The Development of Process Technology for the Friction Stir Welding of Thick Section Aluminium Alloys

Rudolf Zettler

School of Mechanical Engineering
Faculty of Engineering, Computer and Mathematical Sciences
University of Adelaide

July 2006

CONTENTS

ABSTRACT

The ability to join aluminium alloys by Friction Stir Welding (FSW) for a plate thickness of less than 10mm (typically below 6mm) using a generic FSW tool has meant that FSW is now one of the most rapidly expanding processes used for the joining of aluminium and its alloys in the Northern Hemisphere. Attempts however, to exploit this initial tool design for the purposes of welding thicker section (10mm and above) aluminium have proven not as successful.

The purpose of this study is to demonstrate how the interaction of the welding tool, particularly tool pin form in conjunction with rotational speed, applied force and processing temperature can account for joint formation during FSW. A lack of information concerning how the tool pin form influences weld temperatures, process loads and weld formation, when joining aluminium alloys with a plate thickness greater than 12mm has provided the impetus for this current study.

Fundamentally two welding tool pin designs (pin CT1 – conical threaded and pin CT2 – conical threaded with three flats) have been investigated for the FSW of 12.5 and 25mm thick 5083 H111 and 12.5mm thick 7075 O and T651 aluminium alloys. In order to realise processing temperatures in the region of the weld nugget for 25mm thick plate an instrumented FSW tool was designed containing thermocouples embedded in both the shoulder and pin of the joining tool. Results indicate that process temperatures correlate well between those measured in the workpiece (stir zone) and in the tool.

The conclusions from this study are as follows:

- Process parameters are interchangeable when FSW 12.5mm thick 5083 and 7075 aluminium alloys.
- Changes in tool pin geometry do not significantly affect heat generation between tools used under constant FSW parameters for a given alloy.
- Processing temperatures increase with increasing tool rotation speed.
- Changes in tool pin geometry affect processing loads. By minimising the force in the direction of weld travel this helps prevent weld defect formation.
- Adequate tool shoulder contact with the surface of the workpiece is essential if weld defects are to be avoided.
- Although the present study demonstrates tool CT2 is capable of producing sound welds in up to 25mm thick 5083 H111 alloy, this required the spindle motor of the

welder to operate at its maximum capacity. Hence this material thickness was found to be the limit of the FSW machine.

Statement of Originality

This work contains no material which has been accepted for the award of any other degree or diploma in any other tertiary institution and to the best of my knowledge and belief, contains no material previously published or written by another person or persons, except where due reference has been made in the text.

I give consent for this copy of my thesis, when deposited in the University Library, to be made available for loan and photocopying.

Rudolf Zettler

Acknowledgements

This work gratefully acknowledges the support of the Co-operative Research Centre for Welded Structures without whom there would have been no funding, no Friction Stir Welding machine or Friction Stir Welding program.

The supervision of Prof. Valerie Linton, Dr. K. N. Krishnan, Dr. Denny Graham and Dr. M. A. Wahab is also gratefully acknowledged. Of these four supervisors I would particularly like to thank Dr. Denny Graham who first introduced me to the field of FSW. In addition, I would also like to thank Prof. Valerie Linton whose support, patience and understanding in a time of great stress enabled the completion of this document. This will always be greatly appreciated.

I would also like to thank the many staff at the University of Adelaide for the knowledge and friendship they have imparted to me over the years, but most importantly for helping to fabricate the tools and measurement equipment used in this study. For the tools I would like to especially thank Ron Jaeger, Anthony Sherry, Silvio De Ieso, Graham Kelly and Ian Linke.

1. INTRODUCTION

1.1 Background

Friction stir welding (FSW) is a thermo-mechanical solid state joining process i.e. no bulk melting of the base material occurs during joining. The process has its origins in Friction Welding (FW) and was developed then patented by The Welding Institute (TWI) of Cambridge in 1991 [1]. Like FW the mechanisms of heating and forging are readily identified in FSW [2]. In FW the temperature of the components to be joined is raised by frictional heating. The simplest mechanical arrangement involves two cylindrical bars held in axial alignment, Figure 1a)-d). One of the bars is rotated while the other is advanced. Under a pre-selected pressure the parts to be joined are then brought together. Figure 1 (lower caption) presents the FSW process for comparison.

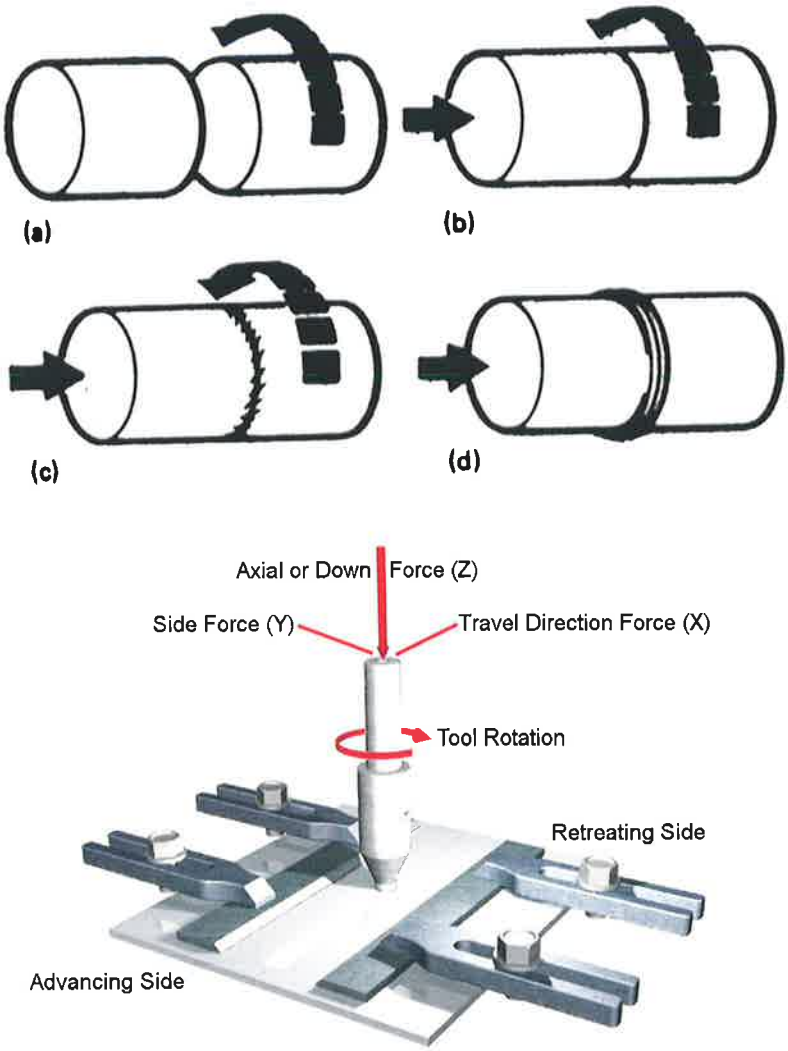

Figure 1 a)-d) basic rotational friction welding: one piece rotates while the other stationary piece is brought into contact with the rotating part. [3]

Once a hot plasticised interface has been established when FW, axial shortening of the workpieces occurs due to the applied pressure. Displacement of plasticised material from the weld interface produces an upset or collar. The collar provides the mechanism by which the heat power (frictional heating from rotation and pressure) is regulated. This is because heat is lost from the weld interface due to conduction, convection and metal which is carrying with it heat being extruded into the collar. Through this regulatory mechanism FW has demonstrated that it is not only possible to join similar but also very different materials [3,4] and that for each material there exists a specific displacement force.

In FSW a rotating non-consumable tool provides for friction heating between typically two components that are to be joined. The tool consists of a threaded pin which is plunged into the workpiece and a shoulder that applies pressure on the surface of the workpiece. Unlike FW the FSW tool with its threaded profile, rotation speed, plunge or axial displacement into the workpiece and weld travel speed are responsible for generating the necessary heat and forging force required to mechanically bind (mix) the thermally softened material from each side of the weld joint. Pressure is applied to maintain intimate contact between the tool shoulder and workpiece, but also to prevent expulsion of any thermally softened material from the weld zone. This pressure is applied in several ways:

- by the tool shoulder over the surface of the join zone,
- by both pin and shoulder profiles which compress, shear and forge the thermally softened material during tool rotation and
- by the pin traversing along the weld join line forcing material to be displaced such that it begins to flow in the direction of tool rotation around the welding tool.

When modeling the FSW process for the joining of relatively thin section aluminium alloys (less than 6mm thick) it has generally been assumed that the majority of heat developed comes from the tool shoulder rubbing against the workpieces [5-18]. The proportion of heat developed by the pin has been considered to be much lower, typically less than 5% of the total heat generated. This however, cannot be said of welds produced in much thicker (greater than 10mm thick) material where heat penetration by the shoulder is limited and thus the welding tool pin must contribute substantially more heat. For thicker section welds Colegrove [19] estimated that up to 20% of the total heat generated may be accounted for in terms of heat developed by the pin.

As with FW, the heat input during FSW must be balanced with any heat lost i.e. through conduction, convection and material flow in and around the weld nugget. Unlike FW however, there is no substantial collar or material upset expelled from the immediate weld zone. Hence heat input and heat lost during FSW must be influenced through means of processing parameters, tool and clamping design to allow for or inhibit the transfer of heat throughout the workpiece.

1.2 Significance

The majority of research work to date has concentrated on FSW aluminium alloys with a plate thickness of around 6mm. Increasing demand however for military [20,21], aerospace [22-26] and transport, both land [27,28] and sea [29,30] applications is driving research to produce tooling and process parameters capable of FSW aluminium alloys in a single pass up to and in excess of 50mm of workpiece thickness.

Limited information exists concerning the design of FSW tools, since much of the work in this area is commercially sensitive and controlled through licenses. Even less information exists on how these tools should be employed i.e. process parameter selection. There is also limited information concerning how tool geometry affects processing forces generated during welding and how these affect both weld quality and the power requirements placed on the FSW machine. One cannot simply upsize a FSW tool just because it was found to be capable of joining a thinner gauge aluminium alloy [32]. This is because increased weld penetration places different demands on the welding tool and these demands may not always change in a linear fashion.

1.3 Objectives

It is proposed that three controlling variables; tool rotational speed, tool shoulder plunge depth into the workpiece (this accounts for axial or down force) and weld travel speed in conjunction with tool pin form can account for the formation of all friction stir welds. By reviewing the processes of FW and FSW it is hoped to discover how these controlling variables along with pin form influence weld parameter selection, process temperatures, weld force, weld energy and weld formation.

Objective 1. Determine a range of FSW parameters capable of successfully joining 12.5mm thick 5083 H111 and 7075 T651 aluminium alloys.

Objective 2. Determine how tool pin form i.e. pin profile influences welding temperatures, welding forces and weld formation when FSW 12.5mm

and 25mm thick 5083 H111 and 12.5mm thick 7075 O and T651 aluminium alloys.

Objective 3. Design a FSW tool pin and demonstrate the feasibility of joining a dissimilar 5083 H111 to 7075 T651 aluminium alloy friction stir weld, for a material thickness of 12.5mm.

2. LITERATURE REVIEW

This thesis is concerned with the FSW of thick section 5083 and 7075 aluminium alloys and the design of a welding tool pin capable of joining these materials both for similar and dissimilar alloy joints. Thick section is used here to define a workpiece thickness greater than 10mm.

The literature review presents an overview relating the material (aluminium) and its properties to that of the joining processes of friction welding (FW) and friction stir welding (FSW). Furthermore the development of tool designs capable of FSW thin (1-10mm) and thick (greater than 10mm thick) aluminium alloys is discussed along with weld parameters. Finally, attempts to visualise material flow are reviewed so as to provide a better understanding as to the nature of weld formation brought about by the joining process.

2.1 Classification For Wrought Aluminium Alloys

Aluminium has a low density (2.7 g/cm^3), approximately one-third that of steel (7.83 g/cm^3). It displays good corrosion resistance in most environments, such as atmosphere, water (including salt water), petrochemicals, and many chemical systems. Pure aluminium and certain aluminium alloys exhibit extremely low strength and hardness values. Some aluminium alloys however can exceed structural steels in comparative strength to weight ratios [32].

For wrought aluminium alloys a four digits system is used to identify alloy family composition. These are designated following the ASM designation system, and reproduced in Figure 2.

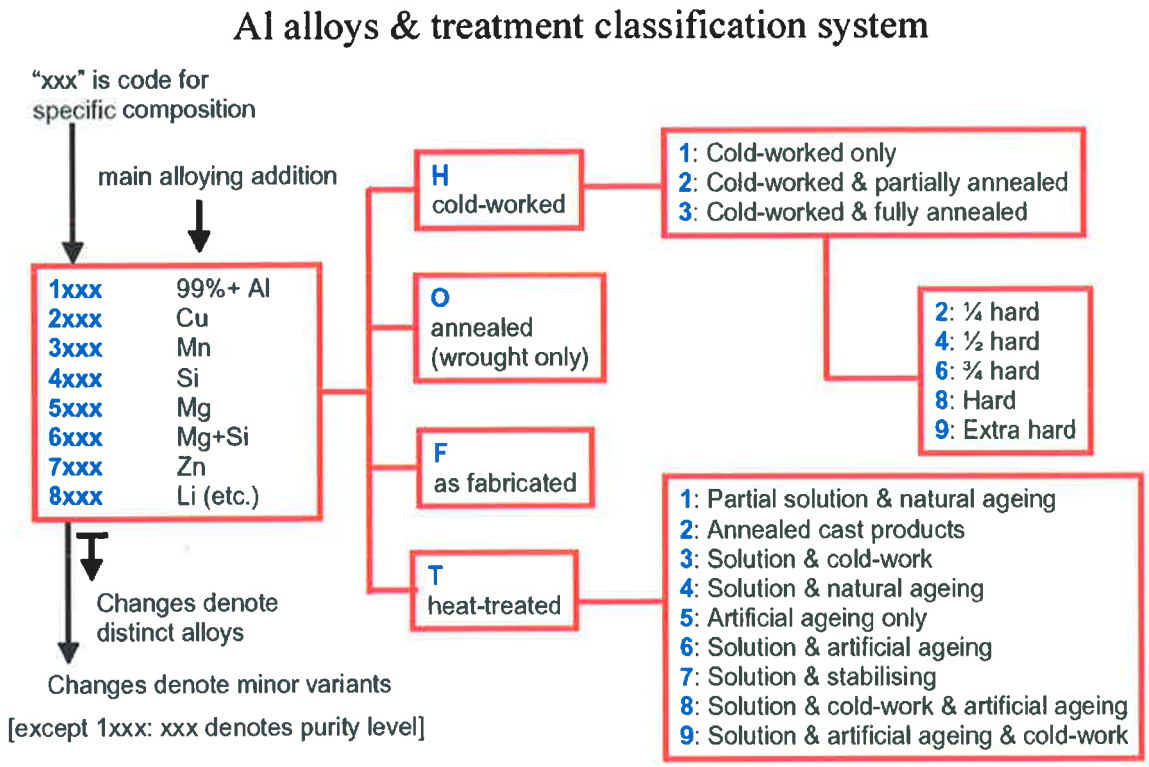

Figure 2 Schematic diagram summarising the aluminium alloy classification system [33].

2.2 Strengthening Mechanisms In Heat-Treatable Aluminium Alloys

Heat-treatable alloys contain elements that have decreasing solubility with decreasing temperature. This feature alone however, does not make an alloy capable of age hardening. The mechanism of strengthening by age hardening involves the formation of coherent particles (clusters) of solute atoms. This creates a great deal of strain as a result of mismatch in size between the solvent and solute atoms. Consequently, the presence of coherent precipitate particles provides considerable strength by obstructing and retarding the movement of dislocations. Heat treatable alloys are thus, solution treated and rapidly cooled followed by aging to produce coherent precipitate particles. Usually, alloys in the 2xxx, 6xxx, 7xxx series are solution heat treatable.

The first step when age hardening an alloy is solution heat treatment. Solution treating is conducted at high temperatures (near the solidus or eutectic temperature where diffusion rates are rapid) so as to maximise solubility. This is followed by rapid cooling or quenching from the solution treating temperature to room temperature, in order to obtain a solid solution supersaturated with both solute elements and vacancies. The supersaturation of vacancies allows diffusion, and thus a much faster rate of

precipitation of strengthening phases to occur upon subsequent aging treatment. The high strength is provided by finely dispersed precipitates that form during aging heat treatment. In practice, hardening is achieved by a combination of solute metastable coherent clusters with a size range of tens of angstroms in diameter called Guinier Preston (GP) zones, and transitional and equilibrium precipitates that can be semi-coherent or incoherent.

Some alloys in which diffusion is very rapid show a spontaneous formation of GP zone structure during exposure at room temperature: this is referred to as *Natural aging*. Heating to a temperature below the GP solvus line (for alloys of all types, the useful range being 120 to 230°C) is required for slow diffusing alloys: this is referred to as *Artificial aging*. During artificial aging, transitional (metastable) precipitates are produced; these remain coherent with the solid-solution matrix and thus contribute to precipitation strengthening. However, heating to higher temperatures or excessive exposure to elevated temperatures (referred to as *overaging*) leads to the formation of large incoherent equilibrium particles and thus softens the material. None the less, for some alloys (for example, the 6xxx series) there may be important differences in detail between the metallurgical processes that occur at different temperatures, particularly in the sequence of phase transformations that constitute the precipitation sequence; this being, the manner in which solute clusters (zones) grow and evolve in shape and crystal structure. Details of these transformations, especially related to the very early stages of solute clustering (precipitation of GP zones) which require experimental investigation at around the atomic level, are still emerging, so it must be emphasised that there is still on-going research in this area [34].

The most widely studied age-hardening alloy system is the Al-Cu 2xxx series, and several commercial alloys based on this system are readily used in aircraft structures today. The high strength of these alloys is provided by dispersed precipitates that form during aging heat treatment. The precipitation sequence is:

SSSS (Supersaturated solid solution) → disk-shaped GP zones θ'' → intermediate θ' → θ (Al_2Cu) [34]

These clusters have a disk shape with a thickness of a few atoms (0.4 to 0.6nm) and a diameter of 8 to 10nm, and are localised on the cubic plane {100} of the matrix. This process is followed by the formation of transitional (non-equilibrium or metastable) precipitates of approximate composition Al_2Cu (θ'' and θ'). The θ'' zones – also called GP2 zones – have a tetragonal shape and they are coherent with the {100} planes of

the matrix. Their dimensions, as the aging process evolves goes from 1 to 4nm of thickness and from 10 to 100nm of diameter. The θ' phase nucleates in a non-homogeneous way particularly on dislocations and are incoherent with the matrix; it has a tetragonal structure with a thickness of 10 to 150nm. The equilibrium θ phase, that is incoherent and has the Al_2Cu composition with a tetragonal structure (a = 0.607nm and c = 0.487nm); forms directly from the matrix or from the θ' phase and does not contribute to precipitation strengthening.

GP zones are more resistant to movement of dislocations through the lattice, particularly the θ'' precipitates which form the most effective strengthening mechanism. The Al-rich corner of the equilibrium Al-Cu phase diagram, includes the metastable solvus boundaries for GP zones, θ'' and θ', Figure 3.

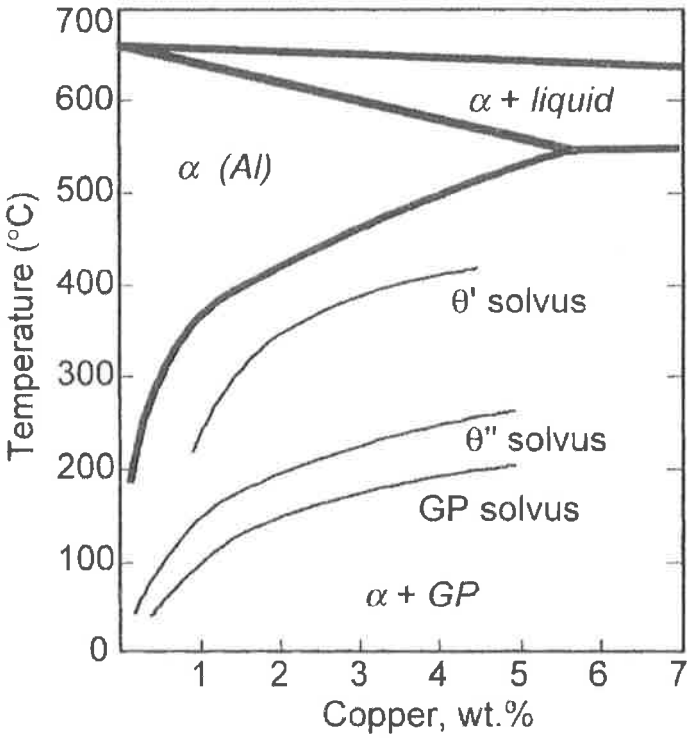

Figure 3 Al-rich corner of the Al-Cu phase diagram showing the metastable solvus boundaries for GP zones, θ'' and θ', together with the equilibrium solvus line for the θ phase. [34]

The complete precipitation sequence can only occur when the alloy is aged at temperatures below the GP zone solvus. The presence of Magnesium (Mg) characteristically accelerates and accentuates precipitation hardening. Also other phases can be identified in several alloys from the 2xxx series because of the presence of Fe, Si, Mg, and Mn, for example: $(Fe,Mn)_3SiAl_{12}$, Mg_2Si, $CuMgAl_2$, Cu_2FeAl_7, Cu_2MnAl_{20} [34]. The 6xxx and 7xxx series aluminium alloys are heat treatable and have similar strengthening mechanisms as described for the 2xxx series alloy.

2.3 Strengthening Mechanisms In Non-Heat-Treatable Aluminium Alloys

When a material is plastically deformed at temperatures that are low relative to its melting point, it is said to be cold-worked. The temperature defining the upper limit of the cold working range cannot be expressed exactly, as it varies with composition as well as the rate and the amount of deformation. Most of the energy expended in cold work appears in the form of heat, but a finite fraction is stored in the metal as strain energy associated with various lattice defects created by the deformation taking place.

When an alloy is plastically deformed many defects are forced into the crystal lattice, and these defects along with elastic strains serve as mechanisms for energy storage in the alloy. X-ray radiography of cold-worked materials has demonstrated that only 5-10 % of the total stored energy can be assigned to elastic strain energy [35].

The most important lattice defects produced by deformation are dislocations and vacancies. The vacancies only account for a small fraction of the total stored energy so that the major portion of the stored energy, generally around 80-90 %, is due to the generation of dislocations. Severe cold working of a material increases the dislocation density from around 10^7 to 10^{11} dislocation per square centimetre. Through the use of transmission electron microscopy (TEM) it has been found that if the dislocations have a low mobility at the temperature of deformation, they appear as a fairly random array in the deformed material. However, if the dislocations are able to cross slip (materials with high stacking-fault energy), they immediately begin to condense into tangles so that the material contains regions of high and low dislocation density. The regions of low dislocation density are called cells or subgrains. Aluminium deformed at room temperature forms a distinct subgrain or cell structure because of its high stacking fault energy which does not inhibit cross slip.

There are four extremely important variables [35] affecting the amount of stored energy. These are:

Purity. The addition of impurity atoms to a metal increases the amount of stored energy at a given strain. The impurity atoms also hinder dislocation motion and thereby produce an enhanced dislocation multiplication.

Deformation. More complex deformation processes, in terms of multiple stress directions produce higher stored energy by increasing the dislocation intersection, thereby giving rise to higher dislocation density.

Temperature. Deformation at lower temperature increases the amount of stored energy. This is because there is less thermal energy to assist in the release of energy and to reduce the interaction between defects during deformation. 5xxx series aluminium alloys unlike the 2xxx, 6xxx and 7xxx series alloys are strengthened through cold working.

Grain size. The amount of stored energy increases as the grain size decreases. This is because as grains decrease in size so does the overall grain boundary area. Thus the stored energy per unit volume can be expressed as the combination of energy derived from dislocations plus energy from new interfaces. The dislocation density produced by strain has been shown to be inversely proportional to grain size. Since the grain boundaries are effective in blocking dislocations, the smaller the grain size the greater the promotion of dislocation interaction and multiplication.

2.3.1 Annealing

It is important to note that the cold-worked state is not thermodynamically stable and by increasing the temperature of the workpiece this state becomes more and more unstable. Eventually the material softens and reverts to a strain-free condition. The overall process by which this occurs is known as annealing. The process of annealing can be divided into three fairly distinct processes: recovery, recrystallization and grain growth [35,36], Figure 4.

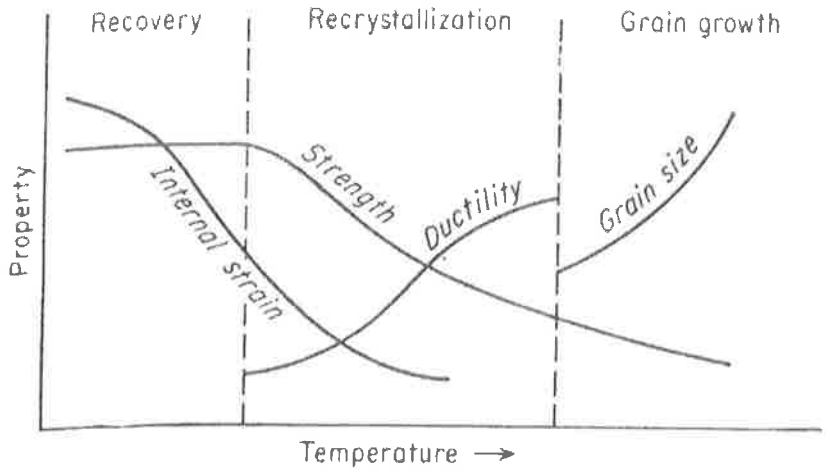

Figure 4: Schematic drawing indicating recovery, recrystallization, and grain growth and chief property changes in each region [36].

2.3.2 Recovery

The most subtle annealing processes is termed recovery. Here no gross microstructural change occurs. However, atomic mobility is sufficient to diminish the concentration of point defects within grains and, in some case, to allow dislocations to move to lower energy positions. This process yields a modest decrease in hardness and can occur at temperatures just below those needed to produce significant microstructural change. The mechanisms operating during the recovery stage can be defined in terms of temperature. At low temperatures migration or combinations of point defects occur. In the intermediate temperature range, the energy level is enough to allow dislocations to rearrange within tangles by two-dimensional movement. At high temperatures the recovery mechanism involves dislocation motion with climb that lead to the polygonization phenomena. This consists of a lining up of dislocations, by slip and climb motion, which produce low-angle boundaries between subgrains [35,37].

2.3.3 Recrystallization

The recrystallization process consists of the nucleation of a strain-free region whose boundary can transform the strained matrix into strain-free material as it moves. In the growth of the boundary out from the nucleus the dislocations are annihilated in the region which is swept. This requires that the moving boundary be a high-angle boundary so that there is a high degree of "misfit" to accommodate the dislocations, Figure 5.

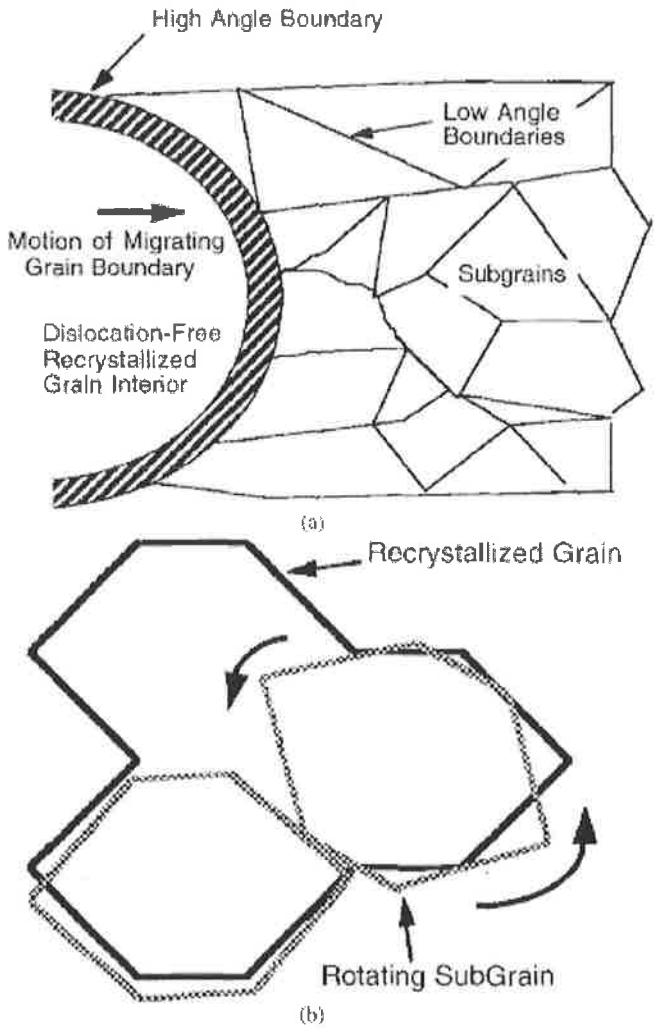

Figure 5: Schematic diagrams of recrystallization by: a) high angle boundary migration through a partially-recovered microstructure; b) subgrain rotation and coalescence. [37]

At least two distinct nucleation mechanisms have been identified for recrystallization. The first is called strain-induced boundary migration, where a strain free nucleus is formed when one of the existing grain boundaries moves into its neighbour, leaving a strain-free recrystallized region behind. The boundary moves into the grain which contains the higher dislocation density in the local region. In the second nucleation mechanism new grain boundaries are formed in regions of sharp lattice curvature through subgrain growth and coalescence. This mechanism seems to predominate at high strains, with nuclei appearing at grain boundaries, twin boundaries, or at inclusions or second-phase particles. [35,37]

2.3.4 Grain Growth

The recrystallised microstructure contains a large concentration of grain boundaries. The coarsening of annealed microstructures by grain growth is a system to reduce these high-energy interfaces, which is not dissimilar to the coalescence of soap bubbles (a process similarly driven by the reduction of surface area). Grain growth is strongly temperature-dependent. Because the driving force for grain growth is appreciably lower than the driving force for recrystallisation, at a temperature at which recrystallisation occurs readily grain growth will occur slowly. Grain growth is also inhibited considerably by the presence of a fine dispersion of second-phase particles, which restricts grain-boundary movement. Under certain conditions, some of the grains of a fine-grained recrystallized material will begin to grow rapidly at the expense of the other grains when heated at higher temperature. This phenomenon is known as exaggerated, or abnormal, grain growth. The driving force for exaggerated grain growth is the decrease in surface energy, not stored energy, but because the phenomenon shows kinetics similar to those of recrystallization it is often called secondary recrystallization. [35,37]

2.3.5 Solid-Solution Strengthening

The main strengthening mechanism in non heat treatable aluminium alloys is solid solution hardening. The introduction of solute atoms into solid solution in the solvent atom lattice produces an alloy which is stronger than the pure metal. The usual result is to raise the yield stress and the level of the stress strain curve as a whole. For this reason it has been concluded that solute atoms have more influence on the frictional resistance to dislocation motion than on the static locking of dislocations [38].

There are two types of solid solution, which are based on the size of the solute atoms [38]. If the solute and solvent atoms are roughly similar in size, the solute atoms will occupy lattice points in the crystal lattice of the solvent atoms. This is referred to as substitutional solid solution. If the solute atoms are much smaller however than the solvent atoms they occupy interstitial positions in the solvent lattice, referred to as interstitial solid solutions.

Solute atoms fall into two broad categories with respect to their relative strengthening effect. Those atoms which produce non spherical distortions, such as interstitial atoms,

have a relative strengthening effect per unit concentration of about three times their shear modulus, while solute atoms which produce spherical distortions, such as substitutional atoms, have a relative strengthening equivalent to their modulus of elasticity in shear divided by 10 [38].

2.4 Friction Welding (FW): A Process Overview

It has been suggested that a better understanding of the FSW process can be gained by studying related friction technology [38]. The earliest form of this technology is FW. Production techniques for friction welds fall into two categories: Direct Drive Friction Welding (DDFW) sometimes called Conventional or Continuous Friction Welding and Inertia Drive Friction Welding (IDFW), also called Inertia Drive Welding or Flywheel Friction Welding [39]. The differences in these techniques relate to how power or energy is supplied to form the welded connection.

In the case of DDFW, power or energy is provided by an infinite duration source (motor) and maintained for a preset period of time, while the workpieces to be welded are brought together under an applied force.

IDFW makes use of the kinetic energy of a freely rotating flywheel. One of the workpieces is connected to the flywheel and the other restrained from rotating. The mass and rotational speed of the flywheel provides the energy required for welding. The workpieces are brought together under axial pressure and then the rotating drive power is shut off. The weld itself becomes the brake and consumes all of the stored energy.

Relationships between Direct and Inertia Drive FW parameters are presented in Figure 6 and Figure 7.

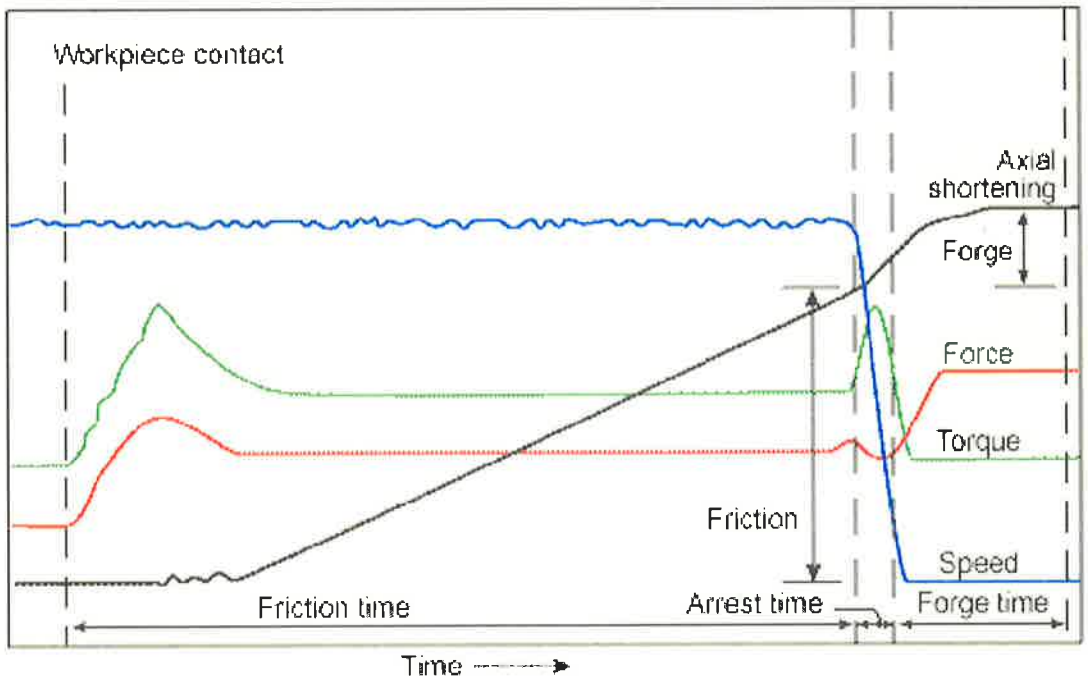

Figure 6 Direct Drive FW parameters characterised [40].

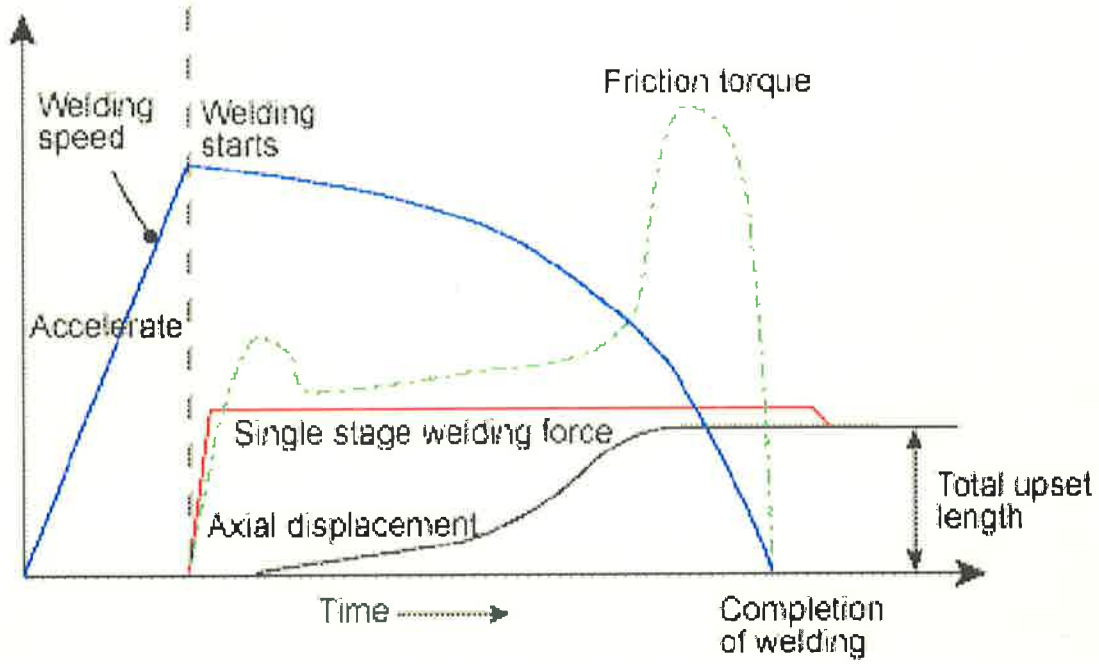

Figure 7 Inertia Drive FW parameters characterised [40]

It has been suggested for all FW systems [3,4], that the relative velocity, axial pressure and heating duration supplied to the parts being welded are the three main controlling

variables. These variables influence both the metallurgical and mechanical properties of the welded joint. For most materials and weld geometries a wide range of FW processing variables i.e. rotational speed, axial pressure and heat duration have been established [41].

2.5 FW: Weld Structure And Weld Formation

If one considers the basic geometry of a conventional friction weld, where one of the workpieces rotates and the other is held stationary, as in Figure 8, then it becomes apparent that two types of welding action occur for the same joint. This distinction has been identified [42] and arises because pressure welding takes place near the centre of the weld interface while true friction welding takes place nearer the periphery of the joint.

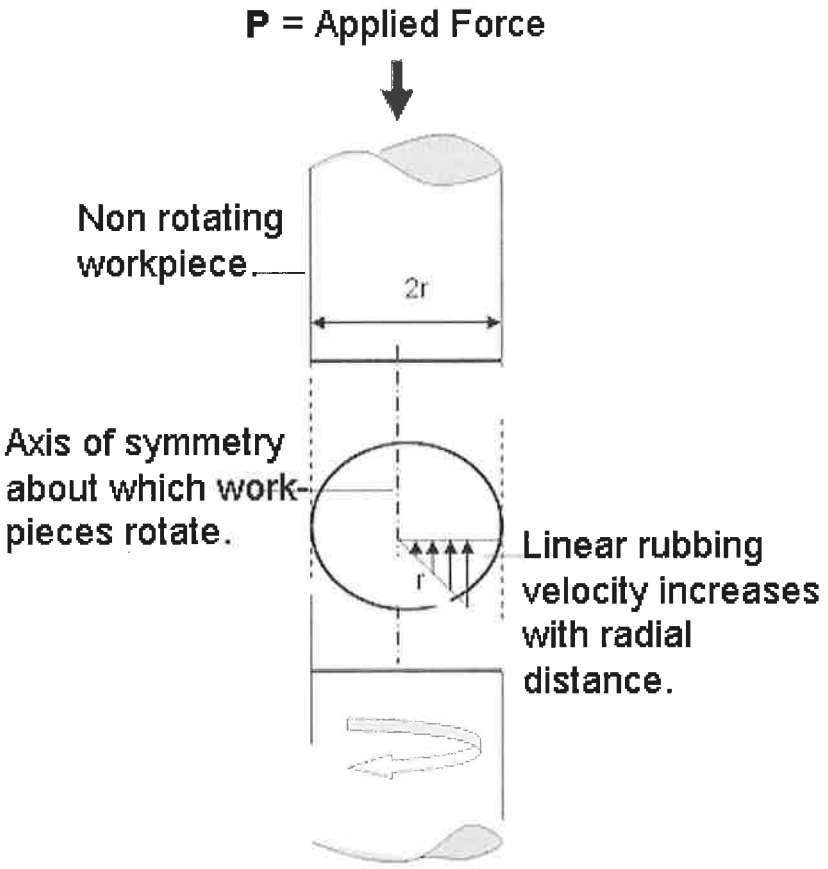

Figure 8 Principals governing Basic Rotational Friction Welding

Friction produced between flat surfaces such as in Figure 8 presents a case for sliding friction. Here the friction force F_r equals a coefficient of friction μ times the normal pressure resulting from the applied force **P**. Rubbing velocity is greatest at the periphery of the workpieces and reduces to zero at the centre. Thus the moment of friction M_f (F_r x r) increases with radial distance, Figure 8 and friction welding initially begins at the periphery of the workpieces.

Determination of friction torque will depend on the nature of the pressure distribution between the contacting interfaces. When the surfaces are newly machined there is likely to be even contact over the entire interfacing area so that the distribution of pressure is also uniform. After a period of time however, the outer surfaces will wear more than the inner surfaces. This is because of the higher linear velocities generated at the periphery of the workpieces causing greater material movement, heat generation and abrasion. The thermally softened material further deforms under the applied force **P** resulting in a pressure decrease in these deforming regions. Maximum pressure then shifts towards cooler regions of the interface i.e. towards the weld centre. Thus pressure increases towards the inner surfaces until they too thermally soften. In all cases it is usually assumed pressure varies with radius across the contacting surfaces. In summary weld surfaces initially heated to higher temperatures become plastic before cooler surfaces, and under the influence of the applied force are flattened out. These hotter surfaces then cease to resist the force and the cooler portions of the friction surface now become the regions for heat generation. As a result temperatures developed between the surfaces are continuously evened out across the interface during the welding process.

In the case of FW it is the influence of rotational speed and the applied force which softens material at the weld interface. The applied force, also known as the forging force is responsible for displacing the thermally softened material outwards from the weld centre forming the upset or collar typical of all friction welds. A photograph representative of the collar for a same diameter friction welded joint can be found in Figure 9.

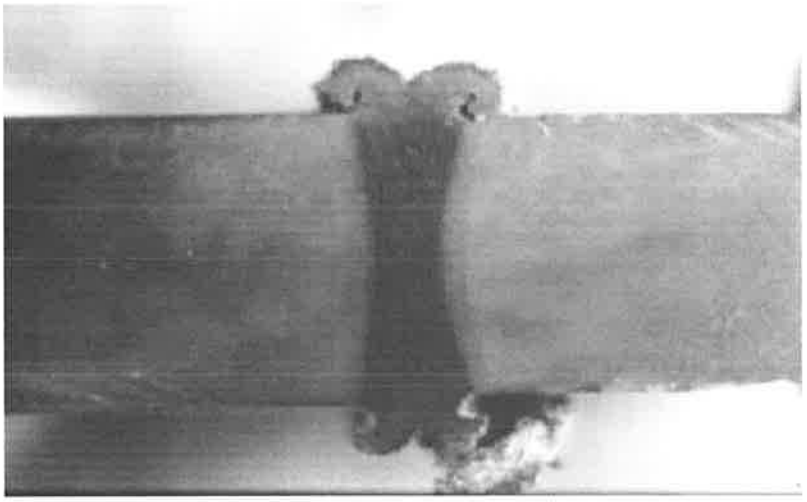

Figure 9 Macrophotograph of equal diameter friction welded steel joint [42].

Friction welds made employing dissimilar materials indicate that the collar may not always be equal and identical for both side of the weld interface. This is typical of joints where one material possesses greater high temperature strength over the other [43]. A weld macro-section of this phenomenon can be found in Figure 10.

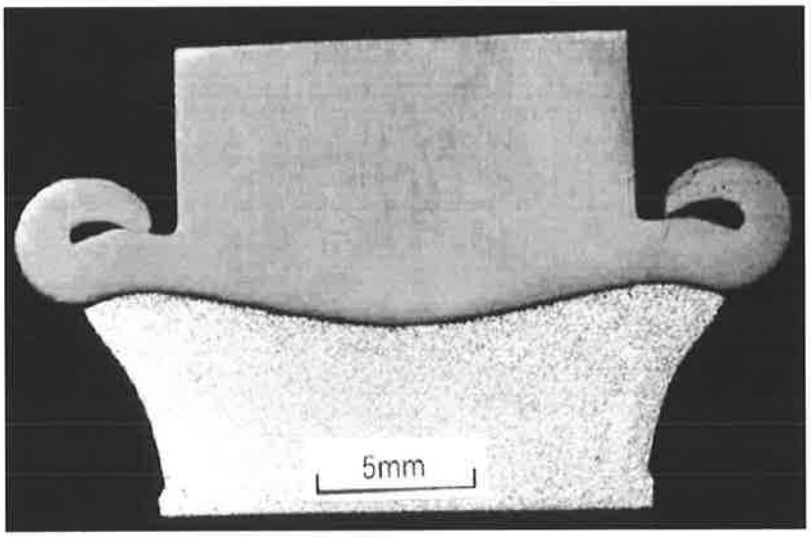

Figure 10 Macrophotograph of friction weld between fine grained Fe3Al-ODS (top) alloy and Haynes 230 (bottom) alloy [43].

Deformation processes as exhibited in Figures 9 and 10 are classified as ones which hot work the material. Hot working is defined as deformation occurring at temperatures above $0.5T_m$ (T_m: is the absolute melting temperature of a material: for pure aluminium this is 940 K) and at strain rates above 10^{-4} s^{-1} [35]. Midling and Grong [44] present a

very detailed process model for the FW of Al-Mg-Si alloys and Al-SiC Metal Matrix Composites (MMC). They point out that strain rates for the contact section for these friction welds are controlled primarily by the rotational velocity. Here the strain rate is often of the order of 1000 s^{-1} or higher. They also point out that in cases where strain rates exceed 10^3 s^{-1} shock waves are generated within the material during deformation.

If one considers that the weld sequence governing all friction welds can be expressed by three distinct phases, these being:

(a) heating of the interfaces,

(b) arrest where welding speed is reduced and then terminated, followed by

(c) bringing together and forging the workpieces

then it is also plausible to characterise the FW process in terms of what is happening to temperature evolution and strain rate during these phases. Besides their effect on macroscopic hot deformation behaviour the phases play a significant role in microstructural development outwards from the weld interface into the body of the workpieces. The zone between the weld interface and the undeformed parent material is classified as the friction welding heat affected zone (FW-HAZ). Midling and Grong [44] identified and divided this region by classifying it in terms of three different reaction zones (1-3), Figure 11.

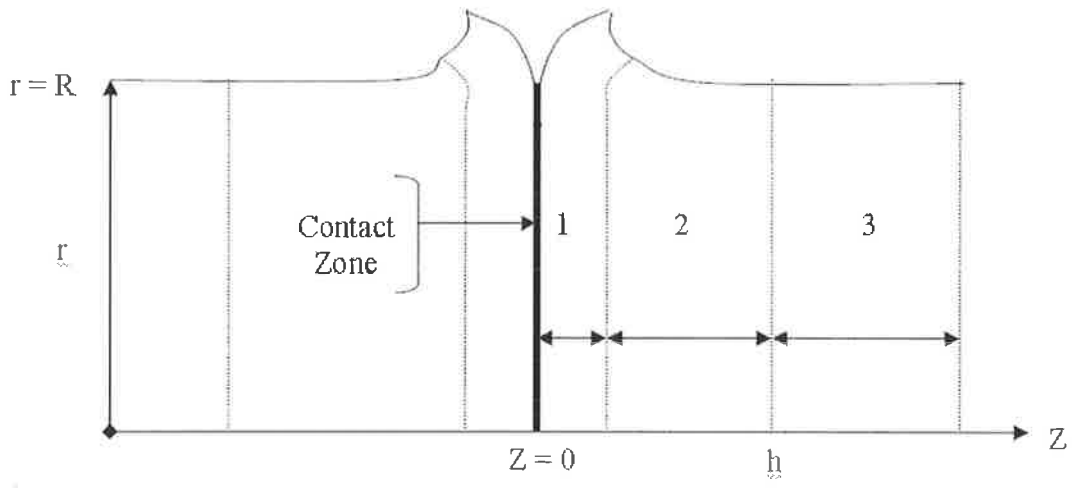

Figure 11 Schematic illustrating the different reaction zones in the HAZ of friction welded components. (Z_{pl}: fully plasticised region = 1, Z_{pd}: partly deformed region = 2, h: total width of plasticised region, Z_{ud}: undeformed region = 3 [44].

During the heating stage the temperature at the weld interface increases steadily until asperity melting occurs. Shortly thereafter temperature at the contact section becomes constant and equal due to a dynamic balance between heat conduction and heat generation. Thermally softened material at the contact section (zone 1, Figure 11) is now able to accommodate plastic strain and does so by means of dynamic recovery or recrystallisation of the microstructure. This mechanism of microstructural evolution is presented in detail by Midling and Grong [44] and as such is not reproduced here. In the partially deformed region (zone 2, Figure 11) the degree of plastic deformation is accommodated by an increase in dislocation density in the matrix grains. In this region the temperature is also sufficient to facilitate dissolution of the base material hardening precipitates. The undeformed region (zone 3, Figure 11) is characterized by partial reversion of the base material precipitates. Although the resulting microstructural changes are similar to those observed in many hot working processes it is obvious that transient effects play a more dominant role in FW because of rapid temperature and strain rate fluctuations during the three process phases.

According to the literature [40,46,47] there are a number of important process parameters and variables which influence the FW process.

Process Parameters:

1. Relative speed of the faying surfaces
2. Normal or axial force on the contact area
3. Heating time
4. Burn-off (displacement of material under rotation) and burn-off rate (rate of axial shortening of a material from its initial pre-weld butted position over time)
5. Time required to stop rotation
6. Forging force and duration

Process Variables:

1. Temperature of the friction surfaces
2. Properties of the weld material e.g. size and nature
3. Presence of surface films and or oxides at the weld interface
4. Rigidity and elasticity of the friction surfaces

Although all of the above FW parameters have relevance during welding, the first four have been found to contribute most to the bonding process. Relative speed however has been found to have the least influence in terms of heat generation [40]. The tendency to believe that increased rotational speed during FW intensifies heat input is erroneous. At high rotational speeds deep tearing of the friction surfaces is replaced by a polishing action [4,48]. Under these conditions plastification of the fraying surfaces will only occur if heating times are increased. Longer heating times however allow for the propagation of thermal energy along the axial direction of the workpieces and as a consequence a greater amount of material is heated. Thus higher rotational speeds lead to lower cooling rates, wider FW-HAZ and hence lower hardness in the contact zone of the weld joint [49]. These conditions have been demonstrated to contribute to significantly lower tensile strengths in the weld region particularly when friction welding steels, while applying low axial forces [49].

A normal or axial force must be applied to a friction weld in order to maintain intimate contact between the faying surfaces. This not only ensures that detrimental substances e.g. oxides are kept out of the weld zone but also helps to avoid oxidation of the weld joint during joining [4, 49]. Although a wide range of axial force may be applied during both the heating and forging stages it is essential to remember that the level of axial force controls three elements, these being;

- temperature gradient in the weld zone,
- the required drive power and
- axial shortening of the workpieces.

The higher the axial force the larger will be the temperature gradient in the weld zone, as will be the required drive power and axial shortening of the workpieces being joined.

The rate of axial shortening and thus the subsequent displacement of material from the weld joint is particularly important in defining the heat distribution in the weld zone. The thermal profile during FW changes as the duration of the heating phase proceeds. If the displacement of material, also known as burnoff i.e. the amount of plasticised material expelled from the weld zone measured as axial displacement or shortening of the rotating workpiece, is too slow this has shown to lead to an increase in the size of the FW-HAZ [48]. However, when the rate of axial displacement and therefore axial force is high the shape of the FW-HAZ changes from an almost parallel sided boundary to a more pinched or double cone, Figure 12.

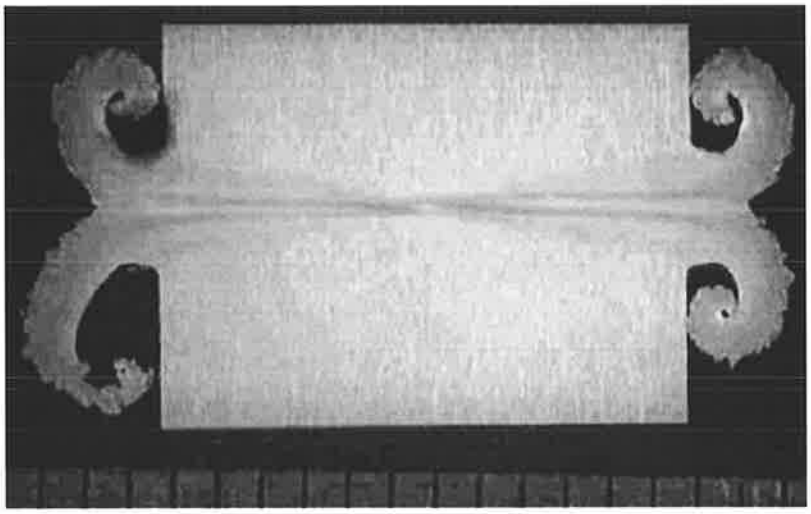

Figure 12 Macrophotograph of a FW between fine grained ODS alloy and itself demonstrating the pinched or double cone profile in the weld zone [43].

By increasing axial force a benefit can be achieved on weld properties. This is because an increase in axial force can change the nature of the microstructure at the weld interface. In the case of friction welded low carbon and low alloy steels a low axial force contributes to the formation of Widmanstätten structures. By increasing axial force it has been demonstrated [49] that this microstructure, changes to a more equiaxed and progressively finer grain sized ferrite. The finer grain size suggests that interface temperatures are reduced since expulsion of material into the weld collar begins at a lower temperature. The high axial force changes the heating conditions as the plasticized material that carries the heat is immediately pressed into the flash.

Plastic deformation during FW is derived from the prevailing temperature conditions. Heating time determines the temperature for the process and consequently this has led some authors [50-52] to suggest the use of temperature itself as the third welding parameter next to relative speed and axial force. The heating time is defined as the period from initial contact of the faying surfaces to the end of the arrest phase. Heating time is reduced as force is increased but is also decreased when using lower rotational speeds [4, 48].

Heating time can be controlled in two ways: the first is by using a suitable timing device which stops rotation at the end of a pre-set time, the second is stopping rotation after a predetermined axial shortening [39]. Heating time is especially important for a low burn-off rate i.e. for limited axial shortening because it not only defines the microstructure of the interface but also controls the depth of heating in the workpiece

by controlling conduction and therefore the width of the FW-HAZ [49]. Failure to achieve a minimum burn-off rate however, has been shown to produce insufficient heating at the weld interface contributing to the presence of lack of bond defects across the plane of the weld. These defects are said to occur as a results of inadequate material flow during joining [3].

The microstructure of the FW-HAZ determines the final strength of the welded joint. Here peak temperatures and cooling rates play a significant role. These are however difficult to measure experimentally due to severe plastic deformation taking place at the weld interface. From a stand point of where improvements can be made to the FW process one must be able to differentiate and control the effects of heating time and cooling rates. Short heating times naturally lead to high rates of intense heat generation. The cooling rate will be affected by heat lost into the surrounding media supporting the joint as well as the welding time combined with the total amount of thermally softened material expelled into the weld collar. If the weld collar is large then heat stored in this mass will be conducted back into the weld thereby reducing the cooling rate and thus affecting the microstructure e.g. lower hardness and tensile strength. For this reason it is preferable to have shorter heating times with minimal formation of the weld collar. Thus the cooling rate will be higher and mechanical properties improved.

The fourth possible way by which the FW process can be influenced and controlled is by influencing the amount of material burn-off. Burn-off not only controls the welding cycle, but also has a significant influence on the joint properties. The applied force and speed of rotation will influence the time needed to reach the pre-set amount of burn-off. The time from initial contact to the end of burn-off becomes shorter as force increases but also a lower rotation speed results in a higher burn-off rate for the same nominal pressure. Since burn-off rate is increased the total welding time is reduced and hence there is less time available for grain growth and homogenization to take place [49].

Controlling the FW process by way of controlling burn-off has its disadvantages too. Vill [4] reported that large burrs, central projections remaining on the surface of the specimen, misalignment of the end cross section and similar surface defects have a negative influence on the quality of the weld when the process is controlled by burn-off.

2.6 Fusion Welding Aluminium

The majority of aluminium alloys can be welded by conventional arc welding processes such as gas manual metal arc welding (GMAW) and gas tungsten arc welding (GTAW)

as well as the high-energy processes of laser-beam and electron-beam welding. Nevertheless, these alloys pose certain risks inherent to all fusion welded aluminium alloys. The risks can be found in the form of tenacious oxides, high thermal conductivity, a high coefficient of thermal expansion, solidification shrinkage almost twice that of ferrous alloys, relatively wide solidification-temperature ranges, high solubility of hydrogen when aluminium is in the molten state and weld porosity. Proper plate surface and edge cleaning, the need for special filler wires, and weld pool shielding via a protective atmosphere are usual practices when fusion welding aluminium alloys. In addition to the formation of gas porosity, which is pertinent to all-alloys, heat treatable Al-alloys, such as the 2xxx, 6xxx and 7xxx series, are more crack sensitive and thus more difficult to fusion weld [53,54] because these cannot withstand the contraction stresses generated when the weld metal solidifies and cools. Cracking can occur in aluminium alloys because of high stresses generated across the weld due to the high thermal expansion (twice that of steel) and substantial contraction upon solidification.

The degree of heat affected zone (HAZ) degradation is also a prime concern in arc welding of aluminium alloys. Conventional arc welding process (TIG, MIG) usually involve the application of 10^3 to 10^4 W/cm^2 arc intensity and at times must be used in conjunction with very slow welding speeds (< 15 mm/s). This can lead to excessive heat input into the weld [55]. A comparison between the heat input produced by MIG and by FSW can be found in Figure 13.

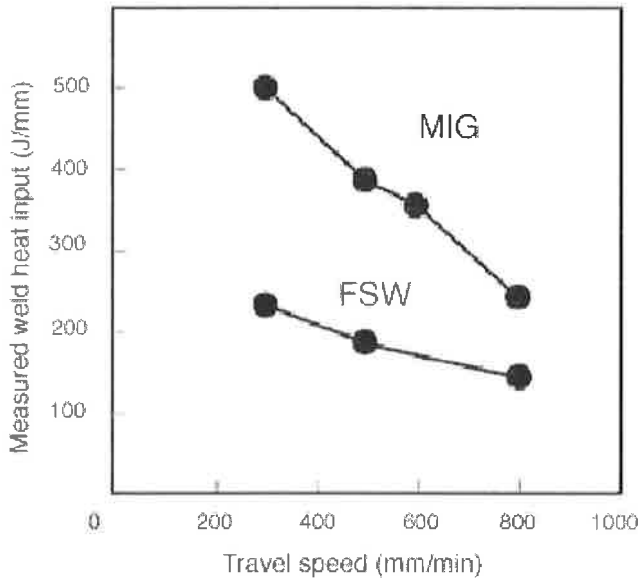

Figure 13 Comparison of weld heat input with FSW and MIG welding to give a full penetration welds for 4 mm thickness plate of aluminium-magnesium alloy. [55]

The higher heat input of the conventional fusion weld results in a coarse fusion zone microstructure characterised by a large dendritic microstructure and a wide HAZ.

The high thermal gradient from the weld into the base material in power beam welding processes, such as laser-beam and electron-beam welding, creates very limited metallurgical modifications and as a result crack sensitivity is reduced. The HAZ produced using these processes is also very narrow due to a low heat input into these regions and thus problems with grain coarsening are limited. However, due to the very high temperature experienced in the fusion zone, the loss of some elements, e.g. vaporisation of Mg, may occur. The loss of any such strengthening elements potentially degrades the mechanical properties of the weld by affecting the weld pool chemistry [54]. Microstructural changes taking place in the region of the weld, i.e. segregation of alloying elements and consequent formation of non-strengthening coarse particles in addition to the depletion of solid solution strengthening elements in the matrix, or loss of strengthening precipitates (dissolution), degrades the mechanical properties in the fusion zone. It also leads to the fact that the strength of the fusion zone cannot be restored to that of the base or parent material via the use of a post-weld heat treatment, principally due to the depletion of these alloying elements. The coarsening of strengthening precipitates in the over aged HAZ also reduces the strength in the HAZ region, which in turn cannot be restored by the use of filler wire [54]. Figure 14 is characteristic of a laser beam weld with very narrow HAZ.

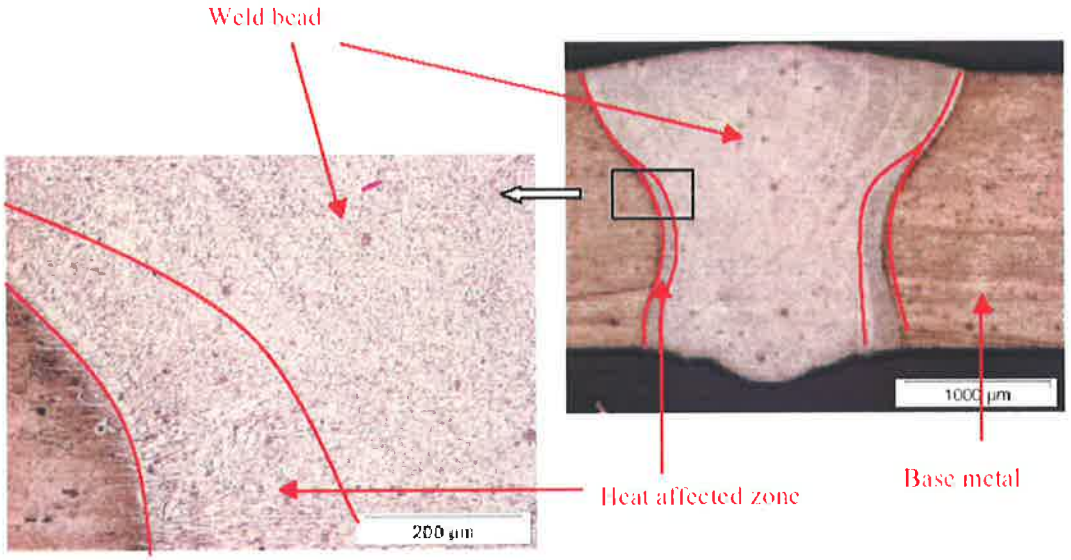

Figure 14 Transverse section of 6056-T4 laser beam welded, see the narrow HAZ. [56]

Microhardness profiles are generally a good indication of the extent and distribution of the heat input into a weld. The higher the hardness value the lower the heat input. Figure 15 highlights that for all processes the lowest hardness value is typically seen to occur some millimetres removed from the weld in the HAZ. In the case of the laser beam weld the smaller HAZ can be attributed to the fact that there exists a tremendous temperature differential between the molten metal and the base material immediately adjacent to the weld. Here heating and cooling rates are much higher than in arc or friction stir welds meaning that the HAZ in a laser beam weld is much smaller.

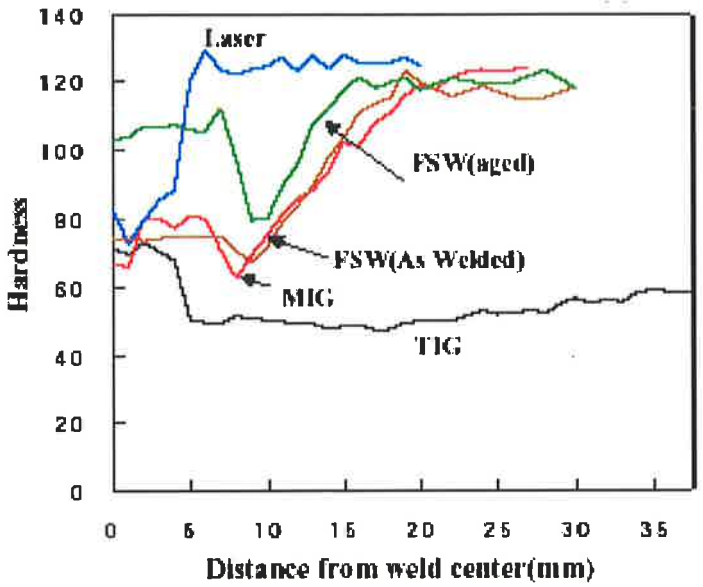

Figure 15 Microhardness profiles as observed for the 6056-T4 alloy welded using different processes. The lowest value for hardness can be seen to occur in the HAZ several millimetres removed from the weld centre line. [57]

2.7 Friction Stir Welding (FSW): A Process Overview

Friction stir welds unlike friction welds are produced by plunging a rotating and non-consumable tool, comprising of a shoulder and a pin into the join line between workpieces. Typically the tool, which possesses a profiled surface, is plunged until a portion of the tool shoulder comes into contact with the top surface of the workpieces. The depth of penetration is determined by setting an axial force for force controlled FSW machines or by estimating a plunge depth for position controlled FSW machines. In both cases the level of shoulder penetration is dependant on the compositon of the alloy, material thickness and rigidity of the welding machine. Relative motion i.e. rotation of the tool in contact with the workpieces then produces heat. This heat allows for a reduction in the flow stress of the workpiece material in the immediate vicinity of the tool. The tool is then traversed along the join between the workpieces. Often the tool pin possesses a special profile, which when rotated enables horizontal as well as vertical movement of the thermally softened material. This softened material is then forced to flow by the forward motion of the tool from the front to the back of the pin where it cools and consolidates [58-67]. A schematic of the process of FSW is presented in Figure 16.

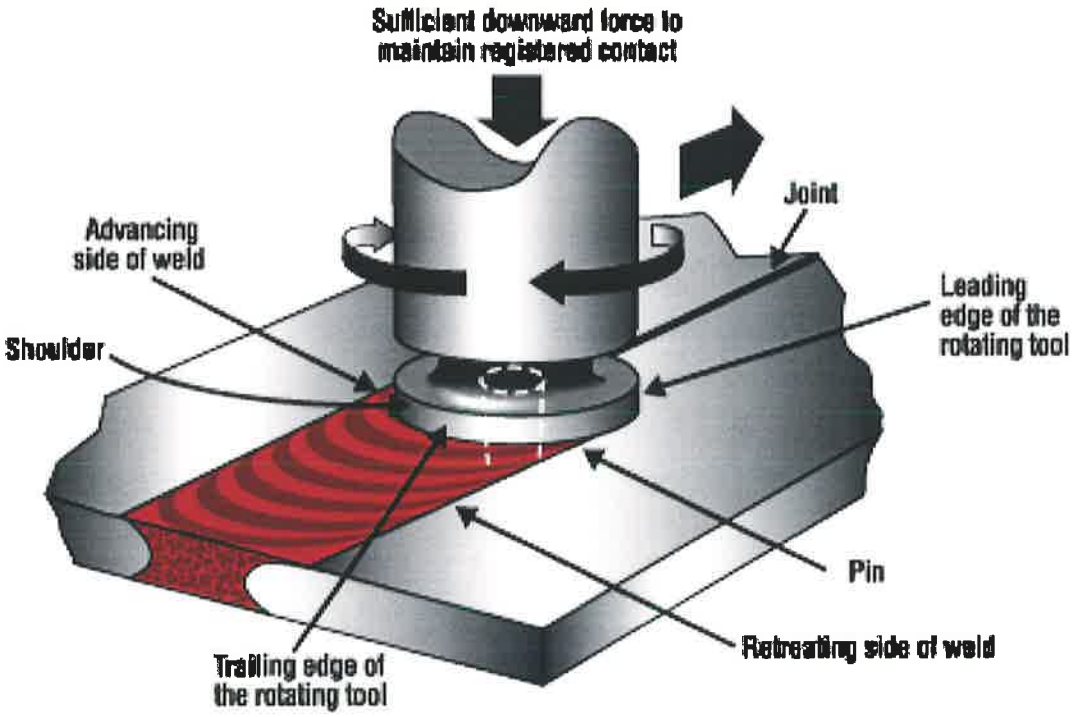

Figure 16 FSW: depicting a plunged and rotating tool traversing the workpiece [68].

Shortly after the invention and subsequent patenting of FSW by TWI [1], the process was systematically examined for the welding of various aluminium alloys with material

thickness ranging between 1.2 and 10mm. FSW tool development for aluminium alloys up to 6mm thick proved so successful that the technology has been used on a number of major industrial applications. These applications include the fabrication of the Space Shuttle external fuel tank for NASA/Lockheed Martin, Delta rocket fuel tanks, and T45 undercarriage doors for Boeing. Further applications include helidecks, bulkheads, the decks of ships in the shipbuilding and maritime industries as well as many applications in the aerospace and to a lesser extent the automotive industry, particularly where structural welds in high strength aluminium alloys are concerned [69-72], Figure 17.

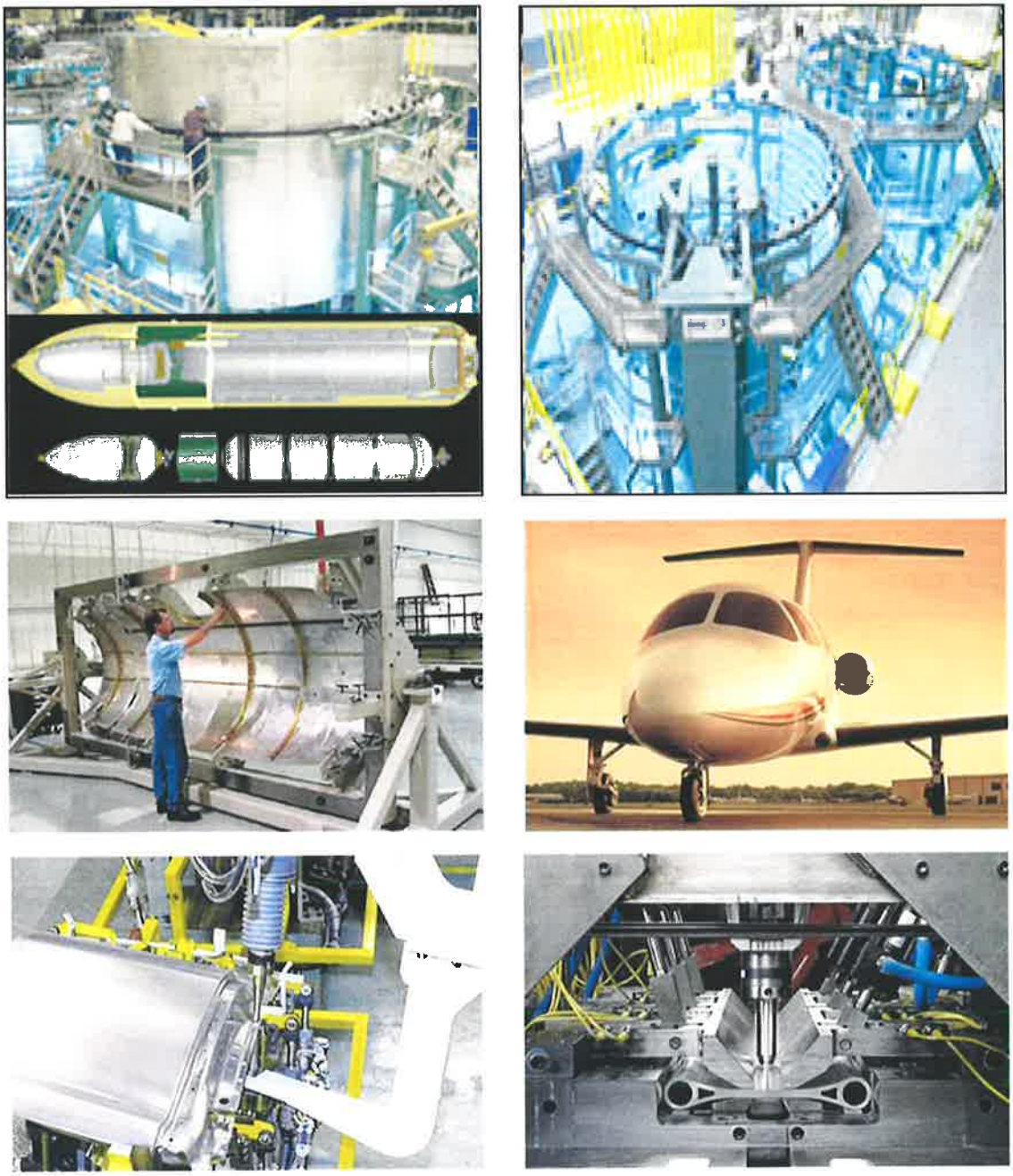

Figure 17 FSW top NASA/Lockheed Martin [69], middle Eclipse [70], bottom Mazda [71] and Ford Motor Co [72].

The process of FSW has demonstrated a number of advantages over competing and conventional arc/fusion welding processes. This is because of the exceptional properties the hot forged friction stir welded joint delivers. Some of the advantages are derived from the fact that:

- FSW occurs with workpiece material in the join zone remaining in a solid state. Hence there is no bulk melting, thereby eliminating the problems associated with hot cracking or porosity development in the weld. Aluminium alloys have demonstrated a tendency to hot crack when the severity of deformation (strain rate) is too great.
- The process produces lower levels of distortion in the workpieces compared to fusion welding as the material remains in a solid state and temperatures generated are thereby very much reduced for FSW when compared to fusion welding.
- No filler wire or shielding gas is required when FSW aluminium and its alloys.
- No fume, no spatter and no UV radiation is produced during FSW, therefore the process can be considered environmentally and OH&S friendly.
- FSW uses readily available machine tool technology and as such is easily automated, thus reducing the need for highly skilled operators.
- FSW can be used in any orientation. The workpiece material remains in a solid state throughout the joining process.
- No special edge or joint preparation is required. Several weld joint geometries are presented in Figure 18.
- FSW can be used to join dissimilar and difficult to weld materials. Apart from aluminium, industrial materials which have been shown capable of being friction stir welded include zinc, lead, copper, magnesium, titanium and steel.
- The FSW process produces a weld with exceptional mechanical properties, which for aluminium alloys equal or exceed those obtained by competing joining processes.

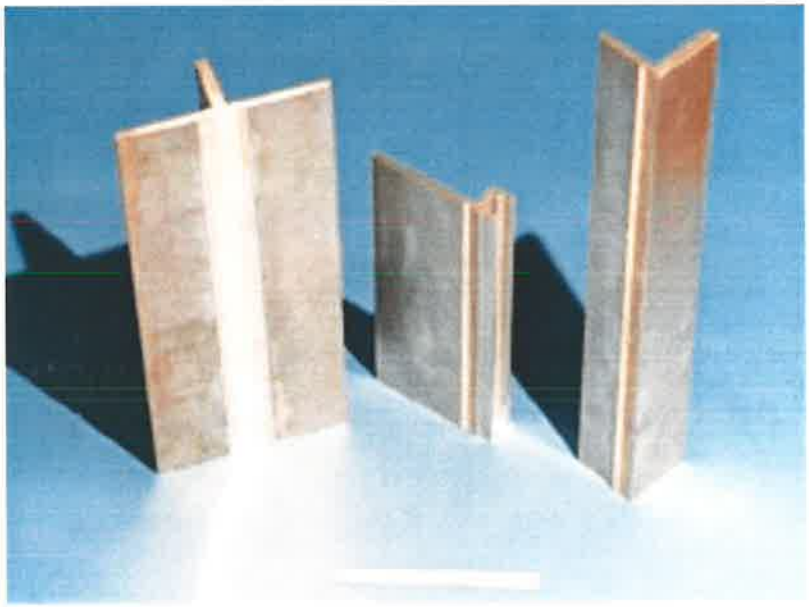

Figure 18 Some possible friction stir weld joint geometries apart from flat plate [73].

A range of tools and welding parameters exist for the production of the various types of friction stir welded joints. Information in the open literature however concerning the design of many of the FSW tools is limited, since much of the work in this area is commercially sensitive.

Although the FSW process has many advantages it does have some disadvantages. One purported disadvantage is that FSW uses a relatively slow weld travel speed in comparison to fusion welding processes such as laser beam welding. This however cannot be said of thick joint welds. Here friction stir welds can be produced in a single pass unlike fusion welds which require multiple passes.

Rigid clamping of the workpiece is seen as another limit of the process. Up to now the workpiece has always been fixed to a backing bar or anvil through mechanical connections and clamping devices like screws, U-bolt, etc. Such a clamping system unfortunately cannot be automated, and so intervention by an external operator is needed whenever clamping and releasing of the workpiece is required. Moreover, these operations require time to be performed and this represents a cost for industry. A recent application for the friction stir welding of thin plates has been directed towards investigating the feasibility of using a vacuum-operated clamping system. This has the potential of making the fixing and release operations on the workpiece faster but does not completely solve the problem associated with an operator whose presence would still be necessary to ensure correct fit up. It should also not be forgotten that the need

for rigid clamping is in response to high axial/forging forces. This means that relatively robust machines are required thus limiting process portability.

Another so called disadvantage of the friction stir welding process is that a hole is left by the pin at the end of each weld. This hole in most cases is not desired and due to non consolidation i.e. a void is left in this region of the weld join, which means that this section at the end of the workpiece cannot be used. Tools such as the retractable pin tool however have demonstrated a methodology by which to overcome this problem [69].

2.8 FSW: Weld Structure And Weld Formation

As with FW, FSW clearly utilises the generation of heat and forging to form the welded connection. Heat arises due to the interaction of the rotating tool with that of the workpiece material. Forging can be said to occur throughout the entire process i.e. via a down force placed on the weld by the contacting shoulder normal to the weld travel direction. The down force placed upon the surface of the workpiece helps to maintain intimate contact between the tool shoulder and the surface of the workpiece. Unlike the process of FW, FSW does not utilise this downforce to displace any of the thermally softened material from the weld joint, rather the tool shoulder in addition to heating helps to prevent expulsion of the thermally softened material. This however means that any oxides or surface impurities present between the join interface (top of the workpiece and join line) have to be disrupted and dispersed throughout the entire weld zone so as to prevent potentially detrimental structures within the weld zone from forming e.g. the alignment of oxide chains which can run through the weld nugget. Such an example can be found in the FSW of cladded alloys. Aluminium and its alloys are typically clad to shield and help protect the underlying alloy from corrosion attack. The problem associated with the FSW of such coated alloys lies in the fact that the coating, typically pure aluminium, is drawn into the weld nugget from both the upper and lower surfaces of the workpiece. In most cases the weld nuggets produced by the FSW of cladded alloys contain finger like projections of the cladding stretching (hooking) into the weld nugget, Figure 19.

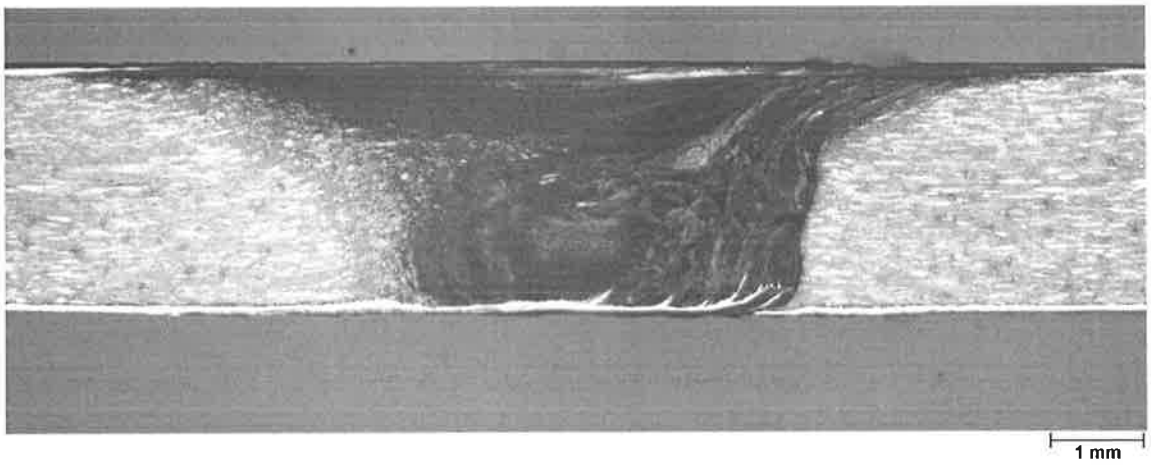

Figure 19 Weld macrograph of a friction stir weld produced by the author in 2.5mm thick cladded 2524 T3 aluminium alloy demonstrating fine finger like projections of the lighter coloured pure aluminium cladding penetrating into the weld nugget.

Due to the introduction of the cladding into the weld nugget this nugget is only as strong as its weakest component, this being the strength of the coating. Hence it is extremely important when FSW that good mixing occurs to prevent potentially detrimental structures from entering the main body of the weld. Since the tool shoulder only has intimate contact with the immediate surface region of the weld nugget this work must be performed by the profile of the welding tool pin in conjunction with appropriate FSW process parameters.

According to the literature [74-76] there are a number of important FSW parameters and process variables when welding aluminium and its alloys.

Process parameters include:

1. Rotational speed of the welding tool. This is a measured of spindle rotation typically in revolutions per minute.
2. Axial displacement of the tool shoulder into the surface of the workpieces whether brought about by co-ordinate or axial load control.
3. Heating or dwell time. This is defined as the time after the tool shoulder has made contact with the workpiece prior to the onset of weld travel where the tool begins to traverse the join.
4. Tool tilt angle. Tool tilt angle is here defined as the angle the tool is tilted away from the vertical as seen from the perspective of the weld travel direction.
5. Weld travel speed. This is a measure of the linear velocity, typically in metres per minute of the tool when traversing the weld join.

Process variables include:

1. Temperature of the weld zone. Particularly the weld nugget and the isotherms generated as a result of the shape of this thermal source.
2. Temper and properties of the parent material.
3. Presence of surface films and or oxides.
4. Weld joint geometry.
5. Clamping and or backing i.e. weld support and containment mechanisms. These influence heat conduction out from the workpiece.

The following definitions are presented to clarify what effects each of the various parameter and process variables have when FSW:

- Tool tilt angle – this influences the area of contact between the tool shoulder and the workpiece surface and thus has implications in terms of the forging force placed on the surface of the weld zone. FSW tools can be tilted away from the direction of weld travel, but some tools have been developed to function at zero degrees of tilt. The greater the angle of tilt however the deeper the heel of the tool shoulder penetrates the surface of the workpiece. This provides for greater anchoring of the tool and also helps limit ploughing into plasticised material that may form in front of the tool.
- Tool rotational speed – this is set so as to provide sufficient frictional heating and material deformation (strain). A more detailed discussion is presented in Chapter 2, section 2.10.
- Shoulder plunge depth – this essentially provides the forging force necessary to consolidate but also to contain the workpiece material within the direct weld zone.
- Dwell time – is the time necessary to uniformly distribute heat between the weld material and tool interface once the tool has been plunged, but prior to the commencement of weld travel. For heat treatable aluminium alloys in peak hardened tempers this also ensures sufficient heating time to dissolve precipitates and thermally soften the material in close proximity to the welding tool.
- Travel speed – is simply the welding speed. The selection of an appropriate weld travel speed is achieved when heat input from friction (rotation or rubbing velocity) and deformation (strain rate) is balanced with that of heat lost through conduction, convection and radiation. Weld travel speed however cannot just be a function of the energy input into a weld. Factors such as reactionary forces developed opposing the direction of tool travel and the hot temperature strength of the tool

material will also determine what travel speeds may be possible given a particular aluminium alloy, FSW tool and FSW machine.

Although the definitions given above can describe and characterise the FSW process they should not be discussed in isolation from material property variables associated with both the tool and the workpiece material. This is because material properties are also seen as influencing the selection of processing parameters as well as the size and shape of the welding tool.

Material properties can be said to influence the welding process through;

1. Thermal and mechanical properties inherent to both the workpiece and tool materials e.g. alloy type and temper, workpiece thickness.
2. Tool geometry and tool profiles e.g. tool static and dynamic displacement volumes and any additional tool profile employed such as a thread form for the FSW pin. These profiles will influence welding force and hence strain placed on the material being joined.
3. Heat sinks i.e. sources into which heat is lost during welding e.g. clamping systems, backing plate and the welding tool.
4. Thermal contact resistance which can restrict heat flow e.g. the interface between abutting workpieces and between workpieces and the backing plate.

A very considerable investment has been made in the pursuit to better understand the mechanisms of joint formation which lie at the heart of the FSW process. This is no more evident than when one considers the numerous papers published in recent years concerning heat [5-19], material flow [13,58-67] and microstructure evolution [77-105] in friction stir welds. Modellers of the FSW process however, still rely on experimental data to validate their model assumptions and as such there is presently no predictive model capable of defining tool geometry or a set of process parameters when it comes to the FSW of aluminium and its alloys. Hence most researchers have turned their attention to interpreting weld structure.

A typical weld structure produced by means of FSW is in many ways similar to that of a weld made using conventional fusion welding techniques, in that the weld can be divided into several distinctly different regions, Figure 20.

The major regions which have been identified and categorized as occurring in a friction stir weld are;

A. The heat affected zone (HAZ).

B. The thermo-mechanically affected zone (TMAZ).

C. The weld nugget.

D. The parent or base material.

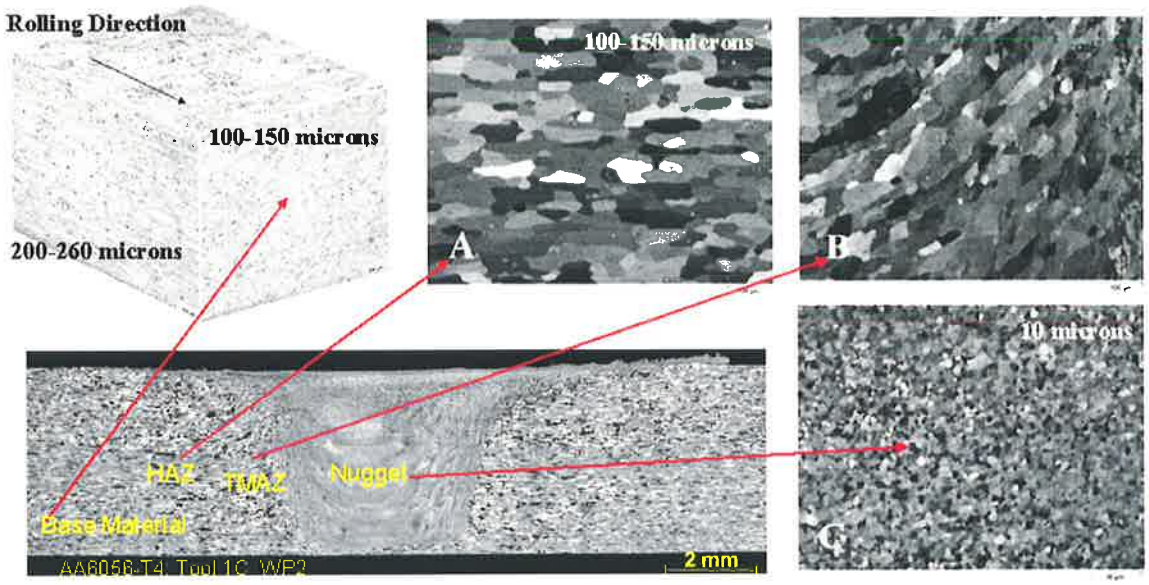

Figure 20 Cross section of a friction stir weld transverse to the welding direction produced by the author in 4mm thick aluminium alloy 6056 T4 [58]. Note the micron ranges define a linear length of the grains as seen in the measurement plane.

FSW is a solid state joining process and so unlike welds produced by means of fusion welding there is no evidence of a solidified or cast structure. Rather these regions typical of fusion welds are replaced by what is generally referred to as a thermo-mechanically affected zone or TMAZ. The material in the TMAZ is deformed extensively by interaction with the welding tool. Workpiece material entering the profile of the tool pin i.e. pin thread is said to be augured downwards towards the weld root. The forward motion of the welding tool and action of the tool shoulder above the surface of the workpiece results in considerable pressure being applied to the weld zone. It can be considered that this pressure when FSW relatively thick section aluminium alloys (greater than 10mm in thickness) translates into very large downward and traversing i.e. weld travel direction forces [106]. An ability to reduce these forces has the potential to reduce the size of the welding tool as well as the required robustness of the machinery and clamping systems used to produce the welds.

The fact that high strains are introduced to the workpiece material during FSW means that a region of the join line (thermally softened zone) is forced to flow.

Inhomogeneous and or sporadic material flow will lead to defect formation. Gross defects can be regarded as volumetric inconsistencies which take the form of surface or sub-surface voids. For such defects not to occur during plastic deformation it is essential that volumetric consistency be maintained between the material moved from in front of the welding tool and that deposited at the rear of the tool.

The fact that material is thermally softened and forced to flow (hot worked) during FSW brings about changes to the original parent material. FSW is a hot-working process in which a large amount of deformation is imparted to the stir zone through the interaction of the pin and the shoulder. Optical micrographs of a friction stir weld reveal that deformation in the stir zone or weld nugget produces a very fine and equiaxed microstructure. Both dynamic recovery and dynamic recrystallisation have been reported as restorative processes that occur in a number of aluminium alloys during FSW [63,64,77,79,92,93,98,100,102,104]. Evidence as to the occurrence of dynamic recrystallisation having occurred as a result of the FSW process is based on the observation that welding completely eliminates the base material (elongated and pancake like) grain structure, replacing it with very fine and equiaxed grains.

Most friction stir welded aluminium alloys achieve mechanical properties very close to those of the parent material. For this to occur a weld must undergo some restorative process i.e. recovery of all or part of the mechanical properties of the material after welding. When a restorative process occurs after deformation this may be referred to as static, while one that occurs during deformation is termed dynamic [107].

Dynamic recrystallization seems to play a significant role in the friction stir welding process [58]. In the current context, dynamic recrystallization refers to the occurrence of recrystallization during the deformation process. When this type of "annealing" process is taking place, both nucleation as well as grain growth occurs in response to the applied strain.

The recrystallization phenomena occurring during FSW has been considered to be created by locally introducing heat through application of frictional rubbing and plastic strain that increases from the TMAZ inwards to the nugget. In the more conventional context, recrystallisation in aluminium and its alloys proceeds by nucleation and growth of new grains surrounded by high-angle grain boundaries. Analysis of optical and TEM microscope studies indicate a high dislocation density with grain growth in the TMAZ in

conjunction with dynamically recovered subgrains. The nugget, in contrast, consists of recrystallized grains demonstrating differing degrees of recovery and absorption of dislocations into the subgrain boundaries inside the recrystallized grains. This suggests that in some instances (perhaps due to the weld parameters) recovery and recrystallization may not be complete or are not continuous in nature [64,77,92], Figure 21.

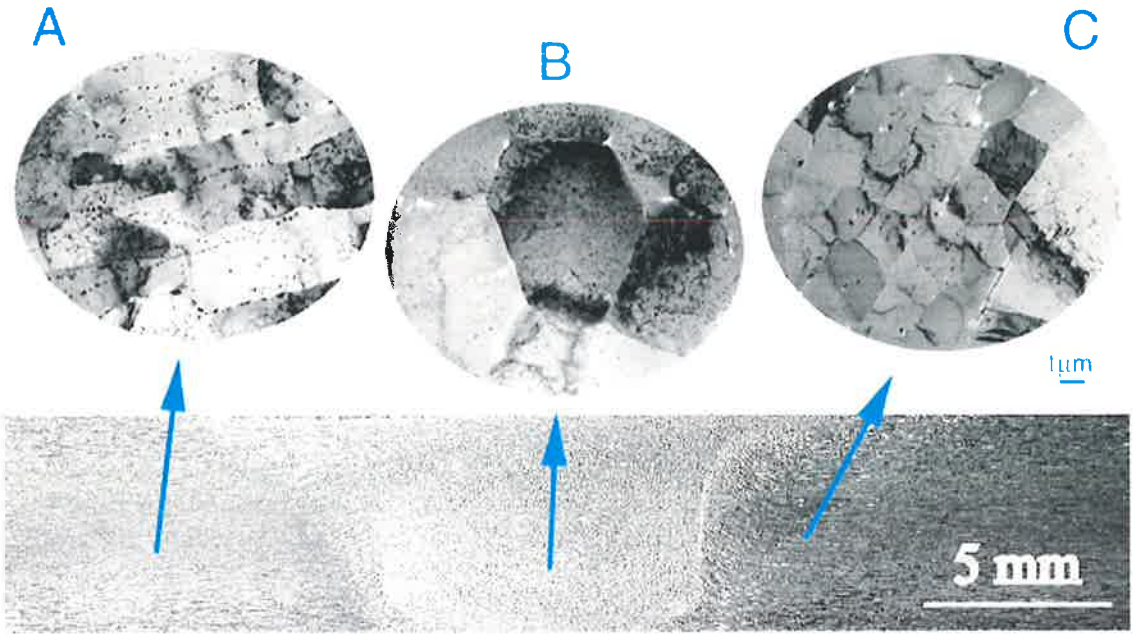

Figure 21 Cross section of a FS weld in Al 7050 and grain structures for different regions by TEM photograph. A) HAZ with low dislocation density and precipitation phenomena; B) Nugget with recrystallized grains (different dislocation structures are showed, zones with high dislocation density and others with low dislocation density); C) TMAZ where subgrain formation is evident. [77]

A sequence that describes the possible evolution of the dynamic recrystallization process in the nugget zone is:

Dislocation introduction: in the early stage of the thermo-mechanical cycle, a large amount of lattice dislocations are introduced by plastic deformation while at the same time grain growth occurs as a result of the elevated temperatures produced during FSW.

Dynamic recovery: in this process, many subgrains are formed intragranularly by dynamic recovery. These subgrains are very small and exhibit low-angle boundaries.

Continuous dynamic recrystallization: during the subsequent thermo-mechanical deformation, dislocations are introduced continuously in the subgrains to accommodate the strain incompatibility of neighbouring subgrains. The small subgrains grow and rotate by repeated absorption of the accommodating dislocations into the subgrain boundaries, resulting in the formation of equiaxed recrystallized grains with high-angle boundaries.

Repeated introduction of dislocation and partial recovery: after dynamic recrystallization, plastic deformation generates additional dislocations within the recrystallized grains. At the end of the thermo-mechanical cycle, partial recovery occurs both in some TMAZ grains and the nugget.

In summary, the recrystallization process is a continuous dynamic recrystallization process based on dynamic recovery. [64,77]

The weld nugget residual microstructure is a grain growth remnant of the dynamically recrystallized grain structure after static grain growth, due to the elevated processing temperature. It has been observed that the temperatures within the weld zone, over a broad range of tool rotation speeds, can vary between 0.6 to 0.9 T_m where T_m is the absolute melting temperature (940 K) of pure aluminium. This is well above temperatures normally required for dynamic recrystallization (~0.5 T_m), even at modest strain rates. [35,64]

Dynamic recrystallization resulting from the FSW process is however extremely complex, as indicated by Figure 22. This is because the ambient temperature, the frictional heating fraction, the adiabatic heating fraction all influence both recrystallization and grain growth rates within the FSW zone and these are in turn dependant on the major process parameters such as down force, rotational and travel speed and the geometry of the welding tool. [64]

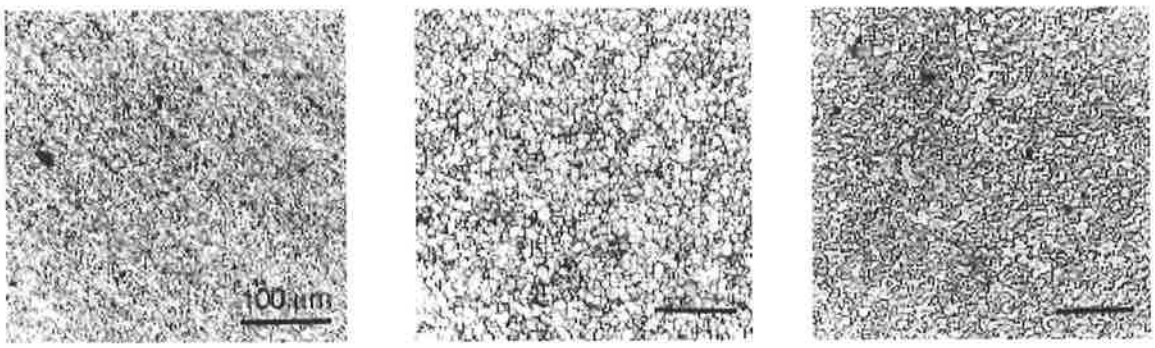

Figure 22 Grain growth remnant of dynamically recrystallized grain structure of 2024-T4 FSW nugget for different tool rotations: from the left 400 rpm, 800 rpm and 1200 rpm with constant travel speed of 1 mm/s, thread pin, concave shoulder (0° axis). [64]

2.9 The Origins Of The FSW Tool For Joining Aluminium And Its Alloys

Of importance to this thesis and subsequent interpretation of results is the FSW tool i.e. tool pin design and how it interacts with the workpiece. It is well acknowledged [74,107,109-111] that tool design lies at the heart of the FSW process. The FSW tool consists of two functioning parts; the shoulder and the pin. FSW tools developed initially for joining thinner gauge aluminium alloys typically less than 6mm thick were produced as one piece tools. An example of such a tool can be found in British Patent Specification, Application No. 940591.3 [112].

When developing the initial FSW process for the joining of aluminium alloys TWI and its group of sponsors undertook a systematic study of some 20 different tool designs [113]. From this study it was found that the most appropriate tool profile for welding the aluminium alloy 6082-T6 consisted of a threaded cylindrical pin with a helix angle of at least 6° coupled to a tool shoulder having a dished recess. This tool has become known as the GSP 5651 tool. The 5651 tool was inclined away from the weld travel direction by approximately 3 degrees and the tool was rotated in a direction so as to cause the threads of the pin to augur the thermally softened material downwards towards the bottom of the workpiece or weld root, Figure 23.

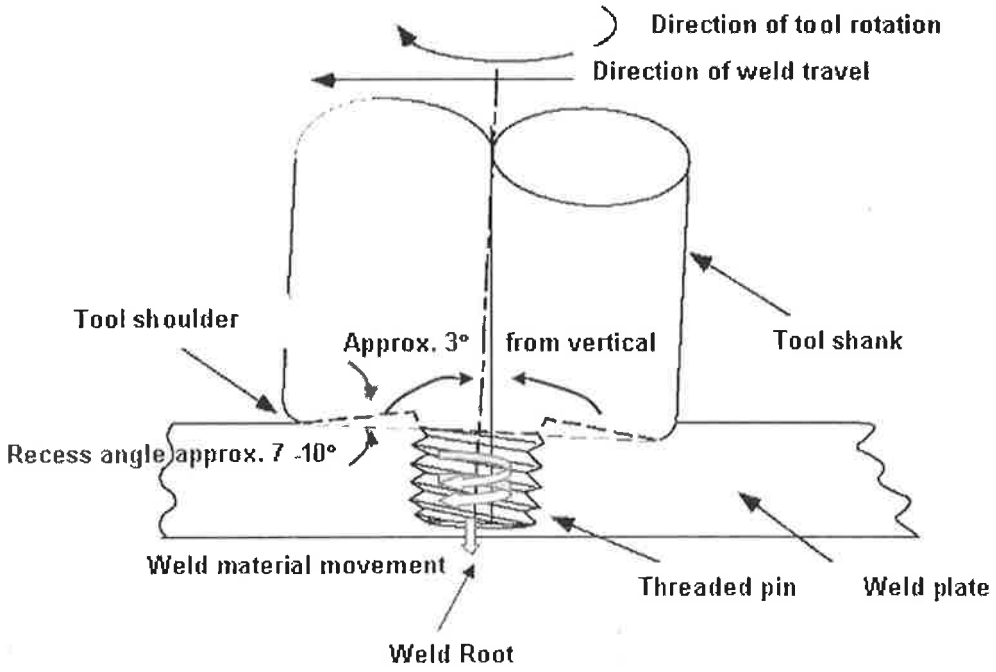

Figure 23 The concept of the GSP 5651 tool and material movement around the welding pin during FSW [67].

During the investigation undertaken by TWI [113] it was found that pins without threads produced welds containing flaws. These flaws appeared in the form of voids i.e. volumetric defects and cold laps (non bonded regions) between the workpieces.

Two tool materials were originally identified by TWI [113] as suitable for the FSW of aluminium alloys. These were AISI H13, 5% chromium hot worked steel and Nimonic alloy 115. Due to the relative cheapness of the 5% chromium hot worked steel, its ease of machining and the ability to heat treat the material, thus further strengthening it, meant that this material became the material of choice for the initial 5651 welding tool.

Further development of the GSP 5651 tool by TWI and its Group of Sponsors [112] demonstrated that wide variations in both tool rotational and weld travel speed were possible when it came to the FSW of most aluminium alloys. The reason for such a wide range of welding parameters may be attributed to the role forging plays in the FSW process. Forgeability of an aluminium alloy improves with increasing temperature. There is however considerable variation in the role temperature plays on the forgeability between the various aluminium alloys. Temperature has the greatest effect in reducing flow stress in the high silicon content 6xxx series alloys but has the least effect on the high strength Al-Zn-Mg-Cu 7xxx alloys. Figure 24 demonstrates the

effect temperature has on the flow stress of aluminium alloy 6061 for a strain rate of $10s^{-1}$.

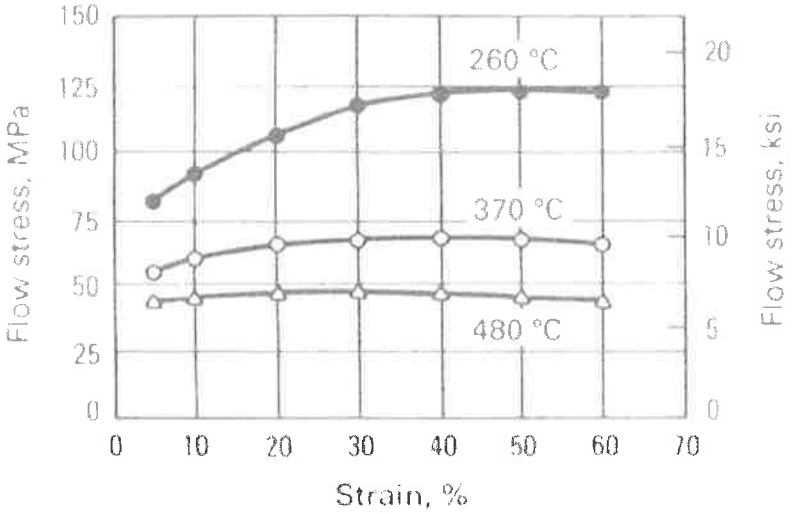

Figure 24 Flow stress vs. strain for aluminium alloy 6061 at three temperatures and for a strain rate of 10 s^{-1} [33].

Increasing temperature can be seen to reduce the flow stress for the 6061 alloy. For alloys that are more difficult to forge however, such as the 2xxx and 7xxx series alloys flow stress increases with temperature resulting in reduced material flow and a greater likelihood for hot tearing to occur during forging [33]. The forging temperature range for aluminium is therefore limited and forging temperature has to be controlled precisely since too high temperatures can destroy the grain structure, while too low temperatures can lead to cracks and die cavities not being completely filled by the forged material.

The generation of temperatures and selection of strain rates for a given forging operation such as occurs during FW and FSW has implications on both the type of equipment used, and in the case of FSW, on tool design. It should be recalled that deformation rates affect not only the forging pressure requirements, but also the severity of deformation, the temperatures being generated and the forces encountered as a consequence of material flow.

2.10 FSW And Tool Rubbing Velocity Relationships

The welding tool is rotated during FSW. This rotation, regardless of tool pin or shoulder form i.e. whether cylindrical or rectangular, will always trace out a circular path whose radius approximates the distance of the furthest extremity from the centre of the tool. The term tool rubbing velocity will now be introduced to identify that a linear

relationship exists between tool rotational speed and material weldability when FSW 5xxx and 7xxx aluminium alloys.

Rubbing velocity can be defined as the linear velocity measured at the periphery of a rotating tool when in contact with a workpiece. This rubbing velocity is responsible for the production of frictional heat that enables localised plastic deformation, confined to a small region at and slightly beyond the tool/workpiece interface.

TWI examined welding parameters (rotational and travel speed) for the FSW of 6.4mm thick aluminium alloys 6082, 5083, 2014, 2219 and 7075 using 5651 tool technology. These studies [112,113] indicated that it was necessary to make small dimensional changes to the welding tool when FSW these alloys; an early indication perhaps that a single FSW tool (size and shape) could not be used to produce defect free welds across all aluminium alloys. A systematic investigation based on matrix studies for tool rubbing velocity versus welding speed was conducted [112]. The major points to come out of this investigation were:

1. Too fine a thread form i.e. 0.75mm as opposed to 1.75mm thread pitch for the welding pin caused the threads to become easily clogged. It was claimed that this hindered the necessary working of the weld material and contributed to the formation of cold laps in the weld joint leading to tensile test failure in these regions.
2. Buttress or saw tooth thread forms e.g. a thread shaped similar to that on the blade of a saw offered no weld formation advantages over conventional thread forms and proved difficult to plunge into the weld material.
3. In order to decrease the load on a cylindrical pin during plunge the pin ends needed to be rounded. It was found that pins with a domed radius of approximately 0.75 that of the pin diameter worked best in decreasing resistance to tool plunge.
4. Tool shoulder size varied in relation to pin size for different aluminium alloys. Too small a shoulder diameter however, effectively expelled plasticised material from the weld zone. This combined with rapid cooling behind the pin led to the formation of weld cavities e.g. open running voids.
5. Examination of shoulder cone angles i.e. the angle of recess, Figure 23, indicated angles of 7° were better suited to large diameter tool shoulders while cone angles between 7 to 10° worked well with small diameter shoulders, particularly for use on thin sheet material.
6. Tool heel plunge depth when FSW relatively thin aluminium plate (under 10mm) was found to be the most sensitive FSW machine setting. The inability to maintain

intimate contact between the surface of the workpieces and the tool shoulder resulted in surface breaking voids.

7. Tool coatings such as chromium nitride and titanium nitride enabled higher tool travel speeds reducing tool clogging. These surface coatings were found to be able to increase or decrease friction forces and thus also influence (decrease) heat generation. This was validated in a study by Midling et. al. [114]
8. It was found that tool rotation speed (rev/sec) for both tool pin and tool shoulder could be associated through the following equation:

$$\text{Tool revs/sec} = \frac{Tool\ pin\ \ rubbing\ \ velocity\ \ for\ alloy\ (m/\sec)}{Pin\ \ circumference\ (m)} \qquad \text{Eq. 1}$$

   Note: Equation 1 refers to a rotational speed based on measurement of a peripheral velocity using pin circumference. This however is equally valid when using the tool shoulder circumference. The fact that two calculations can be made, one for pin and the other for shoulder indicates that there is a dependence between tool pin and shoulder diameters i.e. a ratio appropriate for use when FSW aluminium and its alloys.
9. A relationship for weld travel speed (mm/min) was also determined relative to tool rubbing velocity for the 6.4mm thick aluminium alloys. This was expressed in terms of a given pin thread profile i.e. weld travel speed, mm/min = 35% thread depth (mm) x tool rotation speed (rads/sec), where thread depth = 0.54 x thread pitch (mm).

From the nine major points to come out of the TWI study [112] it is interesting to note that clogging of the tool was seen as detrimental to the process of bonding, point 1. Clogging of the tool threads would imply a stick condition to have occurred between tool pin and workpiece material. It was found that clogging could be avoided as a result of coating the tool with chromium and or titanium nitride, point 7. It has subsequently been demonstrated that coatings have the ability to influence heat generation when applied to FSW tools [114].

It should not be lost on the reader that the objectives of the TWI study [112] were to determine fundamental process parameters and equipment requirements (both tool and machine). In addition the intention of such an investigation was to validate that these aluminium alloys could be welded, so that FSW gain acceptance as a viable alternative for use in the joining of these alloys. Weldability envelopes based on tool shoulder and pin peripheral velocities (tool rubbing speed) versus weld travel speed

could thus be determined. Weldability envelopes for the FSW of 6.4mm thick aluminium alloys 5083 and 7075 are reproduced in Figure 25 and Figure 26 respectively. No information from the study [112] however could be found regarding tool plunge rates, specific shoulder and pin depth into the weld material or dwell times prior to commencement of weld travel.

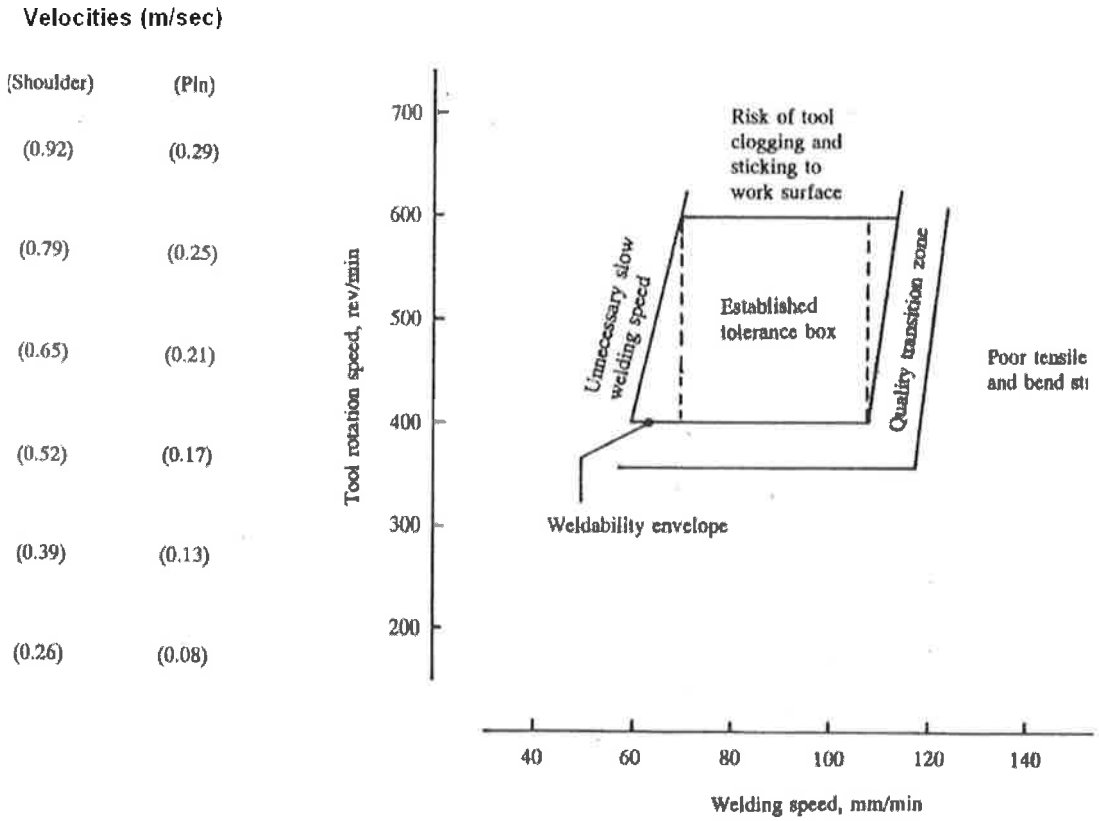

Figure 25 Tool rubbing velocities (shoulder and pin) vs. Welding speed when FSW 6.4mm thick alloy 5083-O and 5083-H321 [112].

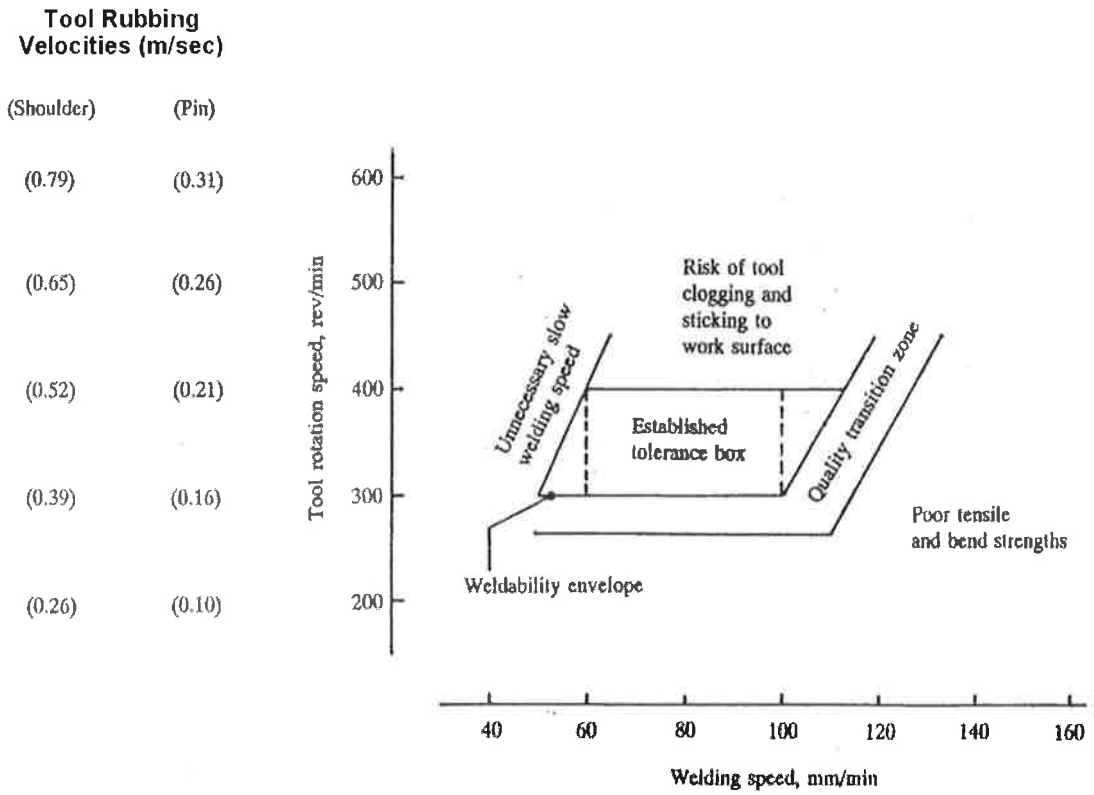

Figure 26 Tool rubbing velocities (shoulder and pin) vs. welding speed when FSW 6.4mm thick alloy 7075-T7351 [112].

Figures 25 and 26 reveal that the shoulder employed during the FSW of the 5083 alloy must have been larger than the one used to weld the 7075 alloy. This can be assumed because tool shoulder rubbing velocity is higher at 0.65m/sec for the 5083 alloy as compared to 0.52m/sec for the 7075 alloy for the identical pin rubbing velocity of 0.21m/sec. The question one has to ask here is why? It could be speculated that when equivalent tool shoulder and pin sizes were employed the temperatures generated in the 5083 alloy were lower than that of the 7075 alloy, hence the need for a higher tool shoulder rubbing velocity and the larger tool shoulder. This however is not revealed in the study [112]. It may equally be the case that the generated FSW temperatures in the 5083 alloy were higher than those produced in the 7075 alloy and as such a greater surface area was required to prevent the tool from ploughing into the workpiece during FSW. Information in the open literature is not readily available to either confirm or deny these assumptions, not only regarding temperature evolution but also the processing forces encountered during FSW.

2.11 Limitations Found To Exist For The Original FSW Tool Design

Although 5651-tool technology forms the basis of most friction stir welds produced in thin gauge (up to 10mm thick) aluminium alloys, limitations of this technology were also identified by the technology initiators [110]. A major drawback was seen to be that the tool had to be tilted away from the direction of travel i.e. at an angle typically between 1 and 3 degrees. This limited the ease with which the tool could be manipulated to make non-linear welds. In addition, the tilt angle at high welding speeds was found to cause the welding tool to partially lift out of the workpiece taking away necessary material from the upper reaches of the pin thread and thus contributing to the formation of surface breaking voids.

One technique found to overcome uplift of the FSW tool has been to couple a threaded pin with a profiled shoulder so as to allow for welding at zero degrees of tilt [111]. The designs of such shoulders and their profiles are many and varied [110,113]. The function of these tool shoulder profiles however, is to mechanically work and direct thermally softened material during rotation of the welding tool towards the welding pin.

Welding trials conducted by TWI [111] demonstrated that by employing a scroll profile on the tool shoulder the workpiece material could effectively be augured and forced to flow towards the tool pin. Previously, the tilted 5651 FSW tool employed the heel of the dished shoulder to compress and through rotation place a high hydrostatic pressure on the surface of the workpiece forcing thermally softened material towards the pin, Figure 23.

In comparison to a dished or concave shoulder the scroll shoulder profile allows for much smaller annuli of plasticised workpiece material to enter its profile. These annuli are said to reduce friction forces because the profile enables a reduction in the energy required to shear and move this workpiece material from the workpiece surface towards the pin, Figure 27.

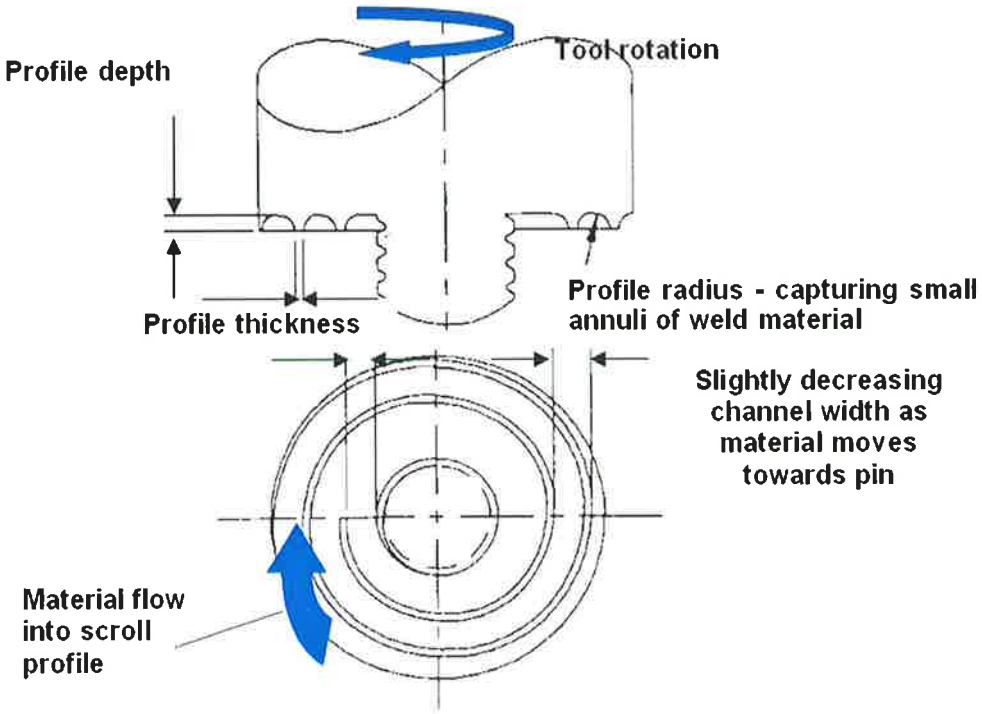

Figure 27 FSW tool with scroll shoulder and cylindrical threaded pin [111].

An improvement of the FSW processing brought about by the use of the scroll shoulder has been the ability to increase weld travel speed for the alloy 5083 as compared with welds made using the dished and tilted shoulder with identical welding pins [111,113].

2.12 Modifications To The Original FSW Tool Pin Design

Not only do tool shoulder profiles have an effect on weld parameters, TWI [115] demonstrated that the pin form also played a key role in weld formation. The first of such studies involved the FSW of 6.4mm thick aluminium alloy 6082. In summary, it was found for this alloy that paddle, whisk and threaded pins produced the best results.

Several tool geometries used in the TWI study [115] are reproduced in Figure 28. Results of the welding trials are summarised in Table 2-1.

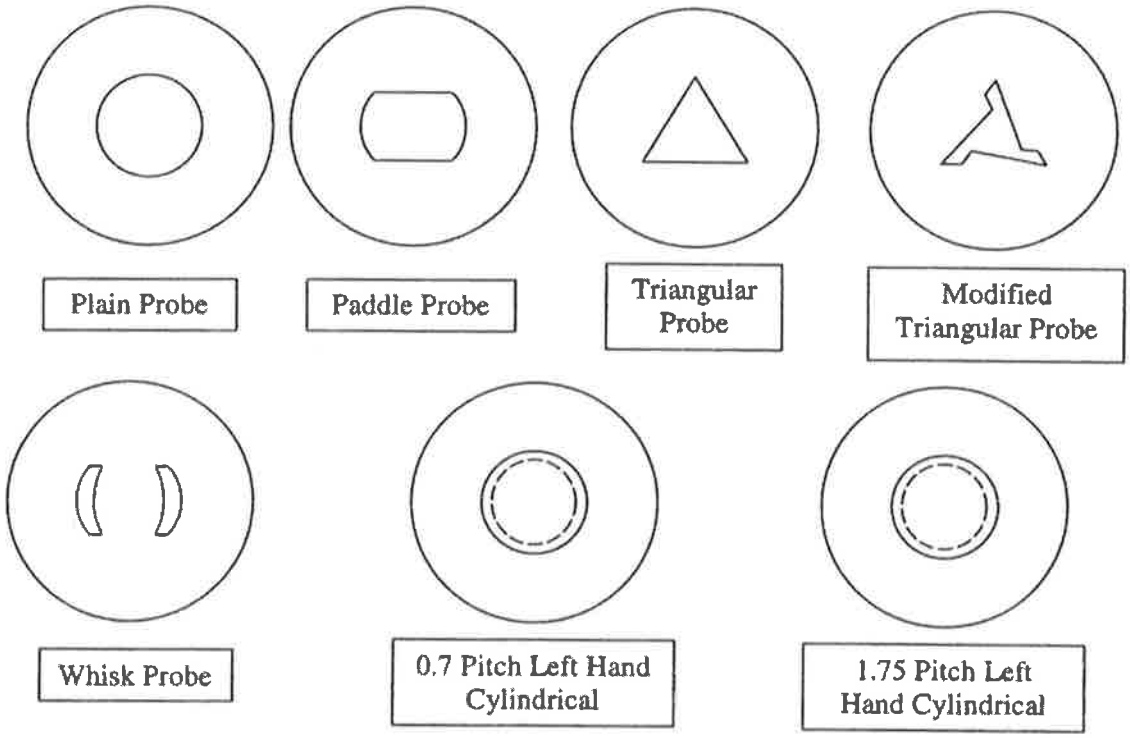

Figure 28 The various tool geometries trialed by TWI when FSW 6.4mm thick aluminium alloy 6082 [115].

Tool Geometry	2mm/sec Travel Speed		14mm/sec Travel Speed	
	No sideways tilt	1.5° sideways tilt	No sideways tilt	1.5° sideways tilt
Cylindrical pin-no thread	#	#	#	#
Paddle pin - 2 faces	4	4	#	4
Triangular pin	4	7	#	7
Whisk pin	4	4	#	7
Cylindrical pin-0.7mm pitch	#	#	#	#
Cylindrical pin-1.75mm pitch	4	4	#	#
Cylindrical pin + concentric ring shoulder	4	4	#	#
Cylindrical pin with reluctant scoops	#	#	#	#

Note: # = welds containing grooves, 7 = no welds made, 4 = welds with no grooves

Table 2-1 Summary of results when FSW with the various tool geometries as trialed in the TWI study [72]. Table 2.1 to be read in conjunction with Figure 28. Note the term groove is used in relation to a defect having been produced as a result of FSW.

The influence of pin geometry on weld formation and mechanical properties has been studied for several aluminium alloys ranging from 4 up to 9.5mm in material thickness [74,75,109,116,117]. Figure 29 shows the various tools used to friction stir weld 8mm thick 2014 aluminium alloy [116]. The details of the tools are reproduced in Table 2-2.

Figure 29 Photo of the various FSW tools examined [116]

Pin No.	Description of Pin	Pin Shank Diameter (mm)	Pin Tip Diameter (mm)	Thread Pitch (mm)
1	Column screw threaded pin	8	8	1
2	Taper screw threaded pin	8	6	1
3	Column pin no thread	8	8	none
4	Taper pin no thread	8	6	none

Table 2-2 Pin geometry of the four FSW tools [116] shown in Figure 29.

In all cases FSW of the 2014 alloy was conducted for a tool rotation speed of 400rpm and a constant weld travel speed of 100mm/min. This meant that the only difference in the experiment was in terms of pin geometry.

Figure 30 shows cross section photos of the friction stir welded joints in the 2014 alloy. Defect free welds were only achieved using pin numbers 1 and 2, captions a) and b) respectively of Figure 30. Defective weld c) was produced using pin 3 while defective weld d) was produced by pin 4.

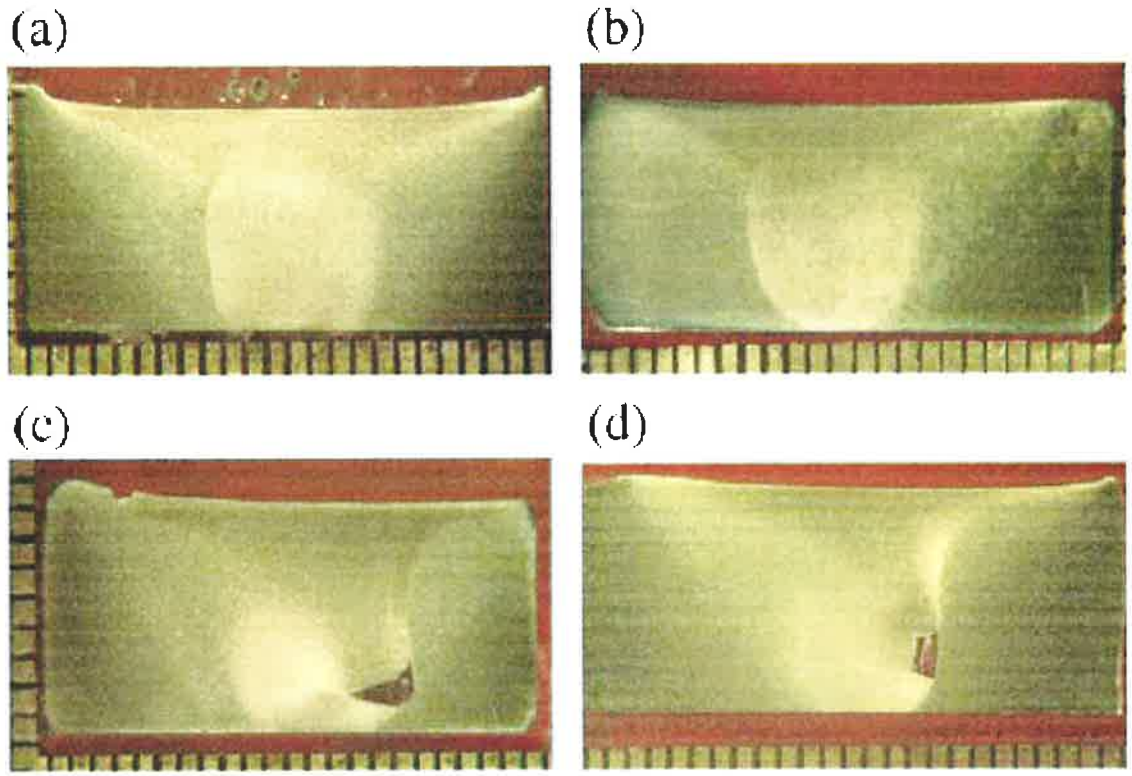

Figure 30 Macrographs transverse to the weld direction [116] of welds made using the tools shown in Figure 29.

The results of the study for the FSW of 8mm thick 2014 alloy [116] indicated that the shape of the pin had a significant effect on weld formation and on the mechanical properties of the joint. It was concluded that for the investigated FSW conditions void defects occurred as a result of FSW using a pin without a screw thread. When the tensile strengths of the welds were compared the taper screw thread (pin 2) proved to provide the best mechanical properties of all four welds.

Colligan [67] had previously demonstrated for the FSW of 6.4mm thick 6061 T6 aluminium alloy that the tool pin threads caused material entering the threads to move downwards during FSW. Figure 31 depicts the welding pin employed by Colligan [67] along side a transverse section taken from the weld around the exit hole at the end of the weld. In the leading edge of the exit hole can be seen a curling of material into the

threads of the welding tool pin. These curls of material can be seen to increase in size as they proceeded downward until the thread space becomes completely filled.

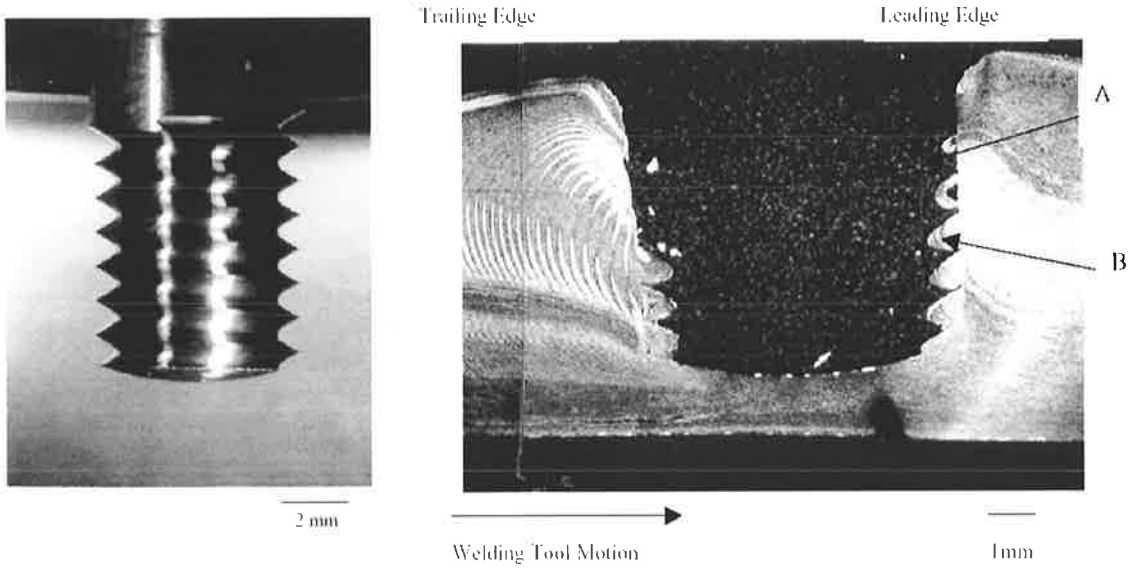

Figure 31 Left caption: Tungsten carbide welding tool pin. Right caption: Transverse section of keyhole [67].

From the appearance of the welds, Figures 30 and 31 it would not be unreasonable to conclude that given the aluminium alloys and welding conditions employed, defect free friction stir welds require a tool pin to posses a threaded profile. This is because welds produced using tool pins lacking the threaded profile are prone to develop a sub-surface void. This assumption is not unreasonable and has been demonstrated to be the case for friction stir welds produced in 4mm thick 2024 T351 alloy over a range of weld travel speeds (100 to 400mm/min) and for a constant rotation speed of 800rpm [117]. It should be noted that three pin forms were trialed in this study [117], whereby all pins were produced from a single pin form (Pin A, conical no thread) and were employed using identical tool shoulders. The pins and cross sections of each weld are reproduced in Figure 32.

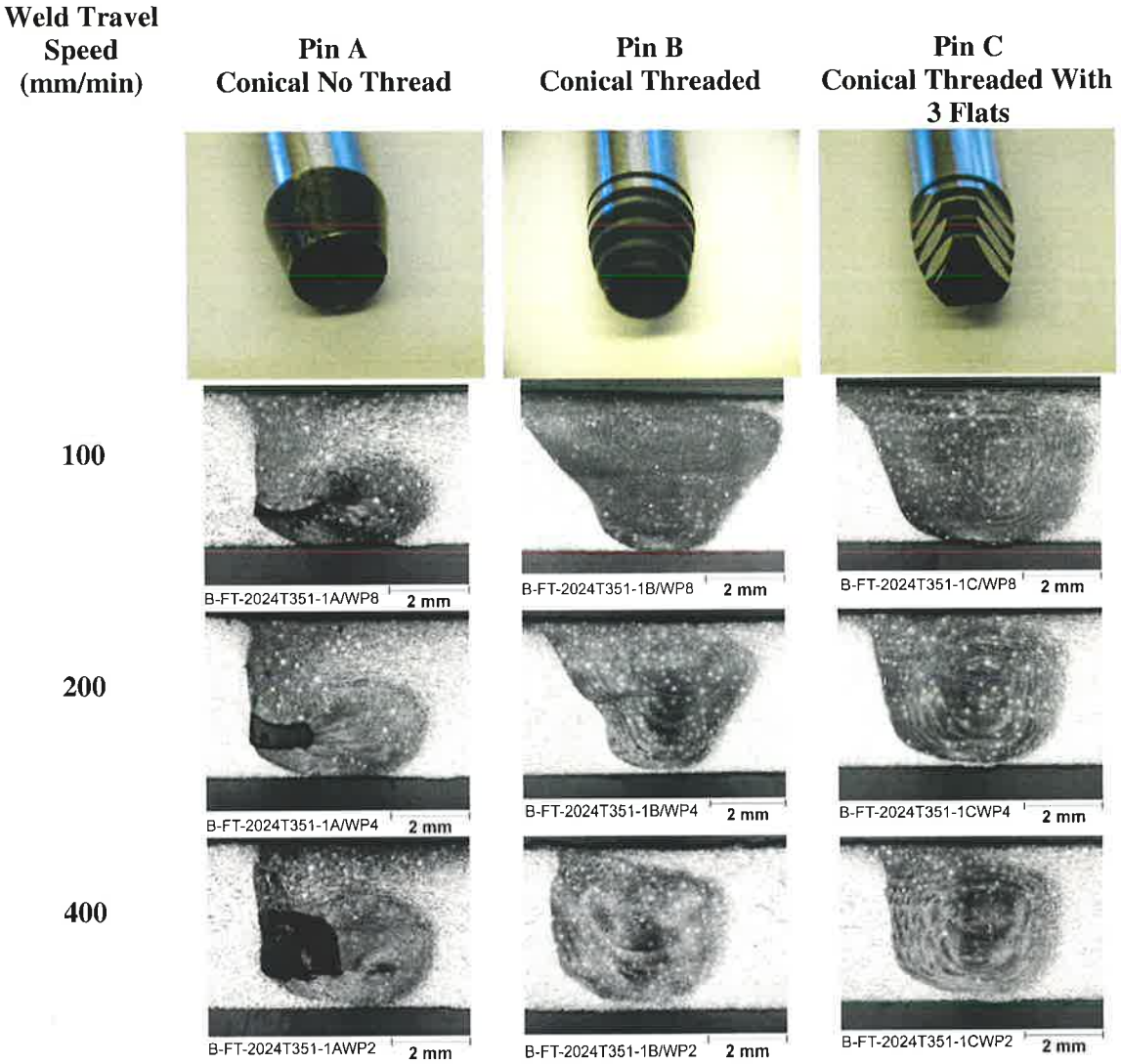

Figure 32 Weld macrographs produced using tool pins A, B and C [117].

The results from the study into the effects of tool geometry and process parameters on material flow and weld properties when FSW 4mm thick 2024 T351 aluminium alloy [117] indicated;

- The area of the stir zone decreased in size with increasing weld travel speed.
- Pin A, the conical non-threaded pin produced a tunnel defect under all process parameters investigated and this tunnel defect grew in response to increasing weld travel speed.
- Both pins B and C were capable of producing defect free welds over the investigated FSW conditions.
- Mechanical testing of the welds indicated that tensile strength and elongation was best for welds produced using pin C and the highest tensile strength and elongation was recorded for the weld travel speed of 400mm/min.

It should be noted that temperatures measured 1 to 3mm below the surface and either side of the workpieces indicated only marginal temperature variation over the welding parameters investigation and that these temperatures were almost identical for welds produced using tool pins B and C.

The fact that defect free friction stir welds could be produced using a conical and threaded pin form where a large portion of the thread is removed, as was the case for pin C, Figure 32 suggests that a minimum thread form and not a continuous thread form is critical for a FSW pin.

The effects of changing tool geometry and process parameters have not only been tested for various tool pin profiles but also for variations in tool pin and tool shoulder diameters [75]. Reynolds and Tang [75] indicated from the results of FSW 8.1mm thick 2195 T8 aluminium alloy that the shoulder diameter was the primary determinant of weld energy (joules) per millimetre of weld length. This was concluded from calculations of weld energy, which is simply weld power (Watts) divided by weld travel speed (mm/sec), where weld power is the spindle rotation rate in radians per second multiplied by the torque and any energy losses obtained (calculated) from the spindle motor.

Although a number of tool pin and shoulder diameters (8 to 12mm and 20 to 30mm respectively) were trialed during the Reynolds and Tang study [75] (it should be noted that all pins were cylindrical and threaded), very little difference could be observed in weld direction force between the various combinations of FSW tools over a constant set of weld travel speeds. For these reasons Reynolds and Tang concluded that all other things being equal, the shoulder diameter of the FSW tool was responsible for exerting the dominant influence on the required Z-axis (axial or down force) and the required spindle motor torque.

The conclusion arrived at by Reynolds and Tang [75] appear sound for the FSW tools and materials investigated. This is not to say however that these relationships are readily transferable to the FSW of aluminium alloys having a thickness greater than 10mm. In the case of much deeper penetrating friction stir welds where the thickness of the aluminium alloys was 25mm, TWI [110] found it necessary to change the shape of the tool pin in order to successfully weld these materials. The reasons given are two fold. Firstly, it was argued that AISI H13, 5% chromium hot worked tool steel did not possess adequate hot shear strength for welding up to 25mm of penetration when

employed using a cylindrical pin form and secondly, that simply changing tool material was not the answer considering the cylindrical pin form contributed to defect formation in these thicker alloys.

The justification for not trialing a new tool material is not immediately obvious. However, if one considers that TWI had invested heavily in researching welding parameter relationships i.e. for the 5651 tool concept based on findings using the AISI H13, 5% chromium hot worked steel for the FSW of 2xxx, 5xxx, 6xxx and 7xxx series aluminium alloys, a change to a new tool material may have rendered these weld parameter relationships between tool and workpiece material no longer valid, thus placing industrial uptake of the process potentially at risk. Work conducted by Midling et. al. [114] has since demonstrated that tool material (coating) can have a significant effect on heat input during FSW and as such will influence processing parameters.

Concerning the tool material i.e. 5% chromium hot worked tool steel not having adequate hot shear strength, a natural conclusion would have been to upsize the tool pin diameter. This however requires the pin to displace and redistribute a larger volume of plasticised material during FSW. It also effectively increases the frictional contact area between tool and the workpiece material. The greater the frictional contact area between welding tool and workpiece the greater will be the friction torque, thus one would expect increasing loads placed on the welding tool and on the machinery supporting and driving the tool (i.e. spindle and associated support structure). A larger welding tool would thus generate greater processing forces and would not have aided in weld consolidation, rather it would have contributed to defect formation.

TWI overcame the problems associated with having to increase tool penetration depth, not by changing tool material, but through the development of a new tool profile. This profile was subsequently trade marked the Whorl™ family of FSW tools [32,38,110, 118]. Essentially the pin takes the shape of a cone. The pin tip however, is not pointed. Rather, a minimum probe tip diameter is left on the end of the welding pin, Figure 33.

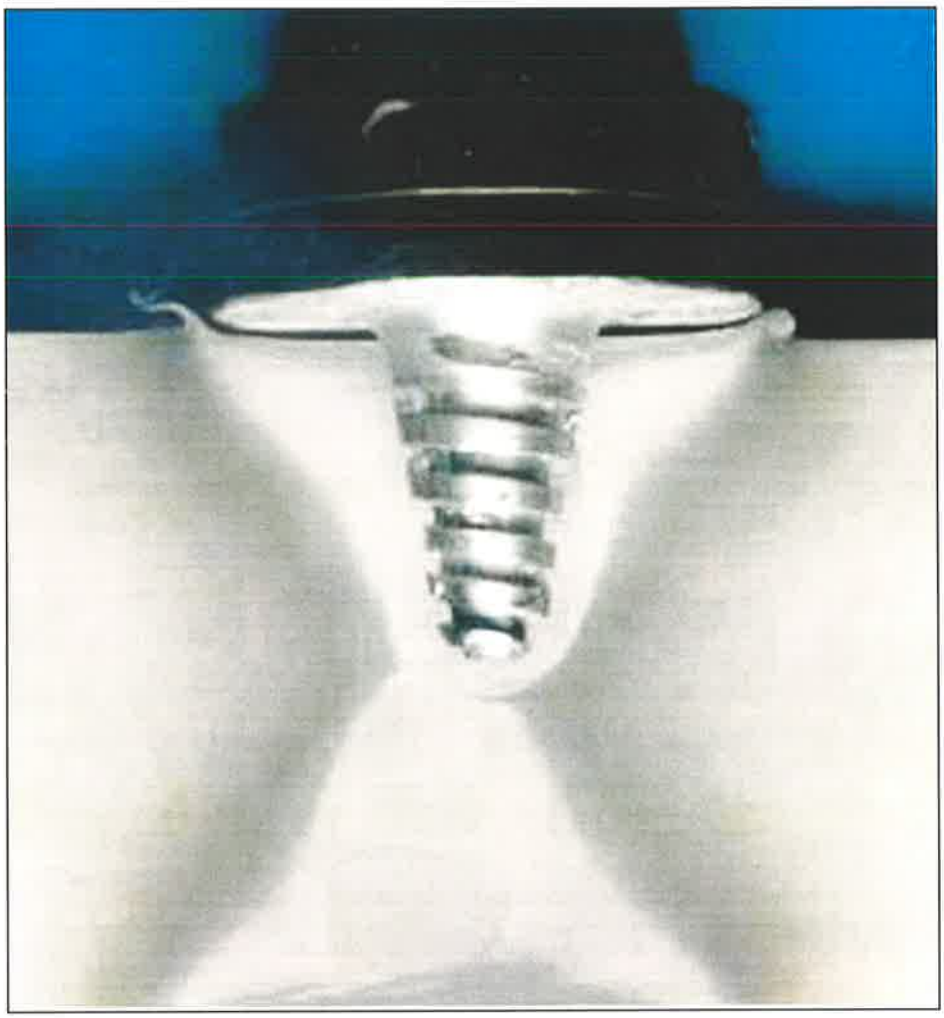

Figure 33 A photo of a Whorl pin developed by TWI and superimposed onto the a cross section of a friction stir weld produced using the same tool [110]

The Whorl pin designed by TWI conforms to principles similar to those used in the design of beams possessing uniform strength [119]. Beams of uniform strength employ a taper which reduces from the largest cross section to approximately one third of this cross section at the tip. This ensures uniformity of stress i.e. shear and torsion by redistributing the forces evenly over the entire unsupported length, which in the case of the welding pin is the threaded region. Like many FSW pins the Whorl pin has a helical profile i.e. threaded profile machined onto the region of the pin plunged into the workpiece material.

TWI tested various tool geometries and profiles for the FSW of 25mm thick aluminium alloys 6082-T6 and 7075-T73511 [32]. The results obtained provided further evidence that tool geometry could influence not only weld formation but also the weld travel speed. A comparison made between three basic but very different tool pin designs where shoulder profiles remained constant was conducted by TWI to verify which tool

form could produce sound butt welds in a single pass for the FSW of the 25mm thick 6082 and 7075 aluminium alloys. The results from this study [32] contributed to the further development of a new tool concept subsequently trade marked by TWI as the Triflute™ family of tools. When compared to a Whorl type tool, Figure 33 and a conventional 5651 technology tool, Figure 34, the MX Triflute tool as it was named, is, considerably removed from either tool, Figure 35.

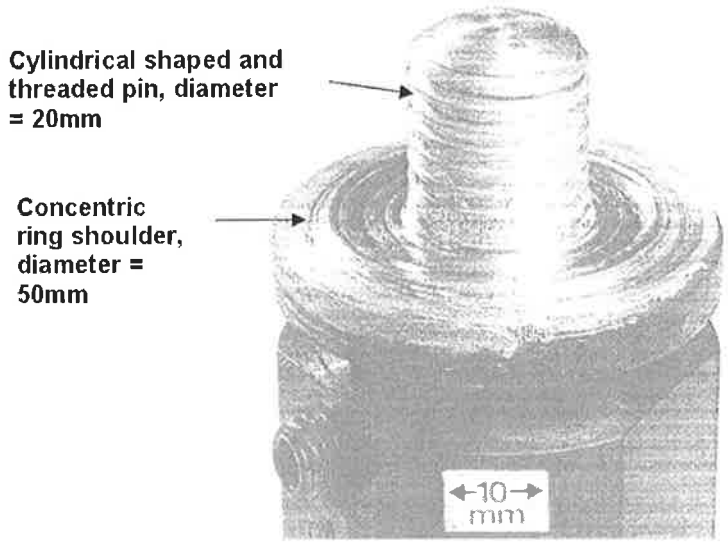

Figure 34 Conventional 5651 tool technology pin i.e. cylindrical and threaded as used in the TWI study [32].

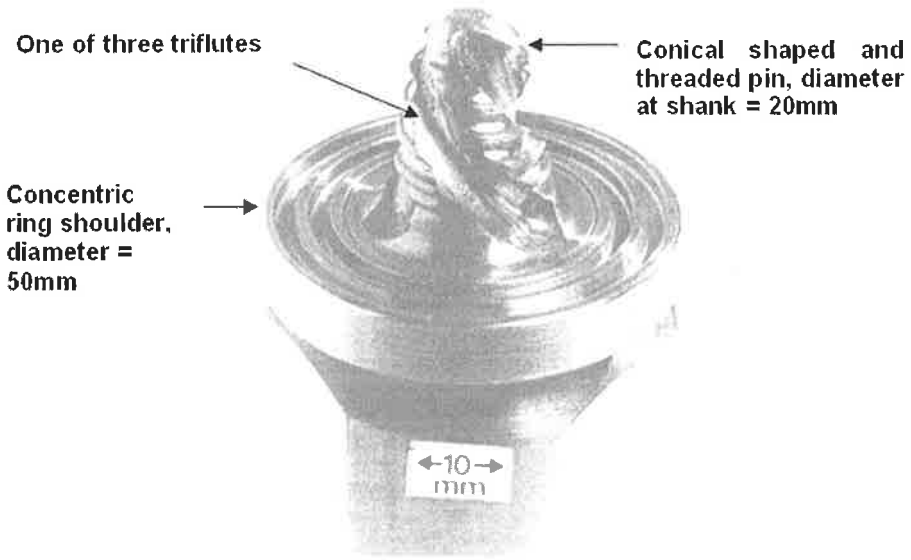

Figure 35 MX Triflute™ tool with conical shaped pin and triflutes [32].

The Triflute tool, Figure 35 in its basic shape can be likened to a Whorl tool, but contains within the body of the conical pin three large helical flutes. Each of these flutes are rotated over approximately 50% the circumference of the pin, i.e. from top to bottom of the pin length.

It is not known if welding temperature measurements were undertaken in the TWI study [32], but rotational speed, travel speed and axial force (this is the downward force transmitted through the welding pin) were recorded. These results are reproduced in Table 2-3.

Tool	Material	Rotational Speed (rpm)	Travel Speed (mm/sec)	Axial Force (kN)	Weld Quality
Convent. Pin	6082	470	0.5-1.5	54	Poor
Whorl	6082	470	2.5	58	Good
Triflute	6082	470	4	46	Good
Whorl	7075	193	0.8	56	Good
Triflute	7075	193	1	54	Good

Table 2-3 Welding conditions and weld quality results for single pass friction stir welds produced in 25mm thick aluminium alloys 6082-T6 and 7075-T7351 [32].

Table 2-3 indicates that for a uniform and constant rotational speed, as applied to each tool and workpiece, the possible travel speed was highest and axial force lowest when FSW with the MX Triflute tool. The lower axial force for the Triflute tool would seem to indicate that force in the weld travel direction must also have been reduced thus allowing for the higher weld travel speed to occur. Note the conventional tool pin was unable to produce sound welds in the 6082 alloy and for this reason there was no attempt made to friction stir weld the 7075 alloy using this tool. Additionally, Table 2-3 indicates that an axial force of approximately 55,000N or 5.5 tonne was necessary to weld the 25mm thick alloys indicating very high processing forces were involved in the production of these welds.

Since all tools employed in the TWI study [32] had the same pin length, pin shank diameter (20mm) and each was coupled to the same concentric ring shoulder (diameter 50mm), the conclusion drawn from the study is that the shape of the MX Triflute tool must have provided for the more efficient flow path for plasticised material transport. This may have been due to the shape of the tool pin as the volume that

each pin statically displaces when plunged in the workpiece material decreases the further one moves away from the cylindrical pin form. In fact TWI [27] confirmed that a Whorl tool's displacement volume lay between 30-61% less when compared to that displaced by the conventional cylindrical pin tool. This displacement volume was further reduced to 74% when comparing the Triflute™ tool with that of the conventional cylindrical pin tool.

An observation that one can make from the results presented in Table 2-3 is the choice of tool rotation speed which was employed for the joining of the 25mm thick aluminium alloys. If one compares the rotational speeds used for the FSW of the 6082 and 7075 alloys and converts rotational speed to rubbing velocity via Eq. 1, section 2.10 (proposed by TWI) then it becomes apparent that the peripheral tool velocity required to friction stir weld the 6082 alloy is more than double that for the 7075 alloy, Table 2-4.

Tool	Material Type	Rotational Speed (rpm)	Rubbing Velocity (m/sec)
Shoulder	6082	470	1.23
Pin	6082	470	0.49
Shoulder	7075	193	0.51
Pin	7075	193	0.2

Table 2-4 A comparison of tool rubbing velocities (shoulder and pin) when FSW 25mm thick aluminium alloys 6082-T6 and 7075-T7351.

Owing to a lack of further information concerning the welding trials conducted on the 6082 and 7075 alloys it is difficult to judge if the selected tool rotation and travel speeds, as presented in Table 2-4 are normal for the joining these alloys and for the level of material thickness being friction stir welded. If a comparison of these rubbing velocities is made against those contained in Figure 26, section 2.10 they suggest that for the 7075 alloy a tool rubbing velocity greater than 0.21m/s for the pin and 0.52m/sec for the tool shoulder should contribute to tool clogging and sticking. The weld quality however as indicated in Table 2-3 was considered to be good for the welds produced using the Triflute and Whorl tools in the 7075 alloy for these same rubbing velocities. This is a direct contradiction of the earlier observations made by TWI, Figure 26. Because of this it can only be concluded that the 7xxx series alloys possess very different FSW parameters when compared to those used for FSW the 6xxx series alloys.

No explanation as to weld travel speed selection is given in the TWI study [32] concerning the FSW of the 25mm thick aluminium alloys 7075 and 6082. An extensive literature search revealed TWI [120] had proposed a methodology for calculating weld travel speed for the 2xxx, 5xxx, 6xxx, 7xxx and 8xxx aluminium alloys, up to a thickness of 30mm. The methodology takes the form of a knowledge based software package and is presented as a final output in the form of Eq. 2 below

$$V_{FSW} = \varphi FSW.\psi FSW.t^{-1} \qquad \text{Eq. 2}$$

here V_{FSW} = welding speed (mm/min), φFSW = material factor, ψFSW = tool factor and t = sheet thickness (mm). V_{FSW} , φFSW and ψFSW data is reproduced in Table 2-4 while data for travel speed vs material and material thickness can be found in Figure 36.

The basis of the factors φFSW and ψFSW (empirical and or material), is not known by this author and was not discussed in the reference source [120]. Similarly, no qualification is made as to how tool factor is assessed i.e. the role pin and shoulder profile play in the production of friction stir welds. It can be observed however, that the values given for φFSW almost resemble rotation speed i.e. tool rpm values and appear realistic when one considers that the softer materials e.g. Lead and 6xxx series aluminium alloys can generally be processed with a tool rotational speed approximately double that of the 7xxx, as was seen to be the case, Table 2-5. Similarly ψFSW appears to resemble area, which would make sense given that V_{FSW} = welding speed (mm/min).

Material	φFSW	ψFSW
Lead	3700	1
Al 6xxx	1200	1
Al 5xxx	700	1
Al 7xxx	600	1
Al 8xxx	600	1
Al 2xxx	600	1
Magnesium	400	1
Copper	300	1
Titanium	100	1

Table 2-5 Data used for calculating FSW travel speed [107].

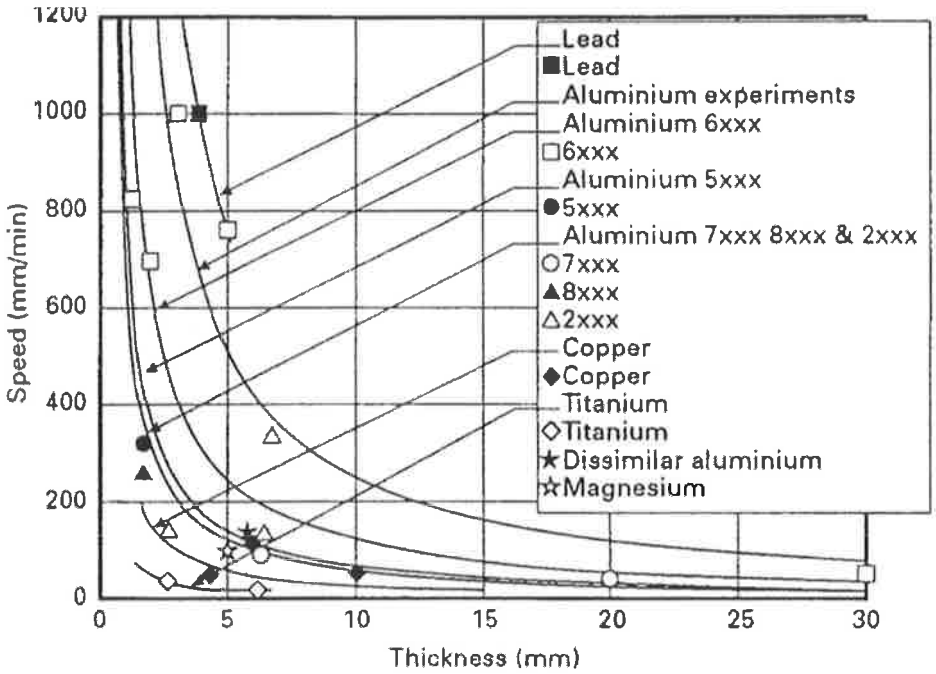

Figure 36 Proposed dependence of travel speed on alloy type and thickness [107].

To check the accuracy of the method for assessment of weld travel speed, Eq. 2 one can utilize the data given in Table 2-5. This would indicate that the weld travel speed for the 25mm thick 6082 friction stir welds should be approximately 0.8mm/sec. For alloy 7075 this becomes 0.4mm/sec. If these values are compared to the values presented in Table 2-3, for the FSW of 25mm thick 6082 and 7075 alloys it becomes clear that this methodology significantly underestimates weld travel speed when FSW using the Whorl and Triflute tools. If all other things are assumed to be equal it would appear reasonable to conclude that the value for tool factor may be somewhat different for both the Whorl and Triflute tools as compared to that indicated in Table 2-5. This however is simply not known.

It can be speculated that a measure of tool factor may lie in its ability to provide for power dissipation through deformation, or through coulomb friction with the workpiece material, both of which are linked to tool rotation speed. Certainly the size of the welding tool and the force placed on the tool during FSW is another critical factor that should be considered. This is because if the forces placed on the tool become too large the tool will break due to bending stresses. One must also consider what effect the FSW parameters have on the FSW machine i.e. is the machine rigid enough to accommodate the high (axial) processing forces and is the spindle motor powerful enough to handle the frictional torque generated during FSW.

It should be recalled that objective 1 of this thesis was to determine a range of FSW parameters capable of successfully joining 12.5mm thick 5083 H111 and 7075 T651 aluminium alloys. This literature review suggests that it should be possible to friction stir weld the 7075 alloy for a tool rubbing velocity of approximately 0.2m/s for the pin and 0.5m/sec for the tool shoulder. What is not clear however is can this rubbing velocity be used for welding the 5083 alloy and if so what effect does it have in terms of heat generation when applied to both alloys. A second question is what travel speed should be used. This can only be determined if one can estimate the welding forces that will be encountered, particularly the axial and reactionary forces i.e. in the direction of weld travel during FSW. These in turn are a function of the tool pin form and can only be determined through welding trials.

2.13 Forces Encountered When FSW

Several FSW studies [74,75,121-123] have reported on the forces that have been measured when FSW aluminium and its alloys. All of the studies highlight the importance of axial or down force during FSW. A schematic depicting these forces can be found in Figure 37.

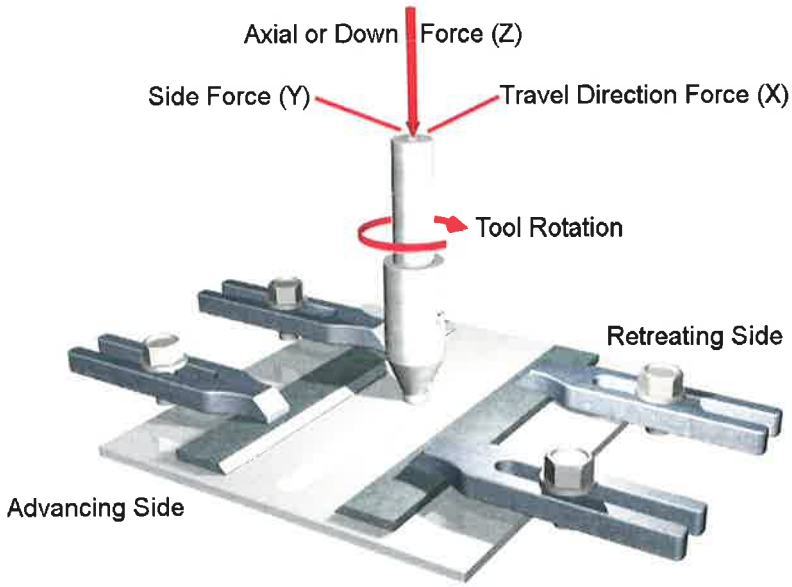

Notes: **X** = force measured in the direction of tool travel i.e. weld direction, **Y** = measurement of side force in the direction of tool rotation, **Z** = measurement of axial or downward force through the welding pin.

Figure 37 FSW force measurement nomenclature [124]

A preliminary force investigation conducted by TWI [121] measured forces for the FSW of 6.3mm thick aluminium alloys 6082-T6 and 5083-O. This study was followed by a much more comprehensive investigation for the FSW of 6082-T6, 2014-T6, 5083-H111 and 7075-T7351 aluminium alloys which ranged in plate thickness from 5.9 to 6.55mm [122]. The FSW tool used throughout this investigation was made of H13, 5% Chromium tool steel and based on 5651 tool technology i.e. a profiled and cylindrical pin coupled to a dished shoulder. Geometric features as to the thread type of the welding tool were not presented in this study. The basic tool dimensions were however given and are reproduced in Table 2-6.

Tool	Shoulder Diameter (mm)	Centre Pin Diameter (mm)	Centre Pin Length (mm)
K1	25	10	6.1
K2	25	8	5.8
K3	20	8	5.6
K4	20	9	6.15

Table 2-6 FSW tool geometries used in weld load study. Reference source [122]

Force measurements in the TWI study [122] were conducted using a Kistler 9123 dynamometer and 9257B force table. FSW force and torque measurements indicated that forces in the direction of welding and transverse to the direction of welding i.e. directions X and Y respectively, were almost identical; that is to say within 5-10% of each other for each of the respective aluminium alloys being friction stir welded. Forces were however considerably larger when FSW the 2014, 5083 and 7075 alloys as compared to that developed when FSW the 6082 alloy. In terms of torque measurements almost the opposite was observed. It could be seen that under identical rotation and travel speeds the torque generated as a result of FSW the 6082 alloy was some 10Nm larger at 55Nm where the torque for the other three alloys ranged between 41-46Nm.

The power delivered to a friction stir weld can be calculated as;

$$\text{Power} = \omega T \eta \qquad \text{Eq. 3}$$

Where Power is in watts, ω is the spindle rotation rate in radians/second, T is the torque as measured for the spindle (Nm) and η is the spindle motor efficiency.

Reynolds and Tang [75] demonstrated that weld power not only varied between alloys but also increased with increasing weld travel speed. Here however shoulder size seemed to be the primary determinant of the power requirement for a given set of welding parameters i.e. rpm and weld travel speed when FSW aluminium alloys with a plate thickness less than 10mm.

Colligan [74] presented results performed to study the influence pin design had in relation to the weld power, specific weld energy, torque, weld forces and weld zone macrostructure when FSW 25.4mm thick aluminium alloy 5083-H131. Here the specific weld energy is simply the Power (watts) given by Eq. 3, divided by the welding speed in mm/second, such as to give the weld energy in (joules) per millimetre.

Colligan's results indicated that specific weld energy decreased with increasing weld travel speed, suggesting lower welding temperatures. This was in agreement with the results from Reynolds and Tang [75]. However, it was also observed that by adding flats or similar features to the pin design this greatly reduced the transverse force on the welding tool and could be considered an enabling feature for making thick section welds in aluminium. Colligan's results also suggested that travel per flat per revolution was an important parameter in determining the transverse in plane force and spindle torque, based on the role the flats played in material flow. It was argued that the travel speed played a role in determining the spindle torque, possibly through its effect on weld temperature and hence the workpiece flow stress. It is not known from the results presented in this study whether this observation has been experimentally validated.

A methodology which could aid in better understanding how load, torque and temperature affect the FSW process and subsequent weld form (i.e. flaws) is through the development of a force and process temperature data acquisition system. Lienert et al [123] presented preliminary results on such a device where data was collected and recorded for friction stir welds made in 6.4mm thick 7075-T6, 5083-O, 6082-T6 and 6061-T6 aluminium alloys. The conclusions drawn from this investigation suggested that in process measurement acquired from a rotating FSW tool was possible and that processing load as well as torque data was very sensitive to flaws produced during FSW making this a very useful tool for future weld quality monitoring or process control in real time.

2.14 FSW: Process Modelling With Reference To Flow Visualisation

Modelling research into FSW has been undertaken to provide information regarding the mechanisms of heating and bonding i.e. microstructural change such as hardness and deformation, which includes the visualisation of material flow taking place during joining. A process model for FSW is seen as critical if reliable estimates of process characteristics such as tool geometry, material properties and the effects of process parameters are to be quantified.

An extensive amount of literature has been published over the years in the field of FSW. Much of the work however has focussed on mechanical characterisation of the welds. This literature review has chosen to focus on material flow behaviour in order to better understand the mechanisms of joint formation.

Material flow resulting from the FSW process has often been studied through the tracking of a tracer material which has been embedded into the aluminium alloy under investigation [58-61,66,67]. The first of such research to openly document a procedure using steel shot as the marker or tracer representative of material flow in and around the region of the stir zone, was performed by Colligan [67]. Results of marker displacement from this method of visualisation could be divided into two categories;

1. the first allowing for the identification of regions where a continuous line of markers was seen to be reoriented and deposited roughly again as a continuous line behind the welding pin, and
2. the second category defined the region where chaotic deposition of marker material had occurred.

Radiographs representative of the reoriented steel shot indicated for most portions of the welds a lifting of the marker to points near the tool shoulder, Figure 38.

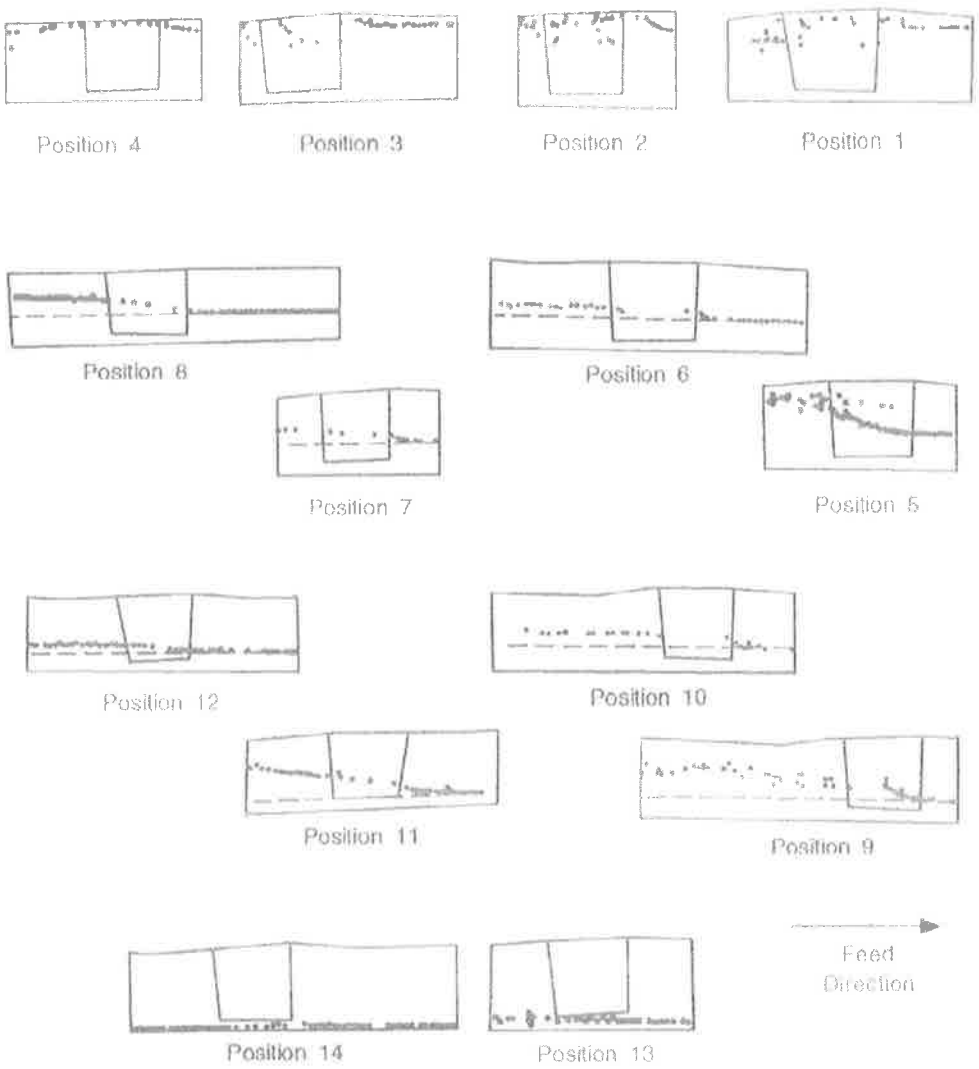

Figure 38 Side view schematic of marker displacement when FSW the alloy [67].

Vertical motion of the marker (steel shot) was however regarded in the Colligan study [67] as being relatively small, primarily because it was observed that the markers stayed roughly at the same depth with regard their original implant plane. The conclusion drawn from the visualisation study was that the FSW process appeared to be a mixture of stirring (chaotic mixing) and extrusion.

The validity of representing bulk material movement through the use of markers such as the steel shot, whose size was larger than the thread forms employed by the welding tool pin and whose material properties were so different from the surrounding alloy has however drawn some criticism. This is because it can be considered unlikely that the steel shot ever flowed into the thread spaces of the tool in the same way as did the plasticised material. As a consequence any vertical flow of the steel shot would at

best have been limited. It has also been observed that the location of steel shot on the advancing side of the weld joint may have affected the movement of this shot due to the geometry and interrelationship between each shot within the joint. Again it has been argued that the shot never entered the threads of the welding pin and therefore because of limited contact between the welding tool and the shot these steel balls could never have actually traveled along the same trajectory as the plasticized material. A further criticism that has been made of the steel shot marker technique has been the suggestion that such large markers (inclusions) can act as large singularities affecting flow path. It has been demonstrated that singularities can dramatically alter particle path dependant upon their release point in the flow [66].

For a marker material to represent bulk material flow during FSW two basic conditions must be met. In the first instance a marker material must be clearly visible within the aluminium alloy after welding, and secondly, the marker material must not disrupt flow of the deforming material i.e. the marker must deform with the workpiece material in such a way that it is itself representative of the bulk flow of the deforming material. As a consequence the representation of material flow resulting from the FSW process has also been attempted through the joining of dissimilar aluminium alloys. The introduction of copper rich aluminium 5454 alloy into a 2195 aluminium lithium alloy [61], such as depicted schematically in Figure 39 is one such example.

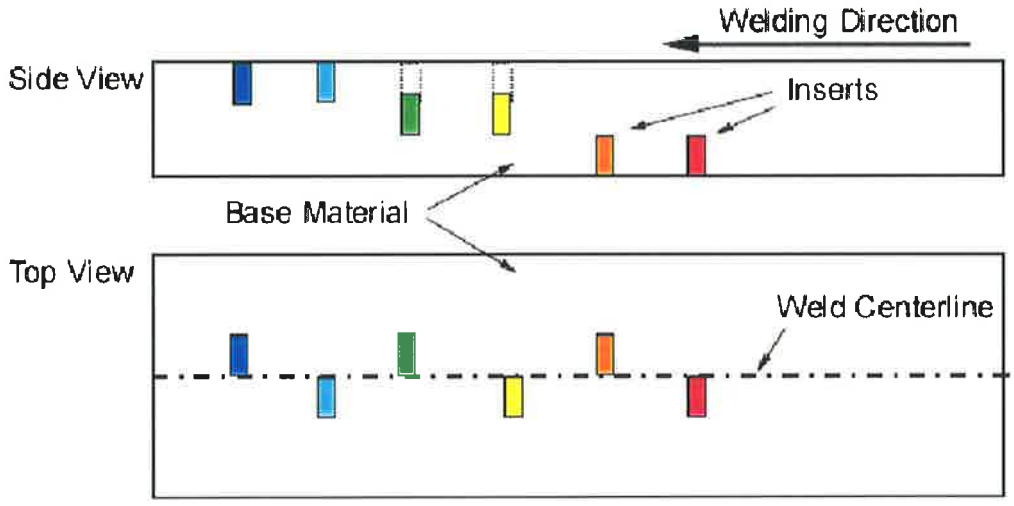

Figure 39 Location of the copper rich 5454 alloy as placed into a 2195 lithium alloy [61].

Marker placed near but outside the periphery of the pin on the advancing side of the weld was observed to be displaced forward while marker on the retreating side was only ever displaced backward, Figure 40.

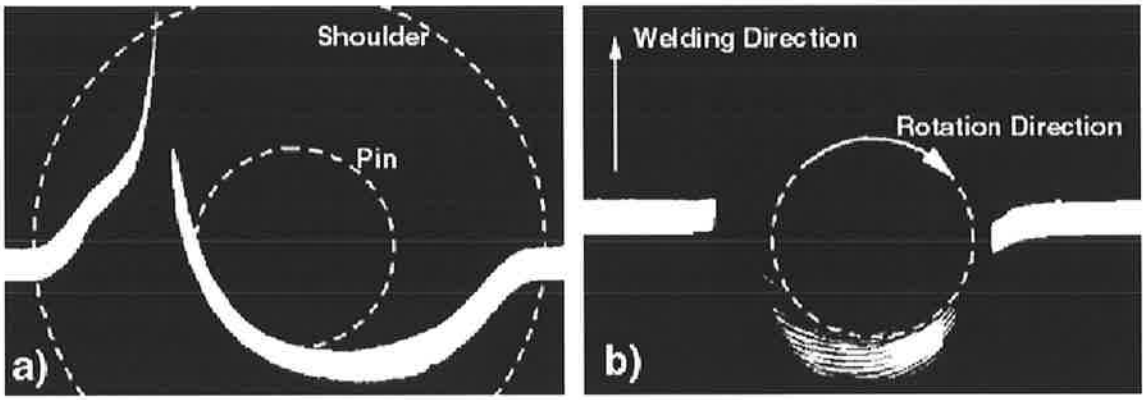

Figure 40 Marker flow as induced by the tool shoulder [61]

Flow paths of the copper rich 5454 alloy marker were digitized and combined to produce 3D material flow maps. These maps again seemed to indicate only modest vertical flow, Figure 41. From the results of the dissimilar aluminium alloy (5454 and 2195 alloy) friction stir welds it was interpreted that the role of the rotating pin was only to provide sufficient frictional heat to make possible extrusion of the thermally softened material.

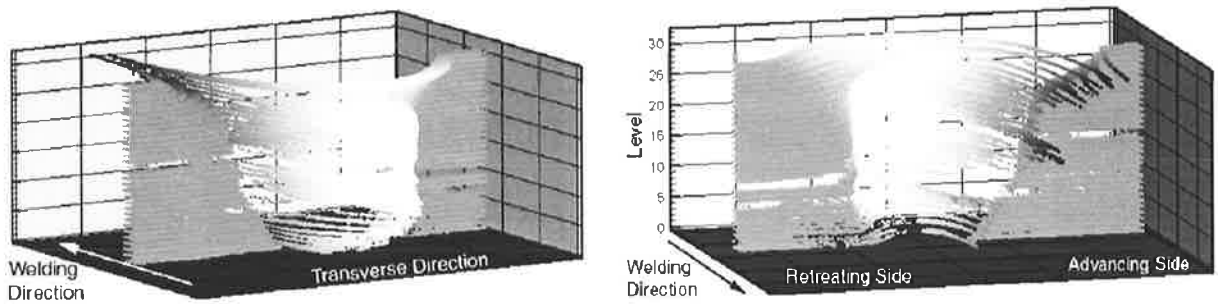

Figure 41 Digitized images of the copper rich 5454 alloy marker flow occurring between both sides of the join line [61].

A criticism of the use of dissimilar alloys to represent material flow occurring for a single alloy system is that in all instances dissimilar alloy friction stir welds demonstrate much more complex swirl like structures in the weld nugget zone as compared to their single alloy counterparts [60,63,64,125,127,128]. Through the use of this technique however different regions within the nugget zone have been identified [63]. The degree of material mixing, the thickness of the deformed aluminium alloy lamellae i.e. banded or onion ring structure and the material flow patterns have all demonstrated to be dependant on their relative positions in the weld nugget, but also on the processing parameters employed during welding [61,63,64]. Distinct differences however, have been observed to occur for plastic deformation, material flow, and mechanical mixing at

both sides of the same and then for dissimilar alloy welds. In fact the microstructure in dissimilar friction stir welds have been shown in some instances to be significantly different from that obtained in welds made from a single alloy, again while using the same tool and welding parameters [63,64]. Not only has it been observed that dissimilar alloy systems with high hardness difference have more pronounced and more complex flow patterns to those produced from a single alloy, but that the location of each alloy in the dissimilar weld, whether placed on the retreating or advancing side of the join line adds to differences in the weld nugget structure [125,127,128], as can be seen in Figures 42-43.

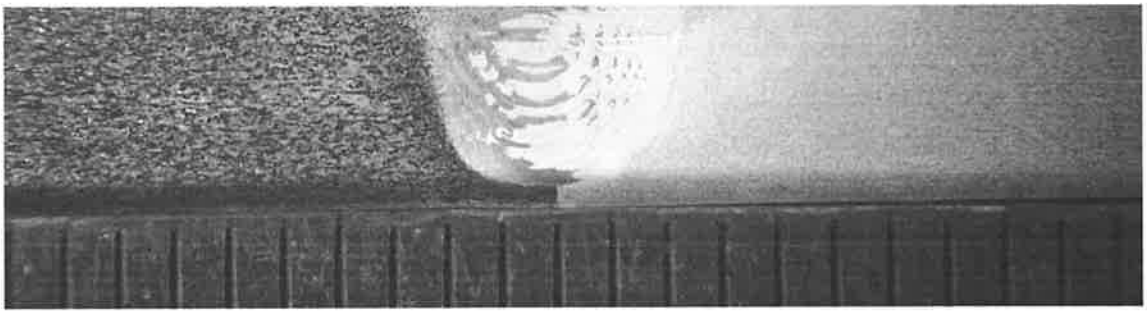

Figure 42 Dissimilar alloy friction stir weld where the 6056-T4 (dark alloy) has been placed on the advancing side and the 7075-T651 (light alloy) on the retreating side [128]

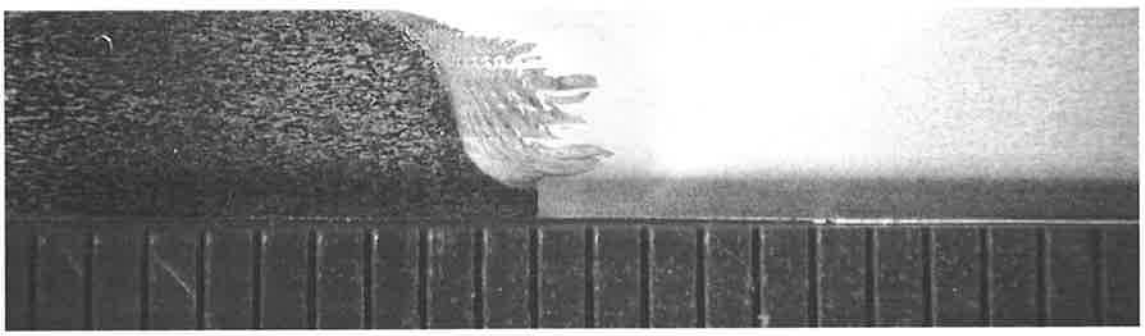

Figure 43 Dissimilar alloy friction stir weld where the 6056-T4 (dark alloy) has been placed on the retreating side and the 7075-T651 (light alloy) on the advancing side [128]

One pioneering methodology [59] that has shed considerably more light on the mechanisms of material flow in the FSW process has been achieved through the use of discrete and continuous markers placed in the workpiece material. Planar markers were inserted into 6.35mm thick 7050-T7451 aluminium alloy plates parallel to the weld join line and across the width of the tool shoulder from advancing to the retreating side of the weld, Figure 44.

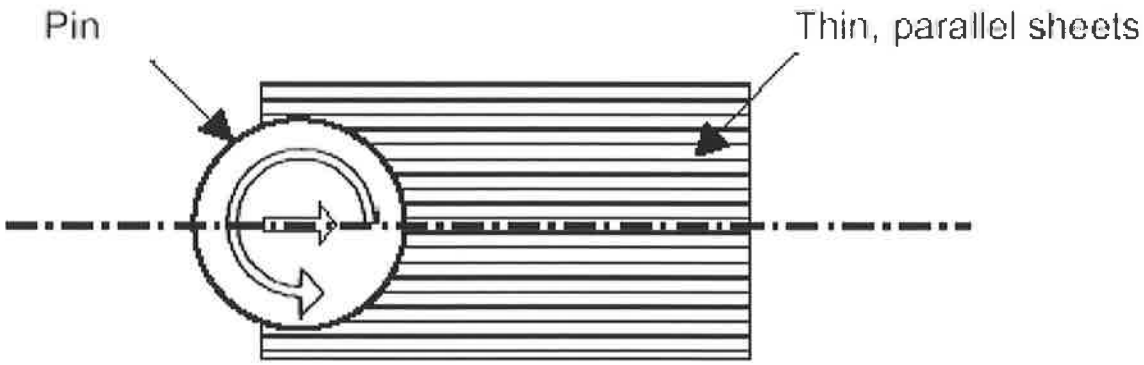

Figure 44 Schematic of planar markers placed parallel to the weld join line [59]

Welding into the line of markers revealed the extent and direction of bending that the marker material experienced ahead of the welding tool, Figure 45.

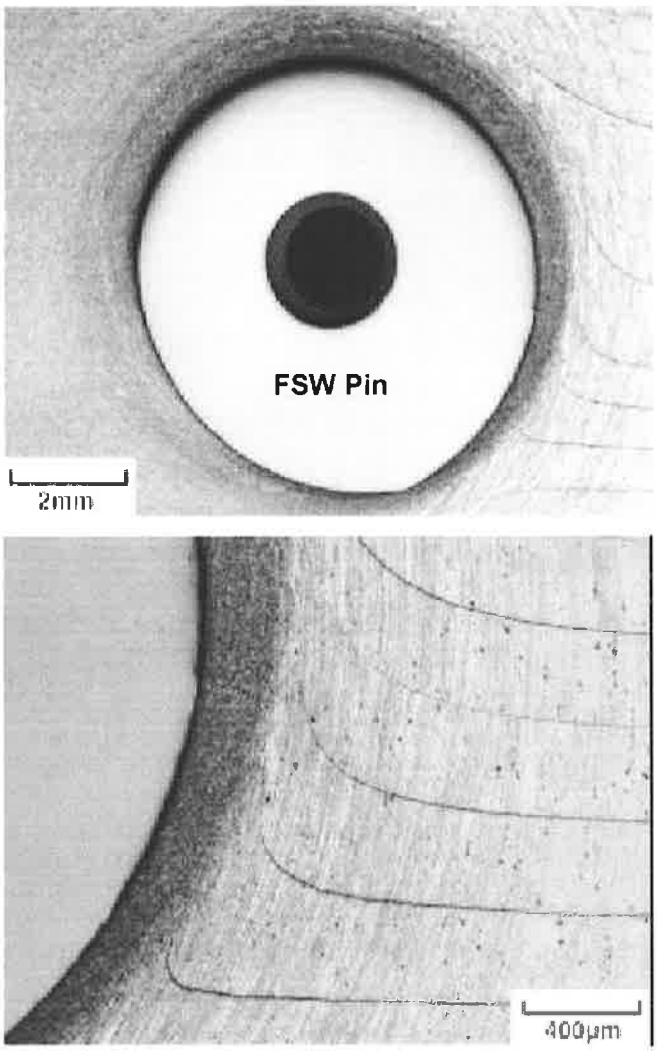

Figure 45 Bending of the markers in the direction of tool rotation ahead of the tool pin [59]

Discrete composite markers in the form of very small discs were also placed in the direct path of the welding tool to establish the thickness and flow direction of the deformation zone ahead of the welding tool, Figure 46.

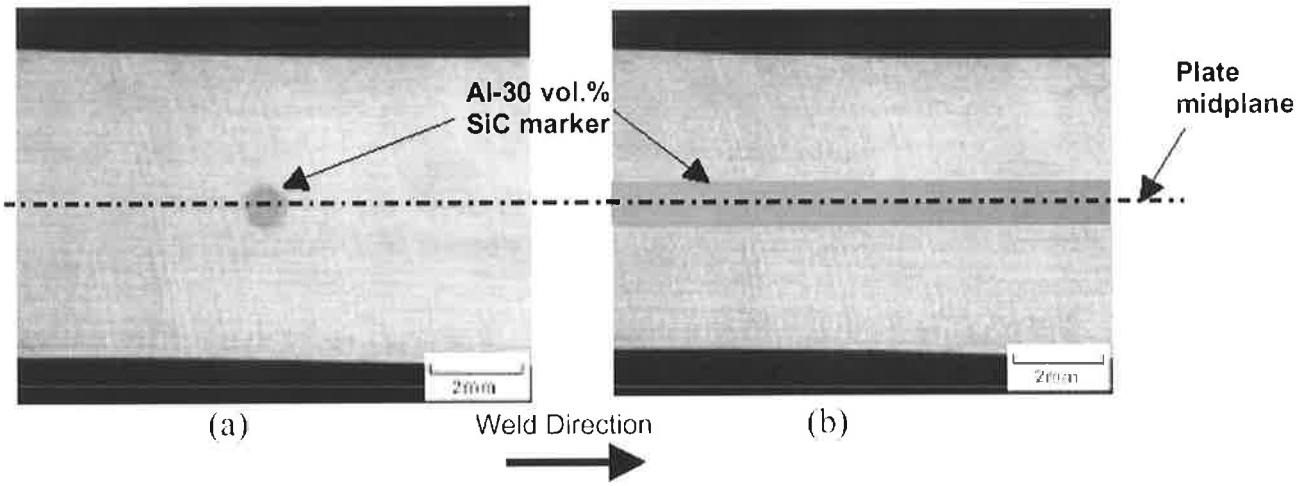

Figure 46 Discrete and continuous marker placed in the deformation zone as seen from the surface of the workpieces [59].

Continuous material markers were placed at two different levels within the thickness of the workpiece to indicate vertical movement of material. In all cases a stop action technique was employed during welding. Here the welding tool came to an instantaneous stop thus allowing for better visualisation of deformed and not deformed marker material from front to back of the embedded welding tool pin, Figure 47.

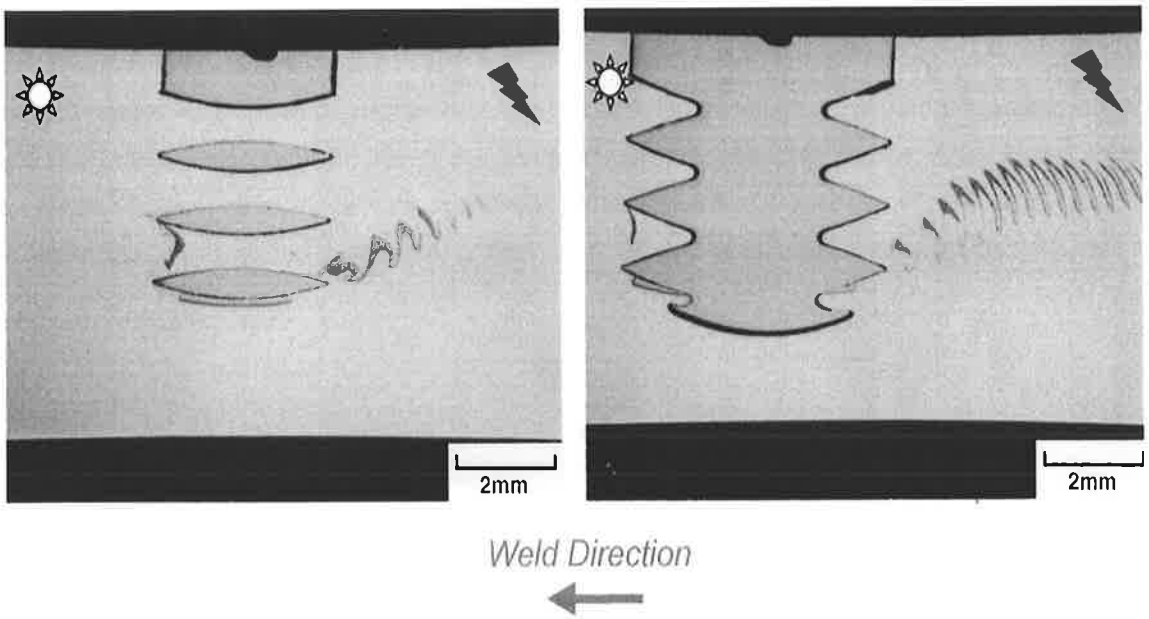

Figure 47 Side view depicting marker flow in the vicinity of the welding pin as seen from the outer extremity of the welding pin (left hand caption) and in the weld join line (right hand caption) [59].

Through the use of the stop action technique where the pin was instantly halted in the workpiece it was possible to identify that;

- material flowed from advancing to retreating side i.e. in the direction of tool rotation across the weld centre line during FSW, and that
- there could be significant material flow toward the top surface of the plate during welding,
- some material rotated more than once around the tool before being deposited in the wake of the weld,
- as the weld progressed, marker material was dropped off behind the pin in streaks – it was thought that the spacing of these streaks may have been an attribute of the geometry of the pin threads and the specific weld parameters employed, but that
- this technique of visualising material flow required significant sample preparation time in that metallographic sectioning was performed through the weld thickness at very small intervals (0.25-0.5mm). In some instances it was also found to be very difficult to discern the marker material from the workpiece material.

In comparing the benefits of using the continuous and discrete markers it was suggested that the continuous markers gave more details of the deformation process than the discrete markers. The discrete marker materials were however better able to indicate the significant uplift of material to the top of the plate as a result of the FSW process. Marker after being moved to the top surface of the workpiece was observed to be sheared as it was translated around the periphery of the pin. Planar markers placed parallel to the butt joint interface across the width of the tool shoulder from advancing to retreating side indicated that as the marker got closer to the pin the material was sheared along a very thin band region near the outer diameter of the pin i.e. the majority of material deformation occurred in a small region constrained by the outer surface of the pin and the non-deforming aluminium alloy approximately 1mm away from the pin itself. As the welding tool traversed along the join this marker material was observed to be dropped off behind the pin in streaks. It was suggested in the investigation [59] that the spacing of these streaks may have corresponded to the geometry of the threads and the specific weld parameters used to create the welds. Band spacing within the weld nugget i.e. the spacing of the onion like rings appearing on the surface of workpieces have also been correlated with welding tool advance during FSW [127,129,130]. This has also been observed in the re-orientation of grain

structures formed within the weld nugget where high temperatures and strain rates are said to reflect characteristics typical of different stages of recrystallisation [83,94,99,131].

Flow visualisation studies all indicate that the flow field around the FSW tool is extremely complicated. Most of the studies performed using material markers however also indicate that there is a significant amount of order in the marker patterns. FSW flow trajectories appear to follow defined paths or streamlines. A FSW model [132] claiming to represent the essential macroscopic features of the flow field occurring around a FSW tool has been synthesized for three incompressible flow fields. The flow field components are depicted in Figure 48.

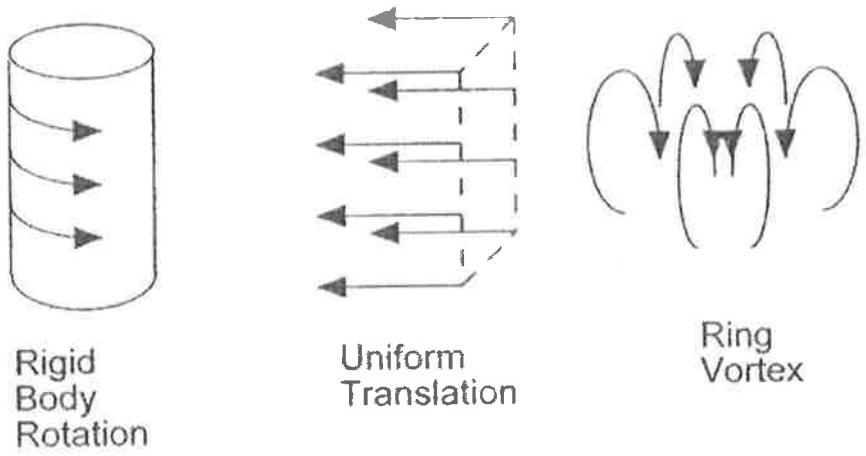

Figure 48 Hypothetical flow fields envisaged to occur during FSW [128]

The hypothetical flow fields as represented in Figure 48 can explain the general macroscopic features of material flow as a result of the FSW process but give no indication as to what effect any variation in tool geometry may have in influencing this flow field. Very few publications [133-135] have attempted to deal with the role tool geometry, particularly that of the welding pin on material flow. Most of the published flow models have assumed that material remains in intimate contact with the tool surface during processing. A critical factor in any attempt to model material flow during FSW is therefore whether one assumes that a stick or a slip condition arises between the tool and workpiece. A stick condition is here defined when workpiece material bonds directly to the FSW tool during welding. Material deformation in this instance will occur a small distance removed from the tool.

The use of the stop action technique where the tool remains embedded within the workpiece has perhaps allowed for the most accurate examination of deformation

zones occurring for all regions of the weld joint. In one such study copper (Cu) foil was placed in the join line just below the surface of a friction stir butt weld made in a 6061 alloy [60]. A plan view at mid thickness of the weld was clearly able to indicate that the weld nugget comprised of several distinctly different zones. These were interpreted as; a rotational zone, a transitional zone and a zone having entrained recrystallised grains not coming from the rotational zone, Figure 49.

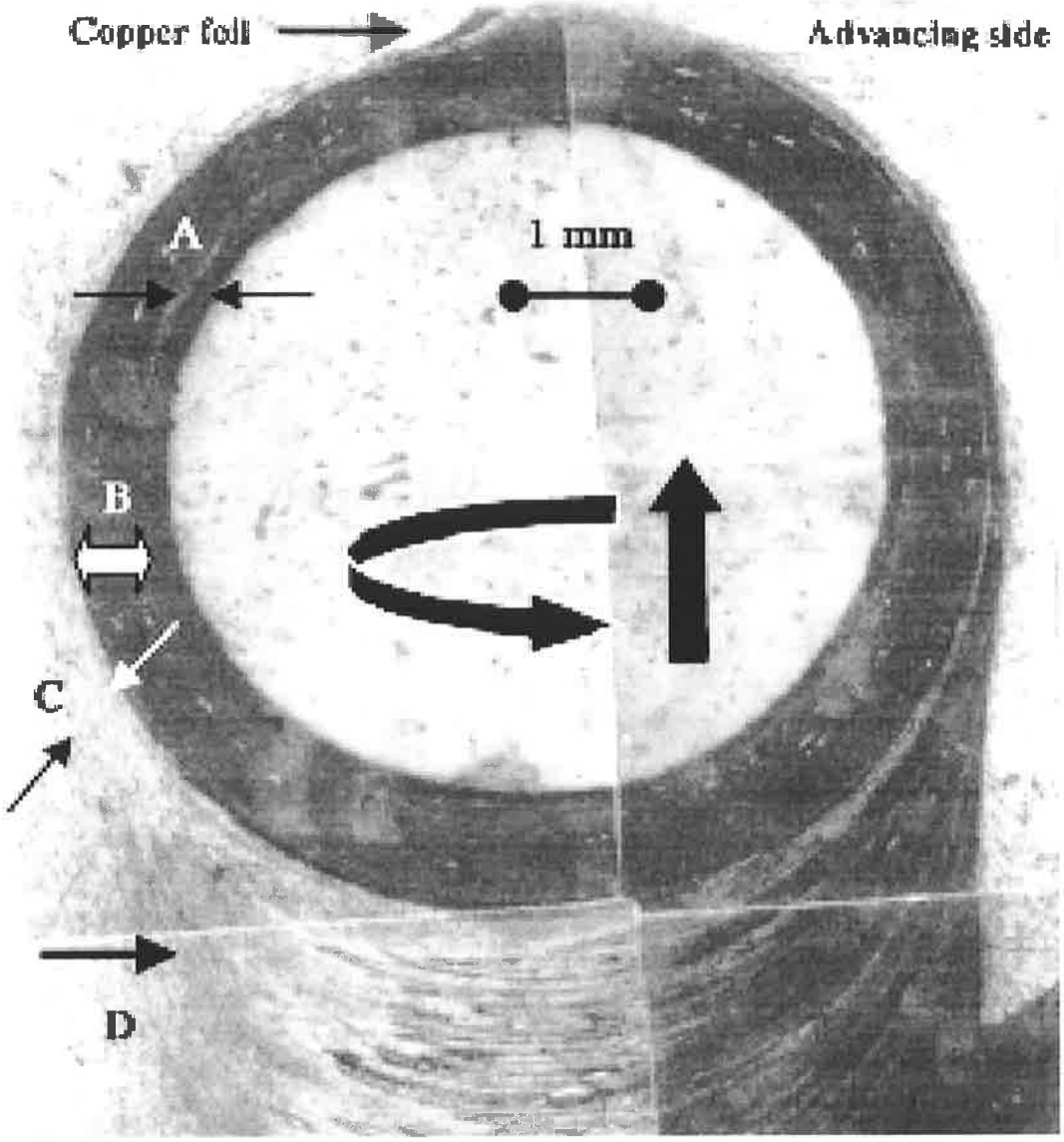

Figure 49 Plan view mid thickness of the workpiece showing the frozen FSW tool surrounded by A; the rotational zone, B; the transitional zone, C; transition zone of material trapped by rotating pin and D; recrystalised and entrained grains [60]

From observation of the deformation occurring for the Cu foil it could be seen that the foil curled in the direction of rotation and sheared as it deformed long before reaching the pin, Figure 50.

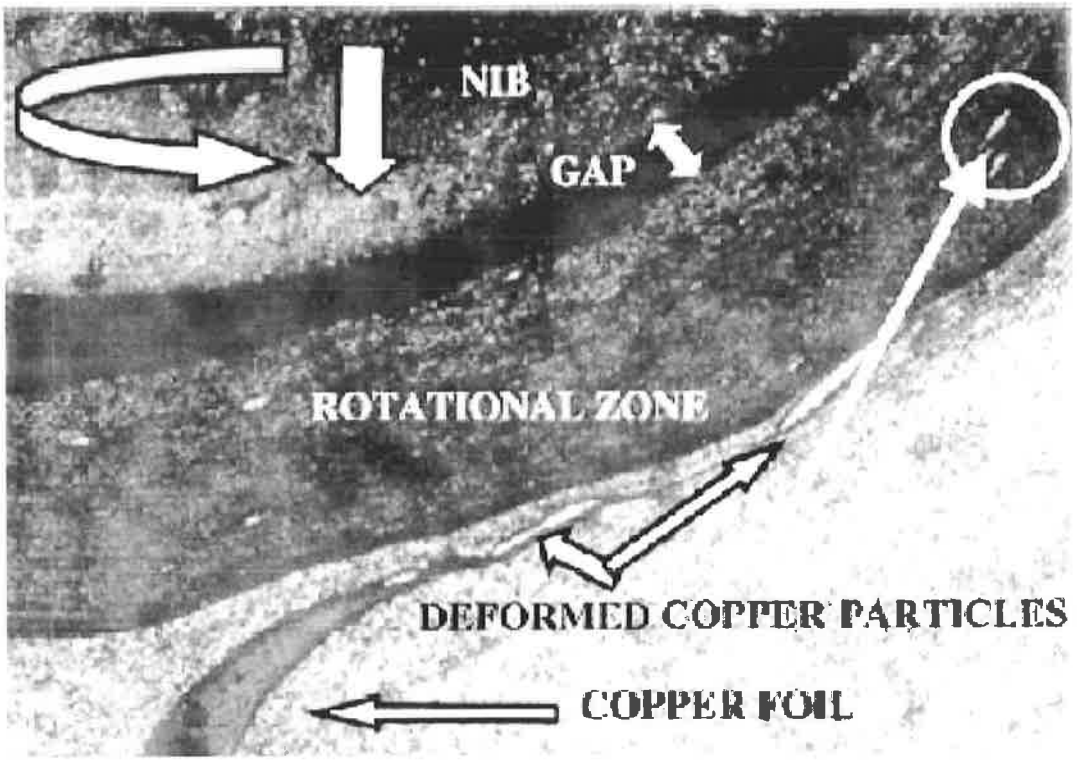

Figure 50 Deformation of the Cu foil ahead of the welding pin [60]

The Cu foil unable to sustain the large strains imposed by the rotating pin, referred to as the nib in Figure 50, appeared to thin rather like wire being drawn. When it was no longer able to sustain this deformation the Cu foil fractured into smaller elongated particles. These particles were seen to enter the rotational zone, which in size was found to measure up to 6 times larger than the distance moved by the pin in one rotation. Between the pin and the rotational zone it could be observed that a small gap existed between the nib and rotational zone, Figure 50, suggesting that a condition of intimate contact between tool and workpiece material was not met for this region of the weld tool. It was further observed that the Cu particles within the rotational zone could be seen to disappear from the plane of viewing indicating vertical movement had occurred for the marker. To verify the vertical movement of marker material a cross section of the frozen pin in the direction of welding was made, Figure 51.

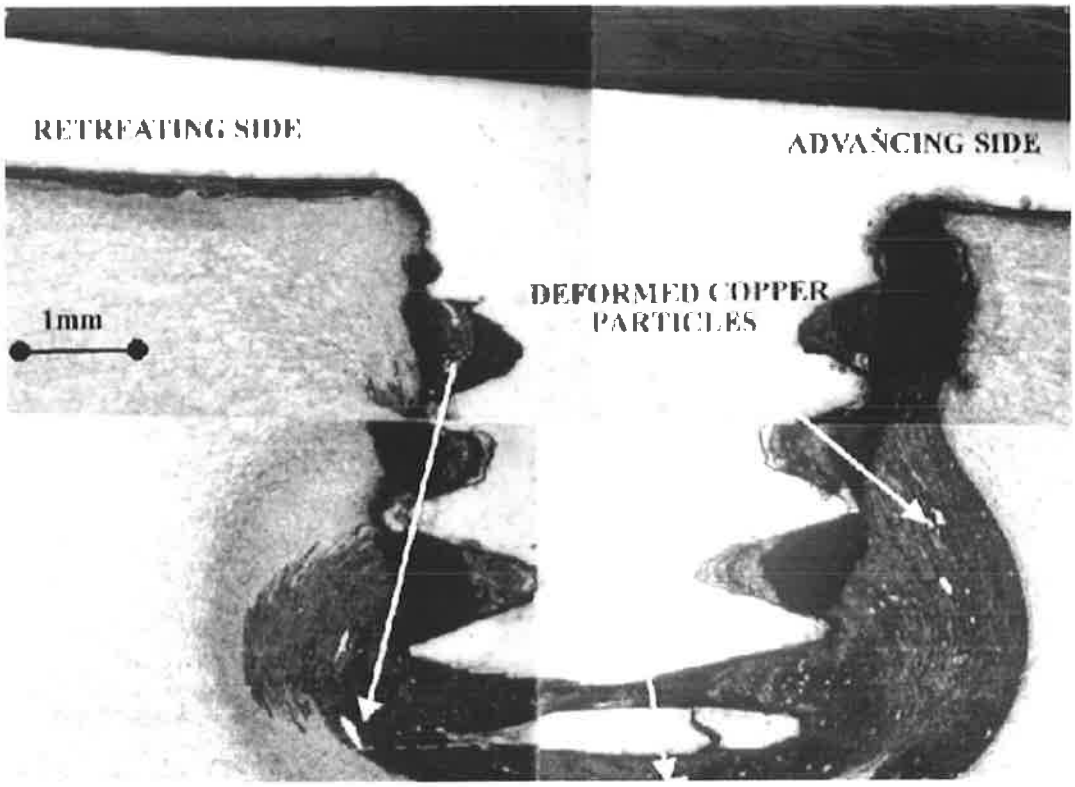

Figure 51 Side view of the frozen pin and Cu particle location [60]

Bright Cu particles were found throughout the entire rotational zone. The constant size of the particles throughout the weld zone suggested that no further shearing occurred for the particles as a result of contact between particles and the welding tool pin. It is interesting to note that in Figure 51 voids between the tool thread and the workpiece material occur around the tool pin.

Outside of the rotational zone was a region defined as a transition zone. Here no Cu particles were found. Grains however in the transition zone were elongated and bent in the direction of tool rotation, Figure 52.

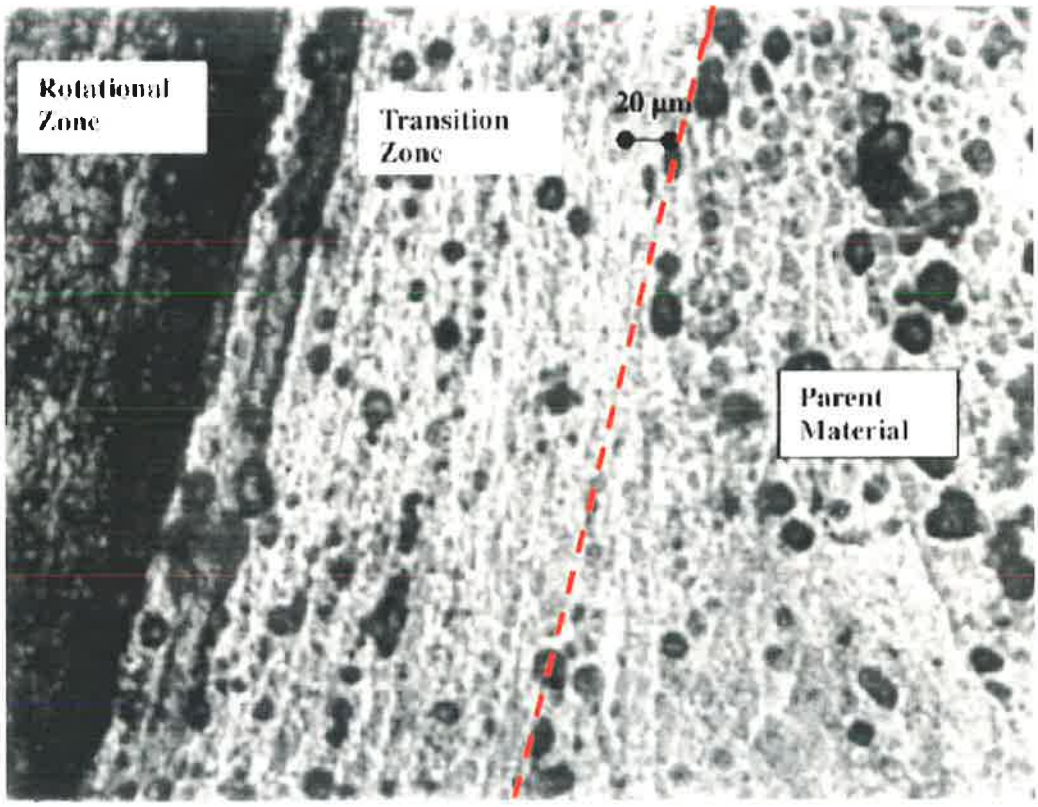

Figure 52 Differences in the microstructure observed between the grains in the rotational and transition zones [60]

The transition zone could be observed to be approximately twice as wide as the rotational zone, an effect perhaps of processing parameters. It was speculated that the transition zone was formed due to extrusion, the die consisting of the hard rotational zone and the parent material outside of the weld zone. Micro-hardness surveys conducted for both rotational and transition zones indicated a higher hardness for the rotational zone. Hardness, grain size and grain morphology were seen to change abruptly at the edge of the rotational zone, but remained the same within this zone indicating that both zones underwent very different thermo-mechanical histories even in such close proximity to the welding tool.

Although there have been many other FSW studies which have attempted to visualise and model material flow arising from the FSW process, the essential details to come out of each study has been comprehensively reported in this literature review. The use of minute embedded marker materials in conjunction with a stop action welding technique, whether viewed through application of metallurgical or radiographic techniques has demonstrated that the marker when entrapped in the flow zone of the friction stir weld rotates in the direction of tool rotation. The marker not only rotates but is also vertically displaced.

To date there has only been one study [58] in which it has been attempted to associate different tool pin geometries with that of marker material displacement resulting from the FSW process, Figure 53. The study [58] has clearly shown that tool pin geometry not only affects marker material flow and deposition but that marker material entrapped in the flow zone around the rotating pin rotates at least once around the pin before exiting the flow region. The use of micro-computer tomography as has the potential to not only define the mechanisms of material flow and bonding associated with the welding tool pin form but also to define the cavity into which material is transported as a result of variation in tool geometry and FSW parameters.

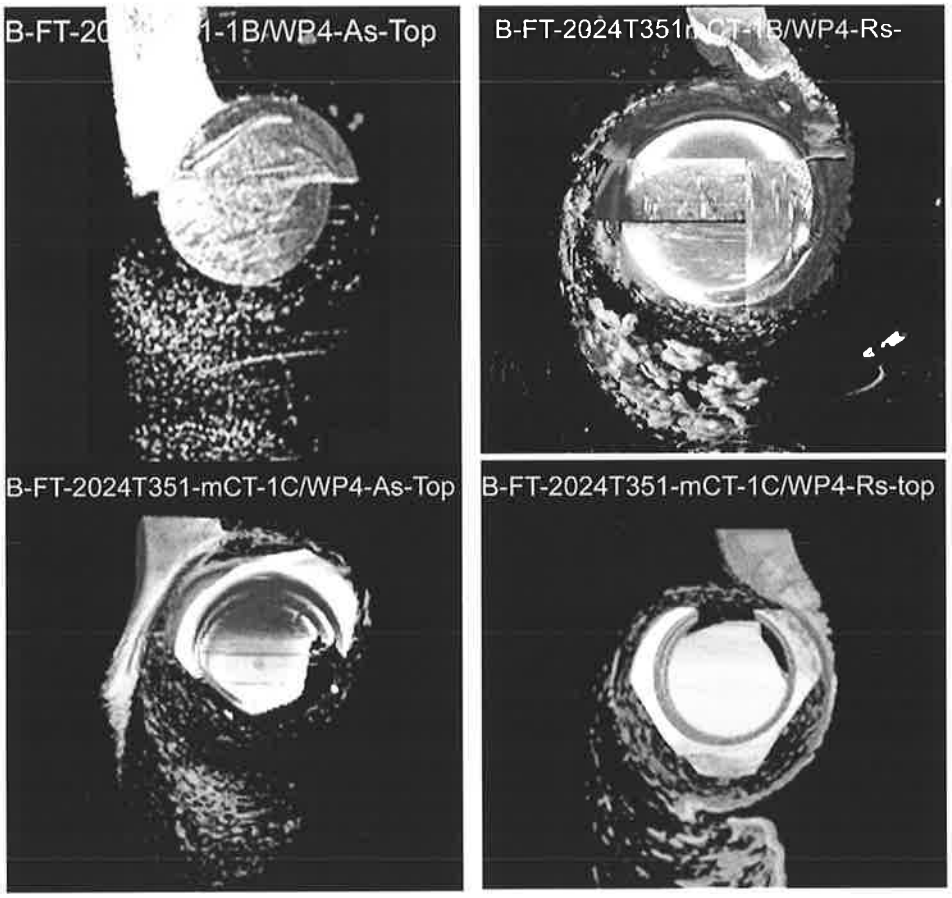

Figure 53 Plan view (computer tomographic images) of the frozen pins engaging the Titanium powder marker material while FSW 4mm thick 2024-T351 aluminium alloy [58]. Note: tool rotation is clockwise and the Ti marker used in the investigation measured 60-90 microns in diameter.

This literature review has indicated that tool geometry and processing forces play a vital role in weld formation. The experimental investigation conducted in this thesis adds further insight into better understanding the weld formation process when FSW thick section 5083 and 7075 aluminium alloys.

2.15 Summary Of Key Points From The Literature Review

A literature review has been undertaken to identify key features of the FW and FSW processes that could help in designing a FSW tool and welding conditions to enable successful joining of 12.5mm and 25mm thick 5083 H111 and 12.5mm thick 7075 alloys.

The literature review has identified that the key factors controlling the process of FSW are tool rotation speed, weld travel speed and axial force (vertical down force) directed through the welding tool and onto the surface of the workpiece. Here the shoulder of the tool exerts the dominant influence both in terms of axial force and torque i.e. frictional load encountered which resists the rotation of the FSW tool.

At the heart of the FSW process lies the design of the FSW tool, particularly the tool pin. The literature review revealed that welding pins required a thread form if volumetric defects in the stir zone were to be avoided. Mechanical test results also indicated that conical and threaded pins provided for superior tensile strength in comparison to cylindrical and threaded pins. In addition it was demonstrated that a continuous thread form was not essential for conical welding pins. In fact tensile tests in friction stir butt welds produced in 4mm thick 2024 T351 alloy that a conical threaded pin containing three flats was superior to the same pin form without flats. This may lie in the fact that material flow and bonding as having been investigated using micro-computer tomographic techniques for observation of marker material dispersion in the stir zone suggests that very different flow regimes and hence weld formation occurs between these tool pin forms even when used under identical welding conditions.

The generic FSW tool consisting of a cylindrical and threaded pin coupled to a concave and recessed shoulder demonstrated that this tool form was unable to successfully join aluminium alloys for a workpiece thickness of 25mm. Defect free welds in this material thickness required the FSW pin to be conical and threaded. Modifications to this design by adding flutes or flats to the pin demonstrated that these did not detract from the quality of the weld, rather they enhanced weld travel speed capabilities.

The literature review makes it clear that the magnitude of the FSW forces, particularly the axial force and the force generated opposing the direction of weld travel are of critical value. The force on the welding tool particularly in the weld travel direction when it becomes too large will break the tool. The magnitude of these forces and their

relationship in terms of tool pin form as well as heat generation and weld formation is as yet poorly understood.

In addition to the uncertainty which revolves around welding forces is the question concerning the selection of FSW parameters such as rotation speed and weld travel speed, in particular how these are influenced by FSW tool form. Clearly the FSW process has demonstrated a wide tolerance in the application of tool rotational speeds for the FSW of aluminium and its alloys. However the literature review could not identify a temperature correlation between FSW conditions and various aluminium alloys i.e. temperature evolution in different aluminium alloys when friction stir welded given a constant set of welding parameters and welding tool. Such studies are of critical importance as they define the processing limits associated with the FSW of a given material in combination to a particular welding tool. This information in addition to processing forces can then be used to select parameters for either microstructure enhancement (coolest welds possible) or for increased productivity i.e. highest weld travel speed.

The literature review was able to find a methodology relating tool rotation speed with that of a rubbing velocity as measured at the periphery of the tool (either pin or shoulder). The rubbing velocity could be calculated and transferred to determine rotation speeds between various tools of different diameters. The validity of this methodology of transferring rubbing velocities between tools of different diameters to establish tool rotational speeds and allow for the FSW of thicker or thinner workpieces has not been demonstrated.

3. MATERIALS, PLANT AND EQUIPMENT

This chapter contains composition, properties and temper details of the various wrought aluminium alloys, as well as the tool materials used during the investigation. In addition this chapter defines characteristics of the FSW welding apparatus, machine operation, clamping arrangements, plate geometry, tool design strategy and measurement equipment (this refers to load and temperature).

3.1 Wrought Aluminum Alloys - Composition and Temper

Details of the wrought aluminium alloys, based on the standard nominal composition [33] for temper and plate thickness used during this study are presented in Table 3-1.

Alloy / Temper	Thick (mm)	Si max.	Fe max.	Cu max.	Mn max.	Mg max.	Cr max.	Zn max.	Ti max.	Other	Al.
5083-H111	12.5, 24.8	0.40	0.40	0.10	0.40-1.0	4.0-4.9	0.05-0.25	0.25	0.15	0.15	rem.
7075-T651	12.5	0.40	0.50	1.2-2.0	0.30	2.1-2.9	0.18-0.28	5.1-6.1	0.20	0.20	rem.
7075-0	12.5	0.40	0.50	1.2-2.0	0.30	2.1-2.9	0.18-0.28	5.1-6.1	0.20	0.20	rem.

Table 3-1 Nominal composition weight %, temper and plate thickness of investigated alloys. (rem.= remainder). Note 0 applies to wrought alloys that are annealed to obtain lowest strength temper. For further details concerning the meaning of the tempers refer to Figure 2 of section 2.1

3.2 Investigated Wrought Al Alloys - Properties

It has been demonstrated that FSW utilises heat, forging and mixing of the workpieces to form the welded connection. The deformation occurring in the stir zone during FSW i.e. weld nugget takes place at temperatures well above 0. $5T_m$ (T_m: is the absolute melting temperature of a material: for pure aluminium this is 940 K). Thus FSW can be classified as a hot deformation process and has led many researchers to investigate processing temperatures in order to explain microstructure evolution as a function of the heat input during welding.

It is known that physical and mechanical properties of an alloy change due to increasing temperature. There is however very little thermo-mechanical and material property data able to correlate processing conditions with that of the flow stress experienced by a material during FSW. Hence, the physical and mechanical property data for the alloys investigated in this study are defined for room temperature only, Table 3-2.

UNS	A97075	A97075	A95083
	A7075-T651 Aluminium	A7075-0 Aluminium	A5083-H111 Aluminium
Density (g/cc)	2.81	2.81	2.66
Hardness Brinell (1)	150	60	81
UTS (MPa)	570	228	300
Ys (tensile, MPa-min)	505	103	190
Elongation % : break	11	16	16
Shear strength (MPa)	330	152	180
Thermal conductivity (W/m.C)	130	173	117
Heat Capacity: J/g.°C	0.96	0.96	0.9
Thermal Diffus. (m^2/sec) x 10^{-3}	0.048	0.048	0.049
Solidus (°C) (2)	532	477	591
Liquidus (°C) (3)	635	635	638

Notes: (1) 500kg load/10 mm ball. (2) Solidus temperature is the highest temperature at which the aluminium alloy will remain a solid. (3) The Liquidus temperature is the lowest temperature for which the alloy remains a liquid.

Table 3-2 Thermal and mechanical properties at room temperature for aluminium alloys 7075-T651 and 5083-H111 [33]

The aluminium alloys 5083, 7075 fall into two basic groups; these being non heat treatable and heat treatable alloys. Both alloys were selected because of their use in a wide range of applications. For example alloy 5083 is used in ship building because of its corrosion resistant properties, and alloy 7075 is exclusively used in the aerospace industry because of its high strength. It should be noted that the alloy 7075 until recently was considered as not being weldable using conventional fusion welding processes and so was of particular interest to the study.

3.3 Welding Apparatus

All welding tests were performed using the Friction Stir Welding Test Bed. Major components 1-10 are identified in Figure 54. This FSW machine was constructed by modifying a Butler Double Housing Planner.

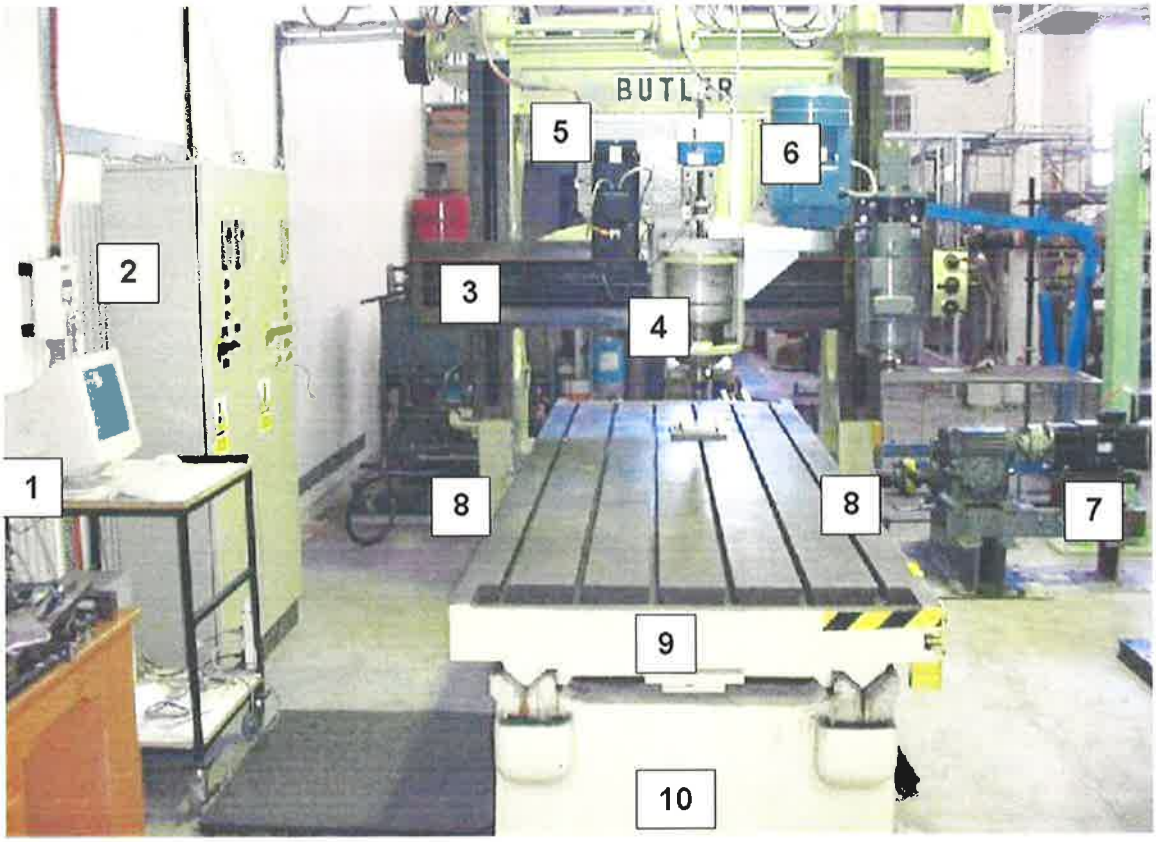

Legend

1. PC
2. ABB ASC 600 Programmable Controller
3. Horizontal welding beam to which the spindle is attached
4. Spindle
5. 4.5 kW Servo motor driving spindle rise and fall
6. 25 kW Induction motor, which governs spindle rotational speed
7. 4.5 kW Servo motor and reduction gearboxes, which drive traversing table
8. Side columns permanently fixed to table support structure
9. Traversing table
10. Table support structure

Figure 54 Friction Stir Test Bed – University of Adelaide, Thebarton Campus.

The Friction Stir Test Bed has a horizontal beam to which the spindle is connected, Figure 55. The beam is attached to two large and permanently fixed side columns from where it can be raised and lowered. The beam also allows for sideways traverse of the spindle. Sideways traverse however, at the time of the study was a manual operation and as such could not be performed during welding.

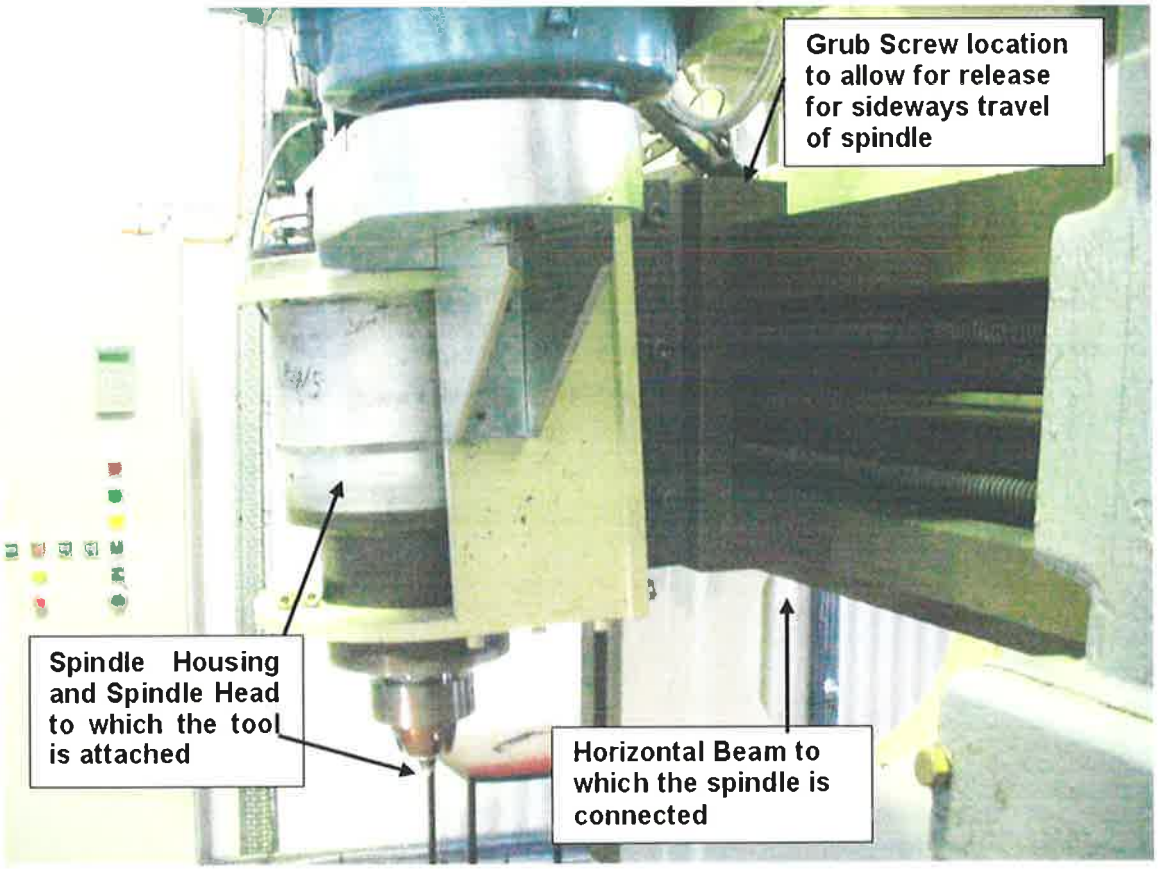

Figure 55 Friction Stir Test Bed spindle and spindle support beam.

It has been demonstrated, Chapter 2 section 2.13, that forces developed during FSW and the management of these forces play an important role in producing defect free welds.

For each applied force encountered during FSW there exists a reactionary force. When a reactionary force equals the applied force a state of equilibrium exists. For example the downforce during FSW is transmitted through the Friction Stir Test Bed spindle, which itself is supported by the spindle support structure i.e. beam to which it is attached. As a consequence of plunging, which initiates the start of the FSW process it was felt necessary that deflection characteristics (bending) of the spindle and associated support structure needed to be established. This was done initially to

ascertain what level of compensation would be required to ensure for correct seating of the tool shoulder into the surface of the workpiece material. Although the motion control program of the Friction Stir Test Bed allowed for tool deflection compensation, refer section 3.3.3 the level of force required to cause the beam to deflect had not been determined. Tests were therefore conducted and a load vs. displacement plot characterising deflection of spindle and spindle support beam of the Butler Friction Stir Test Bed established, Figure 56. These values were obtained by placing a hydraulic jack with a pressure indicator under the spindle head and measuring deflection of the associated spindle support structure using a dial indicator for each given load.

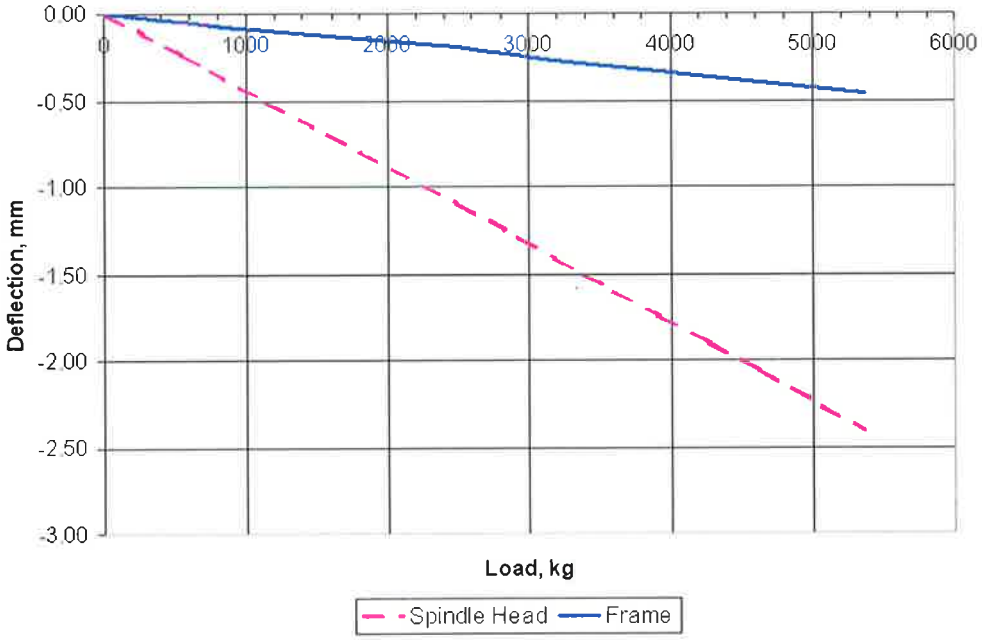

Figure 56 Load vs. Deflection characteristics of the Friction Stir Test Bed spindle and spindle support beam structure. Note maximum deflection occurs for the spindle.

Concurrent to the thesis investigation was an attempt to friction stir weld aluminium alloy 1350 with a penetration depth greater than 25mm (40mm in a single pass) using the Butler Friction Stir Test Bed. This investigation was conducted by the author but due to the commercial interest of the client involved it was not possible to present the work as part of this study apart from highlighting some of the short comings of the welding machine, which needed to be addressed to make possible FSW for this level of penetration. The electric induction motor used to provide motion for the traversing table did not have sufficient power (torque) at low weld travel speeds. It was found that at weld travel speeds below 50mm/min the drive table would stall until such time as the

travel speed was intialised greater than 50mm/min. Consequently shock loading of the tool resulted in tool breakage as the induction motor was incapable of developing sufficient torque at the low rpm range required to start welding.

The initial remedy to prevent shock loading of the tool was the installation of a second reduction gearbox prior to the drive shaft of the Friction Stir Test Bed, Figure 57. The author carried out modifications to the support frame for both the motor and gearboxes.

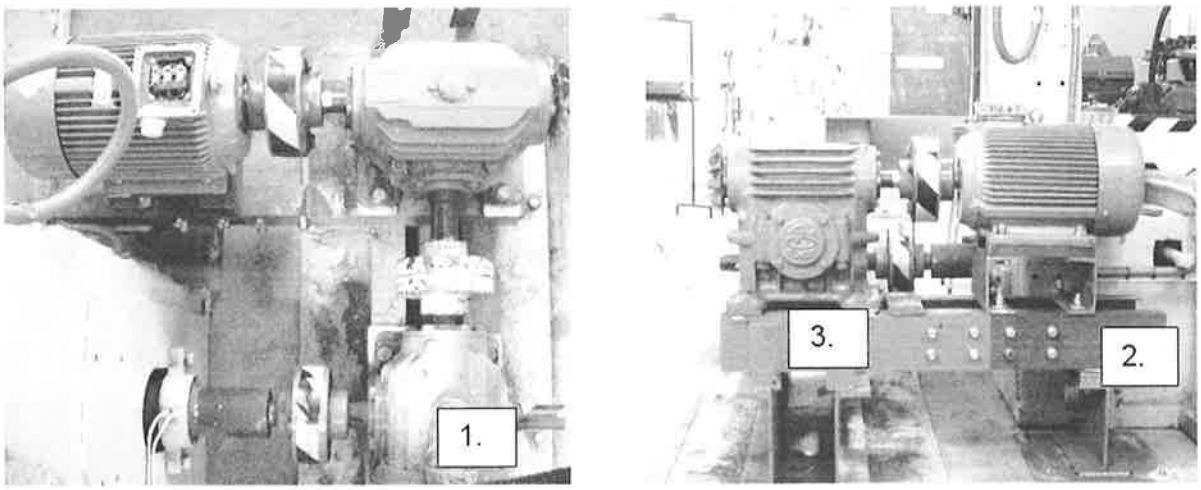

Notes:
1. Introduction of second reduction gearbox.
2. Fabrication of motor support structure and coupling to existing framework.
3. Original position of induction motor.

Figure 57 Gearbox view from above and side view.

The introduction of the second reduction gearbox, although overcoming the problem concerning shock loading of the welding tool severely reduced welding speed (max. = 280mm/min).

As a consequence of the severe knockdown in travel speed for the traversing table a three phase asynchronous Servomotor was purchased to replace the existing induction motor and modifications were again undertaken by the author to fit this to the welder, Figure 58. The servomotor was purchased because its characteristics allowed for the development of very high levels of torque even at low rpm. The biggest advantage however, was that it allowed for an increase in travel speed up to three times that which could be obtained from the original induction motor.

Notes:
1. New asynchronous Servomotor.
2. Modified support structure and repositioning of motor away from Test Bed.

Figure 58 Installation of new servomotor and modifications, as viewed from front.

3.3.1 Basic Machine Control

The main processing or motion control unit of the Friction Stir Test Bed is a DMC-1000 Motion Controller produced by Galil Motion Control, Inc. California. Basic system elements of the DMC-1000 motion control system include amplifiers, motors and encoders. A simplified schematic of these elements is depicted in Figure 59.

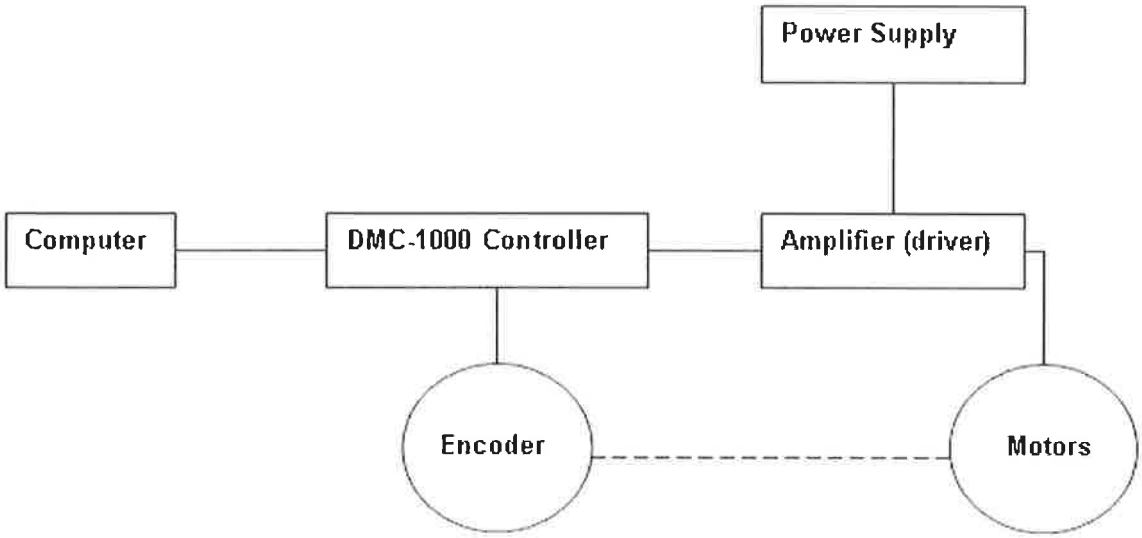

Figure 59 Schematic of basic control system elements of the Friction Stir Test Bed.

The DMC-1000 series motion controller plugs directly into the PC Bus. It provides many modes of motion, including jogging, point to point positioning and raising and lowering of the spindle head. Several motion parameters can also be specified including acceleration, deceleration and slew rates.

3.3.2 Machine Programming

The DMC-1000 can receive commands from a PC/XT/AT or compatible computer. The controller is configured as a standard AT style card that is mapped into the I/O space. Communication between the DMC-1000 and the computer is in the form of ASCII characters where data is sent and received via Read and Write registers on the DMC-1000.

The DMC-1000 instruction set is Basic-like in programming language. Instructions consist of two uppercase letters that correspond phonetically with the appropriate function. For example, the instruction BG means begin motion, and ST means stop motion. Commands can be sent live over the bus for immediate execution by the DMC-1000, or an entire group of commands can be downloaded into the DMC-1000 memory for execution at a later time.

All DMC-1000 programs begin with a label and end with an End (EN) statement. Labels start with the compound (#) sign, followed by a maximum of seven characters. The first character must be a letter, after which numbers are permitted. Spaces are not permitted. Labels are also used to identify one program from another.

A program is typically written in parts. These combine to form program flow instructions, which then complete the program. The first 6 lines of the program following the Label #WELD_AL as can be seen in Figure 60 set program bits which determine the direction of motion e.g. travel of bed towards rear = SB5 and clockwise rotation of spindle = SB6. The bits OFZ=0, OFY=0 also ensure that no motion is carried out until called upon e.g. under each heading “NO APPROACH”, “NO PLUNGE”, “NO WELD” etc.

Program flow instructions evaluate real-time conditions such as elapsed time or motion complete and alter program flow accordingly. Program distances (mm) and speeds (mm/min) are converted either to a voltage or counts per minute values. This is done by double clicking on the UnitConversion header of the Program window. Here conversion tables are accessed to determine the relative machine speeds or positions which are then inputted into a weld program.

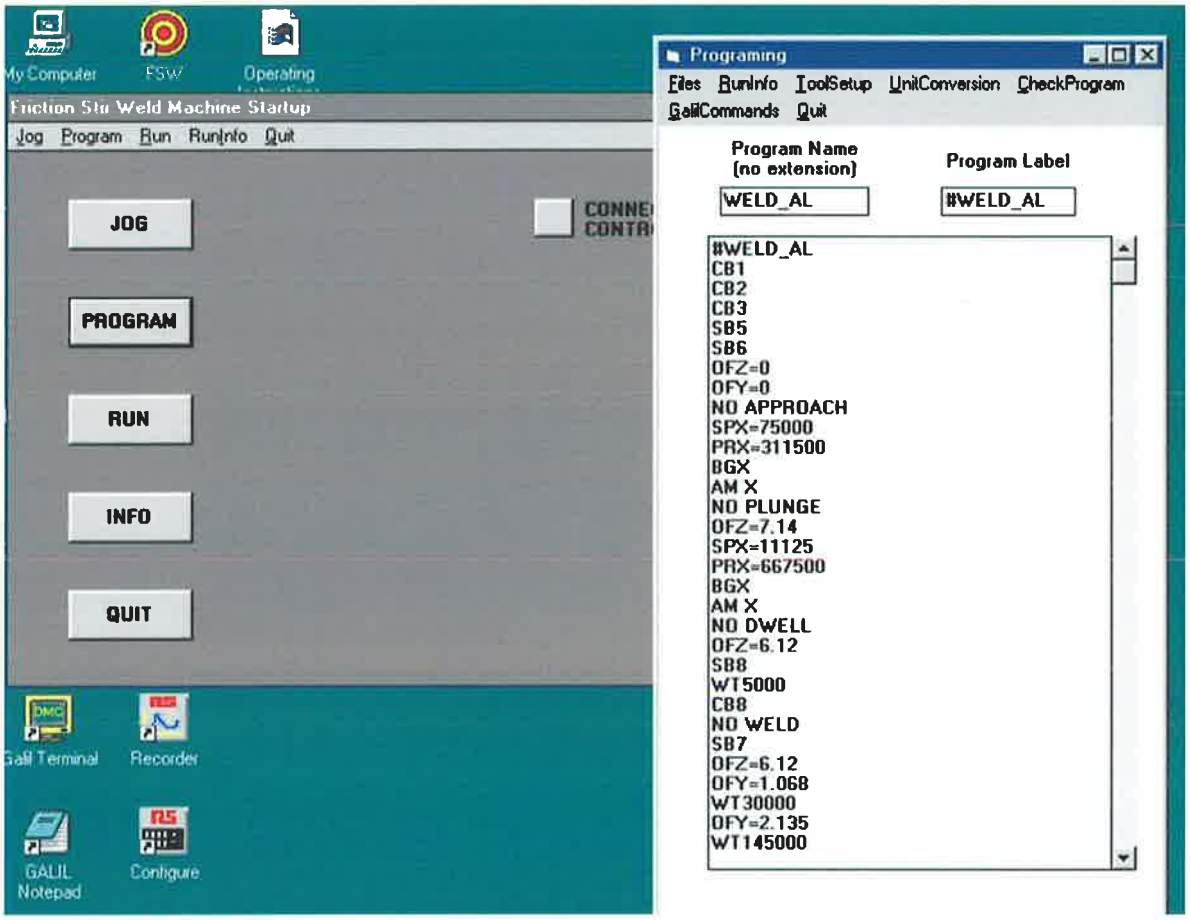

Notes: The entire weld program is not exhibited due to the size of the viewing window. Following the "No Weld" subset of the program are "Exit" and "End" commands. In all programs the first six lines following the Label #... remain constant. SPX=approach speed in mm/min converted to counts/min, PRX=distance mm converted to counts, BGX=begin motion, AMX=after motion complete, NO APPROACH=tool approach phase of program, OFZ=rotational speed rpm converted to volts, NO PLUNGE=plunge phase of program, NO DWELL=dwell phase of program, WT5000=wait 5 seconds, NO WELD=weld phase of program. The header UnitConversion used to convert between relative machine speeds and positions is circled in red.

Figure 60 Sample weld program and flow instruction hierarchy used when FSW with the Butler Friction Stir Test Bed.

3.3.3 Welding

When working with the Butler Friction Stir Test Bed there are several important steps which must be observed before the commencement of a weld. These steps are identified below along with brief comments.

- Clamping of the work pieces – All weld specimens must be securely clamped to the travelling work table. The standard plate holding fixture employed during all welding trials was mounted to the Friction Stir Test Bed as can be seen in Figure 61.

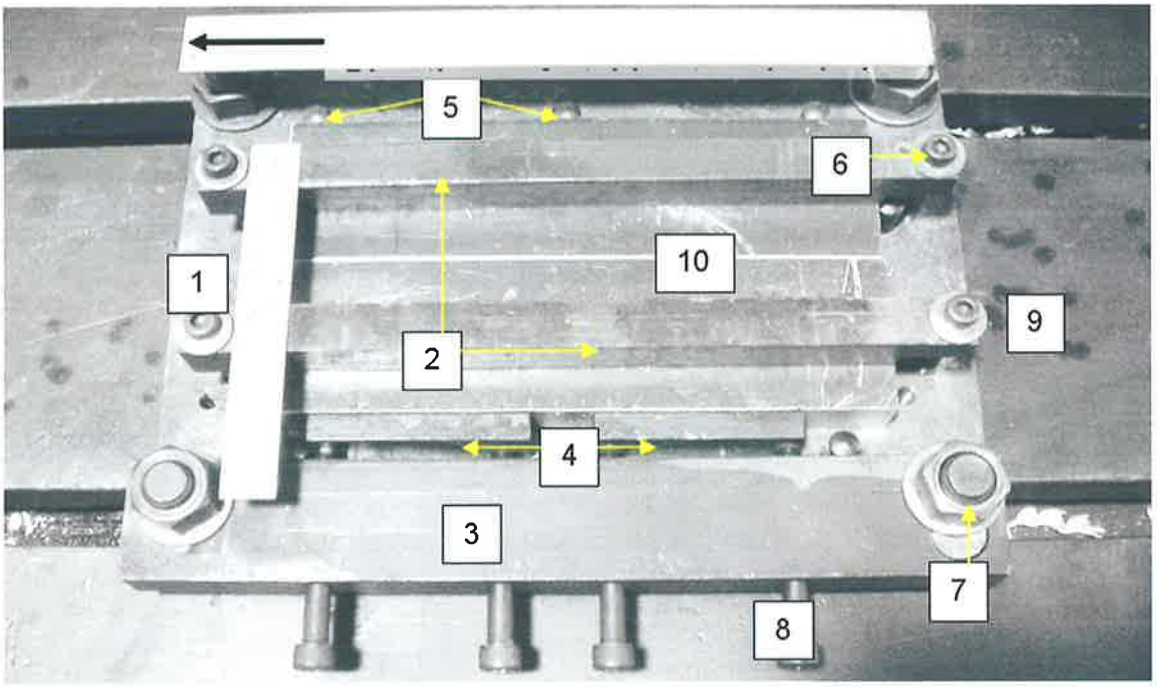

Legend:

1. 300x200x25mm mild steel base plate
2. 280x25x25mm mild steel hold down bars (2 off).
3. 310x50x25mm mild steel bar used to apply sideways force on weld plates.
4. 110x25x12mm mild steel spacers (2 off).
5. 12mm diameter x 25mm protruding mild steel dowels (8 off).
6. M10x50-70mm hex head high tensile bolts (4 off).
7. M20x100mm high tensile T-bolts (4 off).
8. M12x75mm hex head high tensile bolts used to apply side force (4 off).
9. Friction Stir Test Bed traverse table.
10. 240x140x12-25mm aluminium alloy weld plate.

Figure 61 Major components 1-10 of workpiece clamping mechanism.

- Adjustment of pin stick out in the FSW tool – Shims are placed in the tool holder prior to the insertion of the welding pin. A dial indicator is used to gauge pin stickout based on reference measurement of pin tip to shoulder surface. Pin stick out from the tool shoulder for full penetrating welds has been described to be slightly less than that of the thickness of the workpiece material i.e. 0.1mm less than the thickness of the plate to be friction stir welded. Once the correct pin stick out is achieved the pin is then locked into the tool holder by tightening the grub screws located in the tool holder.
- Insertion of the FSW tool into the tool holder of the spindle – The complete tool is inserted into the end of the spindle. Once positioned the grub screws in the head of the spindle are firmly tightened to restrain movement.
- Adjustment of tool tilt angle – The FSW spindle is attached to a horizontal beam, Figure 55. At each side of the spindle three locating screws are presented. By removing the bottom two screws from each side and loosening the top screws adjustment of tilt angle is possible. Two sets of bolt holes allow for the spindle to be tilted towards the beam so as to achieve a tool tilt angle of 3 degrees. When the spindle is tilted away from the beam a tool tilt angle of 0 degrees is achieved. Once tilt angle has been selected all bolts must be replaced and securely tightened.
- Coarse adjustment of spindle height – Prior to adjusting spindle height the four lock nuts (2 can be found at either end of the spindle support beam, rear of the beam when standing in front of the Friction Stir Test Bed) must be loosened. A gear lever which is found on the left hand side of the Friction Stir Test Bed (as viewed from the front) is moved forwards or backwards in order to engage a set of gears to allow for rise or fall motion. Once the direction of travel has been selected the green button on the right hand door of the Control Cabinet (Item 2, Figure 50) can be pressed until the desired travel distance is achieved. Having reached this position the gear lever is then placed in the neutral (middle position) and the four lock nuts securely tightened. These nuts exert the clamping force for holding the spindle support beam to the Friction Stir Test Bed frame.
- Alignment of tool to allow traverse along weld join path – In order to join two separate workpieces by means of the FSW process the tool must be placed so that it traverses directly along the join line between the two abutting surfaces. Positioning of the tool can be done by loosening the large grub screw atop of the horizontal beam (behind the spindle), this allows for release of the spindle so that it can mechanically be traversed from one side of the welder table to the

other. Traverse is carried out by turning the crank handle on the left hand side of the horizontal beam (when viewed in front of the Test Bed). Once the required distance has been traversed the grub screw atop of the horizontal beam is again securely tightened to lock the spindle in position.

- Fine adjustment of weld bed and tool approach (vertical) position – Bed travel and tool approach can be initiated without the need for programming. This is done by double clicking with the mouse on the "JOG" icon, Figure 62. This brings an embedded window into view. By selecting "X" a direction of motion for the bed indicated in the direction of the arrows occurs. By selecting "Z" a direction of motion for the spindle as indicated by the arrows occurs. The icons "Jog" or "Continuous motion" further allow for fine adjustment of the tool approach distance to the work surface. Note the maximum permissible amount of travel allowed for the Z direction is 45mm from the absolute starting point. It should also be noted that when establishing the tool approach to the workpiece surface it is necessary to allow for tool approach combined with plunge to be less than 45mm of the overall tool travel distance.

Having securely clamped the workpiece to the Friction Stir Test Bed table and fastened all clamping screws previously loosened to allow for location of the tool over the workpiece, a weld program specific for FSW of the chosen workpiece material can be accessed or written, and then run.

A weld program is initiated by clicking the "RUN" icon, Figure 62. A new window now appears (green window). This window allows for input and storage of all relevant weld information used in the production of a given weld. To access the data storage facility one clicks the "RunInfo" heading, Figure 62. At this point the weld must be identified by giving it a weld number. The format used throughout this study has been to identify a weld firstly by year, month, day and then the sequence of welds (A,B,C...) produced in any one day e.g. 001213A. To load and then run the weld program one simply clicks on the "OK", "Load", "Go" icons which can again be seen in Figure 62. The weld is then carried out automatically by the Friction Stir Test Bed.

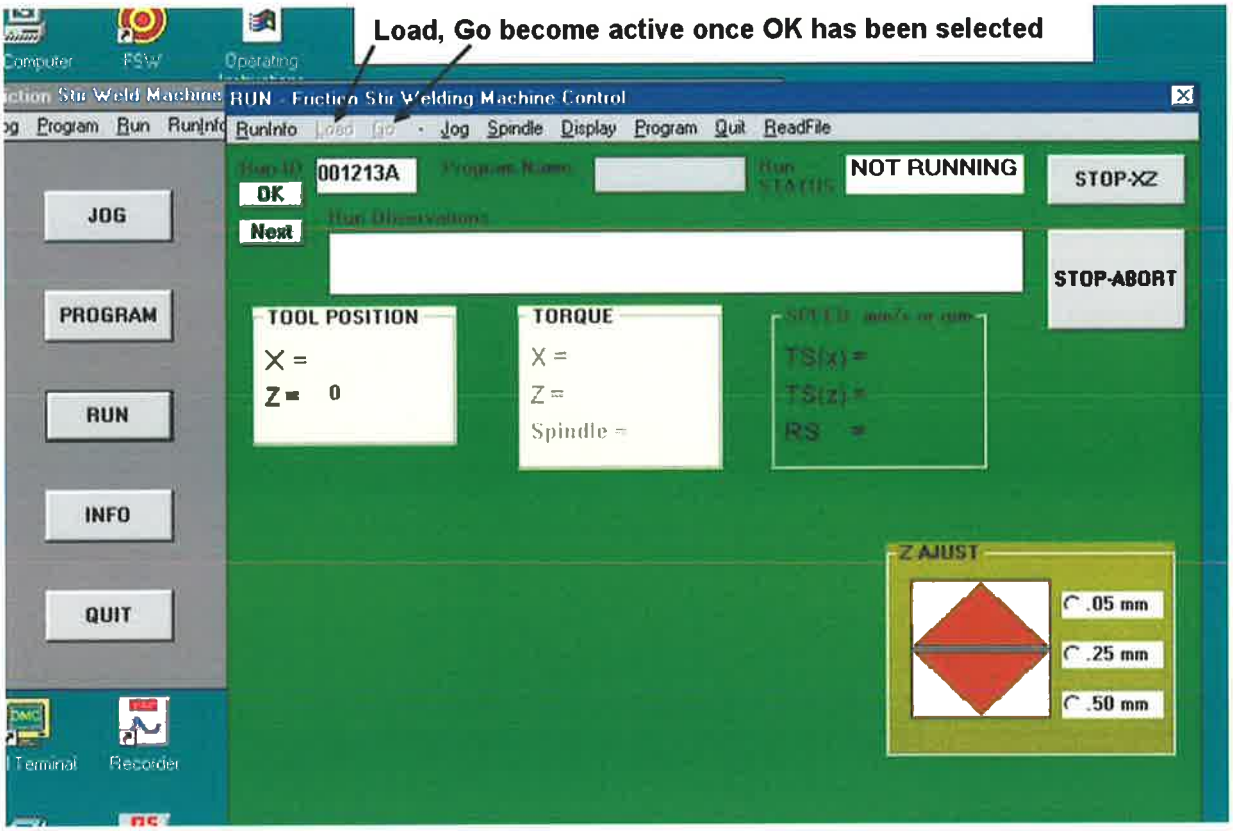

Figure 62 Run display window, which appears during FSW with the Butler Friction Stir Test Bed.

Several functions have been in-built into the control program to allow for adjustment and overriding of the execution program.

During welding, the "Run" display window, Figure 62, allows the operator to make adjustment to the height of the tool. This is done by selecting one of three displayed parameters in the "Z AJUST" box. This is again initiated by using the mouse cursor and clicking on the up or down arrow of this same box.

The weld program can also be interrupted (for weld travel) by clicking on the "STOP-XZ" icon or completely shutting down all motion by clicking on the "STOP-ABORT" icon of the "Run" display window.

The "STOP-XZ" icon allows the operator to interrupt the initiated program without terminating control of any of the three-motion control motors. By opening the "JOG" window the operator can select an axis (X = traverse, Z = spindle) which he/she wishes to control. Care however, must be taken to ensure that the initial program does not time elapse. Each weld program is calculated by the controller to be performed in a given time frame for the selected welding parameters. Once this time has elapsed,

regardless of the interrupt, the friction stir welder will initiate the end of weld sequence and subsequently shuts down all motor motion.

In the event of an emergency the "Run" display window allows the operator to immediately shut off power to the Friction Stir Test Bed. This is done, Figure 62, by clicking the "STOP-ABORT" icon. "STOP-ABORT" should only be activated in the event of an emergency as this cuts power to all machine operations and as a consequence freezes a tool into the workpiece material if the tool has not already been retracted from the workpiece.

3.3.4 Welding - Data Acquisition

The weld sequence when FSW can be described as occurring in several stages. The first stage involves the sample setup. After setup the software controlling the welding program is activated. Upon activation of the software the tool starts to approach the workpiece material and the spindle starts to rotate. The tool is then plunged into the workpiece material until the shoulder of the tool makes contact with the surface of the workpiece. This is then followed by a short dwell period where the workpiece material is further heated through frictional contact between the rotating tool and the workpiece. The tool is then set in motion where it travels along the join line between workpieces. During welding the tool can only be raised or plunged manually such that intimate contact between tool shoulder and workpiece is maintained. This is because the position of the tool is regulated by position and not load control. Once the required weld distance has been achieved the tool is then retracted from the workpiece material.

The DMC-1000 motion controller has an in-built feature which allows for the capture of external data such as tool position, motor loads and also external inputs such as temperature and force measurements.

Four basic data types are automatically captured when FSW. Three of these are given in Figure 63 and include measurement of tool displacement, as well as motor load for spindle rotation and table traverse.

The data from motion and motor torque is stored in the PC according to a weld run file number e.g. 001312A.dmc. All initial run files have the extension ".dmc". These files can be accessed through the Microsoft "Excel Program" and converted to a typical excel plot.

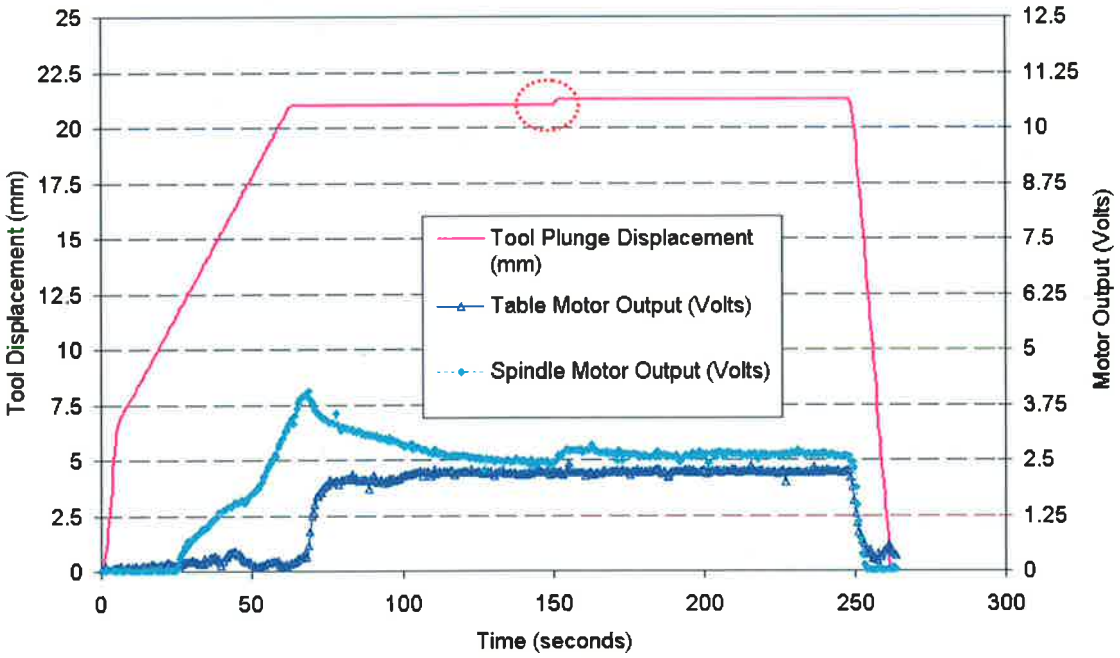

Figure 63 Displacement of the tool during plunge and motor load output (spindle and table motor during FSW) representative of the DMC-1000 data collection system.

Data acquisition is not just limited to tool plunge displacement and motor load measurements as registered in volts during FSW. The motion controller can also compile external data for temperature and force. These are discussed in section 3.6 of this Chapter.

Note the when FSW the tool is typically placed a specified distance above the workpiece. This distance was defined by placing a small steel block between the end of the welding tool pin and the surface of the workpiece to allow for some tolerance if the weld needed to be aborted. These blocks measured 5, 7.5 and 10mm in height and were removed prior to FSW. Upon completion of the weld set up as reviewed in section 3.3.3 of this Chapter the rotating tool would then be plunged and once having made contact with the surface of the workpiece the spindle motor would indicate a load. The value of the load varied between 0 and 10 Volts; 0 Volts indicating no load and 10 Volts indicating maximum load. The value of voltage was independent of the speed of the motor. When the tool shoulder made direct contact with the surface of the workpiece spindle load reaches a peak and shortly there after tool traverse of the joint is set into motion. This is indicated by the increasing load (Volt) of the motor driving the table, Figure 63. The weld is completed when all measurements return to 0.

3.4 Weld Joint Configuration

All friction stir welds performed during this study comprised one of two types: bead on plate (BOP) or Butt. The BOP welds were performed by plunging the welding tool into a single workpiece restrained in the clamping fixture previously shown in Figure 61. The tool was then traversed along the centre of the plate. Plate dimensions (for up to 25mm plate thickness) were 140 ± 2mm wide and between 200-240mm in length i.e. weld travel direction.

FSW butt welds were produced using two 70mm wide abutting plates possessing a square joint with no edge gap in the weld line. The plate edges were squared by mill and lightly sanded prior to fit up. All plates were welded in the as received top surface condition free from scale. Welds were also performed parallel to the plate rolling direction.

3.5 Welding Tools

All welding tools trialed throughout this study were made from H13 (for tool shoulder) and M2 (for tool pin) series tool steel. The welding tool consisted of a two parts – a pin and a pin holder which incorporated the tool shoulder. This was done primarily to allow for flexibility in selecting various combinations of pin and shoulder. It also meant that in the event of tool (pin) breakage the entire tool need not be discarded.

H series tool steels are typically referred to as hot-work tool steels. The M series tool steel, with molybdenum as its major alloying element, is commonly referred to as a high-speed tool steel. The nominal compositions of both H13 and M2 tool steel can be found in Table 3-3.

Type	C	Fe	W	Mo	Cr	V	Si
H13	0.33-0.4	90.95 min.	-	1.33-1.4	5.13-5.25	1.00	1.00
M2	0.78-1.05	81.58	5.5-6.75	4.5-5.5	3.75-4.5	1.75-2.2	0.2-0.45

Notes: wt% composition [86].

Table 3-3 Nominal wt% composition H13 and M2 tool steels.

Chromium tool steel, H13, was chosen for the main body of the tool primarily because this was the tool steel of choice used by TWI in their early FSW tools. Properties which make the H13 tool steel ideal for FSW are that;

1. it resists softening at temperatures up to 800°F (430°C),
2. it possesses very good machinability,
3. it is relatively inexpensive (and comprises the most widely used hot working tool steel in industry)
4. it can be heat treated to increase hardness (to approx. 48 HRC).

M2 tool steel was chosen for fabrication of the FSW pin because;

1. it resists softening up to 1150°F (620°C)
2. it is also the most popular and widely available alloy of all high-speed tool steels
3. it has good machinability
4. can be heat treated to increase hardness (up to approx. 56 HRC)

3.5.1 The Tool Design Philosophy

The thread pitch employed for tool pins designed in this study was 4mm for the FSW of 12.5mm thick plate and 2mm when FSW the 25mm thick plate. A constant thread pitch strategy was employed simply to avoid unnecessary complexity of the tool pin design i.e. tool shoulder and pin design had to be easily fabricated without the need for complex calculations to determine thread pitch variables.

The reason behind selecting the larger thread pitch for pins to be used in the FSW of the 12.5mm thick alloys was to allow for as large a cavity between the body of the pin and each thread. This was done in an attempt to see if this strategy could enhance material flow around the pin. It was feared a 4mm thread pitch when applied to pins for the FSW 25mm thick plate would structurally weaken these pins and therefore it was decided to use a 2mm thread pitch.

3.5.2 Weld Pin Design

The basic pin shape used when designing the welding pin was to give the pin a conical form, with the diameter of the pin reducing from pin shank to approximately one third of this diameter at the pin tip. The length of thread in all cases was equivalent to the thickness of the workpieces to be friction stir welded. A typical pin thread profile can be found in Figure 64. This pin profile is here after referred to as CT1.

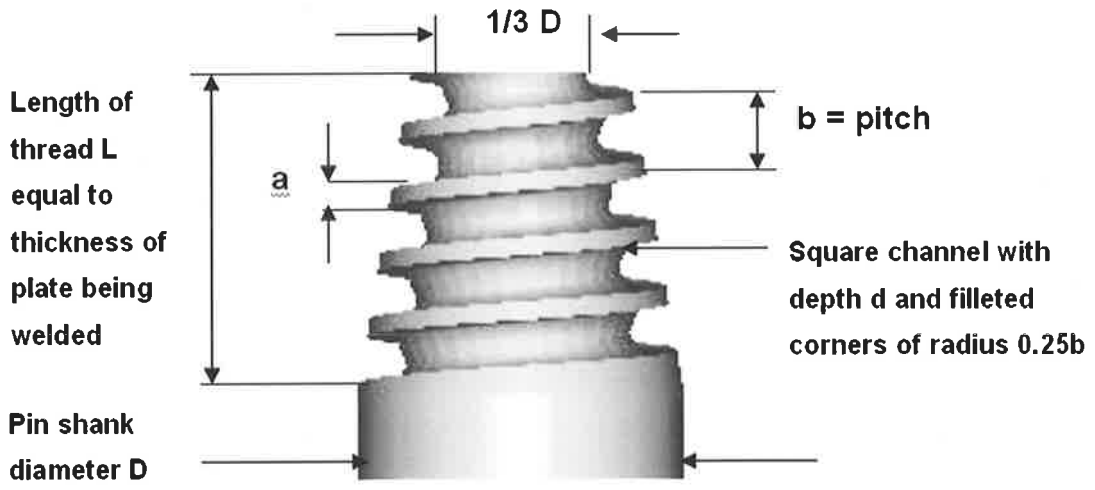

Figure 64 Generic thread profile CT1 trialed throughout experimental investigation. Note a and b were held constant over length L

A second pin profile was designed by the author here after referred to as pin CT2. Although the pin thread profiles remained constant between pin CT1 and CT2, the pin CT2 was altered in form by introducing three flats machined onto the surface of the threaded portion of the pin at a spacing of 120°. This was conducted for pins produced to friction stir weld the 12.5mm and 25mm thick workpieces, Figure 65.

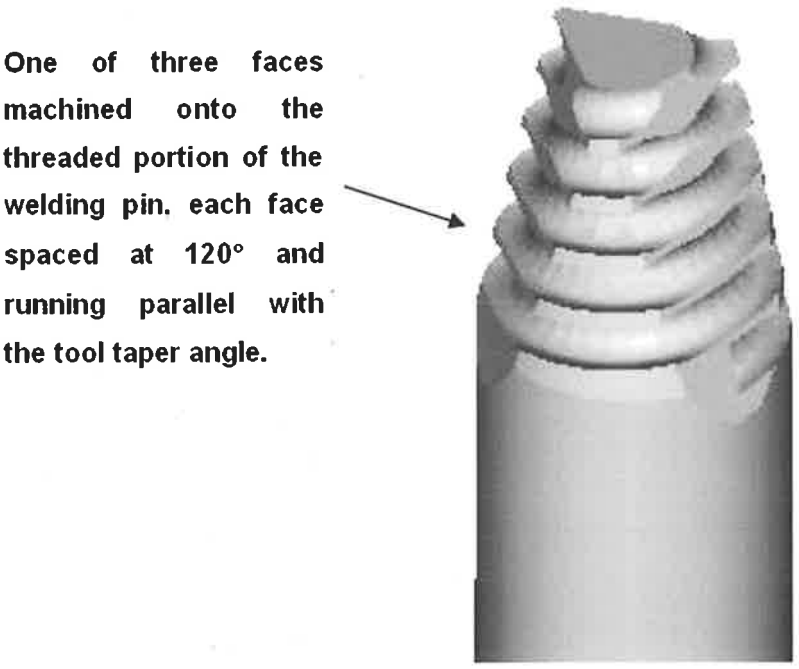

Figure 65 FSW pin CT2 (conical threaded) with 3 flats.

The introduction of flats onto tool pins CT2 was to reduce the overall volume of tool pin plunged into the workpiece material in comparison to tool pins CT1, and thereby it was hoped to reduce processing forces and enhance material flow around the pin.

Pin diameters, lengths and profiles employed during the weld investigation are presented in Table 3-4 (construction drawings for pins can be found in Appendix A). Note terminology giving reference to pin geometry is to be used in conjunction with Figure 64. All welding pins were hardened by heat treatment to between 54-56 HRC. This heat treatment was carried out by Winfield Heat Treatment Services of Adelaide.

Pin I.D.	Length of Thread L (mm)	Thread Pitch b (mm)	Thread Land Thickness a (mm)	Thread Depth d (mm)	Profile, no. of Flats
CT1-14x4	12	4	1.3	1.5	nil
CT2-14x4	12	4	1.3	1.5	3
CT1-20x2	20	2	0.8	1.5	nil
CT2-20x4	20	2	0.8	1.5	3

Notes: Pin I.D. letters and digits reflect from left to right CT = conical threaded, 1 = no flats, 2 = flats, the numbers 14 and 20 = pin diameter. Technical drawings of the pin profiles can be found in Appendix A.

Table 3-4 FSW pin profiles and geometry used during investigation

3.5.3 Tool Shoulder Design

Tool shoulder design consisted of one of two types:

1. Shoulders incorporating the tool holder.
2. Shoulders separate from the tool holder.

Shoulder types 1 and 2 can be found in Figure 66 and Figure 67 respectively.

Figure 66 Tool holder type 1 incorporating tool shoulder.

Figure 67 is representative of the tool design where the shoulder remains separate from that of the tool holder. This shoulder type was employed for the instrumented tool to allow for seating of the tool embedded thermocouples into both the pin and shoulder. Refer section 3.6 of this Chapter for further details.

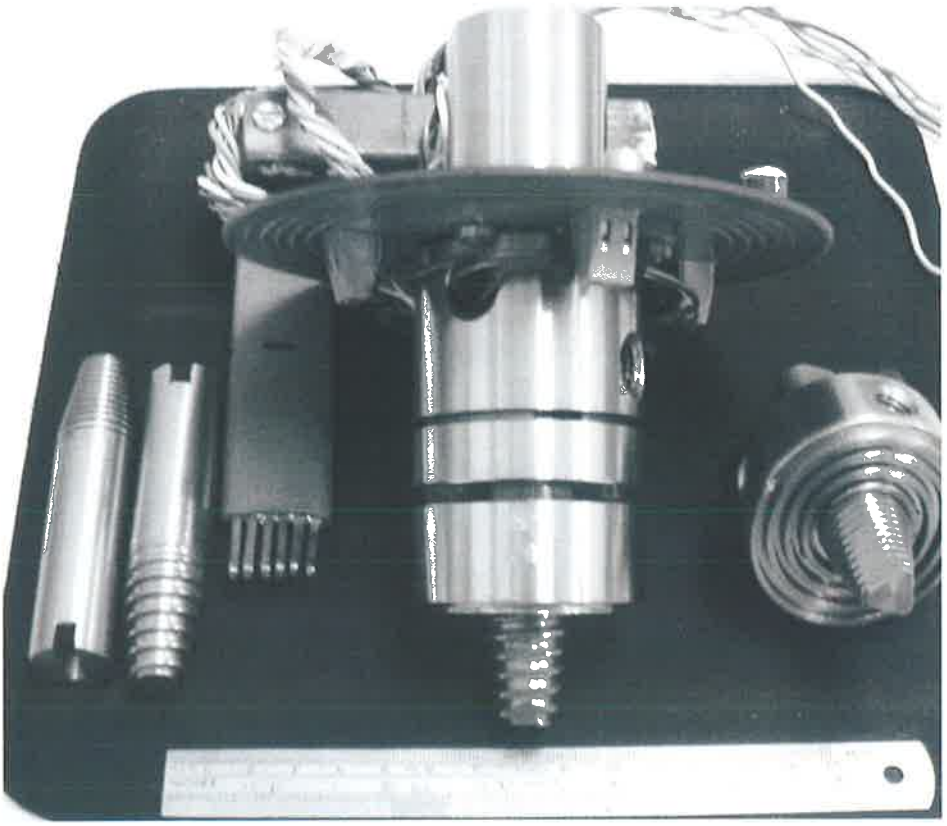

Figure 67 Tool holder types 2 with separate shoulders and pins.

Tool shoulder diameters, profiles and heat treatments employed during the welding trials can be found in Table 3-5.

Shoulder I.D.	Temper (HRC)	Concavity (°)	Pitch (mm)	Thickness Of Profile Thread (mm)	Depth Of Profile Thread Into Shoulder (mm)
30Cc14	nil	7	nil	nil	nil
50CR20	46	nil	4	2	2

Notes: Shoulder I.D. digits and letters reflect from left to right firstly shoulder outer diameter, followed by shoulder type Cc = concave, CR = concentric ring, followed by pin diameter. Technical drawings of the shoulder profiles can be found in Appendix A.

Table 3-5 Tool shoulder geometry and profile description

3.6 Measurement Apparatus

An in-built feature of the DMC-1000 motion controller highlighted in section 3.3.4 of this Chapter was that it could allow for the capture of data such as tool position and motor loads as measured in Volts. The controller however, also enabled the capture of external inputs, e.g. temperature and load cell measurements. The equipment and methodology employed to measure temperature and load will now be discussed.

3.6.1 Temperature Measurement

Temperature measurements were made on 12.5mm thick 5083 H111 and 7075 T651 aluminium alloys. FSW temperatures were also measured when welding 25mm thick 5083 H111 alloy. Two methodologies were used to measure temperature. The first method involved embedding thermocouples directly into the workpieces, in and around the region to be welded. This was performed for both the 12.5mm and 25mm thick workpieces. A schematic depicting the location of thermocouples in a typical weld plate allowing for variable plate thickness can be found in Figure 68.

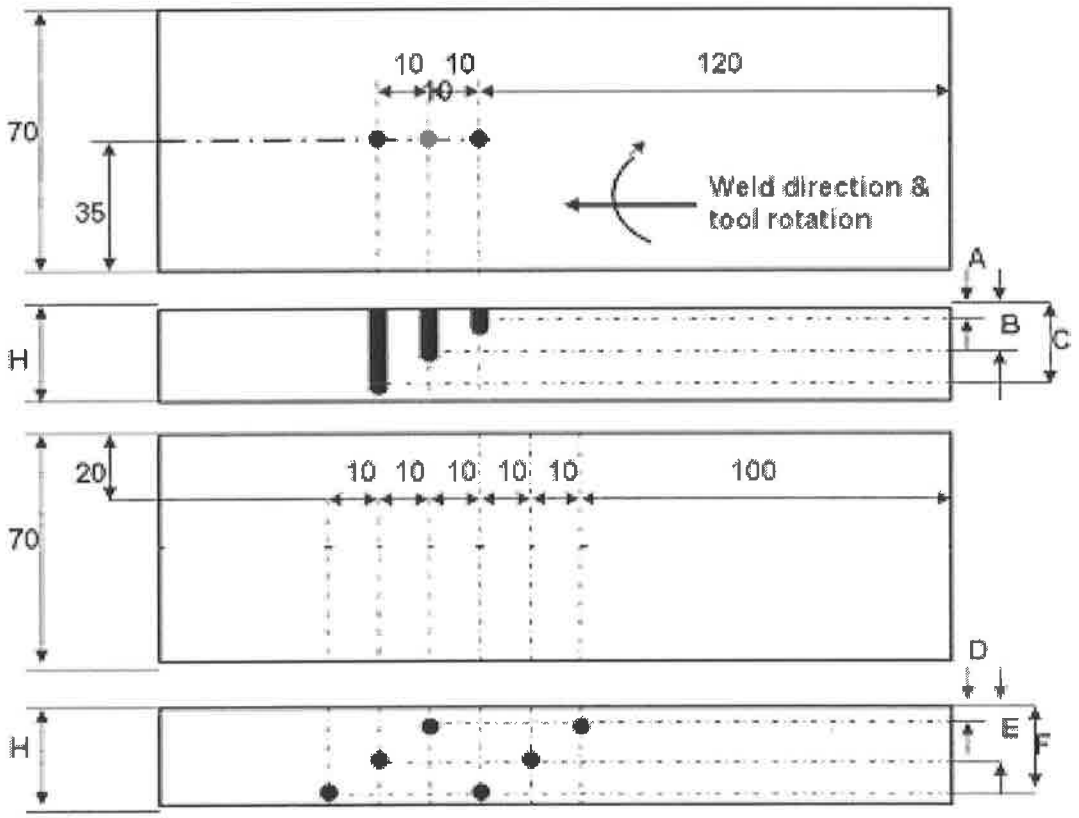

Figure 68 Location and depth of thermocouple holes (A-F) to be read in conjunction with Table 3-6. Note all dimensions are in millimetres. The captions top to bottom are retreating side top view, retreating side interface (join), advancing side top view and advancing side join.

Alloy	A (mm)	B (mm)	C (mm)	D (mm)	E (mm)	F (mm)	H (mm)
5083-H111 7075 T651	3	6	9	3	6	9	12.5
5083-H111	3	12.5	19	3	12.5	19	25

Table 3-6 Depth of thermocouple A-F and plate thickness H used during temperature measurement. To be read in conjunction with Figure 68.

Chromel-Alumel K-type thermocouple wires with a diameter of 0.23mm were resistance welded onto sheet steel. Excess sheet was then removed from the joint. Thermocouples were then inserted into 2mm diameter drilled holes made in the aluminium alloy plate.

Chromel-Alumel, K type thermocouples were chosen to ensure rapid response of the thermocouples to temperature. Thermocouple wires were 150mm long and connected to 1.58mm extension grade wire using male/female type thermo connectors. The

extension wire was then connected to a Data Scan 7220 RS 629-415, 16 Channel Measurement Processor, Figure 69.

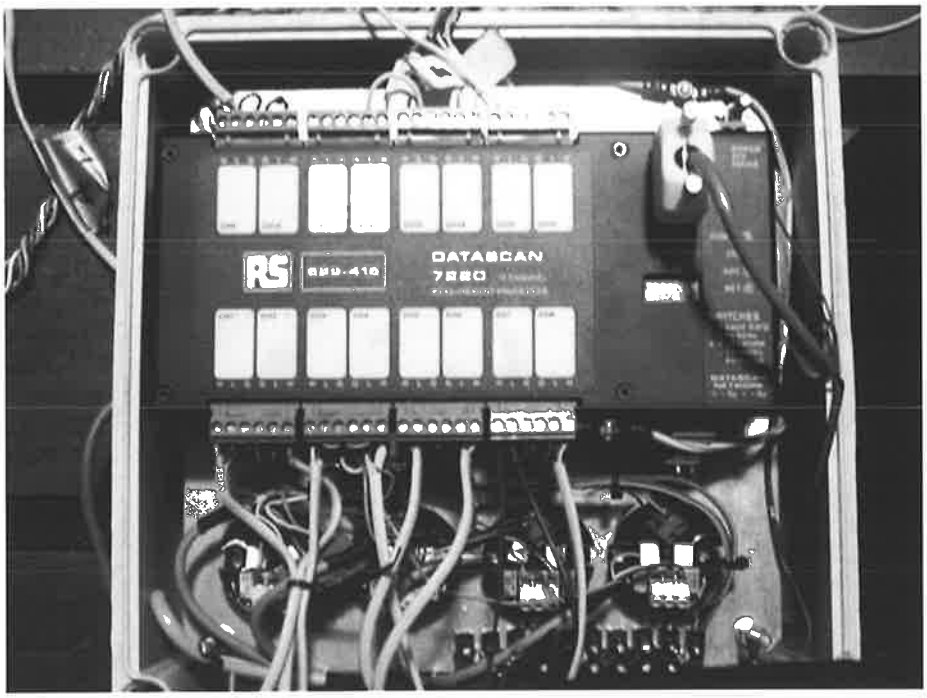

Figure 69 Data Scan 7220 RS 629-415 Recorder

The Data Scan Recorder has a sampling rate of 40Hz. The unit averages the sampled data set (40 samples per second) and then sends this sample average to the PC, where it is recorded.

The second method of temperature measurement employed during the weld investigation involved the use of an instrumented tool developed by the author. Type K, 1.5mm diameter, MIT-S MIMS thermocouples, (sheathed in a stainless steel casing), with standard type insulated junction were placed into the type 2 FSW tool (3 in the pin and one in the shoulder, Figure 70. The tool was then used in conjunction with the 0.23mm K type thermocouples embedded in the weld material to allow for comparison of tool temperature with that recorded for the workpiece material.

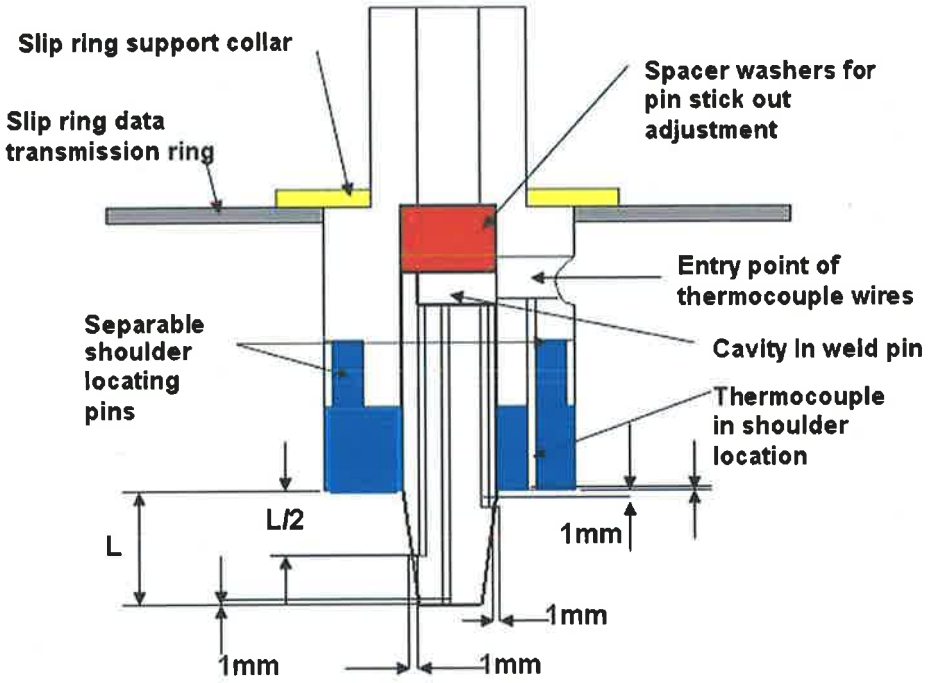

Figure 70 Schematic of Type 2 FSW tool showing location of thermocouple sites. A technical drawing of the tool can be found in Appendix A.

Temperature readings obtained using the instrumented tool were transferred from the tool embedded thermocouples to the RS Data Scan unit via copper brushes which made contact with copper grooves contained on the underside of the slip ring, Figure 71. The data was then sent to the PC where it was stored for access and processing.

Figure 71 shows the tool holder, the underside of the slip ring containing grooves where the cooper brushes make contact and the thermocouples used to measure the tool temperature. Figure 72 depicts the general assembly as used during welding.

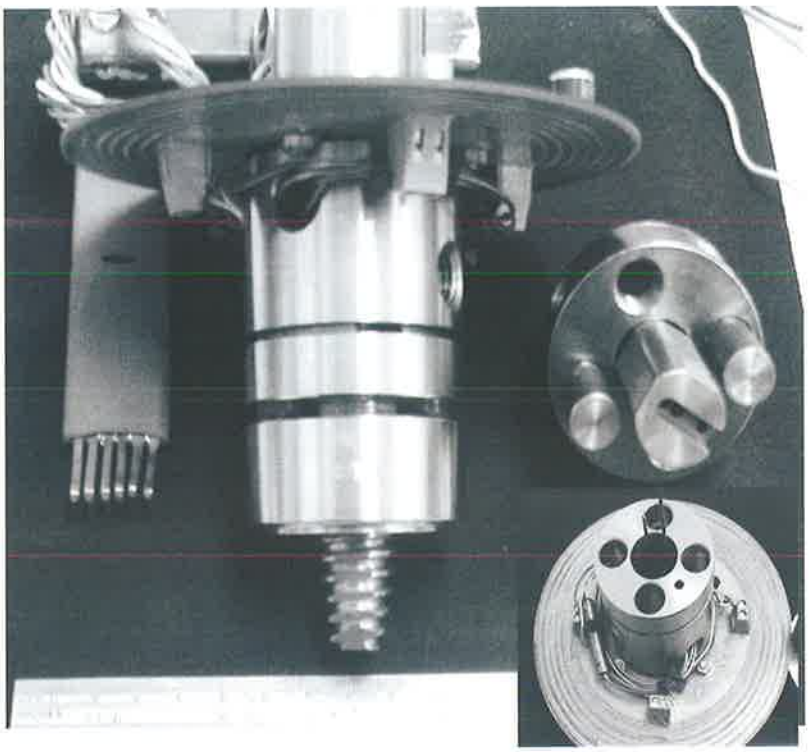

Figure 71 Type 2 FSW tool and slip ring assembly.

Figure 72 Type 2 FSW tool with combined instrumentation. Note the plate clamping arrangement for use with load cell when measuring welding load.

The instrumented tool required a power supply providing a voltage (approx. 15 Volts) to four A/D 597 set point controllers carried on the slip ring (refer Appendix B). Thermocouples embedded in the welding tool under the influence of heat modify the input voltage (rather like resistors). This voltage signal was then outputted to the Data Scan 7220 RS 629-415 unit via the copper brushes which make contact with the slip ring.

Calibration of the slip ring and thermocouples was undertaken to gauge the accuracy of temperature measurement. The test revealed a temperature gain of only 3°C at 250°C which increased to 11°C at 500°C over the four thermocouples. The temperature gain was put down to a difference in the junction point material between thermocouple and slip ring connectors.

Initially the data collected using the instrumented tool could not allow for the measurement of temperature fields during tool plunge. This was because the arm carrying the slip ring brushes was rigidly fixed. Temperature measurements were therefore performed only when the copper brushes made contact with the slip ring. This however only occurred when most of the tool plunge distance had been traversed and thus excluded valuable information concerning transient temperature fields during most of tool plunge. The problem however, was overcome by designing a spring loaded pivot arm as can be seen in Figure 73 and Figure 74.

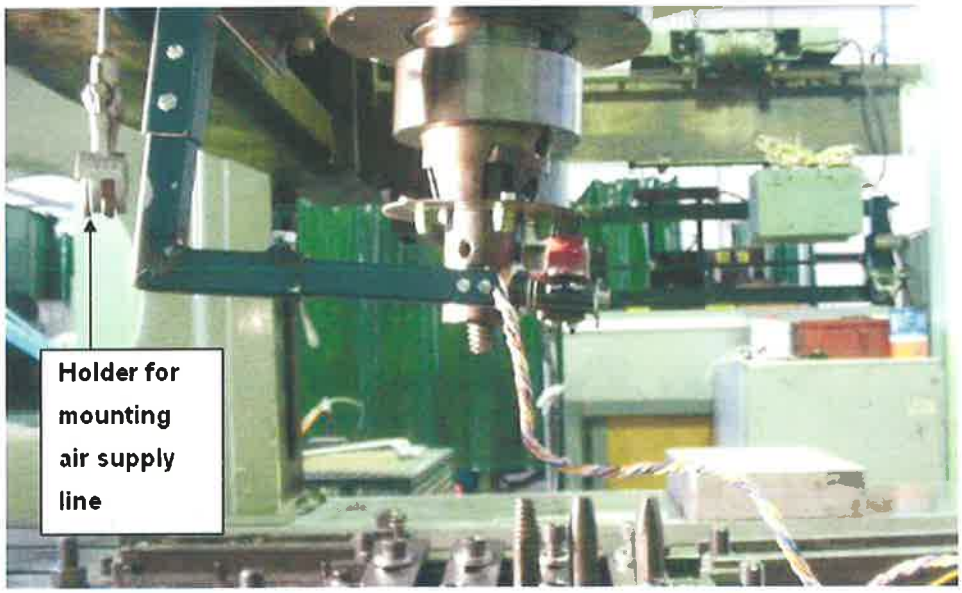

Figure 73 Type 2 FSW tool as mounted in spindle with slip ring and brushes in contact with the slip ring.

Note: In order to avoid overheating of the A/D 597 set point controllers carried by the slip ring, air was blown over the unit. To further reduce heat transfer to the slip ring insulation was also used between the slip ring and the slip ring support collar.

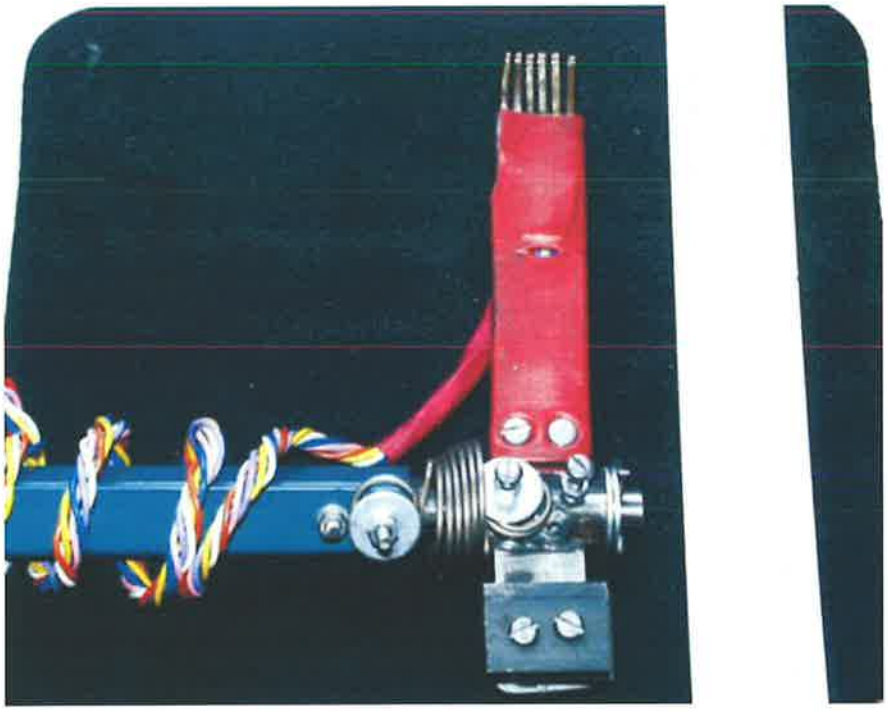

Figure 74 Pivot mechanism employed for the arm supporting the brushes. This enabled the brush arm to make continuous contact with slip ring over the entire tool plunge distance.

3.6.2 Load Measurement

Traverse or weld travel direction load was measured using a load cell and the plate clamping arrangement as can be seen in Figure 75 and Figure 76. A 5-ton load cell was mounted between an angle iron brace which was bolted firmly to the Test Bed table. The workpiece holder was mounted in a cradle supported by steel rods. These rods enabled movement of the workpiece holder in the direction of tool traverse. Vertical movement of the plate however, was restrained by application of small plates placed on either side of the workpiece holder which restricted vertical movement.

Figure 75 Top view of the load measurement assembly.

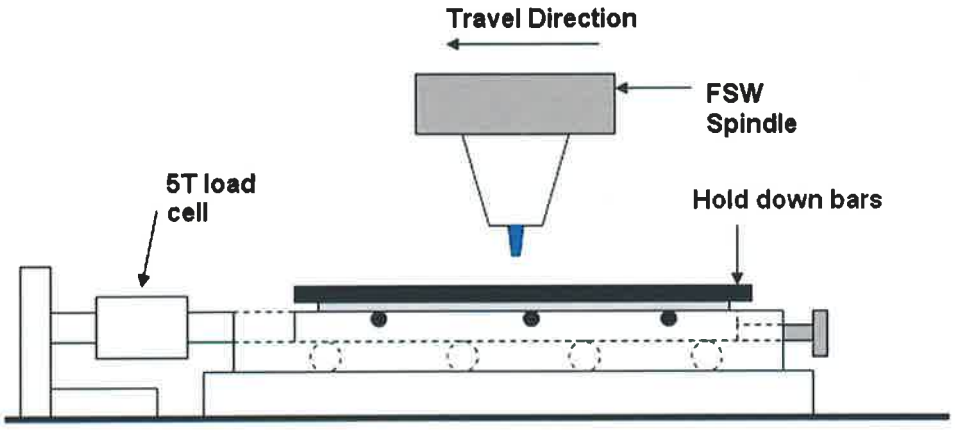

Figure 76 Schematic of the load measurement assembly (side view)

Plates were mounted in the clamping fixture. The load cell was then placed under compression during welding and load cell readings (kg) were continuously recorded on the PC connected to the Friction stir Test Bed.

4. EXPERIMENTAL

In order to define the experimental program it is important to recall what the objectives of this thesis are;

Objective 1. Determine a range of FSW parameters capable of successfully joining 12.5mm thick 5083 H111 and 7075 T651 aluminium alloys.

Objective 2. Determine how tool pin form i.e. pin profile influences welding temperatures, welding forces and weld formation when FSW 12.5mm and 25mm thick 5083 H111 and 12.5mm thick 7075 O and T651 aluminium alloys.

Objective 3. Design a FSW tool pin and demonstrate the feasibility of joining a dissimilar 5083 H111 to 7075 T651 aluminium alloy friction stir weld, for a material thickness of 12.5mm.

The essence of the three objectives as listed above are to design and fabricate a FSW tool pin and establish welding conditions such that 12.5mm and 25mm thick 5083 H111 and 12.5mm thick 7075 T651 alloys can be successfully friction stir welded.

In order to achieve these objectives it will be necessary to firstly determine the load vs. deflection characteristics of the spindle and its associated support structure. The literature review made it clear that it was essential when FSW that the tool shoulder remain in intimate contact with the surface of the workpiece. Axial loads in particular could be expected as high as 60kN. Measurements were therefore necessary to determine the load vs. deflection characteristics of the spindle and support beam. A calibration plot can be found in Figure 56. This plot will be useful in determining the level of adjustment required during plunge to intimately seat the tool shoulder into the surface of the workpiece as well as giving an estimation of the axial force required to produce the weld.

FSW tools need to be designed and fabricated. The literature review was extremely useful in giving guidance as to the basic shape of the tool pin (conical); however the question remained as to what form the thread profiles should take. The literature review again made it clear that the pin required threads and that these threads needed to function like a screw extruder, firstly to transport thermally softened workpiece material

vertically, and secondly to maximise material flow between each thread thereby helping to prevent clogging of the thread forms, particularly at the higher rubbing velocities i.e. above 0.2m/sec for the pin and 0.5m/sec for the shoulder. Hence the thread pitch should be large.

Two FSW pin profiles CT1 and CT2 were fabricated for investigation. A 14mm diameter pin was to be used to friction stir weld the 12.5mm thick alloys while a 20mm diameter pin was to be used when FSW the 25mm thick 5083 alloy. The investigation centred around determining to what extent the thread forms (CT1 conical and threaded and CT2 conical, threaded with three flats) influenced heat generation, welding forces, power requirements of the FSW machine, specific weld energy and weld formation when FSW the 5083 and 7075 aluminium alloys.

In relation to temperature measurements very little information could be found in the open literature concerning heat generation at the tool / workpiece material interface. In an attempt to accurately assess the temperature profiles as near as possible to this interface a FSW tool was designed and fabricated to accommodate both the 20mm diameter CT1 and CT2 pin forms such that tool temperatures could be measured in several locations; three in the FSW pin and one in the tool shoulder. These temperatures were to be compared to those measured in the workpiece material.

To validate the findings both in relation to the tool designs and processing conditions it was decided to prove the optimum FSW tool pin form by producing firstly a 2 metre long single pass friction stir butt weld in 25mm thick 5083 H111 aluminium alloy. This was to be followed by a dissimilar alloy friction stir weld combining the 5083 H111 and 7075 T651 alloys in 12.5mm of thickness.

The following experimental investigations were conducted firstly to examine the effect welding parameters such as tool position had on weld formation. Tool pin geometry was then examined in relation to its effects on processing temperatures and welding forces i.e. force in the direction of weld travel when FSW 5083-H111, 7075-O and T651 aluminium alloys whose material thickness ranged between 12.5 and up to 25mm.

Welds are identified in terms of aluminium alloy, temper, plate thickness, joint type, tool geometry, tool tilt and rotation as well as weld travel speed. All welds were performed using the Butler Friction Stir Welding Test Bed and as such a number was recorded

against each weld. For brevity only the last three digits and a letter of the alphabet identifying weld sequence has been used to identify each weld.

4.1 Weld Formation In Response To Tool Shoulder Position When FSW 12.5mm Thick AA5083 H111

Table 4-1 summarises the parameters used to produce three B.O.P. welds in 12.5mm thick alloy 5083. The welds were produced using tool pin CT1-14: conical and threaded in conjunction with concave shoulder: 30Cc14 under identical welding parameters with the exception that tool shoulder penetration depth into the surface of each workpiece varied over approximately 1mm between the maximum and minimum penetration depth.

Al Alloy	Temper	Pin Stick Out [mm]	Weld Type.	Weld No.	FSW – Process Parameters						
					Tool Type	Tool Tilt [°]	Plunge [RPM]	Plunge Rate 1 [mm/min]	Plunge Rate 2 [mm/min]	Weld [RPM]	Max. Travel Speed [mm/min]
5083	*H111*	*11.7*	*BOP*	*313B*	*CT1-14 30Cc14*	*3*	*300*	*5*	*5*	*350*	*100*
5083	*H111*	*11.7*	*BOP*	*614C*	*CT1-14 30Cc14*	*3*	*300*	*5*	*5*	*350*	*100*
5083	*H111*	*11.7*	*BOP*	*614D*	*CT1-14 30Cc14*	*3*	*300*	*5*	*5*	*350*	*100*

Table 4-1 Weld parameters B:O:P: welds 313B, 614C and 614D. Note 14 = pin diam.

In all cases the tool pin rubbing velocity as calculated for the pin shank diameter employing equation 1, section 2.10 was 0.26m/sec for the 14mm diameter pin and 0.55m/sec for the 30mm diameter shoulder.

4.2 Temperature, Torque And Load Measurement When FSW 12.5mm Thick Al Alloys 5083 and 7075

Table 4-2 identifies the FSW parameters used to compare torque (spindle motor torque), weld force (in the direction of welding) and thermal cycles as measured by workpiece embedded thermocouples when FSW 12.5mm thick aluminium alloys 7075-O and 7075-T651.

Al Alloy	Temper	Pin Stick out [mm]	Weld Type.	Weld No.	FSW – Process Parameters						
					Tool Type	Tool Tilt [°]	Plunge [RPM]	Plunge Rate [mm/min]	Dwell [sec.]	Weld [RPM]	Travel Speed [mm/min]
7075	*O*	*11.7*	*BOP*	*614A*	*CT1-14 30Cc14*	*3*	*300*	*15*	*5*	*350*	*30, 60, 90,100*
7075	*T651*	*11.7*	*BOP*	*614B*	*CT1-14 30cc14*	*3*	*300*	*15*	*5*	*350*	*30, 60, 90,100*
7075	*O*	*11.7*	*BOP*	*614F*	*CT1-14 30Cc14*	*3*	*450*	*15*	*5*	*350*	*30, 60, 90,100*
7075	*T651*	*11.7*	*BOP*	*615A*	*CT1-14 30cc14*	*3*	*450*	*15*	*5*	*350*	*30, 60, 90,100*
7075	*O*	*11.7*	*BOP*	*615D*	*CT1-14 30Cc14*	*3*	*450*	*15*	*5*	*350*	*30, 60, 90*
7075	*T651*	*11.7*	*BOP*	*615E*	*CT1-14 30cc14*	*3*	*450*	*15*	*5*	*350*	*30, 60, 90*
7075	*O*	*11.7*	*BOP*	*615K*	*CT1-14 30Cc14*	*3*	*450*	*15*	*5*	*350*	*30, 60, 90*
7075	*T651*	*11.7*	*BOP*	*615L*	*CT1-14 30cc14*	*3*	*450*	*15*	*5*	*350*	*30, 60, 90*

Table 4-2 Weld parameters employed for the FSW of 12.5mm thick aluminium alloys 7075-O, 7075-T651.

Note the travel speed as appears in Table 4-2 was conducted over the length of a single weld. In all cases the weld length was 160mm with the first 10mm of weld length programmed for 30mm/min of weld travel speed. This was followed by a weld length of 50mm at 60, 90 and then 100mm/min. In the case of welds 615D, 615E, 615K and 615L above, the weld length for the weld travel speed of 90mm/min measured 100mm.

4.3 Process Loads And Weld Temperature Relationships When FSW 12.5mm Thick Aluminium Alloys 5083 H111 & 7075 T651 Using A Conical Threaded Pin, CT1-14 vs. Conical Threaded Pin With 3 Flats, CT2-14.

Table 4-3 summarises the welding parameters used in the production of friction stir butt welds in 12.5mm thick aluminium alloys 7075-T651 and 5083-H111. Unlike the welds produced in Table 4-2 all welds were performed for a single weld travel speed of 60mm/min.

Al Alloy	Temper	Pin Stick out [mm]	Weld Type.	Weld No.	FSW – Process Parameters						
					Tool Type	Tool Tilt [°]	Plunge [RPM]	Plunge Rate [mm/min]	Dwell [sec.]	Weld [RPM]	Travel Speed [mm/min]
7075	*T651*	*11.7*	*Butt*	*403A*	*CT1-14 30Cc14*	*3*	*450*	*15*	*5*	*300*	*60*
7075	*T651*	*11.7*	*Butt*	*403B*	*CT2-14 30Cc14*	*3*	*450*	*15*	*5*	*300*	*60*
7075	*T651*	*11.7*	*Butt*	*403C*	*CT1-14 30Cc14*	*3*	*450*	*15*	*5*	*450*	*60*
7075	*T651*	*11.7*	*Butt*	*403D*	*CT2-14 30Cc14*	*3*	*450*	*15*	*5*	*450*	*60*
5083	*H111*	*11.7*	*Butt*	*405A*	*CT1-14 30Cc14*	*3*	*450*	*15*	*5*	*300*	*60*
5083	*H111*	*11.7*	*Butt*	*405B*	*CT2-14 30Cc14*	*3*	*450*	*15*	*5*	*300*	*60*
5083	*H111*	*11.7*	*Butt*	*405C*	*CT1-14 30Cc14*	*3*	*450*	*15*	*5*	*450*	*60*
5083	*H111*	*11.7*	*Butt*	*405D*	*CT2-14 30Cc14*	*3*	*450*	*15*	*5*	*450*	*60*

Table 4-3 Weld parameters employed for the FSW of 12.5mm thick aluminium alloys 5083-H111, 7075-T651. Note CT1 = Conical threaded pin no flats, CT2 = Conical threaded pin with flats

4.4 A Comparison Of Temperature Evolution When FSW Using Tool And Workpiece Embedded Thermocouples

Table 4-4 summarises the welding parameters used when measuring temperature and spindle motor torque for the FSW of thick section (25mm thick) aluminium alloy 5083-H111.

The location of the material embedded thermocouples is illustrated in Figure 68, Chapter 3. Tool embedded thermocouples are illustrated in Figure 70, Chapter 3.

Al Alloy	Temper	Pin Stick out [mm]	Weld Type.	Weld No.	FSW – Process Parameters						
					Tool Type	Tool Tilt [°]	Plunge [RPM]	Plunge Rate [mm/min]	Dwell [sec.]	Weld [RPM]	Travel Speed [mm/min]
5083	*H111*	*20*	*Butt*	*215B*	*CT1-20 50CR20*	*3*	*350*	*5*	*10*	*200*	*50*

Table 4-4 Weld parameters employed while FSW 25mm thick 5083-H111 for the purpose of temperature measurement.

Table 4-5 summarises the welding parameters used when measuring temperature in the FSW tool while using a two stage plunge when FSW 25mm thick aluminium alloy 5083-H111.

Al Alloy	Temper	Pin Stick out [mm]	Weld Type.	Weld No.	FSW – Process Parameters						
					Tool Type	Tool Tilt [°]	Plunge [RPM]	Plunge Rate 1 [mm/min]	Plunge Rate 2 [mm/min]	Weld [RPM]	Travel Speed [mm/min]
5083	*H111*	*20*	*Butt*	*822A*	*CT2-20 50CR20*	*3*	*350*	*5*	*2*	*200*	*50*

Table 4-5 Welding parameters used for the purpose of determining plunge rates for the FSW of 25mm thick aluminium alloy 5083-H111.

4.5 Tool Plunge Depth, Weld Travel Speed And Spindle Motor Output When FSW 25mm Thick AA5083

Table 4-6 summarises the welding parameters used when investigating tool uplift while FSW 25mm thick aluminium alloy 5083-H111 with a tool pin having 3 flats.

Al Alloy	Temper	Pin Stick out [mm]	Weld Type.	Weld No.	FSW – Process Parameters						
					Tool Type	Tool Tilt [°]	Plunge RPM	Plunge Rate 1 [mm/min]	Plunge Rate 2 [mm/min]	Weld [RPM]	Travel Speed [mm/min]
5083	*H111*	*22*	*BOP*	*625A*	*CT2-20 50CR20*	*3*	*400*	*5*	*2*	*250*	*70*
5083	*H111*	*22*	*BOP*	*625B*	*CT2-20 50CR20*	*3*	*400*	*5*	*2*	*250*	*100*
5083	*H111*	*22*	*BOP*	*625C*	*CT2-20 50CR20*	*3*	*400*	*5*	*2*	*250*	*60*

Table 4-6 Weld parameter investigation to investigate the relationship between weld travel speed, tool plunge and tool uplift while FSW 25mm thick alloy 5083-H111

4.6 The Production Of A 2m Long Friction Stir Weld In 25mm Thick AA5083

Table 4-7 summarises the welding parameters used when FSW the 25mm thick aluminium alloy 5083-H111 for a weld length of 2m using the conical threaded pin with three flats.

Al Alloy	Temper	Pin Stick out [mm]	Weld Type	Weld No.	FSW – Process Parameters						
					Tool Type	Tool Tilt [°]	Plunge [RPM]	Plunge Rate 1 [mm/min]	Plunge Rate 2 [mm/min]	Weld [RPM]	Travel Speed [mm/min]
5083	*H111*	*22*	*Butt*	*716A*	*20A25.2 50CR20*	*3*	*400*	*5*	*2*	*250*	*60*

Table 4-7 Weld parameters used to investigate weld formation for a 2m long Butt weld produced in 25mm thick alloy 5083

4.7 Weld Structure Investigation For Dissimilar Al Alloy Weld

Table 4-8 summarises the weld parameters employed when FSW the 12.5mm thick dissimilar alloy (7075-T651 and 5083-H111) friction stir weld using the tool pin with 3 flats.

Al Alloy	Temper	Pin Stick out [mm]	Weld Type.	Weld No.	FSW – Process Parameters						
					Tool Type	Tool Tilt [°]	Plunge [RPM]	Plunge Rate [mm/min]	Dwell [sec.]	Weld [RPM]	Travel Speed [mm/min]
7075 *5083*	*T651* *H111*	*11.7*	*Butt*	*820A*	*CT2-14* *30Cc14*	*3*	*450*	*5*	*10*	*350*	*60*

Table 4-8 Weld parameters used to investigate extent of material mixing when FSW 12.5mm thick alloy 7075 to 12.4mm thick alloy 5083

5. RESULTS

The following sections contained within Chapter 5 present the results of the experimental investigation whose aim it was to determine weld parameters, which included identifying the tool plunge depth required to successfully weld 12.5mm and 25mm thick 5083 and 12.5mm thick 7075 aluminium alloys. In addition the experimental investigation was to determine how welding conditions i.e. tool rotation speed, tool plunge depth and tool pin form, affected weld temperature, weld forces and weld joint formation for the 5083 and 7075 alloys. Two tool pin forms were investigated for these purposes (CT1 conical, threaded and CT2 conical threaded with three flats). An appropriate welding parameter in conjunction with the best performing welding tool was then to be used to verify the results by producing a single pass friction stir butt weld in 25mm thick 5083 H111 alloy and a dissimilar 5083 H111 and 7075 T651 alloy weld in 12.5mm of plate thickness.

Results from the experimental investigation are presented both in a graphical and tabular format. A typical plot of the measurement data collected during each welding trial i.e. graphical representation of the measurement data can be found in Figure 77.

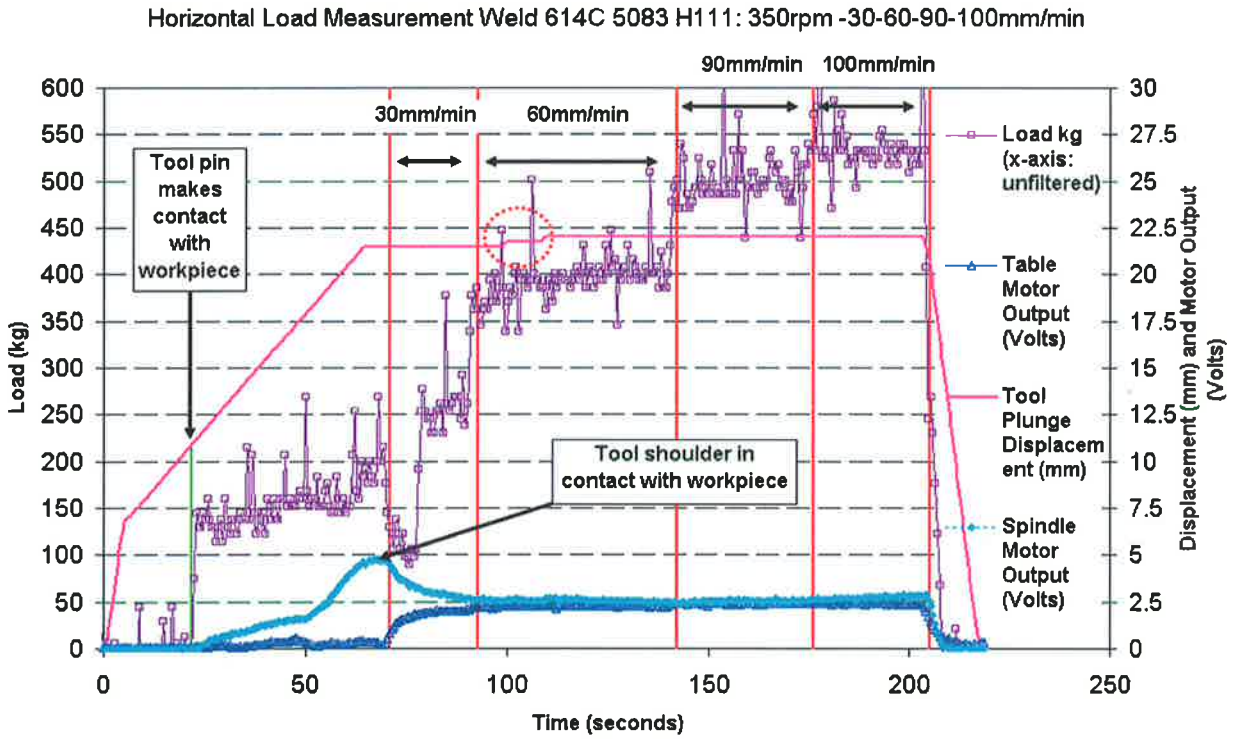

Figure 77 Motor output (spindle, table) and load as measured in the direction of weld travel in response to weld travel speed for a friction stir weld produced in 12.5mm thick 5083 H111 aluminium alloy. Note travel speed was programmed to occur for 30, 60, 90 and 100mm/min.

Figure 77 is representative of load (kg), tool plunge displacement (mm) and motor output (Volt) measurement data collected while FSW a 12.5mm thick 5083 H111 aluminium alloy. The load measurement was recorded using the setup described in section 3.6.2 of Chapter 3 and schematically presented in Figures 75 and 76.

The data plot, Figure 77 indicates that the tool was positioned a small distance (approximately 10.5mm) above the workpiece prior to being plunged. This is substantiated by the fact that both the load and spindle motor output increase as a result of the tool pin making contact with the surface of the workpiece. There after it can be seen that both steadily rise until a peak is reached. This peak corresponds to the tool shoulder having made contact with the surface of the workpiece. Shortly after the peak spindle motor output declines as the workpiece material softens and weld traverse is initiated i.e. weld travel of the tool through the join begins. Correspondingly there is an increase in table motor output, Figure 77.

The weld travel speed used in the production of all friction stir welds in sections 5.1 and 5.2 is given in Table 5-1 below.

Weld Speed (mm/min)	Speed (mm/sec)	Length of travel (mm)
30	*0.50*	*10*
60	*1.00*	*50*
90	*1.50*	*50*
100	*1.67*	*Remainder of weld length*

Table 5-1 Weld travel speed parameters used to produce all welds presented in sections 5.1 and 5.2. Note the minimum weld length was 160mm.

For all subsequent friction stir welds, sections 5.3 through to 5.7 a single weld travel speed was initiated. This weld travel speed is indicated for each weld in the relevant sections of the results. It should be noted that Figure 77 also includes the results of load as measured in the direction of weld travel. This load fluctuates somewhat over the range of weld travel speeds investigated. The fluctuation occurred primarily because of two factors; natural oscillation of the welding tool during FSW and because of a small tolerance between the guides, rollers and end stop of the cradle supporting the load measurement table, onto which the workpiece was mounted. The fluctuation in load was more notable in the measurements conducted for welds produced in sections 5.1 and 5.2

simply because of the step wise initiation of the various weld travel speeds, which occurred during the production of each friction stir weld. This problem was not encountered for load measurements in welds produced in section 5.3 simply because a single weld travel speed was initiated throughout the entire weld length.

5.1 FSW 12.5mm Thick AA 5083 H111: The Initial Weld Formation Investigation

The objective of the investigation, presented here in section 5.1, was to determine if the FSW tool pin CT1-14, designed by the author was capable of producing defect free welds in 12.5mm thick AA5083 H111 and to gauge the reproducibility of the FSW process given a constant set of welding parameters. The weld parameters consisted of a rotation speed of 350 rpm and a peak weld travel speed of 100mm/min. The tool pin employed during welding can be seen in Figure 78. This tool pin was used in conjunction with a 30mm diameter concave profiled tool shoulder 30Cc14. The tool was tilted away from the direction of weld travel by 3°.

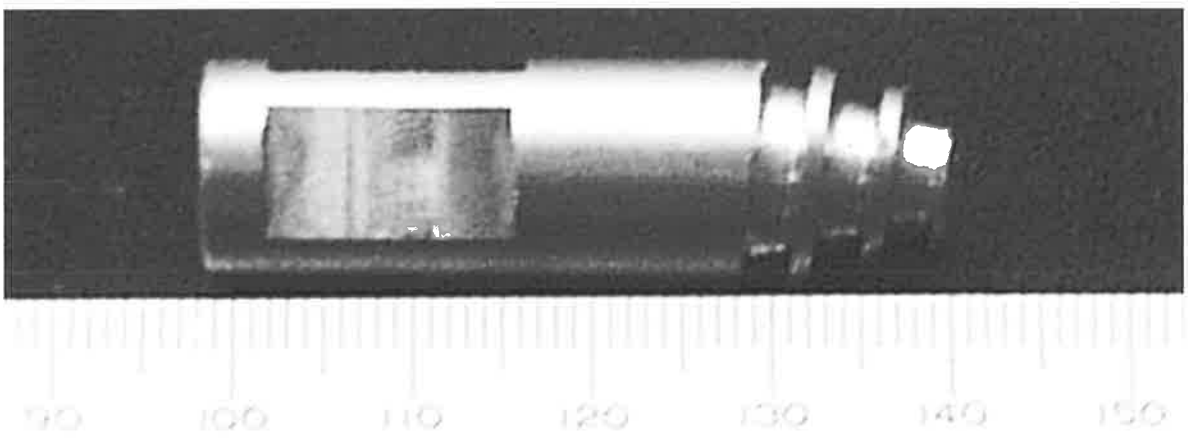

Figure 78 Tool pin CT1-14: conical and threaded pin, with no flats. This tool pin was used in conjunction with tool shoulder 30Cc14: concave 30mm diameter shoulder.

Three welds were produced. These welds are identified as welds 313B, 614C and 614D. Of the three friction stir welds only weld 313B could be considered to be free from defect, Figures 79 and 80. Welds 614C and 614D on the other hand suffered from volumetric defects in the form of open running voids. These were clearly visible from visual examination of the surface of each workpiece. The largest void was produced for weld 614D, Figure 81.

Figure 79 Weld 313B - top view

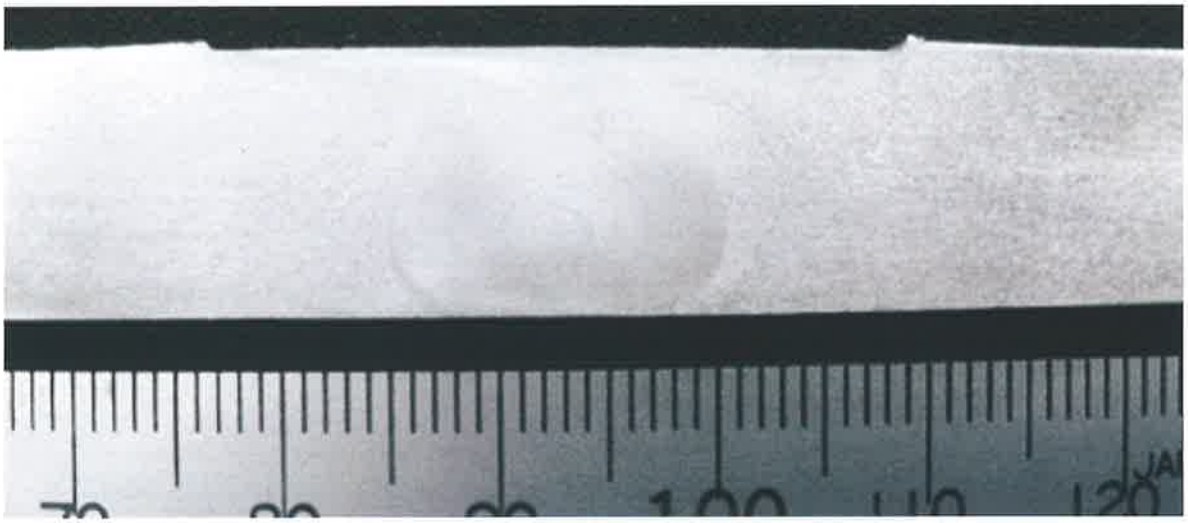

Figure 80 Weld 313B – transverse to the weld travel direction

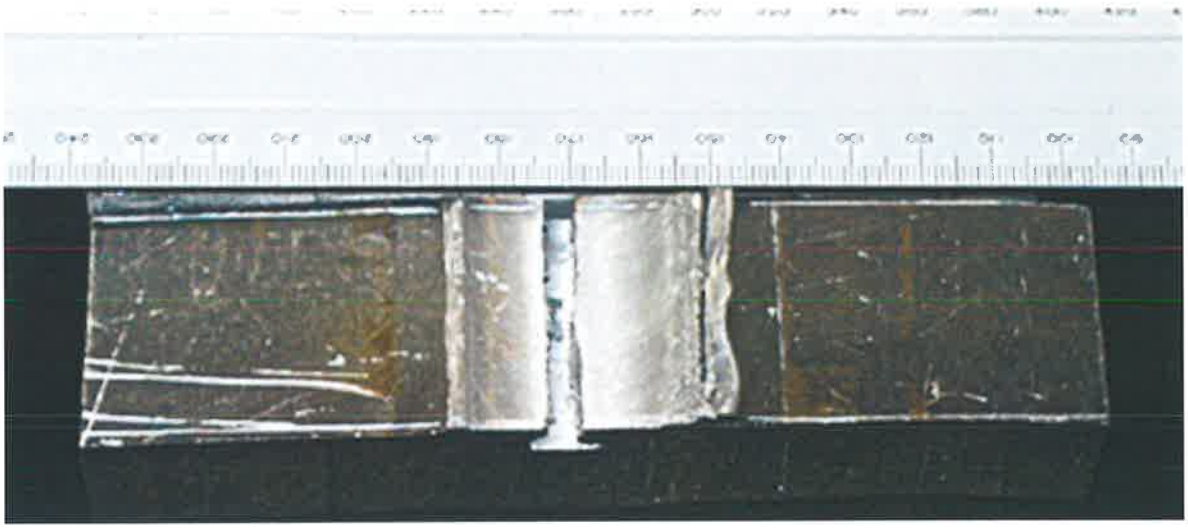

Figure 81 Weld 614D – top view demonstrating a large surface breaking cavity

Although all three welds 313B, 614C and 614D were produced using the same set of welding parameters it was found when comparing the spindle motor output, weld load in the direction of tool travel and tool plunge depth that weld 313B was considerably different from subsequent welds 614C and 614D. The variation in spindle motor output between the three welds is presented in Figure 82.

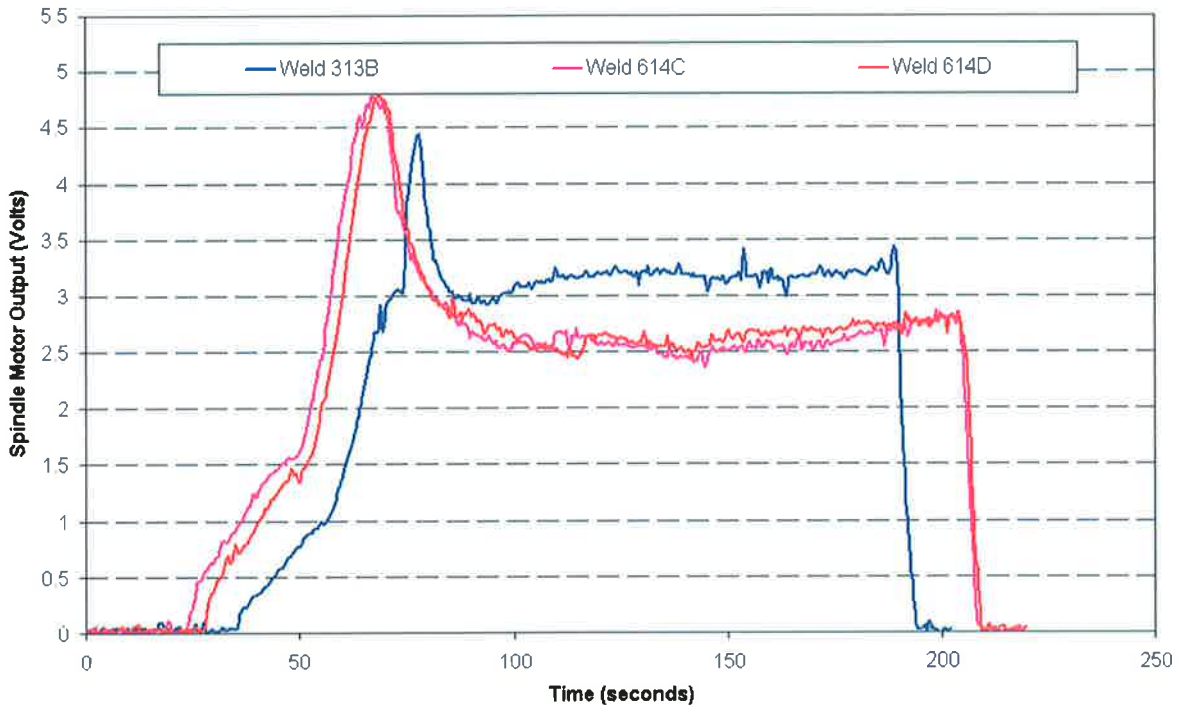

Figure 82 Spindle motor output as measured for welds 313B, 614C and 614D.

Figure 82 indicates that spindle motor output was largest for weld 313B. No discernable difference however could be observed in the spindle motor output between welds 614C and 614D.

Although there may have been no real difference in the spindle motor output between welds 614C and 614D this could not be said of the load as measured in the direction of weld travel. Load was measurably smaller for weld 614D (the weld possessing the larger volumetric defect), Figure 83.

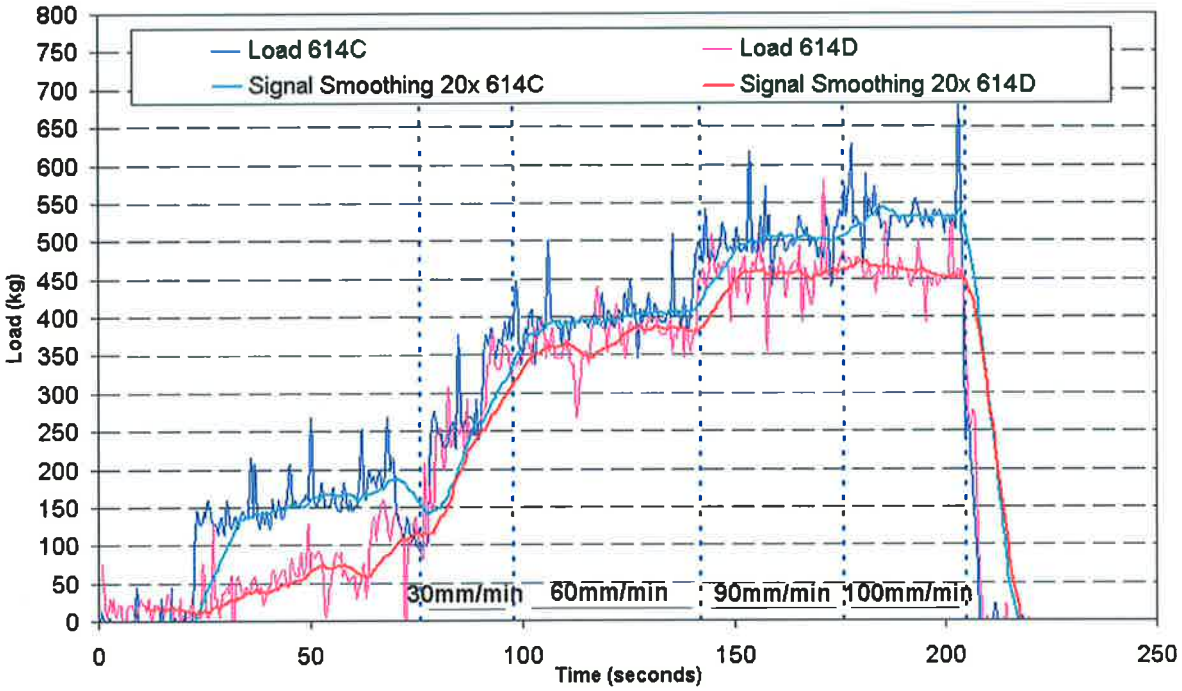

Figure 83 Load in the direction of weld travel for welds 614C and 614D. Note welding speed did not greatly alter the load measured between 60-90mm/min.

When a comparison was made between the plunge depth of the tool for each weld, Figure 84 it could clearly be seen that weld 313B had the greater plunge travel distance and thereby penetration depth in comparison to welds 614C and 614D. It should be noted however that the tool first made contact with the workpiece after 20 seconds of initiation of each weld program. Figure 84 indicates that after the initial 20 seconds the tool has been plunged by 10mm for both welds 614C and 614D and 9.5mm for weld 313B. Table 5-2 summarises the true plunge displacement of the tool in relation to the overall plunge depth.

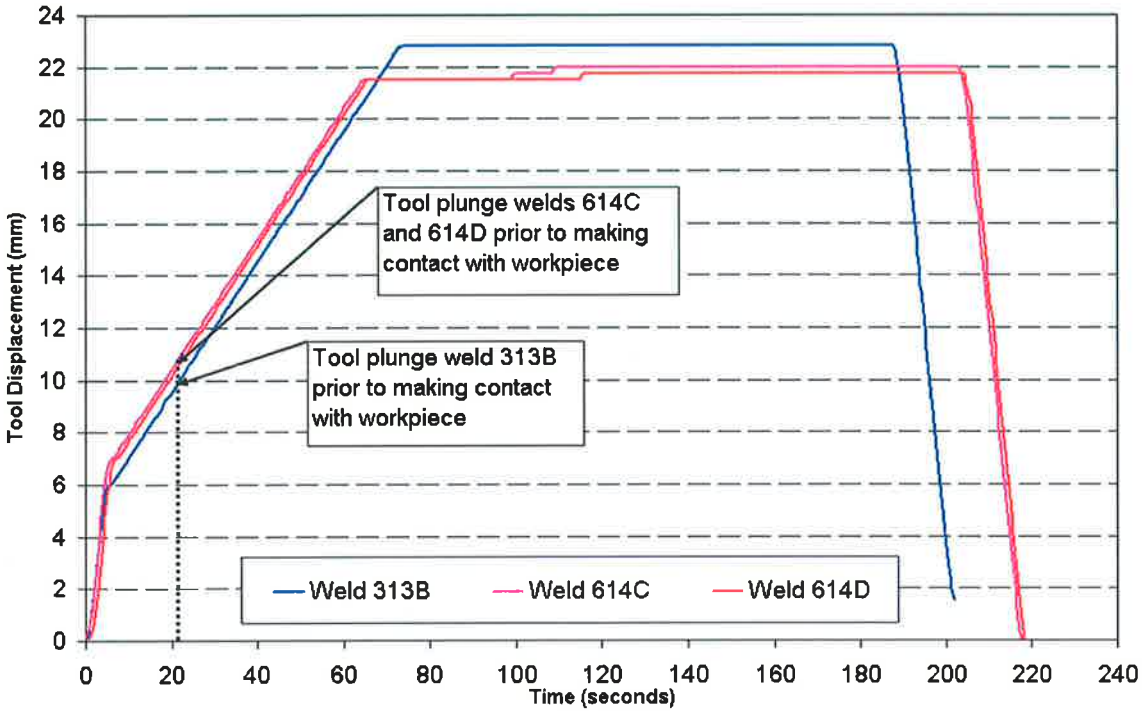

Figure 84 Tool plunge displacement for welds 313B, 614C and 614D. Note the vertical line at 20 seconds into the weld indicates tool plunge distance at the time the FSW tool first made contact with the workpiece. Note also the steps in the plots for tool displacement depth, welds 614C and D were an attempt during FSW to plunge the tool further into the workpiece.

Weld No.	Pin Stick out (mm)	Overall Plunge Displacement (mm)	Plunge Displacement to Workpiece (mm)	Plunge Depth Compensation Into Workpiece (mm)
313B	*11.7*	*22.8*	*10*	*1.1*
614C	*11.7*	*22*	*10.75*	*-0.45*
614D	*11.7*	*21.7*	*10.75*	*-0.75*

Table 5-2 Plunge depth in relation to plate thickness for friction stir welds 313B, 614C and 614D. Note welds 614C and 614D are negative values indicating insufficient plunge.

Table 5-2 indicates that for weld 313B, which contained no defect, there was a difference of 1.1mm between the pin stick out and the actual plunge depth into the workpiece i.e. Plunge Depth into Workpiece minus Pin Stick out. Although the pin stick out measured 11.7mm and the workpiece thickness was 12.5mm, hence a difference of 0.8mm, a plunge of 1.1mm did not result in the pin making contact with the backing bar. For this not to have occurred there must have been some vertical deflection which allowed for an uplift of the tool.

Both welds 614C and 614D suffered from a surface breaking volumetric defect. This defect occurred primarily because both tools were inadequately plunged into their respective workpieces. A measure of the difference between the pin stick out and plunge depth into workpiece, Table 5-2 reveals that weld 614C lacked 0.45mm of plunge in order to achieve a plunge equivalent to the pin stick out, where as weld 614D lacked 0.75mm. Plunge depth or rather the lack of shoulder contact with the surface of the workpiece appeared to be a key factor in determining whether a sound or defective weld formed when FSW the aluminium alloy 5083 using the tool pin CT1-14 in conjunction with the tool shoulder 30Cc-14.

Figure 56 of section 3.3, Chapter 3 indicates that the spindle and associated support structure will deflect vertically under sufficient axial loading. Although weld 313B, Figure 79 developed some flash it can also be seen that the through thickness of the workpiece approximates that of the original parent material, Figure 80. Taking into account that weld 313B was produced with 1.1mm of over penetration compared to the pin stickout, this would indicate from Figure 56 that a vertical load of between 2000 and 3000kg (20 to 30kN axial force) had been generated during FSW. Note the value of the force was calculated by multiplying the deflection load (kg) by acceleration (gravitational constant). The defects observed in welds 614C and 614D had occurred simply because there had been insufficient down force acting on the workpiece, brought about by a lack of plunge depth into the surface of the workpiece.

5.2 Process Loads, Spindle Motor Output, Weld Power and Weld Energy Relationships When FSW 12.5mm Thick Aluminium Alloy 7075-O and T651 Using The Conical And Threaded Pin CT1-14

In section 5.2 of the results measurements for weld load in the direction of weld travel and spindle motor output were compared for defect free welds produced in 12.5mm thick aluminium alloy 7075 under two temper conditions, T651 (peak hardened, artificially aged) and O (annealed). The spindle motor output for all welds (Volts) was then converted to reflect spindle motor torque (Nm) and these values used to calculate weld power (Watts) for the investigated welds.

All welds were performed using the CT1-14 welding tool pin as was used in section 5.1, and depicted in Figure 78. This pin was coupled to the concave tool shoulder 30Cc14 where a tool rotation speed of 350rpm and an incrementally increasing travel speed starting at 30mm/min and terminating at 100mm/min was employed. The initiation of weld travel speed was identical to that which had been employed and summarised in Table 5-1 of section 5.1.

A series of nine welds was investigated. These welds are identified in Table 5-3.

Al Alloy	Temper	Weld No.
7075	*O*	*614A*
7075	*T651*	*614B*
7075	*O*	*614E & 614F*
7075	*T651*	*615A*
7075	*O*	*615D*
7075	*T651*	*615E*
7075	*O*	*615K*
7075	*T651*	*615L*

Table 5-3 Weld material temper and weld number designation.

The data plot for the initial weld 614A, Figure 85, produced in the 7075 O tempered alloy was performed to calibrate tool plunge depth. Figure 85 shows that "Tool Plunge Displacement" was activated during welding i.e. during the time Table Motor Output was greater than zero. Initiation of tool plunge during weld travel was performed because the

programmed plunge depth had not provided for sufficient contact between tool shoulder and the surface of the workpiece i.e. the shoulder could physically be seen to riding slightly higher than the surface of the workpiece.

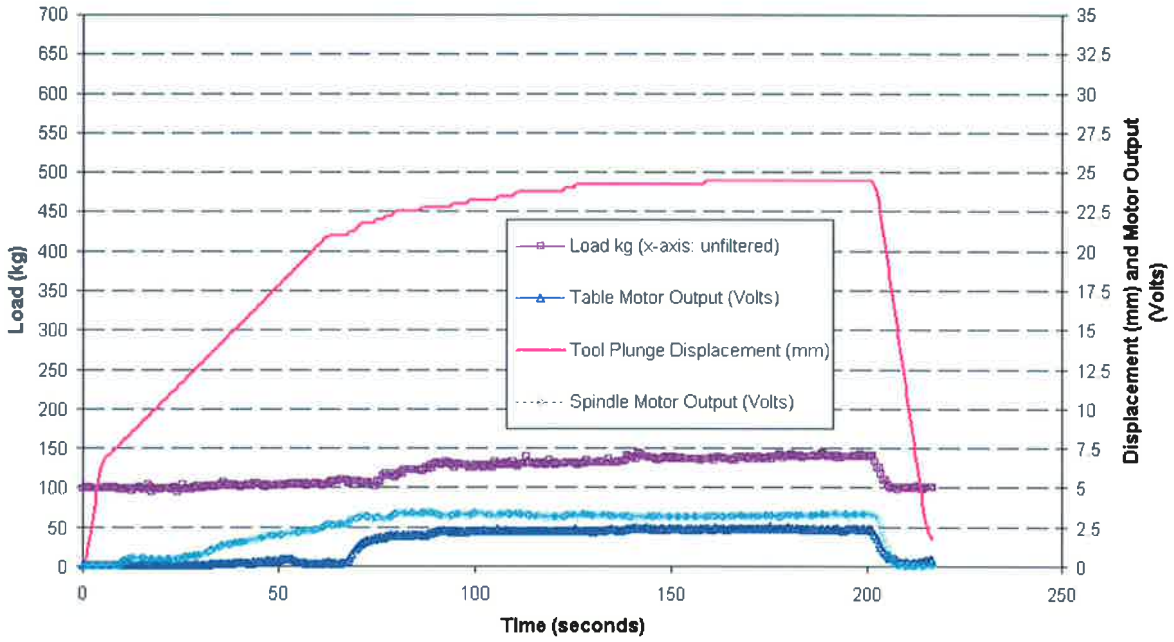

Figure 85 Load, tool displacement and motor output plot for weld 614A, AA7075 O. Note it was necessary to plunge the tool during welding to seat the tool shoulder onto the surface of the workpiece.

It should also be noted that weld 614A was conducted while using the load measurement table, as described in section 3.6.2 of Chapter 3. FSW was performed with the load cell slightly pre-tensioned. This was achieved by tightening the grub screw, at the rear of the measurement table and then releasing this screw once weld travel was initiated. The reason for pre-tensioning was to minimise load fluctuation during plunging of the tool. It was observed during the production of the welds, section 5.1 that once the tool pin made contact with the workpiece there was a tendency for the table supporting the workpiece to move backwards and forwards until the pin had penetrated the surface of the workpiece i.e. by some 1 to 2mm. From the shape of the load plot, Figure 85, particularly the flat profile prior to commencement of weld travel it is possible that too much tensioning may have restricted movement of the table against the load cell during FSW and thus was responsible for the relatively low and desensitised load measurement data. For this reason it was decided for all subsequent welds not to over tension and immediately release the grub screw once plunge was completed.

The calibration for tool plunge was again attempted via a second weld, 614B. This was conducted for the 7075 alloy but in the T651 temper condition. The measurement data from this weld is presented in Figure 86.

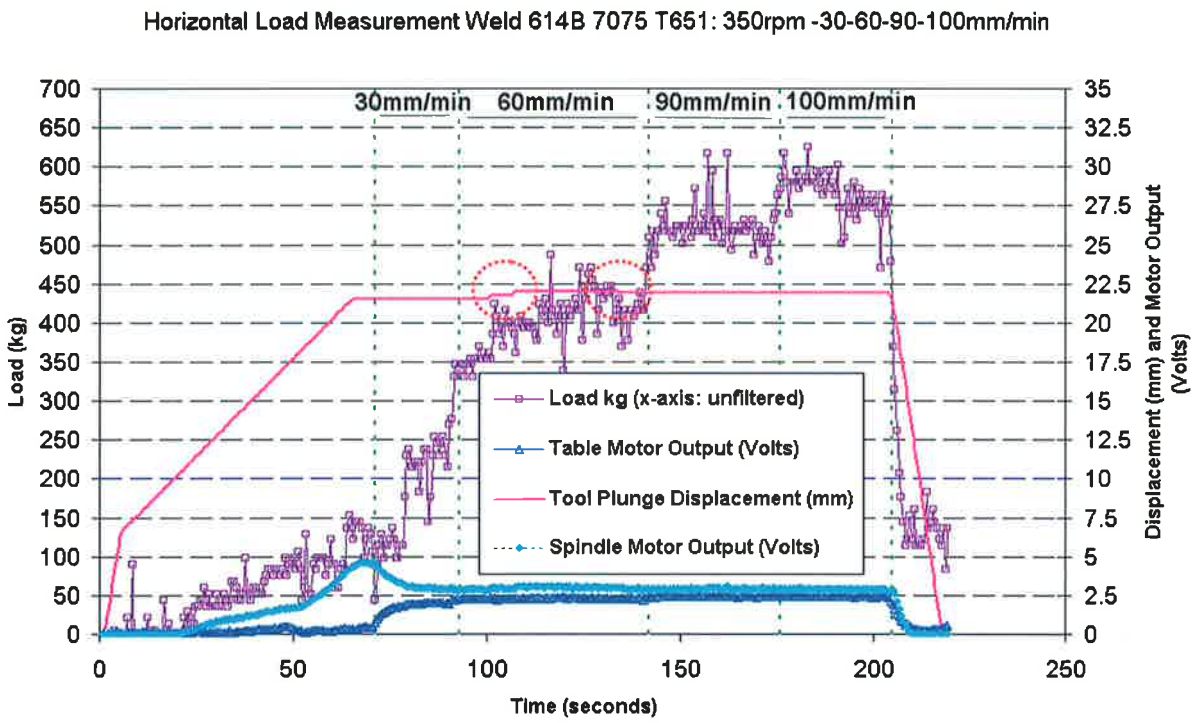

Figure 86 Load, tool displacement and motor output plot for weld 614B, AA7075 T651. Note during welding the tool was further plunged (circled region) into the workpiece.

Weld 614B was performed using the same welding parameters as were used to produce weld 614A. In both cases the welds suffered from surface breaking voids, which appeared directly after activation of weld travel, and which could not be healed by means of further plunging of the tool during weld traverse.

Although the results of welds 614A and 614B indicated that considerable differences existed in the weld load as measured in the direction of weld travel, the fact that the tool plunge displacement varied between both welds suggested that this may have influenced the outcome of the results. As such two further welds 614F and 615A were produced for the alloy 7075 in both the O and T651 temper conditions. These welds all shared a rotation speed of 350rpm and an incrementally increasing weld travel speed starting at 30mm/min, which then increased to 60, then 90 and finally 100mm/min. The welds were performed using the CT1-14 pin in conjunction with the concave shoulder 30Cc14. Tool tilt measured 3° away from the direction of weld travel.

Figures 87-88 demonstrate that an overall tool plunge displacement of 22mm was used in the production of both welds 614F and 615A.

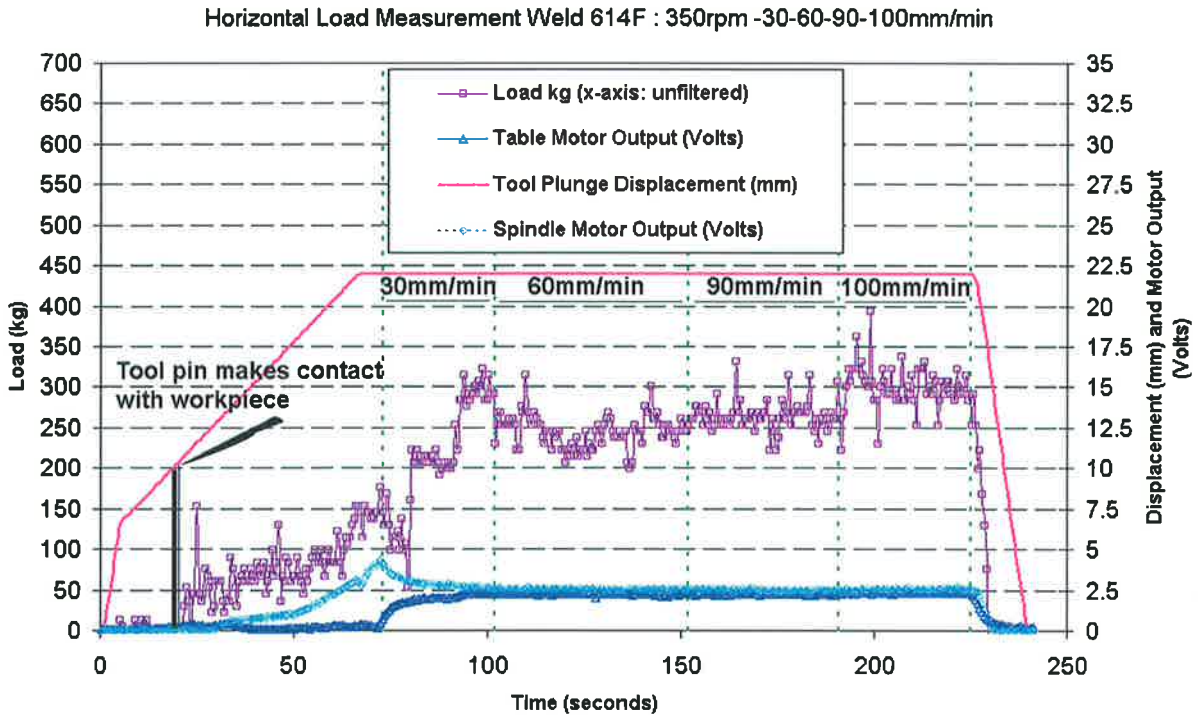

Figure 87 Load, tool displacement and motor output plot for weld 614F, AA7075 O.

Weld 614F produced in the 7075 O temper, Figure 87 had a step wise increasing weld travel speed. The load measurement in the direction of weld travel indicated that this load remained relatively constant for the majority of weld length. This was not the case however for weld 615A produced in the 7075 T651 alloy, Figure 88.

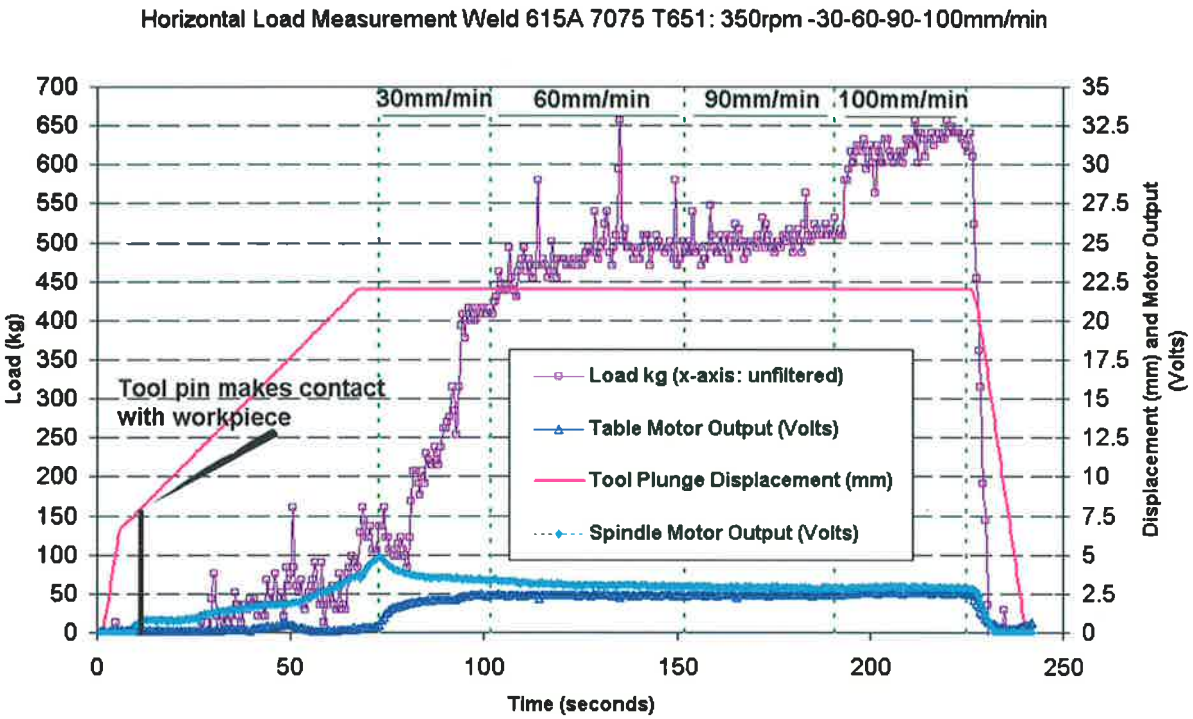

Figure 88 Load, tool displacement and motor output plot for weld 615A, AA7075 T651

Although the overall tool displacement for welds 614F and 615 A were identical the distance between the starting position of the tool as measured from tool tip to workpiece was not. This was indicated in both Figures 87 and 88. Table 5-4 summarises this difference.

Weld No and Alloy Temper.	Pin Stick out (mm)	Overall Plunge Displacement (mm)	Plunge Displacement to Workpiece (mm)	Plunge Depth into Workpiece (mm)
614F 7075 O	*11.7*	*22*	*10*	*12*
615A 7075 T651	*11.7*	*22*	*8.5*	*13.5*

Table 5-4 Plunge depth in relation to plate thickness for B.O.P. welds 614F and 615A produced in 7075 O and 7075 T651 aluminium alloys respectively

The tool displacement, Table 5-4 remained constant for all subsequent welds presented in section 5.2.

Visual inspection of the welds 614F and 615A, particularly around the region of the exit hole revealed that both welds were free from defect but that the imprint left by the tool

shoulder in this region varied between welds, Figures 89 and 90. Weld 614F, Figure 89, having been produced in the 7075 O temper had the smaller plunge depth, refer Table 5-4 into the workpiece but produced the larger tool shoulder imprint compared to weld 615A produced in the 7075 T651 temper alloy, Figure 90. The implication here is that although the plunge depth was over 1.5mm deeper for weld 615A the resistance to penetration of the 7075 alloy in the T651 temper condition was much greater under the processing conditions as witnessed by the imprint left on the surface of the workpiece. The difference between the tool pin stick-out length and plunge depth into workpiece, Table 5-4 is 1.8mm. From the imprint left by the shoulder of the tool, Figure 90 it can be seen that the shoulder was at the same height as the workpiece for the middle of the exit hole. For this to have occurred based on the load vs. deflection characteristics, Figure 56 for spindle and support beam it can be assumed that an axial load of between 35 and 40kN was generated when FSW the 7075 T651 alloy. If the same comparison is made for the weld 614F produced in the 7075 O temper the axial load is approximately 10kN.

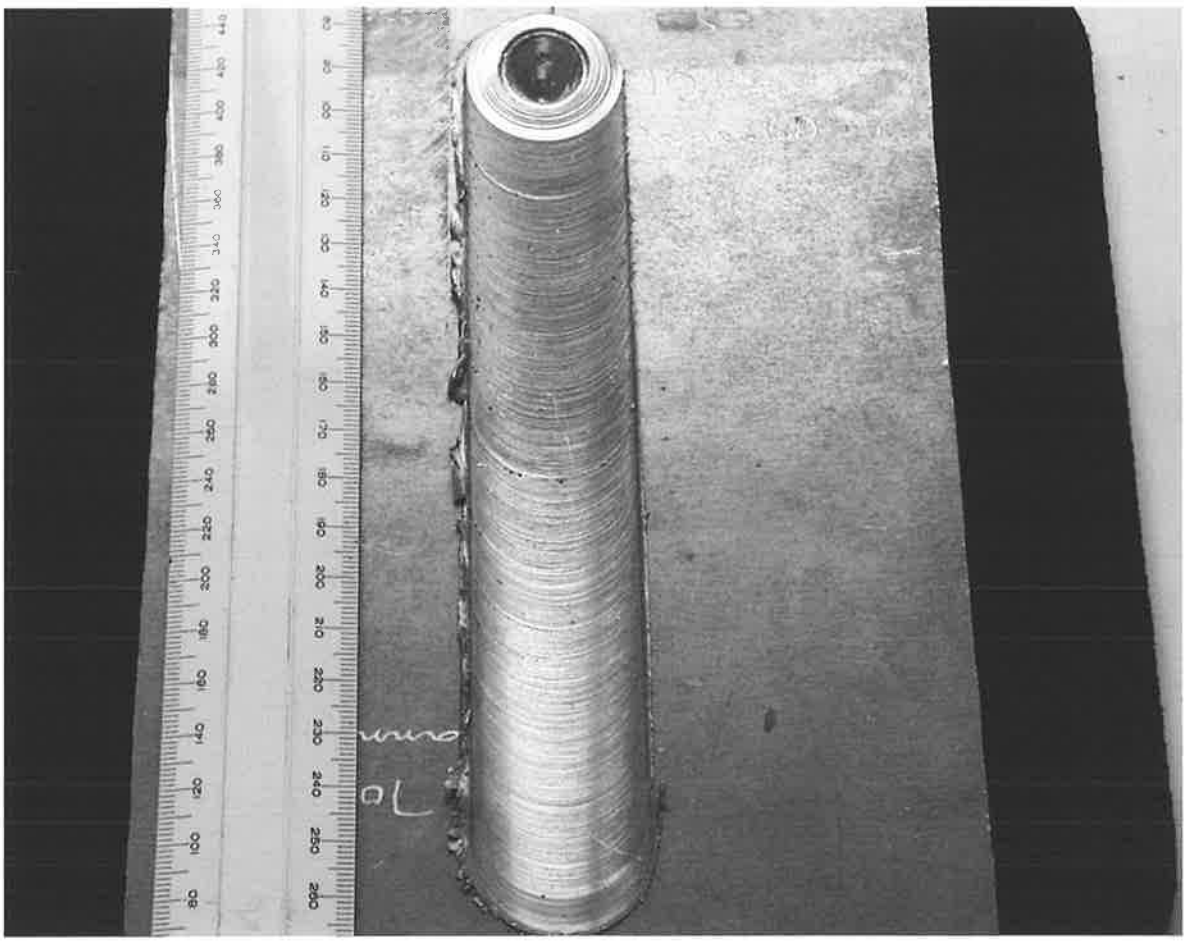

Figure 89 Top view B.O.P. weld 614F made in AA7075 O

Figure 90 Top view weld B.O.P. weld 615A made in AA7075 T651

A comparison of the spindle motor output, Figure 91, between welds 614F and 615A revealed that a relatively small difference measuring approximately 0.5 volts occurred between each weld. This difference was marginal in comparison to the difference that could be observed in the load as measured in the direction of weld travel, Figure 91.

Although the overall trend for weld direction load in both welds 614F and 615A appeared to be similar the processing load generated for weld 615A, produced in the 7075 T651 alloy was approximately twice as large as that of weld 614F, produced in the 7075 0 alloy. It could further be observed, Figure 9, that the load in the direction of weld travel for weld 615A dramatically increased at the weld travel speed of 100mm/min.

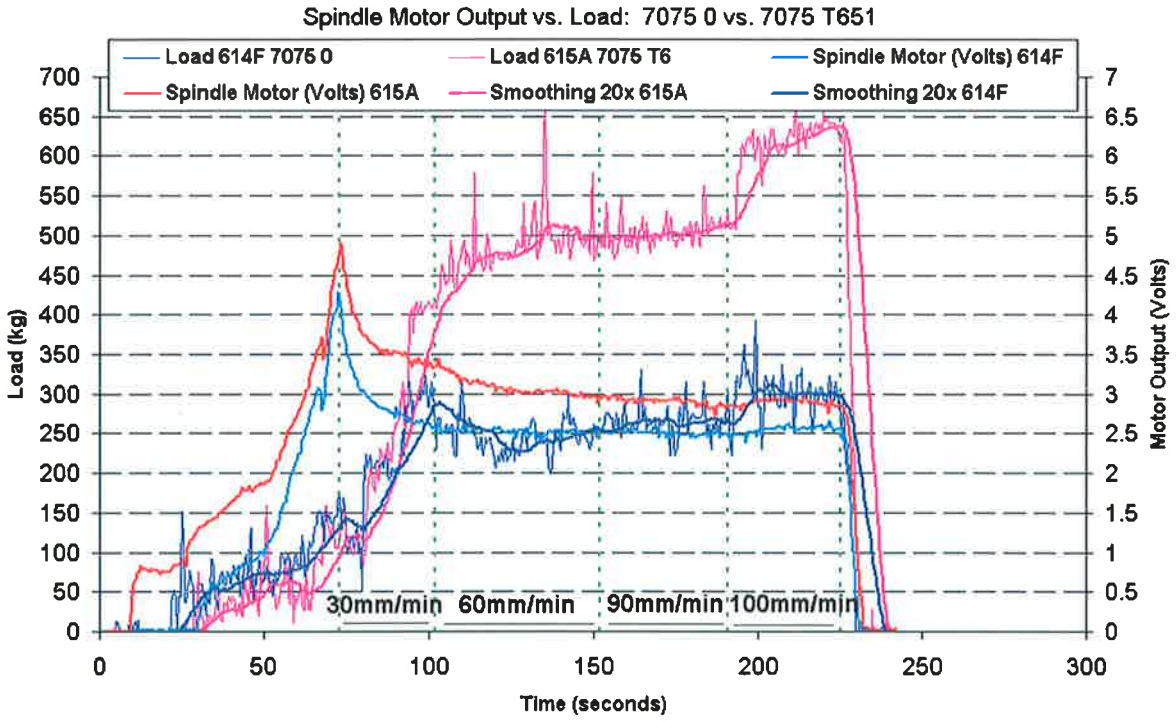

Figure 91 Plot for load in the weld direction vs. spindle motor output for welds 614F, 615A, produced in AA7075 O and 7075 T651 respectively

To test and verify the reproducibility of the data generated from welds 614F and 615A a further set of four friction stir welds were undertaken, both in the 7075 O and T651 temper conditions. These welds classified 615D, 615E, 615K and 615L and their respective temper conditions were indicated at the start of section 5.2, Table 5-2. The welding parameters used in the production of each weld remained constant having a rotation speed of 350rpm and an incrementally increasing weld travel speed starting at 30mm/min and increasing to 60 and terminating at 90mm/min. The terminating travel speed was 10mm/min slower as compared to the previous welds 614F and 615A. The travel speed of 100mm/min was not employed because of the high processing forces previously encountered.

The CT1-14 pin was again employed in conjunction with the 30Cc14 concave shoulder tool. Tool tilt measured 3° away from the direction of tool travel. Data plots for the first two welds 615D and 615E, representative of the four welds can be found in Figures 92 and 93 respectively.

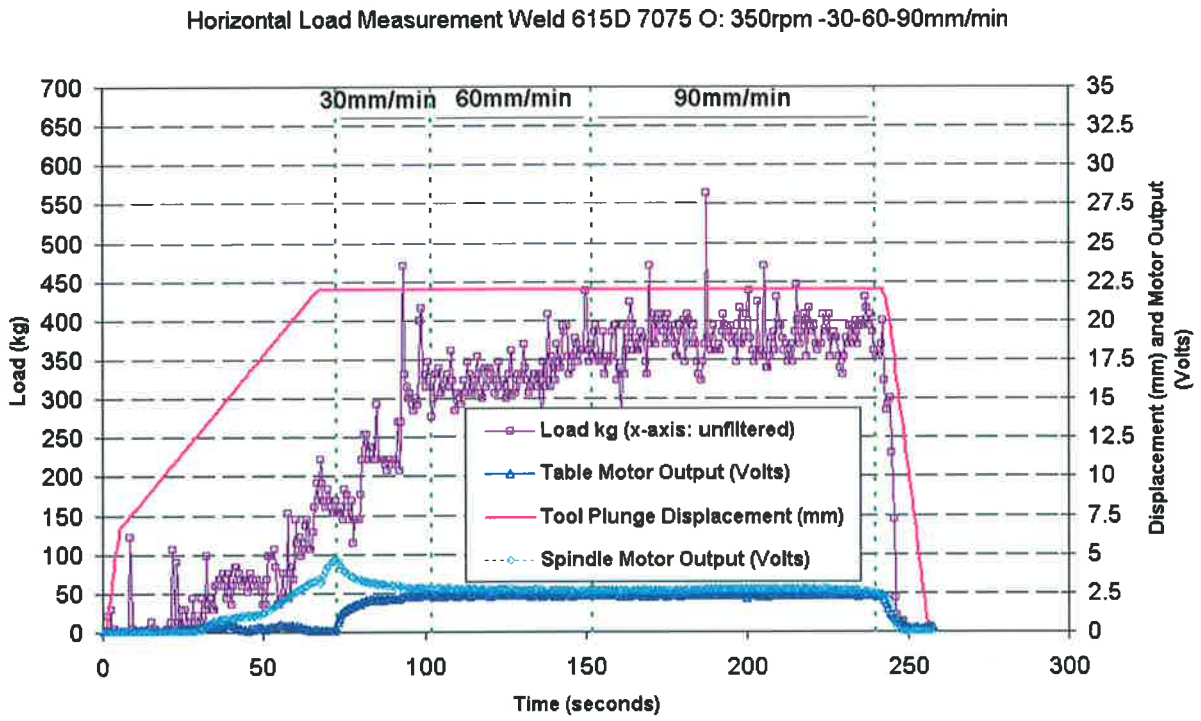

Figure 92 Load, tool displacement and motor torque plot for weld 615D, AA7075 O

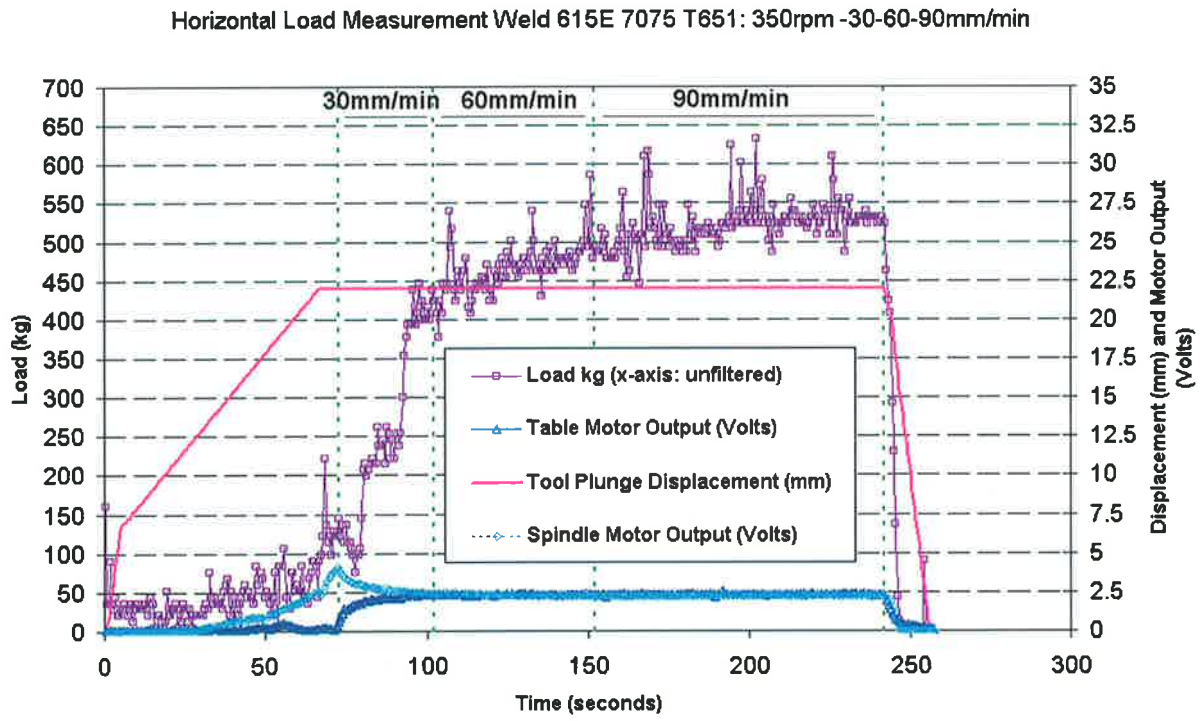

Figure 93 Load, tool displacement and motor torque plot for weld 615E, AA7075 T651

Figure 94 combines and highlights the differences appearing in motor output and weld load in the direction of weld travel between welds 615D and 615E. It can be seen that the

difference in spindle motor output measured approximately 0.5 volts between welds, while the difference in weld travel direction load was over 200kg. No discernable difference however could be observed for the table motor output between these two welds, suggesting that table motor output was relatively insensitive to the difference in travel direction load between the two welds.

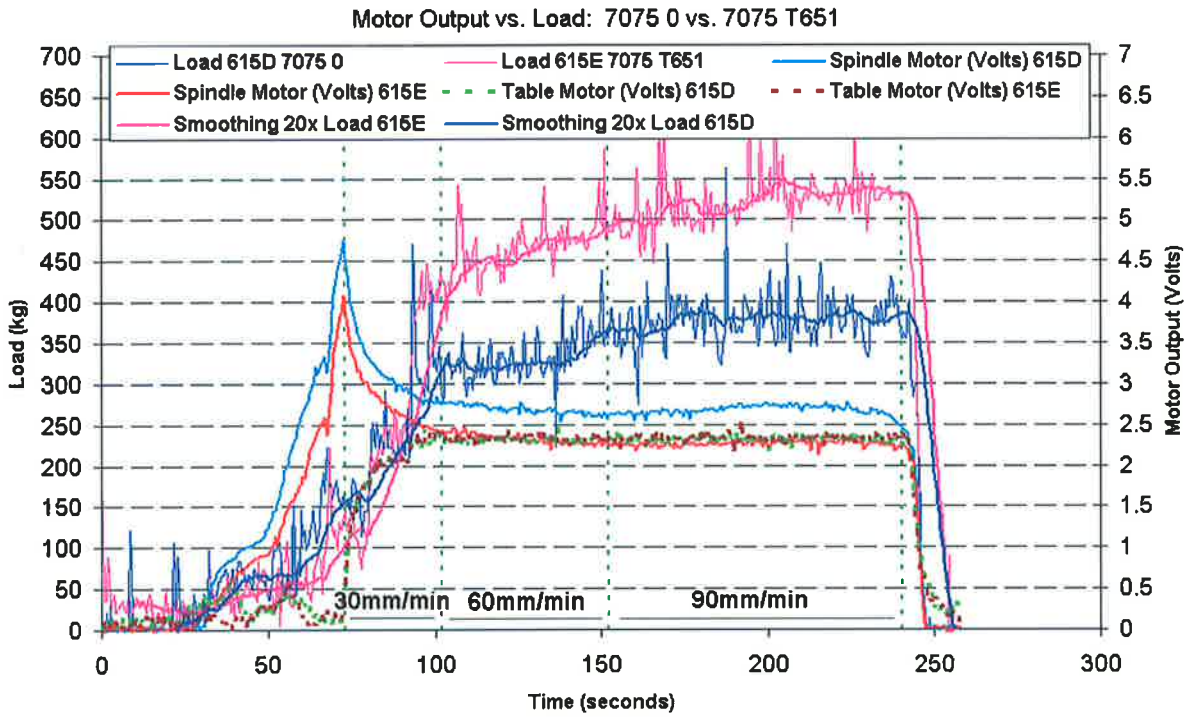

Figure 94 Plot for load in the weld direction vs. spindle motor output for welds 615D, 615E, produced in AA7075 O and 7075 T651 respectively.

It should be noted that both welds 615D and 615E were visually free from defect and produced under identical tool plunge displacement as welds 614F and 615A, Table 5-4.

A review of spindle motor output and weld travel direction load for friction stir welds produced in both the 7075 O and 7075 T651 alloys indicate that considerable differences exist as a consequence of alloy temper condition. This was also observed in the plunge depth compensation required to produce successful friction stir welds in each temper.

If a comparison of spindle motor output and weld travel direction load between a friction stir weld produced for the 5083 H111 (weld 614D, section 5.1) and 7075 T651 alloy (weld 614B), both of which employed the same welding parameters and welding tool, it can be

seen that the spindle motor output and load are slightly higher when FSW the 7075 T651 alloy, Figure 95.

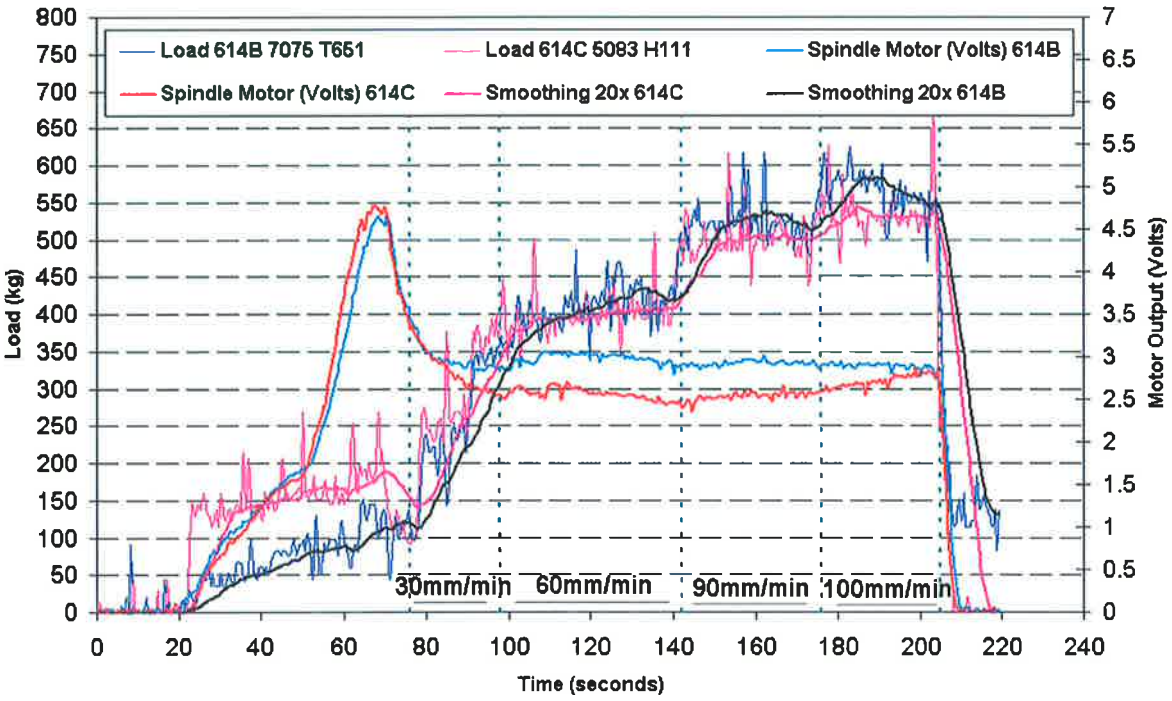

Figure 95 Plot for load in the weld direction vs. spindle motor output for welds 614B, 614D, produced in AA5083 H111 and 7075 T651 respectively.

Summarising the load data as measured for friction stir welds produced in 12.5mm thick 5083 H111 (section 5.1), 7075 O and 7075 T651 alloys it can be observed, Figure 96 that although considerable differences exist between welds produced in the 7075 O and T651 tempers there is only a marginal difference in load between the 7075 T651 and 5083 H111 alloys.

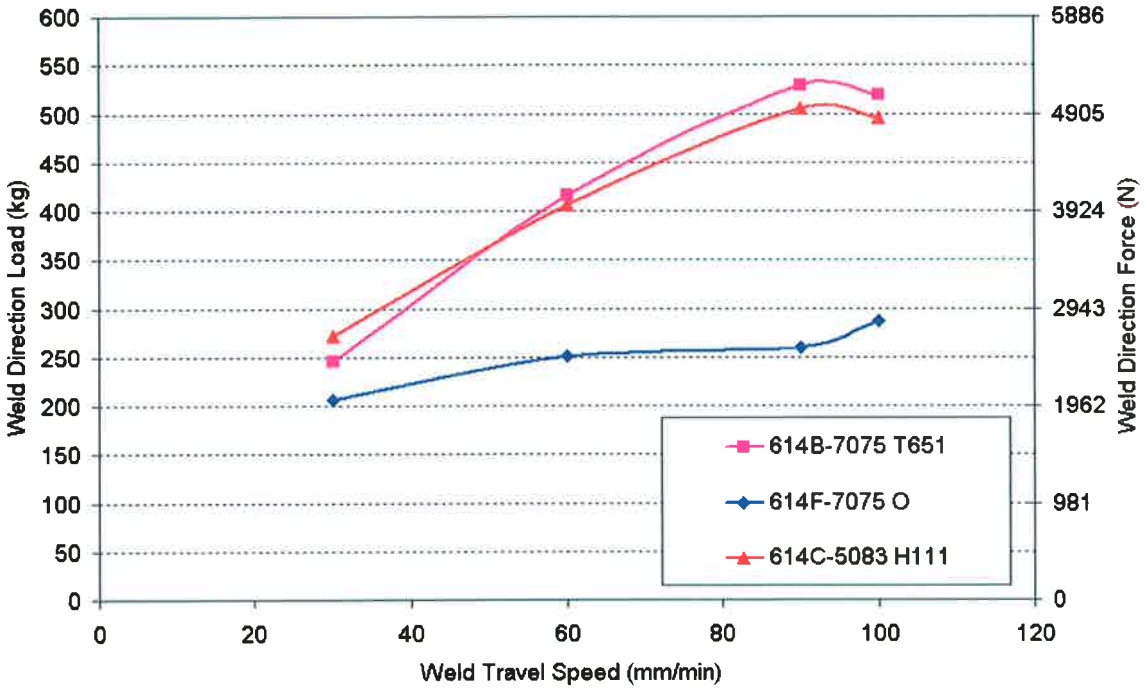

Figure 96 Weld force as function of welding speed for the alloys 7075 T651, 7075 O and 5083 H111. Note data for the 5083 alloy was obtained from weld 614C, Figure 82 for comparison purposes only.

Correlation between processing loads, spindle torque, weld power and weld energy give a further insight and help to enhance our understanding of the FSW process. With sufficient understanding of the resultant effects processing parameters have on processing loads, spindle torque, weld power requirements and the specific weld energy delivered into a weld it may be possible to predict many of the effects without the need for time consuming trial and error experimentation.

In nearly all cases the power input that goes into producing a friction stir weld has been calculated from torque measurements derived from the FSW spindle. In order to quantify the magnitude of spindle motor output (Volts) of the friction stir welder and relate this to a spindle torque (Nm) a calculation was performed using a methodology developed by Colegrove [134]. This methodology can be found in Appendix C.

Figure 97 demonstrates a linear relationship was determined by Colegrove [136] between the spindle motor output (Volt) and spindle motor torque (Nm).

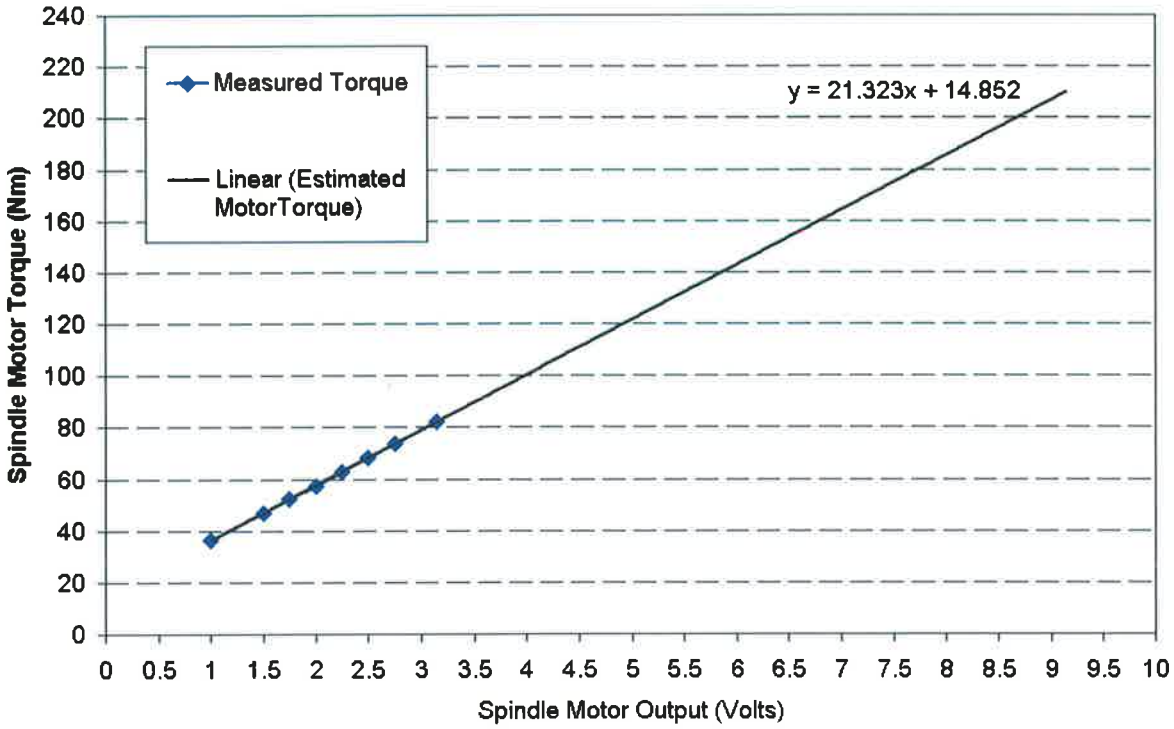

Figure 97 Spindle Motor Torque (Nm) as a function of Spindle Motor (Volt) output.

Colegrove [136] determined that a spindle motor output of 3.15 volts resulted in a heat input of 2.96kW. The corresponding power output of the motor he calculated as being 3.34kW based on a nominal load of 147Nm. Hence there was a 12.9% energy loss through the drive system. To verify heat input (Power = Watts) into the workpiece however, it was essential to know not only the torque produced at the motor but at the FSW spindle since there existed a 2:1 reduction gear between the motor and spindle. Verification of torque at the spindle was performed by Colegrove [136] using a brake drum attached to the end of the spindle, refer Appendix C for details. Here a horizontal arm connected a brake drum to a load cell. A breaking load was applied to the drum and measured at the load cell. This load was then compared to the spindle motor output over a range of rotation speeds. This calibration curve as determined by Colegrove [136] is reproduced in Figure 98.

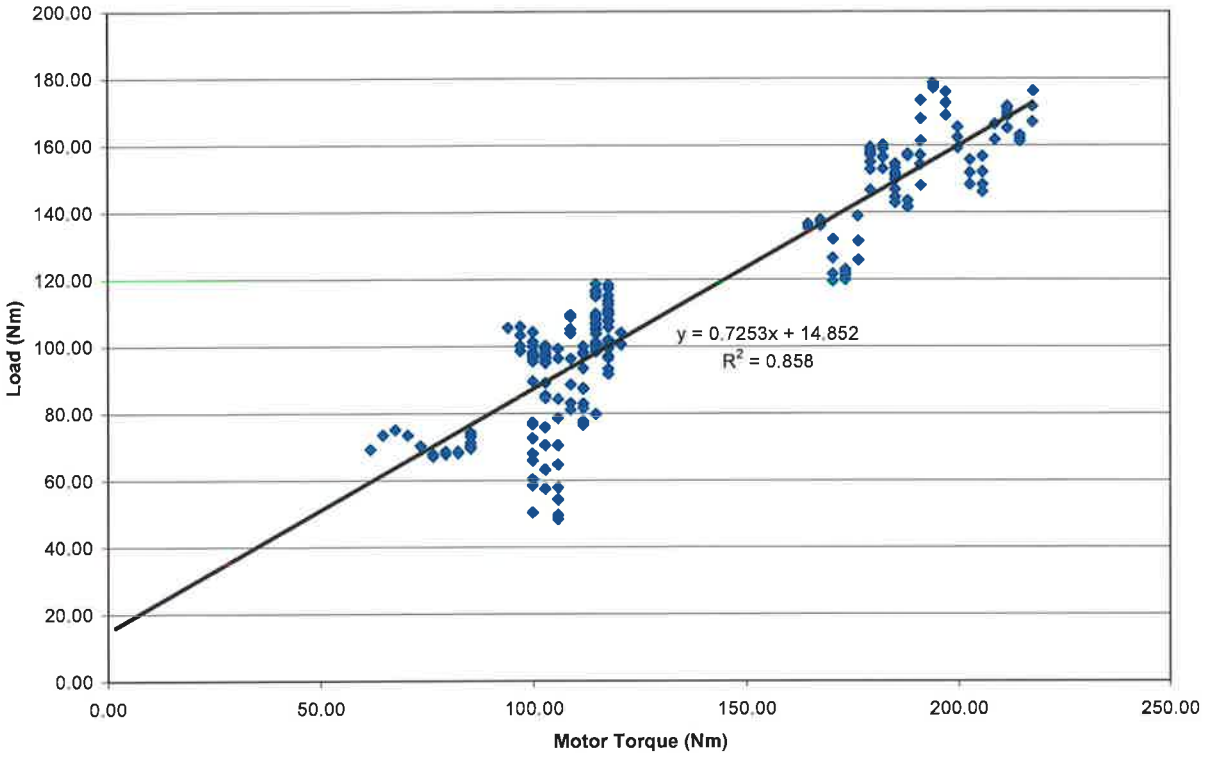

Figure 98 Linear approximation of torque at the spindle as a function of load cell torque [136].

Figure 98 demonstrates that a linear relationship was determined by Colegrove [136] between the spindle motor torque and the torque as measured at the spindle. The spread of the data is minimal for a range of motor torque between 50-100Nm i.e. for spindle torque between 60-80Nm. An explanation for the rather large spread of data points in Figure 98, for values of torque above 100N is given by Colegrove [136]. He observed during the measurements how for a given setting on the hand brake, the load on both the load cell and spindle motor reduced over time. This was particularly noticeable for higher rotation speeds and braking loads. Colegrove [136] attributed this to the brake pads heating up and losing their efficiency. However, since all the welds presented in sections 5.1 and 5.2 do not exceed 3.5 Volts or 80Nm of motor torque it is reasonable to assume that the linear approximation of torque, Figure 98 allows for quite accurate assessment of both the weld power (Watts) and specific weld energy (joules) per millimetre of weld length for friction stir welds produced in 12.5mm thick 5083 and 7075 alloys.

The weld power (Watts) is a function of the spindle torque and spindle rotation speed (radians/sec). A comparison of weld power in relation to spindle torque and spindle motor output is presented in Figure 99, derived from the calibration curve, Figure 98.

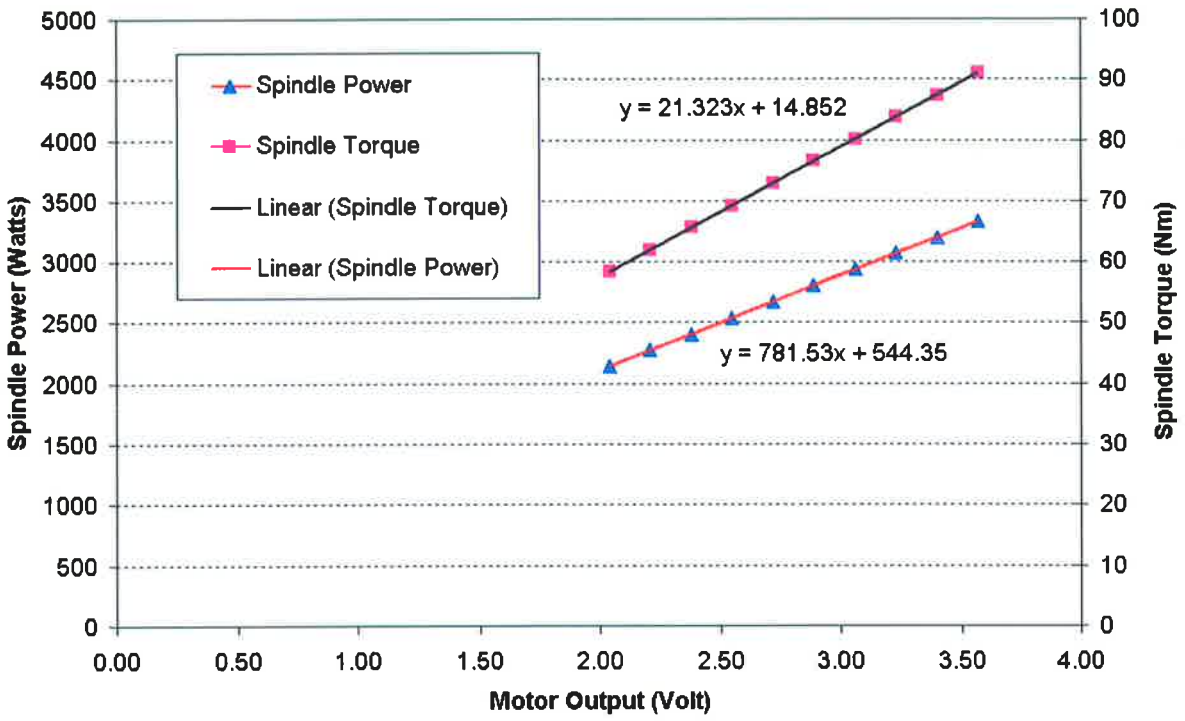

Figure 99 Weld power at the spindle as a function of spindle torque (Nm) and motor output (Volts).

Figure 99 summarises a relationship between spindle motor output (Volt), spindle torque (Nm) and spindle power (Watts). Lacking from Figure 99 however is clarity concerning how weld travel speed and in turn the force in the direction of weld travel influence the calculation of weld power. Figure 96 previously revealed that forces developed in the direction of weld travel increased in relation to weld travel speed and as such were a function of weld travel speed.

Figure 100 reveals that spindle power as a function of weld travel speed differs between alloys and alloy temper for materials welded under identical processing parameters and when friction stir welded using the identical FSW tool. The welds 614B, 614C, 614F and 313B, depicted in Figure 100 were all produced for a tool rotation speed of 350rpm and a weld travel speed that incrementally increased from 30 through to 100mm/min of weld travel speed. The tool used to produce these welds was tilted 3 degrees from the direction of weld travel and consisted of the tool pin CT1-14 in conjunction with tool shoulder 30Cc14. It should be noted that weld 614C, refer section 5.1 and produced in the 5083 H111 alloy contained a surface breaking defect unlike its counterpart weld 313B.

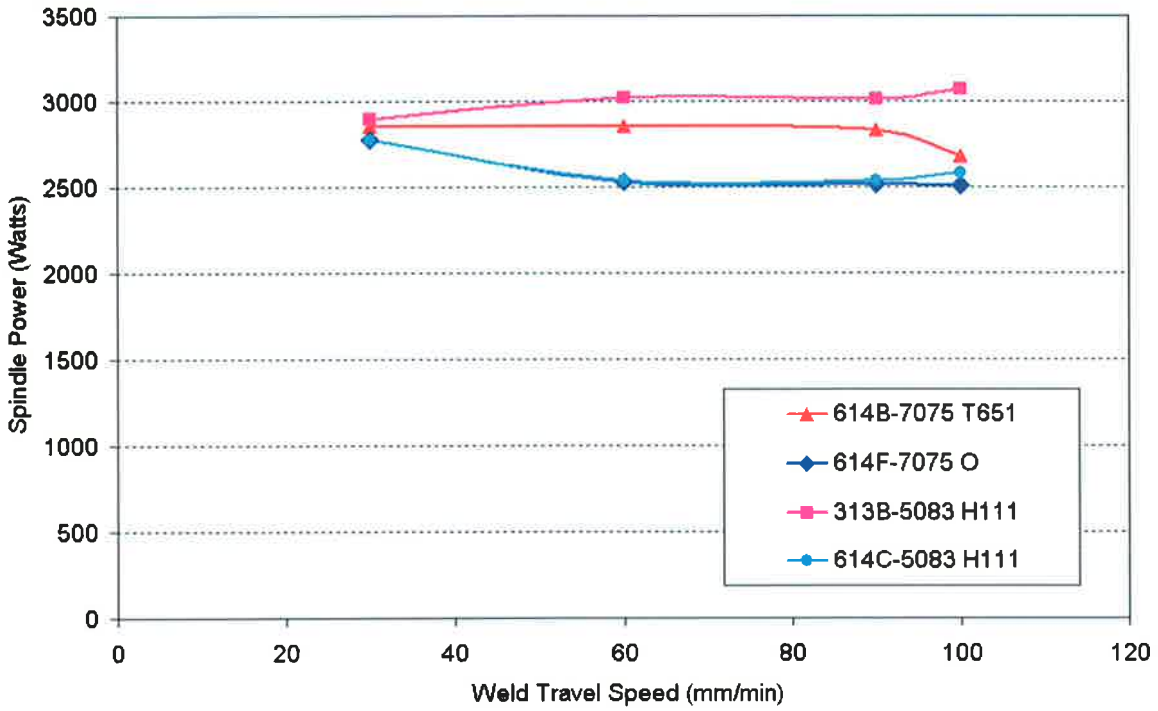

Figure 100 Weld power at the spindle as a function of weld direction force and weld travel speed, for friction stir welds 614B, 614C and 614F produced in 12.5mm thick 7075 T651, 5083 H111 and 7075 O aluminium alloys respectively.

Figure 100 reveals that weld power slightly increases over the investigated weld travel speeds for welds produced in the 5083 H111 alloy (weld 313B) and the 7075 T651 alloy (weld 614B). This however was not the case for welds produced in the 7075 O temper (weld 614F) and the weld containing the surface breaking defect, weld 614C, produced in the 5083 H111 alloy. Figure 100 also demonstrates that the change in weld power over the weld travel speed range is relatively small for each individual weld. From these observations it can be assumed that travel speed up to 90mm/min and indirectly force as measured in the direction of welding (because force has been shown to be a function of weld travel speed) had minimal effect on the level of weld power generated during each weld. Certainly weld power calculated from the mean value of the spindle torque measurement is only capable of providing an estimate of the input power delivered into the weld.

If a constant weld power (Watts) is divided by the weld travel speed (mm/sec), it is possible to calculate weld energy in terms of (joules) per millimetre of weld length. When this is performed, for example for weld 313B produced in 12.5mm thick 5083 H111 alloy,

Figure 101 it reveals that specific weld energy into the weld decreases in relation to weld travel speed.

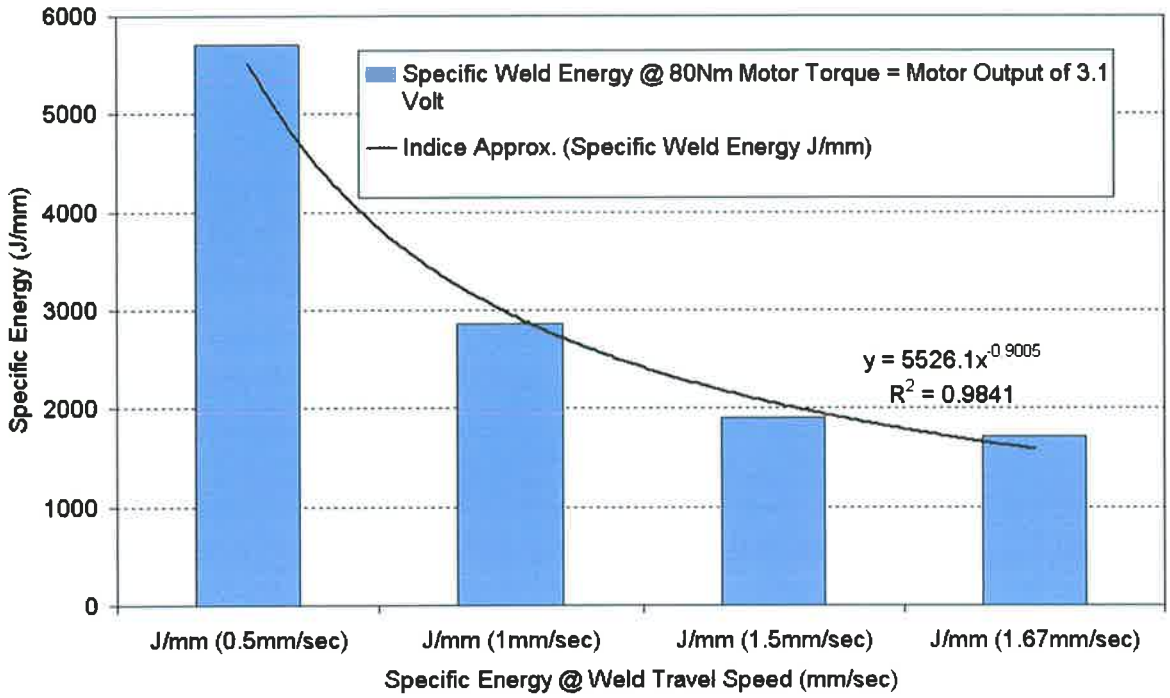

Figure 101 Specific weld energy (J/mm) as a function of weld travel speed (mm/sec) for 12.5mm thick friction stir welded 5083 H111.

If the true weld power however is used in calculating each range of weld travel speed investigated and applied to welds produced in both the 7075 and 5083 alloys, Table 5-5 then specific weld energy demonstrates measurable differences not only in the level of weld energy arising for a particular alloy but more accurately for the level of energy as related to a specific region of the weld, Figure 102.

614B-7075 T651	Travel Speed (30mm/min)	Travel Speed (60mm/min)	Travel Speed (90mm/min)	Travel Speed (100mm/min)
Volt	*2.96*	*2.96*	*2.92*	*2.73*
Load (kg)	*246.11*	*415.85*	*529.51*	*519.79*
Spindle Torq. (Nm)	*77.95*	*77.95*	*77.23*	*73.06*
Spindle Power (W)	*2857.13*	*2857.13*	*2830.55*	*2677.69*
Specific Power (J/mm)	*5714.26*	*2857.13*	*1714.28*	*1606.61*

614F-7075 O	Travel Speed (30mm/min)	Travel Speed (60mm/min)	Travel Speed (90mm/min)	Travel Speed (100mm/min)
Volt	*2.86*	*2.54*	*2.52*	*2.51*
Load (kg)	*206.79*	*250.88*	*260.09*	*286.8*
Spindle Torq. (Nm)	*75.78*	*69.07*	*68.52*	*68.34*
Spindle Power (W)	*2777.38*	*2531.48*	*2511.54*	*2504.9*
Specific Power (J/mm)	*5554.76*	*2531.48*	*1674.36*	*1502.94*

313B-5083 H111	Travel Speed (30mm/min)	Travel Speed (60mm/min)	Travel Speed (90mm/min)	Travel Speed (100mm/min)
Volt	*3.01*	*3.17*	*3.16*	*3.22*
Load (kg)	*n.a.*	*n.a.*	*n.a.*	*n.a.*
Spindle Torq. (Nm)	*79.04*	*82.49*	*82.3*	*83.76*
Spindle Power (W)	*2897.01*	*3023.28*	*3016.63*	*3069.8*
Specific Power (J/mm)	*5794.01*	*3023.28*	*2011.09*	*1837.89*

614C-5083 H111	Travel Speed (30mm/min)	Travel Speed (60mm/min)	Travel Speed (90mm/min)	Travel Speed (100mm/min)
Volt	*2.86*	*2.55*	*2.55*	*2.6*
Load (kg)	*272.16*	*406.2*	*505.88*	*496.23*
Spindle Torq. (Nm)	*75.78*	*69.25*	*69.25*	*70.34*
Spindle Power (W)	*2777.38*	*2538.13*	*2538.13*	*2578*
Specific Power (J/mm)	*5554.76*	*2538.15*	*1692.08*	*1546.8*

Table 5-5 Load, spindle torque, spindle power and specific weld power relationships for B.O.P. welds produced in both the 7075 O and T651 alloys as well as for the 5083 H111 alloy for 12.5mm of plate thickness.

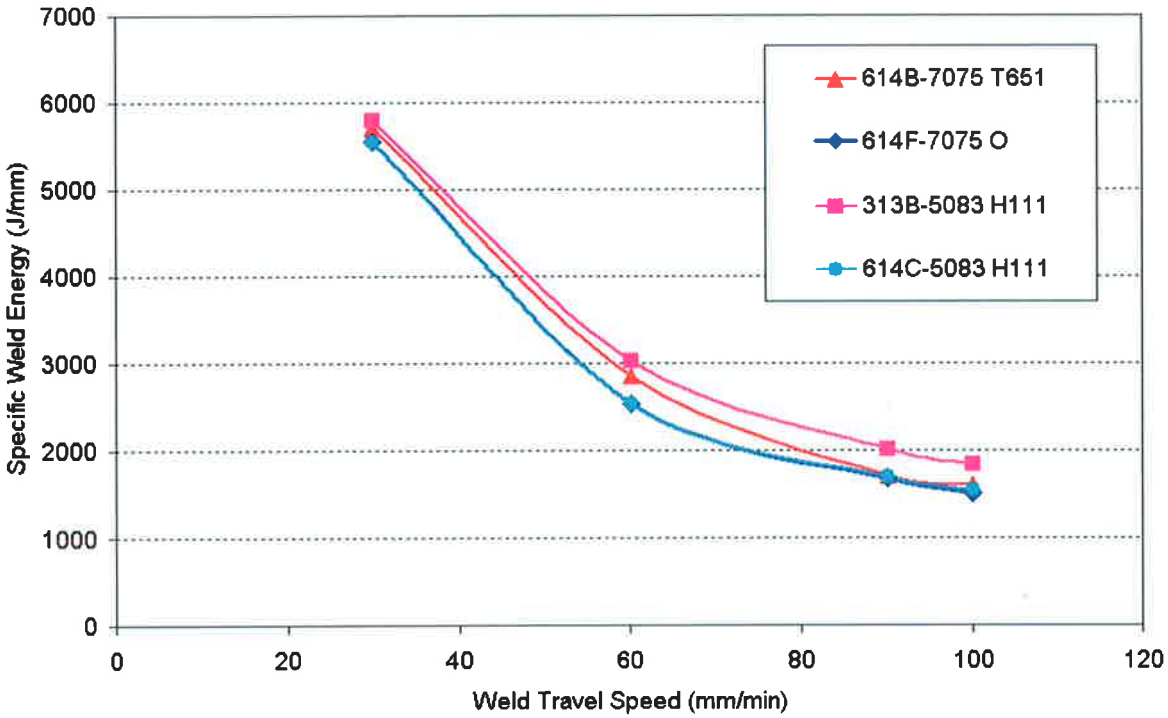

Figure 102 Specific weld energy as a function of weld travel speed. Note the difference between defective weld 614C and successful weld 313B, both produced in the 5083 alloy

Figure 102 reveals that it is the level of weld energy in relation to weld travel speed that may provide a much more telling assessment as to how friction stir welds produced under identical welding parameters, using the same friction stir welding tool differ in relation to weld travel speed, and indirectly weld force. Figure 102 clearly shows that the defective weld 614C in comparison to the non defective weld 313B, both of which were produced in the 5083 H111 alloy had a noticeably lower weld energy over all weld travel speeds. It should not be forgotten however that both welds differed in relation to the level of shoulder penetration into the workpiece, which was over 1.5mm greater for weld 313B, refer Figure 84 of section 5.1.

The information derived from measurements of spindle motor output were used to calculate weld power and specific weld energy. This methodology indicates that specific weld energy is considerably affected by weld travel speed, which itself is a function of the weld load experienced by the FSW tool. The results of welds produced in sections 5.1 and 5.2 suggest that calculations of specific weld energy can differentiate welds produced free from defect and containing defects, such as was the case between welds 313B and 614C, Figure 102. The fact that weld force as measured in the direction of FSW can be easily measured and associated with travel speed offers a relatively quick and

inexpensive way to appraise not only the effects of process parameters but also of tool pin geometry on weld formation.

In the early days of FSW, most welding was performed on modified machine tools such as the Friction Stir Test Bed used in this study e.g. Shaper Planers and modified milling machines. These machines had limited instrumentation for process monitoring and thus a great deal of speculation has developed on the quantitative effects of process variable and tool geometry changes. The level of instrumentation currently available for process monitoring in FSW machines has increased markedly but so has the cost of these machines. In this study the motor torque that was used to calculate specific weld energy was estimated from calibration curves. The exact level of specific weld energy is therefore limited to the accuracy of the calibration. Load measurements may offer a much more cost effective and accurate way of assessing tool geometry affects on friction stir weld formation. Section 5.3 presents results which build on this investigation.

5.3 Process Loads And Weld Temperature Relationships When FSW 12.5mm Thick Aluminium Alloys 5083 H111 & 7075 T651 Using A Threaded Pin vs. Threaded Pin With 3 Flats.

The results from sections 5.1 and 5.2 have demonstrated that it was possible to friction stir weld 12.5mm thick aluminium alloys 5083 H111 and 7075 T651 using a common set of welding parameters with the tool pin CT1-14 in conjunction with tool shoulder 30Cc14. For successful defect free welds to be produced however it was necessary to determine the level of plunge the tool shoulder needed to be compensated for such that the shoulder was able to maintain firm contact with the surface of the workpiece during FSW. These values and an estimate of axial force can be found in Table 5-5.

Aluminium Alloy (12.5mm) Thick	Plunge Depth Compensation (mm)	Estimated Axial Force (kN) At 100mm/min Travel Speed
5083 H111	*1.10*	*25*
7075 O	*0.50*	*10*
7075 T651	*1.50*	*35*

Table 5-5 Weld plunge depth compensation i.e. the value added to pin stick-out length when the tip of the pin makes contact with the workpiece for the FSW of 12.5mm thick 5083 H111, 7075 O and 7075 T651 alloys.

The results presented in section 5.3 were generated in an attempt to define what roll the pin profile played with regard to temperature and weld force evolution as measured in the direction of weld travel. As such a modification was made to the original CT1-14 pin form, Figure 103. This was carried out by applying three flats at a spacing of 120° along the threaded region of the pin, to the point where the thread was completely removed in the region of the flats. This pin, again designed by the author was named CT2-14, and can be found in Figure 104.

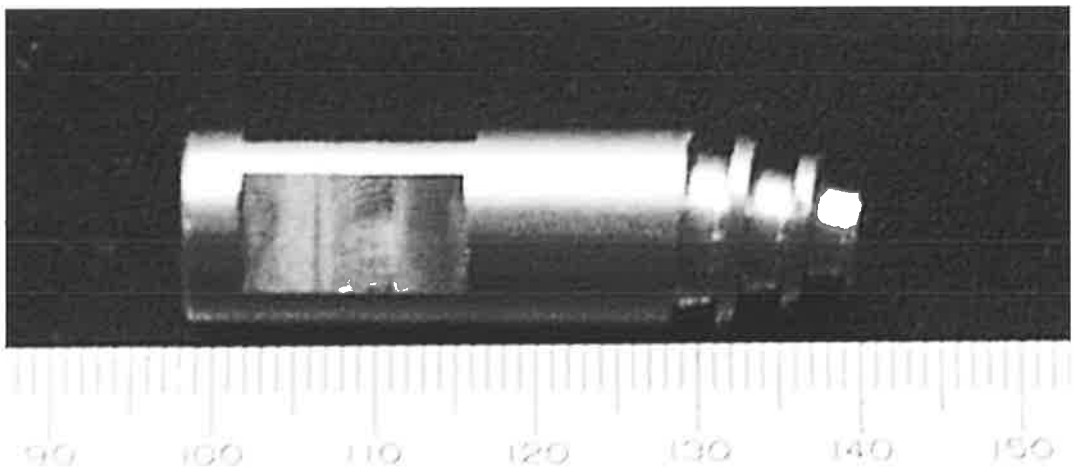

Figure 103 Pin CT1-14 = Conical threaded pin with no flats.

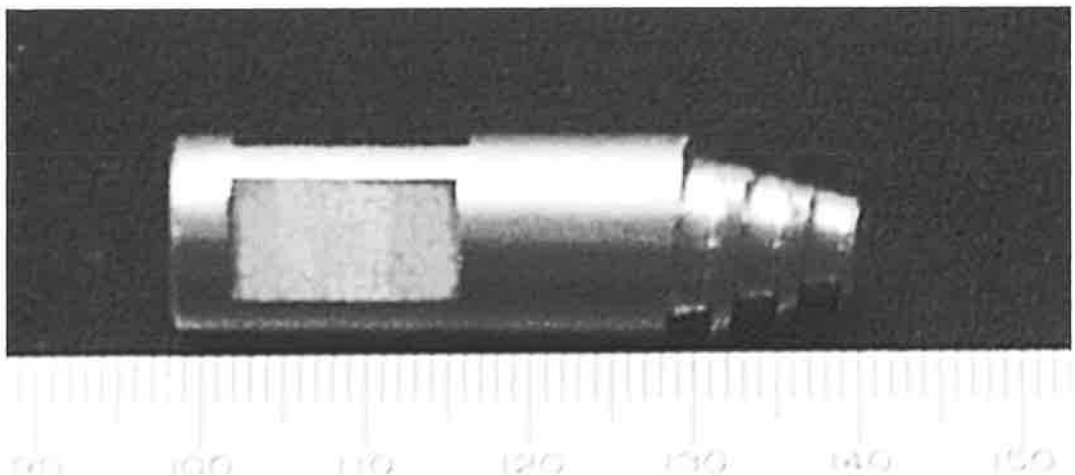

Figure 104 Pin CT2-14 = Conical threaded pin with three flats.

The reason for application of the flats was to enhance the difference between the dynamic and static volumes displaced in the workpiece compared to pin CT1. It should be noted that the diameter of the two pins CT1-14 and CT2-14 remained essentially the same although tool pin CT2-14 had a smaller volume than pin CT1-14. Hence under tool rotation the circumferential volume defined by a rotation of each tool also remained the same. This is because the size of the circular path that each tool follows under rotation is dependant on the outer periphery of each welding tool pin and since these are equivalent the dynamic volume swept by each tool pin should also remain the same. This however cannot be said of the two tool pins in terms of the static volume each would displace when statically plunged into the workpiece. Tool pin CT2-14 having the smaller static displacement volume, was envisaged to be capable of sweeping more material which entered the dynamic orbit of the pin than pin CT1-14. It was also envisaged that the greater efficiency in material transfer provided by tool pin CT2-14 should also help in

generating lower processing forces in the direction of welding because of this ability. It was furthermore reasoned that by achieving lower processing forces this would help in preventing volumetric defects from occurring in the weld nugget. To verify these assumptions four identical welds were conducted in both the 7075 T651 and 5083 H111 alloys. The welds are identified in Table 5-6.

Al Alloy	Weld No.	Tool Type	Rotation Speed (rpm).
7075 T651	*403A*	*CT1-14 30Cc14*	*300*
7075 T651	*403B*	*CT2-14 30Cc14*	*300*
7075 T651	*403C*	*CT2-14 30Cc14*	*450*
7075 T651	*403D*	*CT1-14 30Cc14*	*450*
5083 H111	*405A*	*CT1-14 30Cc14*	*300*
5083 H111	*405B*	*CT2-14 30Cc14*	*300*
5083 H111	*405C*	*CT2-14 30Cc14*	*450*
5083 H111	*405D*	*CT1-14 30Cc14*	*450*

Table 5-6 Aluminium alloy, weld no., weld tool and rotation speed identification for friction stir welds produced in section 5.3

Two tool rotation speeds were trialed; 300rpm and 450rpm. These rotation speeds when converted to peripheral tool rubbing velocity, using equation 1, section 2.10 of Chapter 2 indicated a maximum velocity at the pin shank of 0.22m/sec for 300rpm and 0.33m/sec for 450rpm. The rubbing velocity of the tool shoulder was calculated to be 0.47m/sec at 300rpm and 0.71m/sec at 450rpm. All welds were performed using a single weld travel speed of 60mm/min and each weld had the same tool plunge displacement. In contrast to the levels of tool plunge compensation given in Table 5-5 for the 5083 H111 and 7075 T651 alloys it was decided that a value of 0.9mm be used across all welds. This was 0.2mm less displacement than for welds produced in the 5083 alloy, section 5.1 and 0.6mm less than used for welds produced in the 7075 T651 alloy, section 5.2 of this Chapter. The reasons for reducing the weld plunge displacement was firstly to compensate for the lower weld travel speed used in this investigation as compared to welds produced in section 5.1 and 5.2, and secondly it was hoped that by not plunging as

deeply weld defects could be initiated thus differentiating the performance of the two tool pins. Hence welding parameters remained identical for all welds. Tool tilt was also maintained at 3° inclined away from the direction of weld travel.

The surface appearance of the four welds produced in the 7075 T651 alloy, Figure 105 demonstrates that a surface breaking void occurred while FSW using pin profile CT1-14, welds 403A and 403D. No such defect could be seen for welds produced using welding pin CT2-14, i.e. welds 403B and 403C.

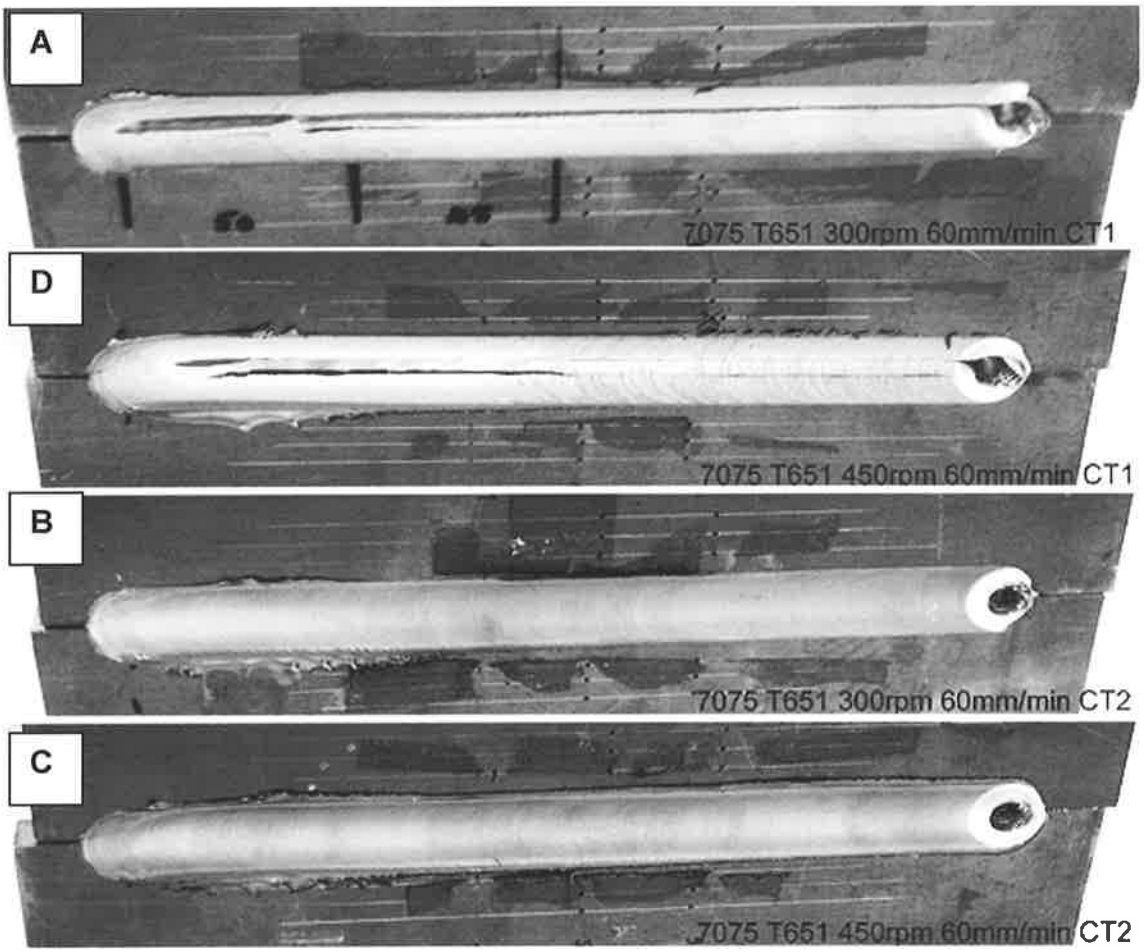

Figure 105 Welds produced in AA7075 T651 from top to bottom 403A, D, B and C. Note welds 403A and D were produced using tool pin CT1-14 and suffer from an open running void.

Temperature measurements were conducted for thermocouples embedded at a spacing of 20 and then 25mm either side from the join line and at mid plate thickness. FSW temperatures indicated that only marginal differences occurred in the workpieces as a result of changes in tool pin geometry over both of the investigated tool rotation speeds, Figures 106-109.

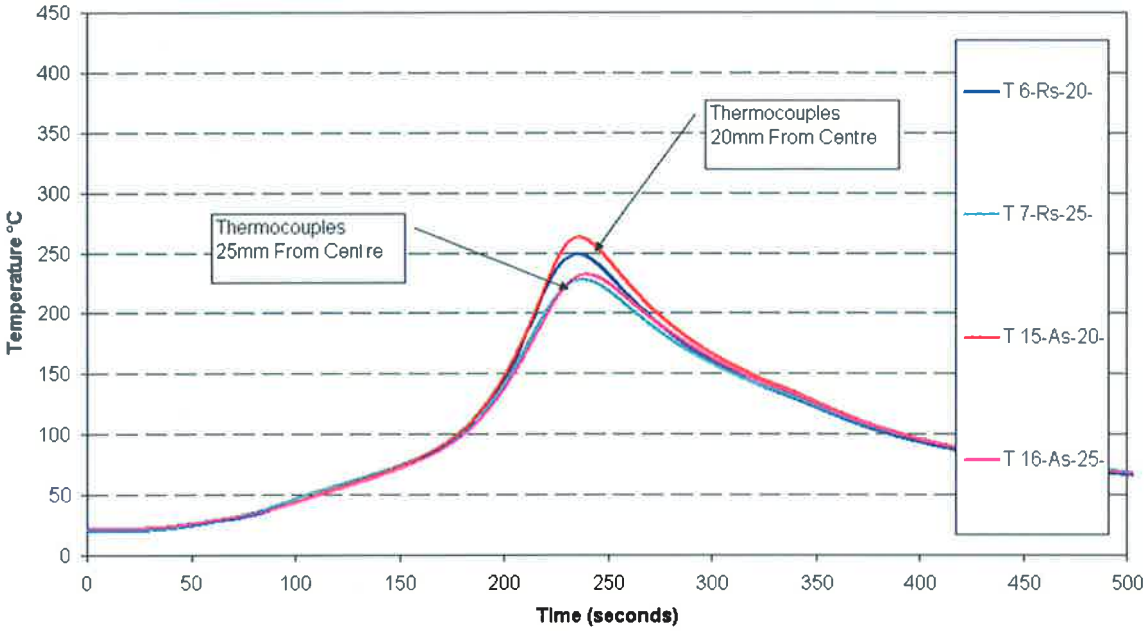

Figure 106 Temperature profiles as measured in workpiece for weld 403A, while FSW using tool CT1-14 for a rotational speed of 300rpm. Note As in the Legend refers to advancing side and Rs retreating side of the weld.

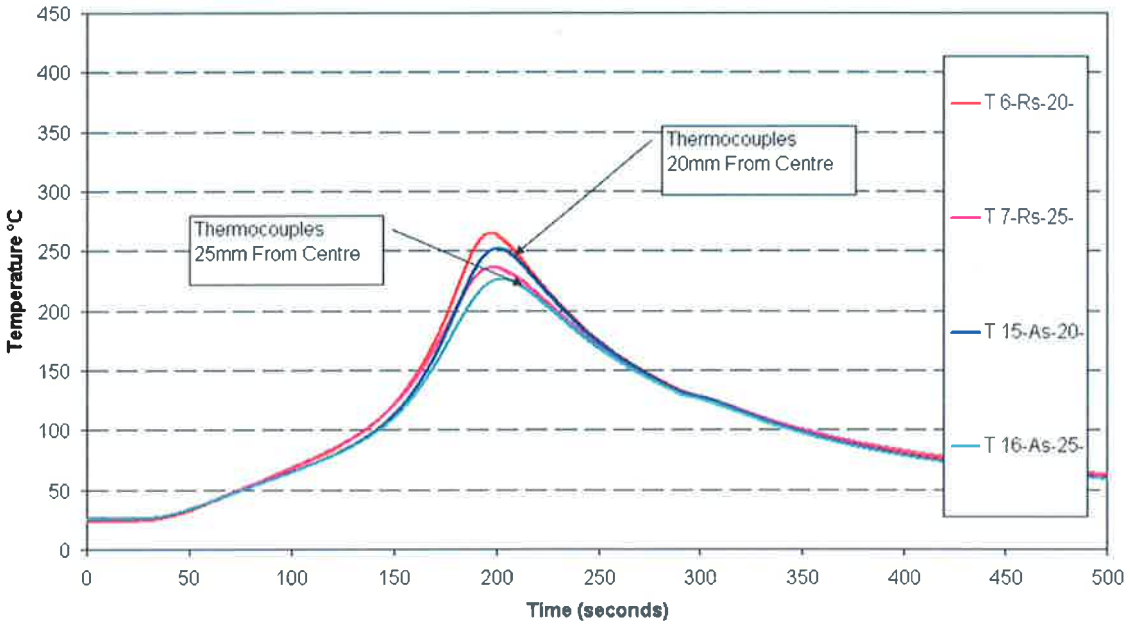

Figure 107 Temperature profiles as measured in workpiece for weld 403B, while FSW using tool CT2-14 for a rotational speed of 300rpm. Note As in the Legend refers to advancing side and Rs retreating side of the weld.

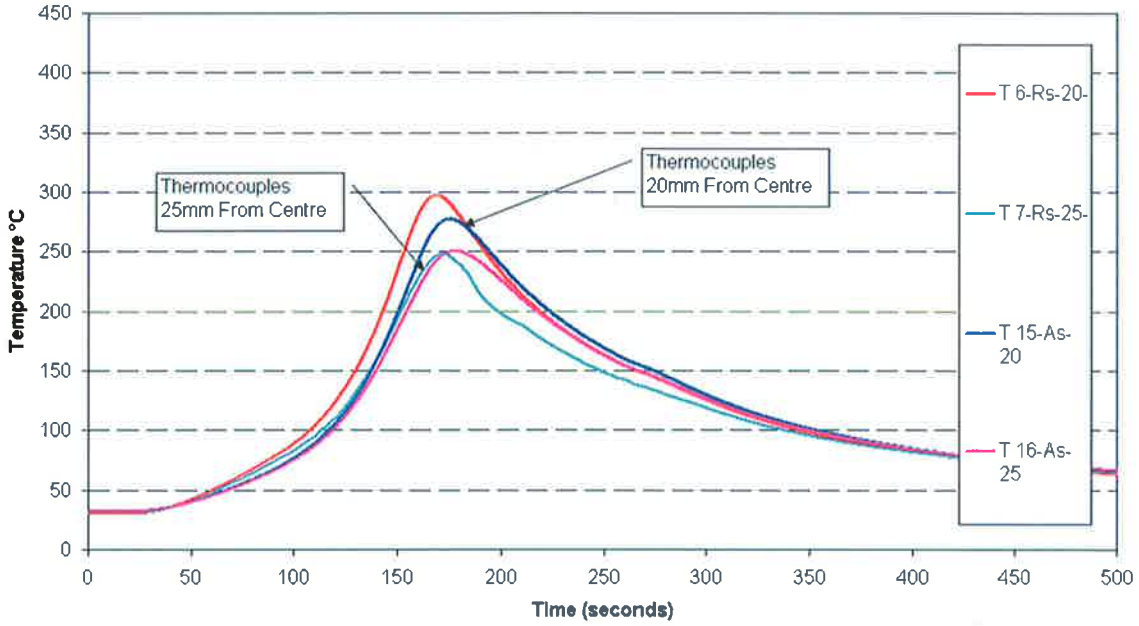

Figure 108 Temperature profiles as measured in workpiece for weld 403C, while FSW using tool CT2-14 for a rotational speed of 450rpm. Note As in the Legend refers to advancing side and Rs retreating side of the weld.

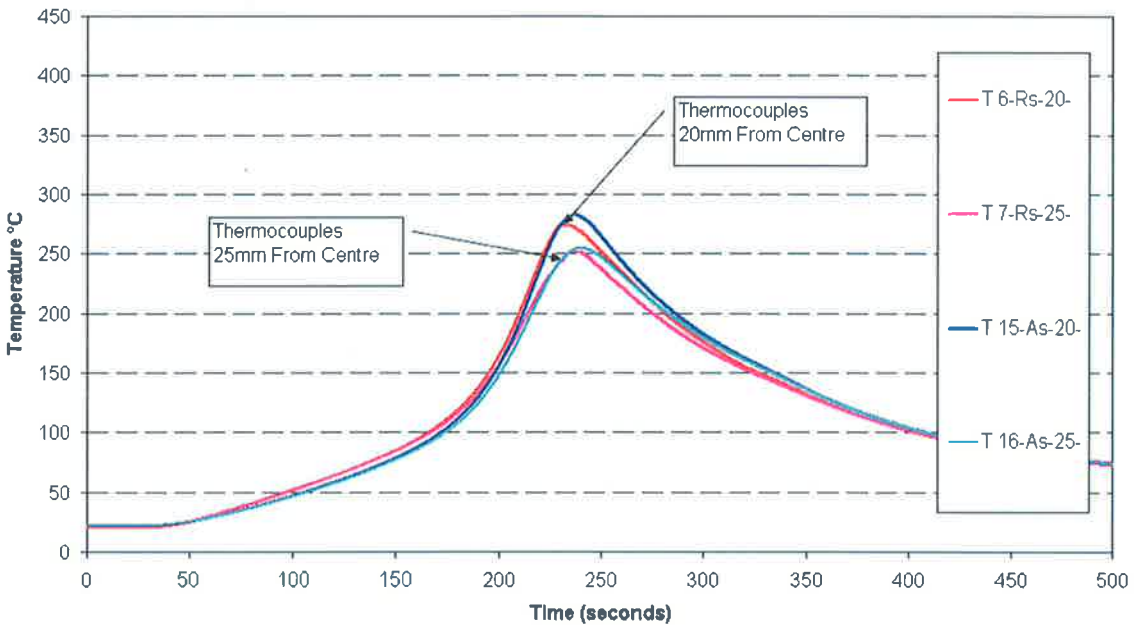

Figure 109 Temperature profiles as measured in workpiece for weld 403D, while FSW using tool CT1-14 for a rotational speed of 450rpm. Note As in the Legend refers to advancing side and Rs retreating side of the weld.

When the same tests were conducted in the 5083 H111 alloy using identical welding tools and weld parameters as for the welds produced in the 12.5mm thick 7075 T651 alloy, it could again be observed that welds produced using pin CT1-14, welds 405A and 405C suffered from surface breaking defects, Figure 110.

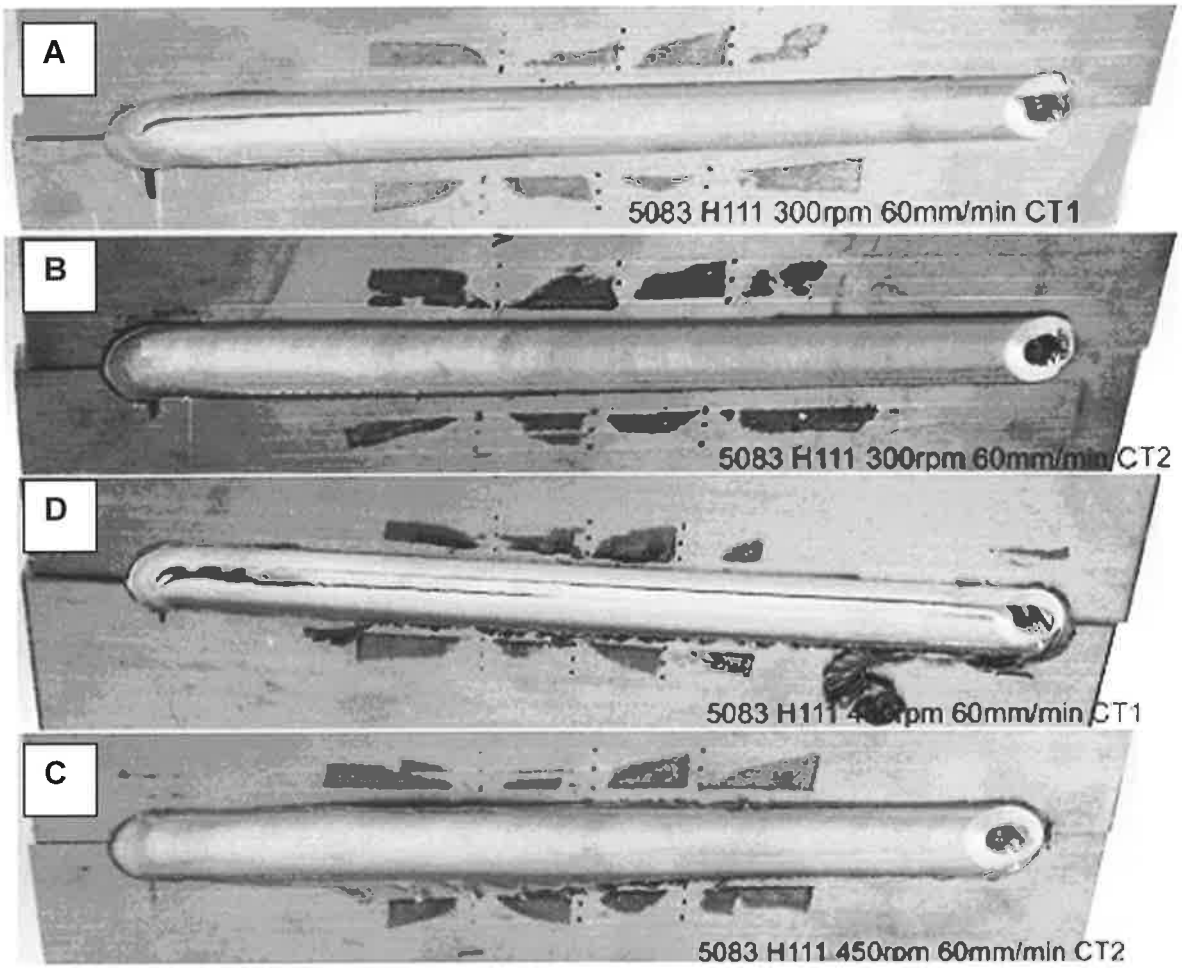

Figure 110 Welds produced in AA5083 H111 from top to bottom 405A, B, D and C. Note welds 405A and D were produced using tool pin CT1-14 and suffer from an open running void.

Weld temperature measurements again measured at 20 and 25mm either side of the weld join line and at mid plate thickness for the welds produced in the 5083 H111 alloy confirmed little difference in the processing temperatures of each workpiece as a result of FSW tool pin form, Figures 111 and 112. A summary of the peak processing temperatures as measured 20mm from the weld join line for both tool pins CT1-14 and CT2-14 when FSW the 5083 and 7075 alloys can be found in Figure 113.

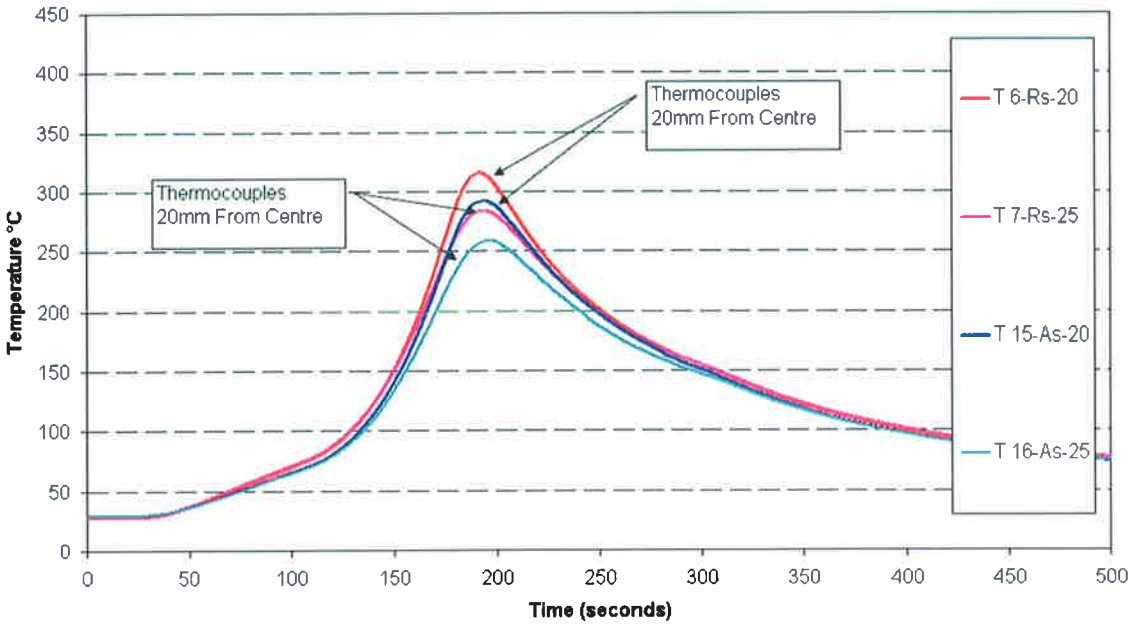

Figure 111 Temperature profiles as measured in workpiece for weld 405C, while FSW using tool CT2-14 for a rotational speed of 450rpm. Note As in the Legend refers to advancing side and Rs retreating side of the weld.

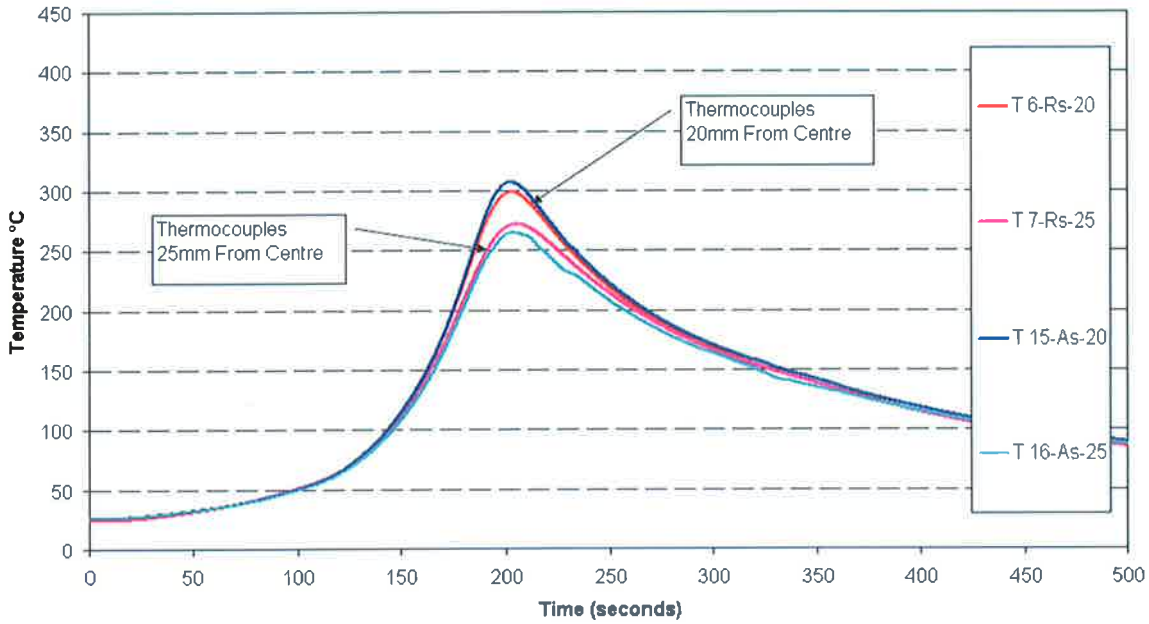

Figure 112 Temperature profiles as measured in workpiece for weld 405D, while FSW using tool CT1-14 for a rotational speed of 450rpm. Note As in the Legend refers to advancing side and Rs retreating side of the weld.

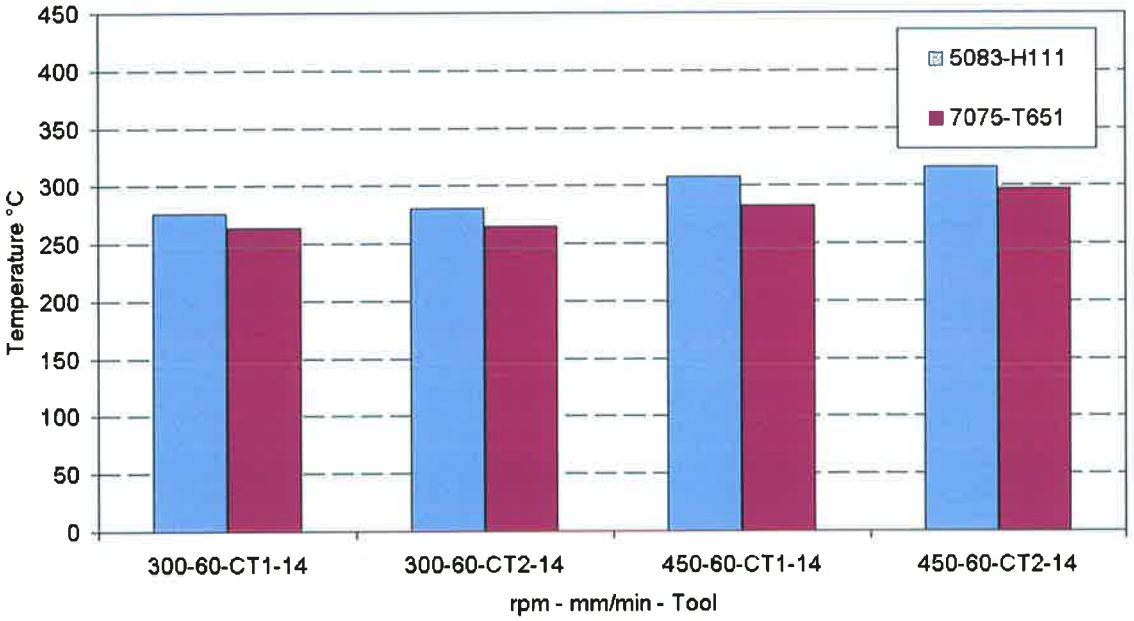

Figure 113 Summary of the peak temperatures as measured in the workpiece for welds produced in alloys 5083 and 7075 using tool pins CT1-14 and CT2-14.

Figure 113 reveals that for welds (5083 H111 or 7075 T651) produced under constant tool rotation speeds of 300rpm and 450rpm, the temperature as measured in the workpiece in response to FSW using tool pin types CT1-14 and CT2-14 varied by little more than 10°C. What is of interest however is that the 5083 alloy could be seen to generate measurably higher processing temperatures than those produced in the 7075 alloy for identical processing conditions. This could be observed not only for the welds containing defects but also those which were defect free. This may be due to the lower thermal conductivity of the 5083 alloy in comparison to the 7075 alloy. It may also be in response to a difference in the frictional heat generated between the two alloys during FSW. It should be recalled that the determination of friction torque between the tool and the surface of the workpiece will depend on the nature of the pressure distribution between the contacting shoulder and workpiece interface. Of greater interest however is the fact that volumetric defects were seen to increase in size as a result of the higher rotation speed when FSW both alloys using tool pin CT1-14. This would indicate that an increase in temperature on its own is unable to aid material flow and close the defect. It also suggests that weld parameters which can be used to friction stir weld the 5083 and 7075 alloys are in part a function of the tool pin form and the axial load placed on the surface of the workpiece.

When process loads (kg) in the direction of weld travel were compared, firstly for the 7075 T651 alloy, Figures 114-117 and then for the 5083 H111 alloy, Figures 118-121 it could be

observed that under identical processing parameters the CT1-14 tool pin always generated the higher loads for the direction of weld travel. A summary of these loads when converted to force (N) through the multiplication of load (kg) by acceleration (gravitation constant) can be found in Figure 122.

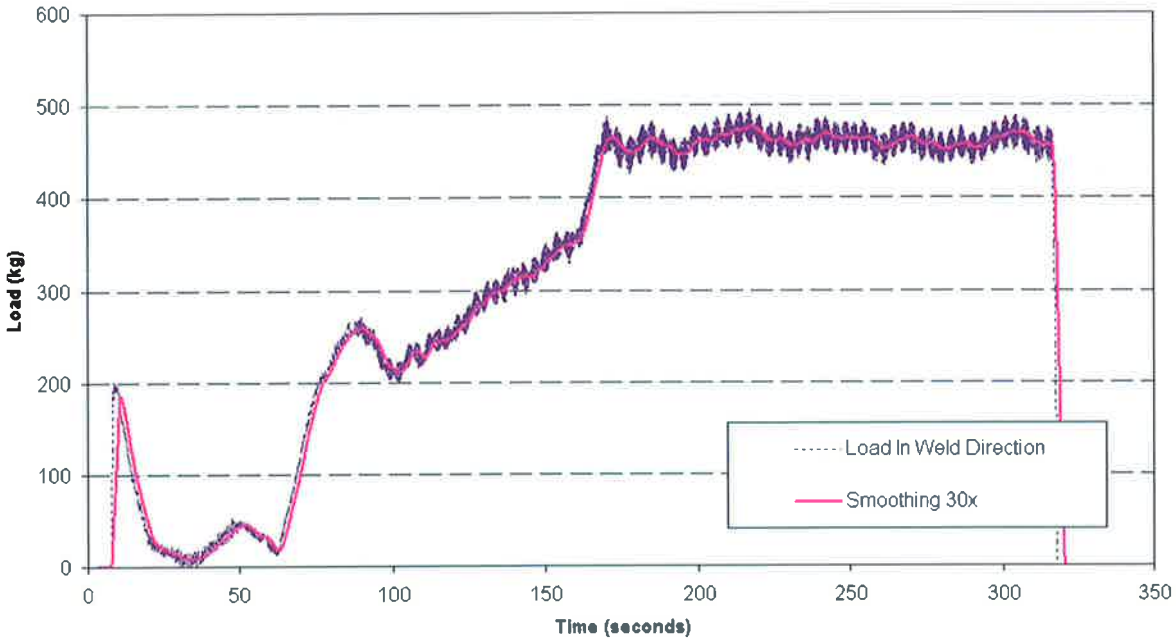

Figure 114 Load in the direction of weld travel for weld 403A (AA7075), while FSW using tool CT1-14 for a rotational speed of 300rpm

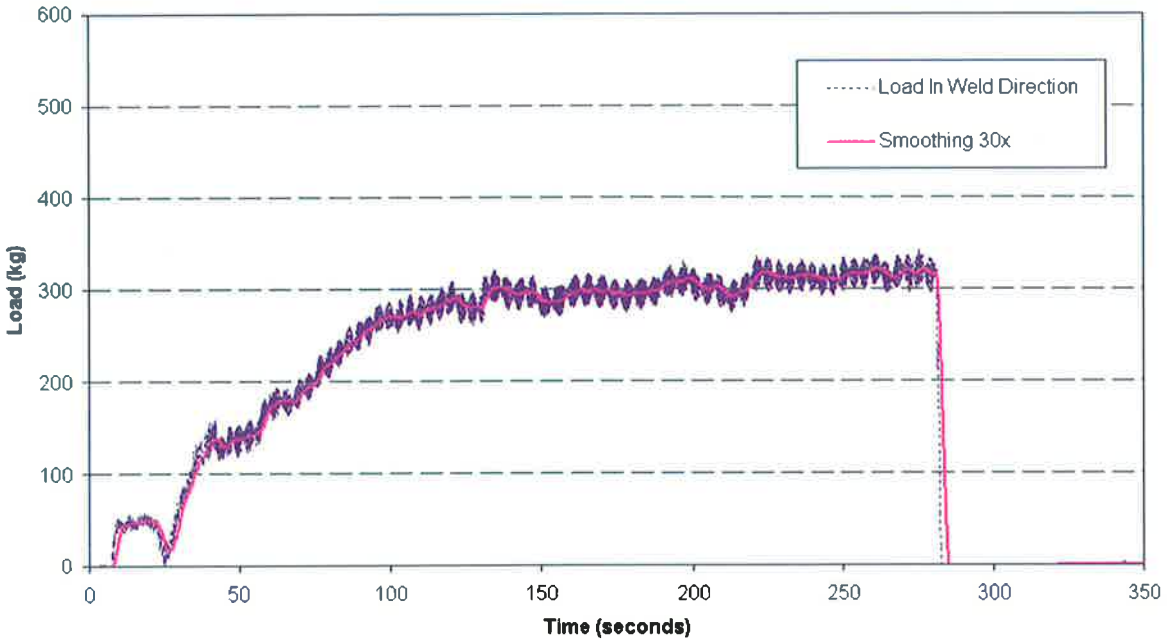

Figure 115 Load in the direction of weld travel for weld 403B (AA7075), while FSW using tool CT2-14 for a rotational speed of 300rpm

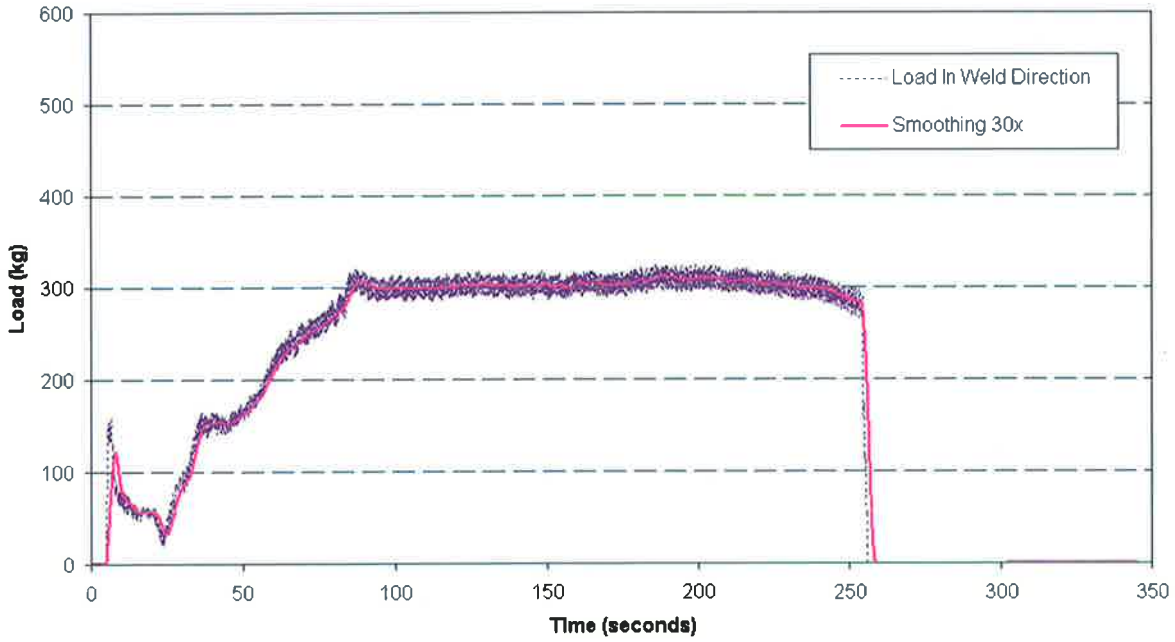

Figure 116 Load in the direction of weld travel for weld 403C (AA7075), while FSW using tool CT2-14 for a rotational speed of 450rpm

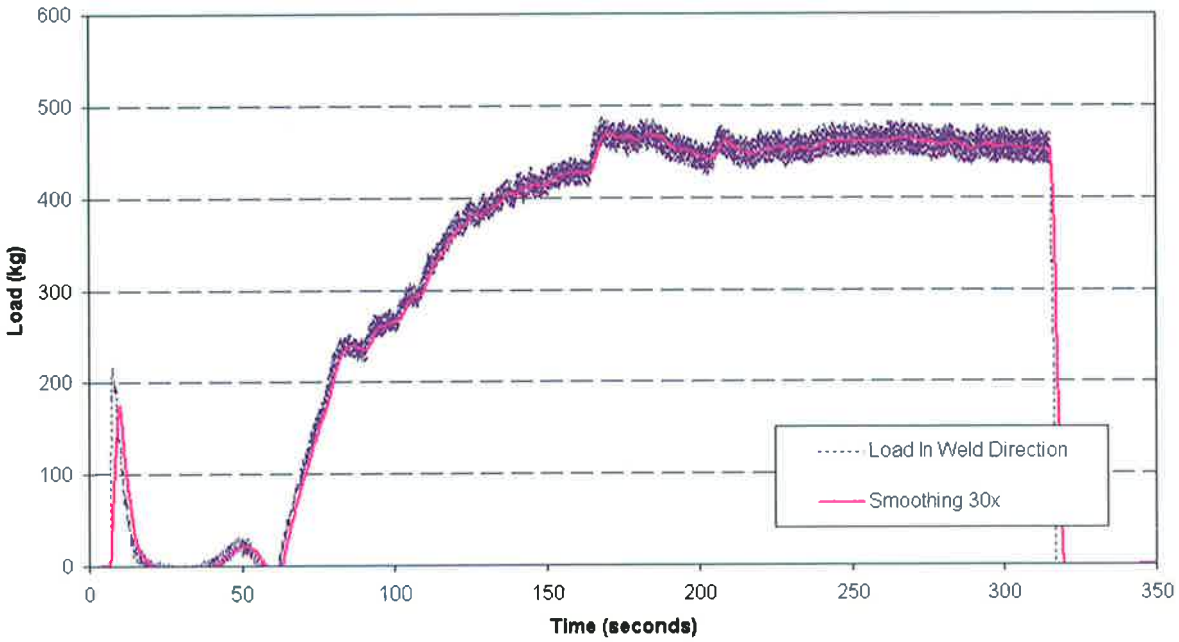

Figure 117 Load in the direction of weld travel for weld 403D (AA7075), while FSW using tool CT1-14 for a rotational speed of 450rpm

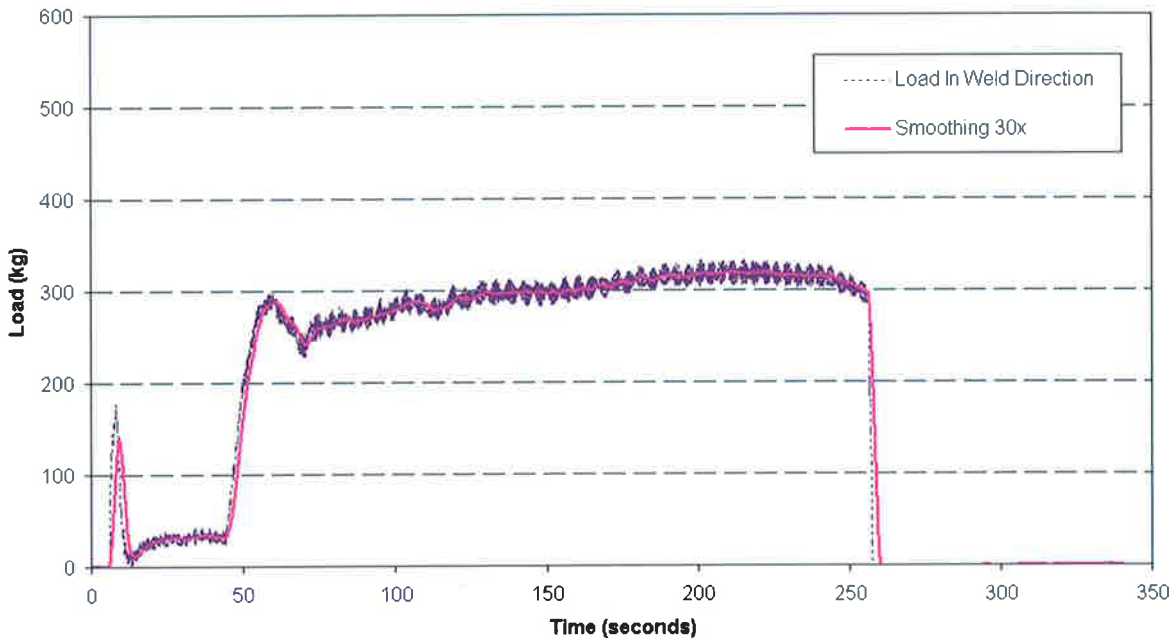

Figure 118 Load in the direction of weld travel for weld 405A (AA5083), while FSW using tool CT1-14 for a rotational speed of 300rpm

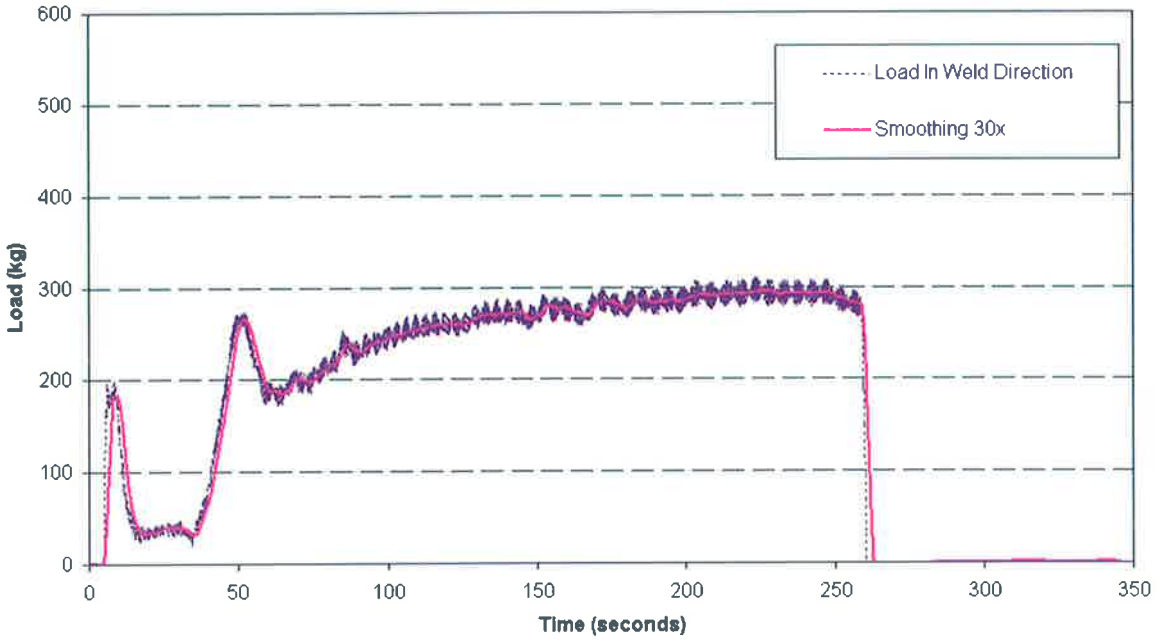

Figure 119 Load in the direction of weld travel for weld 405B (AA5083), while FSW using tool CT2-14 for a rotational speed of 300rpm

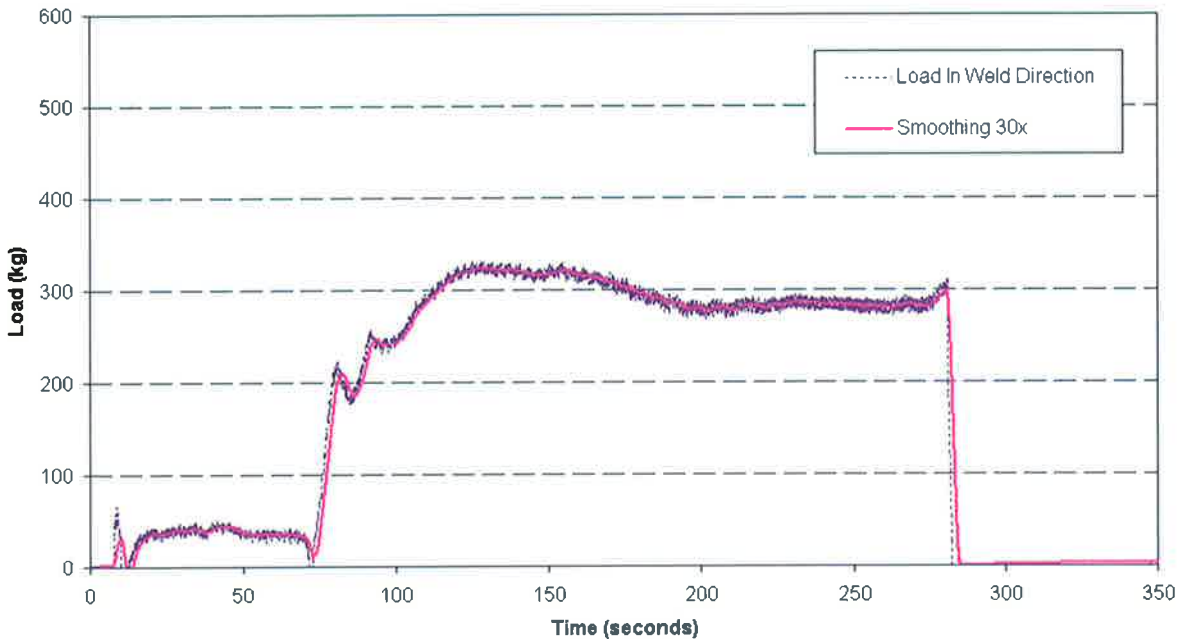

Figure 120 Load in the direction of weld travel for weld 405C (AA5083), while FSW using tool CT2-14 for a rotational speed of 450rpm

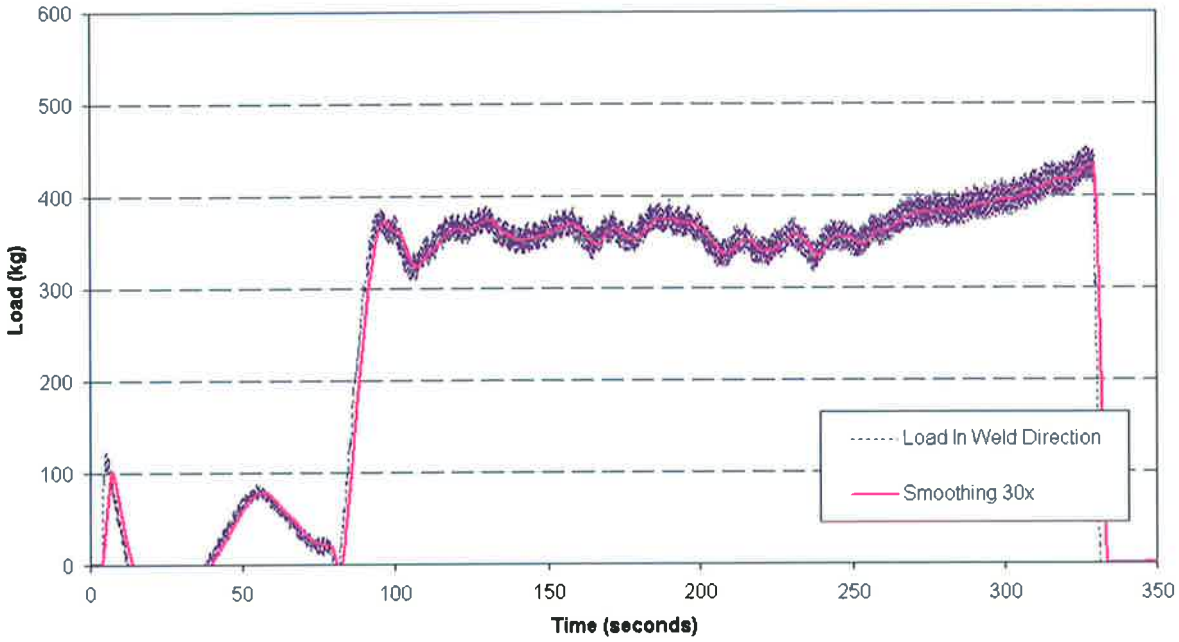

Figure 121 Load in the direction of weld travel for weld 405D (AA5083), while FSW using tool CT1-14 for a rotational speed of 450rpm

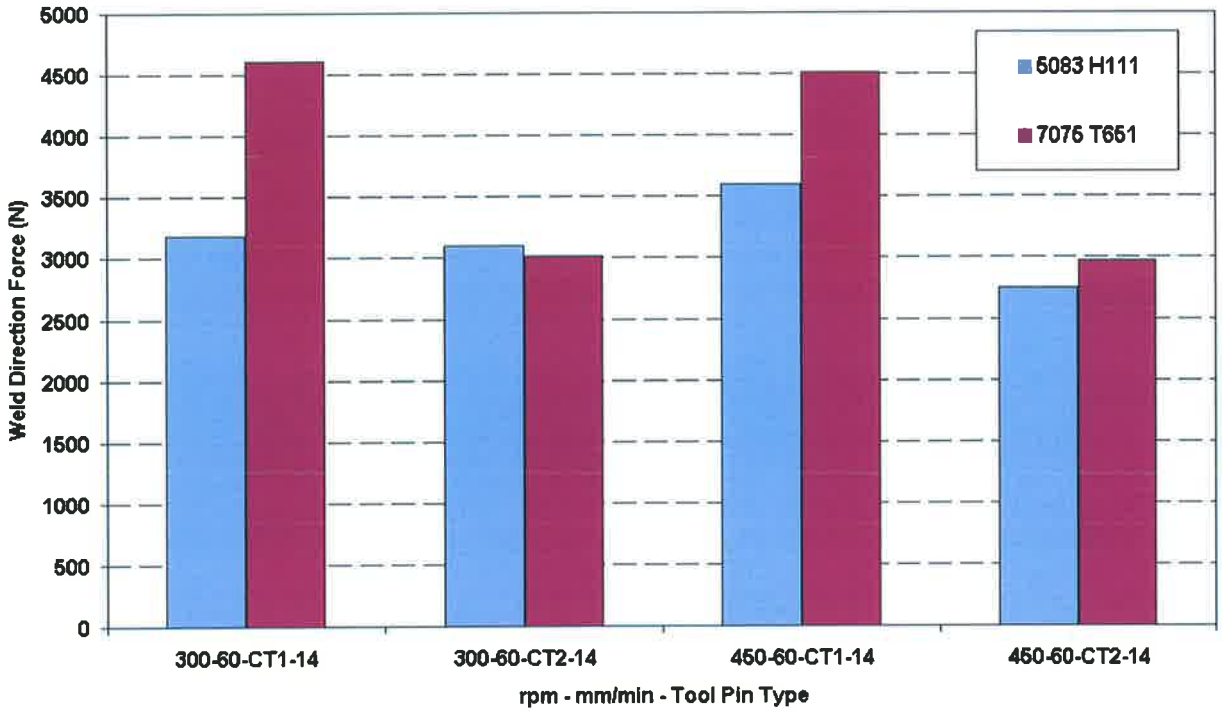

Figure 122 Summary of peak forces (N) for the direction of welding as a function of tool pin profile (CT1-14 and CT2-14) for welds produced in alloys 5083 and 7075.

Processing forces as summarised in Figure 122 reveal that for each tool pin the force generated in the direction of weld travel decreased with increasing tool rotation speed. In all cases however tool pin CT2-14 possessing the three flats demonstrated the lower processing force. It is believed that this reduction in weld force for the direction of welding in each alloy occurred in response to the tool pin profile and not because of increased welding temperatures. This reduction in force also enabled the production of defect free welds when using tool pin CT2-14 where tool pin CT1-14 could not. The reason that weld defects formed for welds produced using tool pin CT1 can be put down to the fact that the axial force placed onto the surface of each workpiece i.e. 0.9mm of compensatory plunge was insufficient to maintain intimate contact between tool shoulder and surface of the workpiece. Pin CT1 having a continuous thread enabled the tool to climb slightly out of the workpiece during welding. This was not the case of tool pin CT2 as the threads were interrupted for a large proportion of the pin due to the flats.

In terms of processing temperatures it should be recalled that these were measured in the far field i.e. at 20 then 25mm from the weld join line, for each workpiece. These temperature measurements are therefore only capable of reflecting the temperature as appears in the HAZ of the workpiece and do not allow for an intimate assessment of temperature isotherms i.e. the shape of the heat source generated in the region of the stir zone. As such it could be argued that weld temperatures as measured in direct contact with the welding tool pin may vary substantially in relation to pin form and thus render meaningless any observation of FSW temperatures conducted in the far field between the two tool pin forms. To assess this hypothesis it was decided to design a FSW tool capable of recording FSW temperatures in four locations of the tool, 1mm removed from the tool and workpiece interface. This tool was designed by the author and allowed for interchangeability of tool pins. The assessment of tool temperature relationships during the FSW process is the subject of section 5.4.

5.4 Tool And Workpiece Temperature Relationships When FSW 25mm Thick Aluminium Alloy 5083-H111

Unlike fusion welding the processes of friction and FSW rely on heat being generated by the physical interaction of typically two contacting bodies. In the case of FSW this interaction is between the welding tool and the workpiece. When two contacting solids are pressed together, the temperature of the contiguous friction surfaces do not remain constant and may vary within the friction surfaces. This is due to the fact that the energy utilized for overcoming the friction forces (molecular-mechanical interaction of the surfaces) is firstly generated as heat on the elementary physical contact surfaces. At these points (known as asperities) temperature peaks may appear causing a sudden increase in temperature of the micro projections. These temperatures may drop just as quickly because of an intensive dissipation of heat from within the body to the surrounding medium. Heat will therefore flow into two solids, partitioned, dependant on their geometry, the nature of the heat source and material flow as well as material thermal properties. The results of the experimental investigation reported here in section 5.4 were an attempt to answer the question as to what extent FSW temperatures as measured in the welding tool were influenced by tool pin geometry and its relationship with the workpiece. These measurements were performed for the FSW of 25mm thick 5083 H111 aluminium alloy using the instrumented tool designed by the author, section 3.6, Figure 71.

The initial welding trial, weld 215B was performed using a conical threaded pin, CT1-20, Figure 123 coupled to a 50mm diameter concentric ring shoulder, 50CR20. The weld was performed for a tool tilt of 3° away from the direction of weld travel using the parameters indicated in Table 5-7 below.

Rotation Speed (rpm)	Weld Speed (mm/min)	Length of travel (mm)
200	*50*	*160*

Table 5-7 Weld parameters used to produce weld 215B made in 25mm thick AA5083 H111. Note for 200rpm using equation 1, section 2.10 of Chapter 2, the linear rubbing velocity at the pin shank = 0.21m/sec and 0.52m/sec at the tool shoulder periphery.

It should be recalled that the rotation speed selected for FSW the 25mm thick 5083 alloy produced the identical tool rubbing velocity as was employed to friction stir weld 12.5mm thick 5083 H111 alloy in section 5.1.

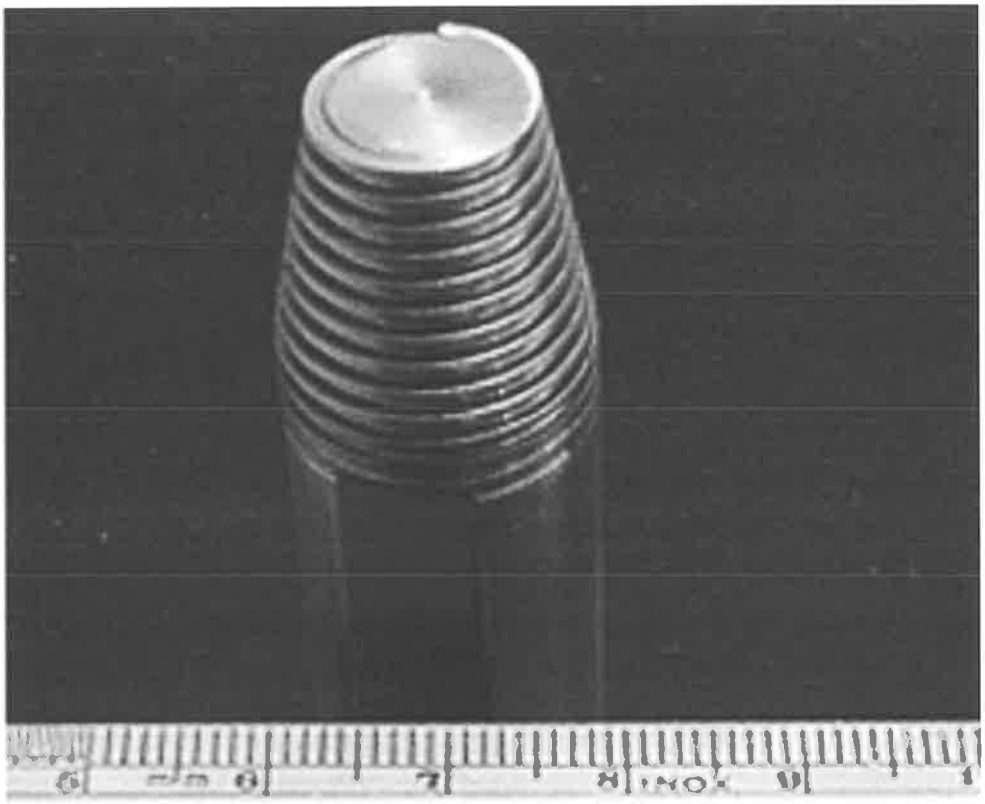

Figure 123 Weld pin CT1-20 used to produce weld 215B

During the production of weld 215B it was not possible to measure temperature in the tool during the entire tool plunge distance. This was because the brushes which were to make contacted with the slip ring, Figure 71, section 3.6 were not capable of sufficient bending to allow for continuous contact with the slip ring over the entire plunge distance. As such the tool had to first be plunged approximately 75% of the overall distance into the workpiece before contact between slip ring and brushes was possible. This is reflected by a lack of temperature data for the tool embedded thermocouples, Figure 124, in the region 0-200 seconds of weld time. In addition to the tool embedded thermocouples, k-type thermocouples were also placed in and around the path of the FSW tool but within the workpiece. The FSW temperatures as registered for both tool and workpiece embedded thermocouples can be found in Figure 124. A comparison of weld temperatures reveals that weld 215B was produced with an average temperature (maximum) of approximately 510°C. This temperature maximum was recorded by both the instrumented tool and thermocouples placed in the workpiece stir zone.

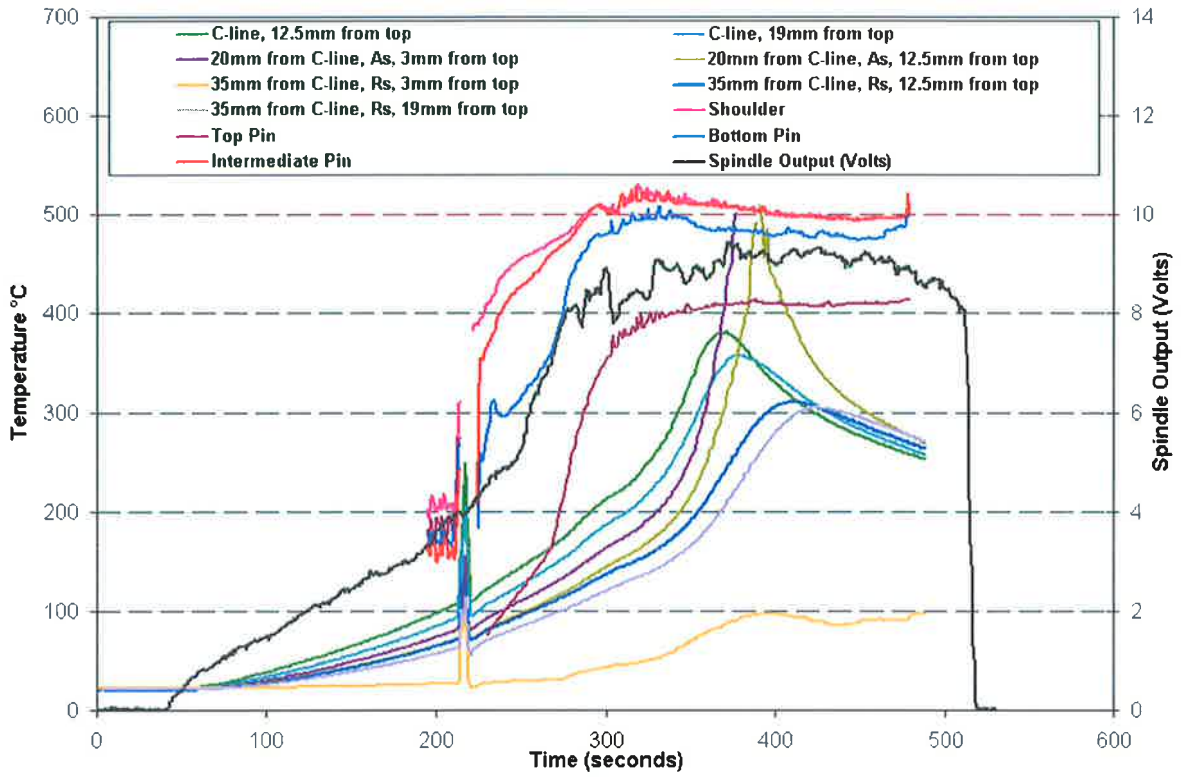

Figure 124 Spindle output and FSW temperatures as measured in the FSW tool (pin CT1-20) and workpiece material. Note As = advancing side, Rs = retreating side of weld.

Although the instrumented tool demonstrated it was possible to measure and compare processing temperatures within and around the weld nugget, weld 215B contained a substantial subsurface volumetric defect as can be seen in Figure 125, placing the validity of some of the temperature measurements in and around the stir zone in doubt.

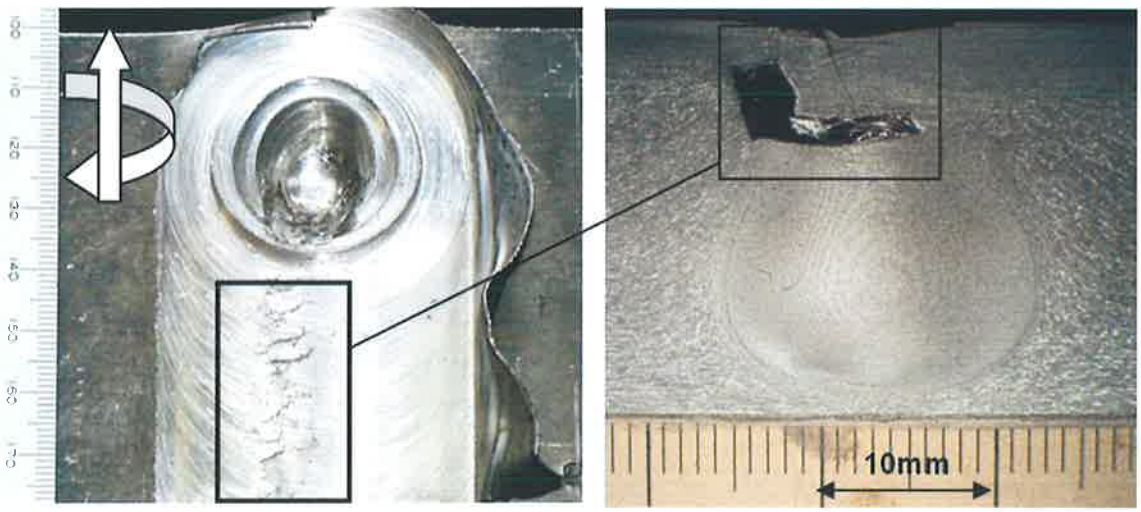

Figure 125 Weld 215B top view left and macrograph right with volumetric defect highlighted by the boxed section of the weld.

The large volumetric defect, which can be seen in the weld macrograph, Figure 125 was not immediately apparent from visual inspection of the weld surface. This defect could however be clearly seen when the exit hole was examined. Weld 215B also suffered from a considerable amount of weld flash. In this case the weld flash occurred because of too deep a tool plunge of the shoulder into the surface of the workpiece.

Weld 215B was reproduced using tool pin CT2-20. This weld 822A set out to compare whether the weld pin form (CT2) was capable of producing a defect free weld under identical processing conditions as was used to produce weld 215B but also to answer the question as to what extent FSW temperatures as measured in the welding tool were influenced by tool pin geometry. Pin CT2-20, Figure 126 was identical to pin CT1-20, Figure 123 but had three flats milled at a spacing of 120° along the entire length of the threaded portion of the pin, such that the threads were no longer visible in these regions of the pin.

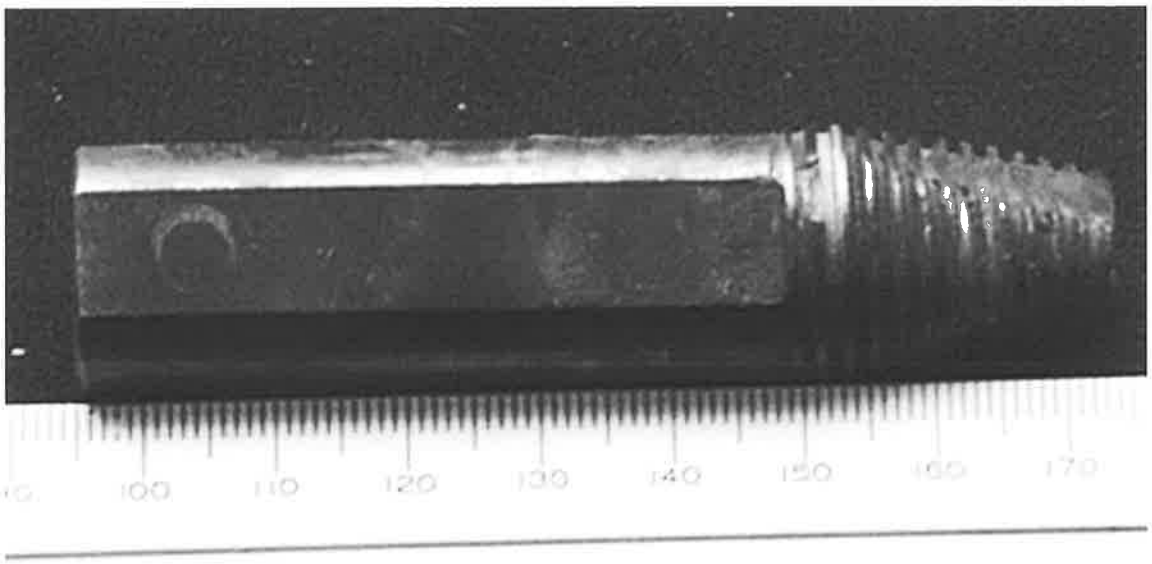

Figure 126 Weld pin CT2-20 used to produce weld 822A

A modification was also undertaken for the instrumented tool which measured temperatures in the pin and shoulder. This was carried out on the support arm carrying the brushes that were to make contact with the slip ring of the instrumented tool. Here a return spring was installed. This allowed for vertical movement of the arm carrying the brush thus allowing for the brushes to make permanent contact with the slip ring during the entire tool plunge. These modifications can be seen in Figure 74, section 3.6.

Temperatures as measured in the FSW tool during plunge for weld 822A, Figure 127 reveal that the tip of the pin was the hottest part of the welding tool until around 300 seconds after initiation of plunge. At this point weld travel is initiated and here after temperatures as measured for the next 60 seconds in the four locations of the tool i.e. pin tip, pin at mid length, pin near shoulder and shoulder) begin to converge suggesting that the welding tool had perhaps reached temperature saturation and that welding had achieved steady state thermal processing.

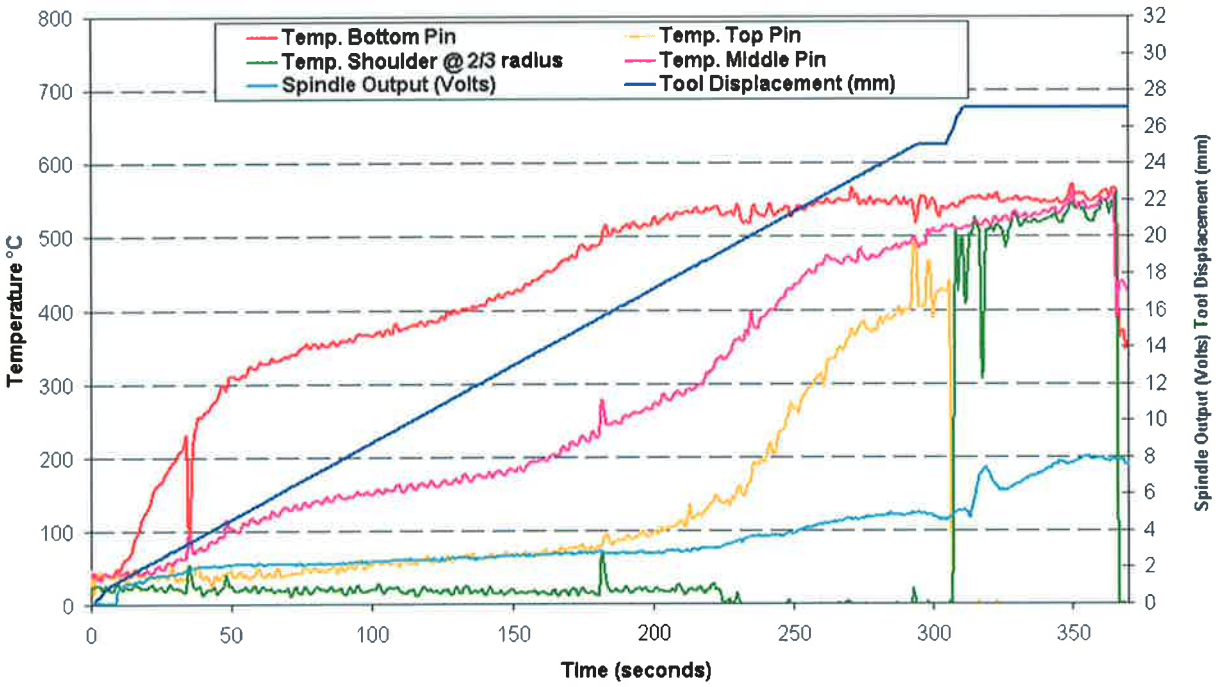

Figure 127 Spindle output and FSW temperatures as measured in the FSW tool (pin CT2-20) for weld 822A.

Tool temperatures as measured for both weld 215B and 822A, Figures 124 and 127 respectively indicate that bulk tool temperature under the investigated FSW parameters, as given in Table 5-7 of this section varied by less than 30°C between the two welding tools. Weld 822A unlike weld 215B did not suffer from a volumetric defect and as such this was probably the reason for the slightly higher tool temperature, which was recorded for this weld. A temperature difference of approximately 30°C between both welds is however relatively small when one compares the overall tool temperature recorded (approximately 540°C).

The fact that the bulk FSW temperatures of both tools was not significantly affected by changes made to the welding tool pin form suggests that welding parameters such as tool rotation, travel speed and axial load are the main precursors of heat generation and not tool pin geometry. More significant however to the heat developed in the tool was the fact

that tool pin CT2-20 used to produce weld 822A unlike tool pin CT1-20-2 was capable of producing a defect free weld, Figure 128.

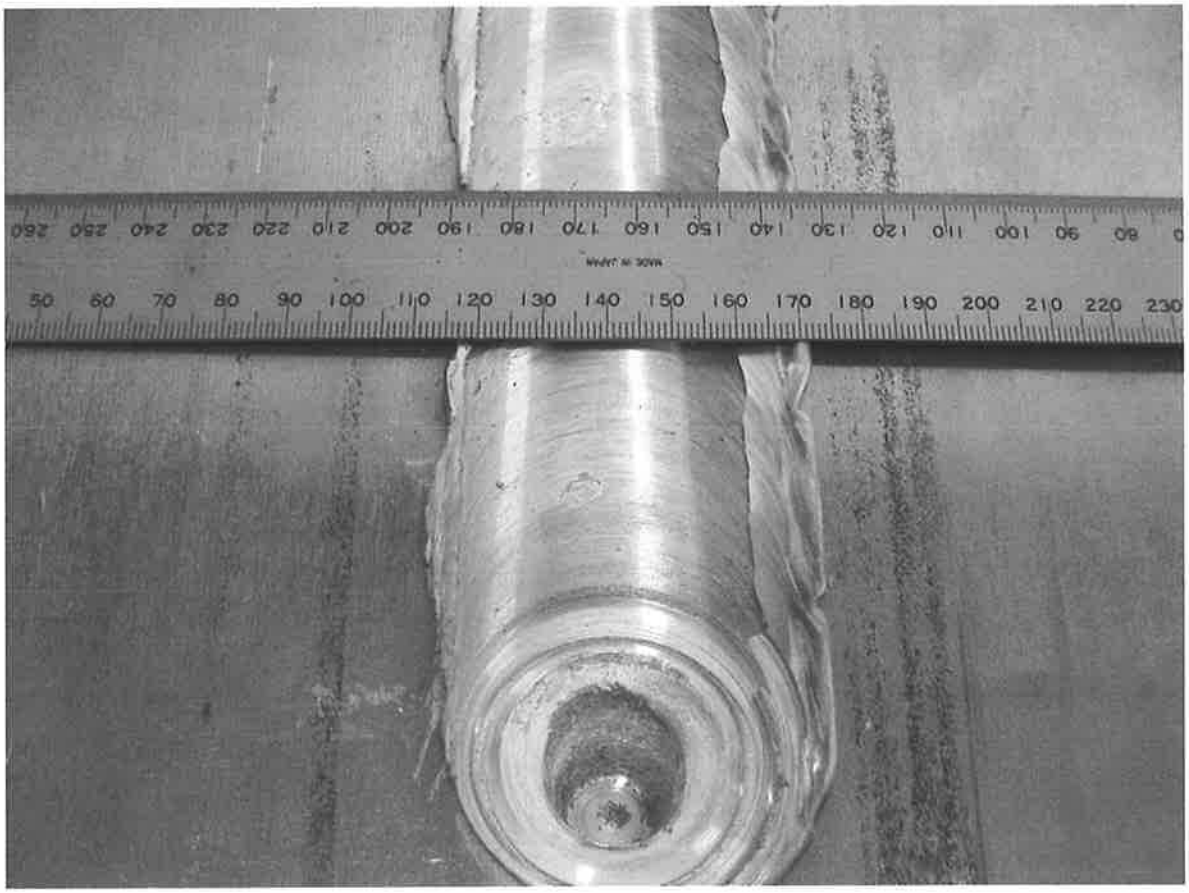

Figure 128 Weld 822A produced in 25mm thick 5083 H111 alloy using tool pin CT2-20. Note no defect could be seen in the region of the exit hole.

Figure 128 reveals that weld 822A did not suffer from a sub-surface volumetric defect as was evident from inspection of the exit hole in weld 215B. Although it was not possible to measure FSW load in relation to the FSW of 25mm thick plate, simply because the test bed cradle for mounting the workpiece holder was not robust enough for use with this thickness of plate, Figures 124 and 127 give an indication as to the amount of the load the spindle motor was encountered while producing the two welds. Spindle motor output (Volts) can be seen to be approximately 9 Volt for weld 215B, produced using tool pin CT1-20 while for weld 822A, produced using tool pin CT2-20 this value is 8 Volt. Section 5.2 of this chapter had previously indicated that the larger the spindle motor output the higher was the load observed in the direction of weld travel. From these observations it would seem plausible that welding temperature alone did not dictate whether a friction stir weld would be free from defect.

5.5 Tool Plunge Depth, Weld Travel Speed And Spindle Motor Output Relationships When FSW 25mm Thick Aluminium Alloy 5083-H111

The FSW trials conducted in section 5.4 not only demonstrated that tool pin CT2-20 when combined with tool shoulder 50CR20 was capable of producing defect free friction stir welds in 25mm thick 5083 H111 alloy but that tool rubbing velocities as calculated for the pin and shoulder were capable of being transferred for use in friction stir welds where workpiece thickness differed i.e. between 12.5mm (refer section 5.1) and 25mm thick plate.

The weld travel speed attempted when producing 25mm thick friction stir welds in section 5.4 was maintained at 50mm/min for fear of damage the instrumented tool. This was justified considering the high spindle motor load that was encountered.

Section 5.5 reports the results of welding trials conducted in 25mm thick aluminium alloy 5083 H111 where welds were attempted over a range of weld travel speeds. Three welds, 625A-C were produced using tool pin, CT2-20, previously shown in Figure 126 coupled to tool shoulder 50CR20. The slip ring and thermocouples were removed from the FSW tool prior to welding and all welds were performed as B.O.P. for a constant tool rotation speed of 250rpm and a tool tilt away from the direction of weld travel of 3°. The welds are further identified in Table 5-8.

Weld No.	Weld Speed (mm/min)	Length of travel (mm)
625A	*70*	*160*
625B	*100*	*160*
625C	*60*	*160*

Table 5-8 Weld parameters used to produce welds 625A-C made in 25mm thick AA5083 H111. Note for 250rpm using equation 1, section 2.10 of Chapter 2, the linear rubbing velocity at the pin shank = 0.26m/sec and 0.65m/sec at the tool shoulder periphery.

It should be noted that for a tool rotation speed of 250rpm the tool pin has a rubbing velocity of 0.26m/sec while the tool shoulder achieves 0.65m/sec. These values are slightly higher than those attempted for friction stir welds produced in section 5.4. The higher tool rotation speed was selected in order to generate slightly higher processing temperatures as a means of compensating for increasing weld travel speed.

Section 5.1 of the results had demonstrated that it was important to seat the shoulder of the FSW tool a certain distance into the surface of the workpiece if defect formation i.e. open running voids were to be avoided. The level of compensatory plunge distance for the selected weld parameters needed to be established. Table 5-9 identifies the level of plunge depth compensation used for weld 625A.

Weld No.	Pin Stick out (mm)	Overall Plunge Displacement (mm)	Plunge Displacement To Reach Workpiece (mm)	Plunge Depth Compensation Into Workpiece (mm)
625A	*20*	*25.5*	*2.0*	*3.5*

Table 5-9 Plunge depth settings for friction stir weld 625A

Table 5-9 indicates that the overall plunge distance was 25.5mm. This was performed in two stages. The first stage plunged the tool 24.3mm at a plunge rate of 5mm/min. There after the tool was plunged a further 1.2mm at a plunge rate of 2mm/min.

Weld 625A was produced using a weld travel speed of 70mm/min. From the appearance of the surface of the weld it looked as if the weld was free from defect. Examination of the exit hole suggested otherwise as there could be seen a number of small sub-surface voids, later confirmed by the weld macrograph, right hand caption of Figure 129.

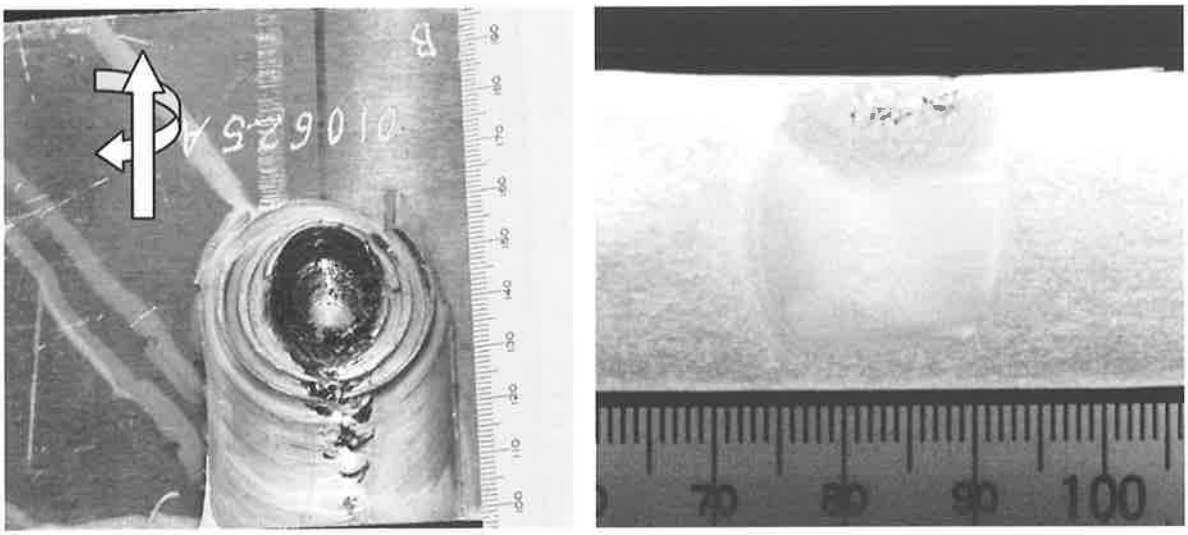

Figure 129 Weld 625A top view left and weld macrograph right demonstrating the small sub-surface voids.

It should be noted that during the FSW of weld 625A several attempt were made to further plunge the tool into the workpiece during weld traverse, Figure 130. This was initiated to enable greater tool shoulder contact with that of the surface of the workpiece.

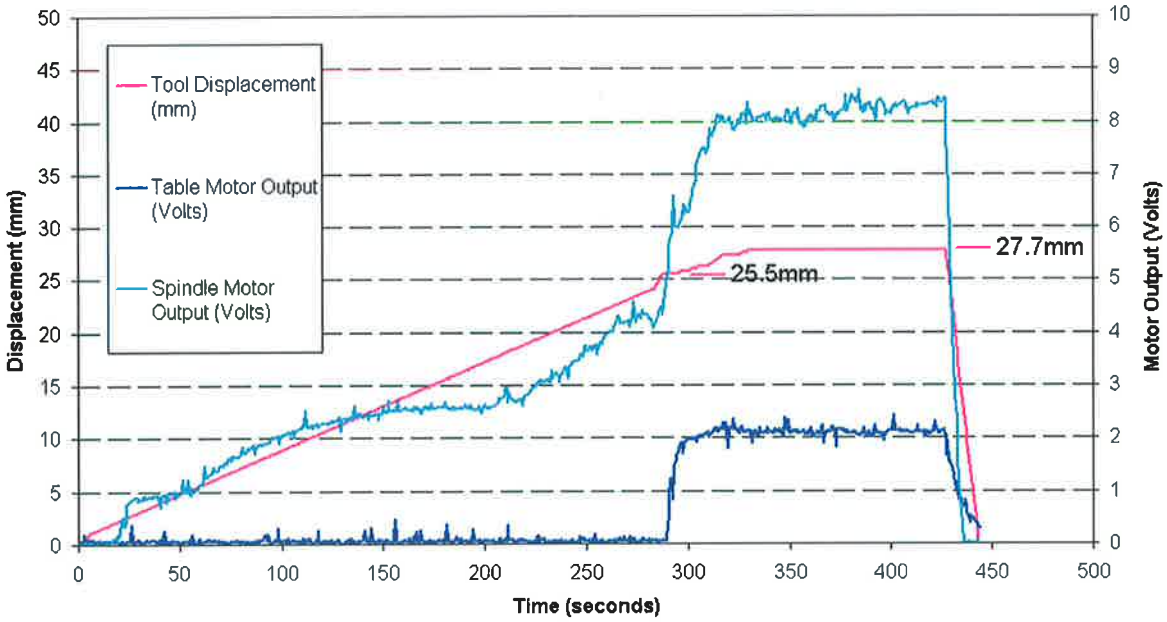

Figure 130 Tool displacement vs. motor output plot for B.O.P. weld 625A.

The volumetric defect encountered when producing weld 625A was put down to inadequate seating of the tool shoulder prior to commencement of weld travel. As such tool plunge compensation was increased for weld 625B, Table 5-10.

Weld No.	Pin Stick out (mm)	Overall Plunge Displacement (mm)	Plunge Displacement To Reach Workpiece (mm)	Plunge Depth Compensation Into Workpiece (mm)
625B	*20*	*27.7*	*2.5*	*5.0*

Table 5-10 Plunge depth settings for weld 625B

It was hoped that by employing a two stage plunge whereby tool depth displacement was programmed at an initial travel speed of 5mm/min for the first 24.3mm of plunge displacement followed by a further reduced plunge travel speed of 2mm/min for a distance of 3.2mm that the problem concerning the seating of the tool shoulder, weld 625A could be eliminated, Figure 131. Weld 625B was attempted for a weld travel speed of 100mm/min. No further plunging of the tool occurred during welding.

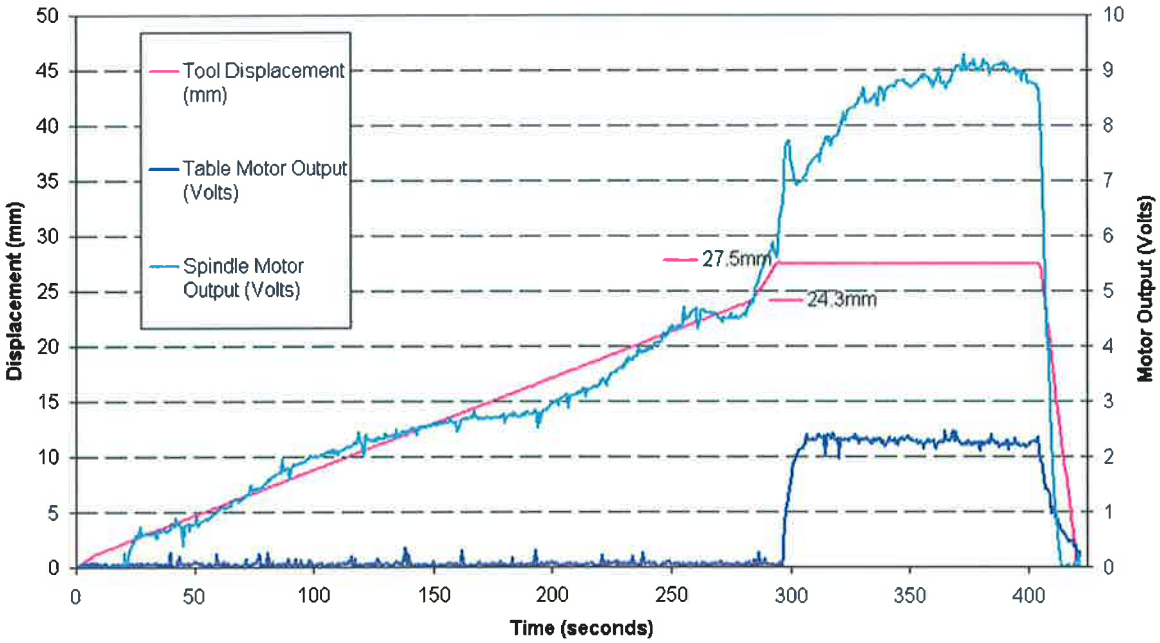

Figure 131 Tool displacement vs. motor output plot for B.O.P. weld 625B.

Although the tool shoulder was successfully seated into the workpiece material prior to commencement of weld travel for weld 625B it was obvious from the surface appearance of the weld, Figure 132 that a volumetric defect in the form of an open running void had occurred. A macrograph made of the weld transverse to the weld travel direction, (right hand caption of Figure 132) clearly demonstrates the extent of this defect. Here it can also be seen that the workpiece had grown in thickness indicated by a swelling of the workpiece in the region of the stir zone directly below the tool shoulder.

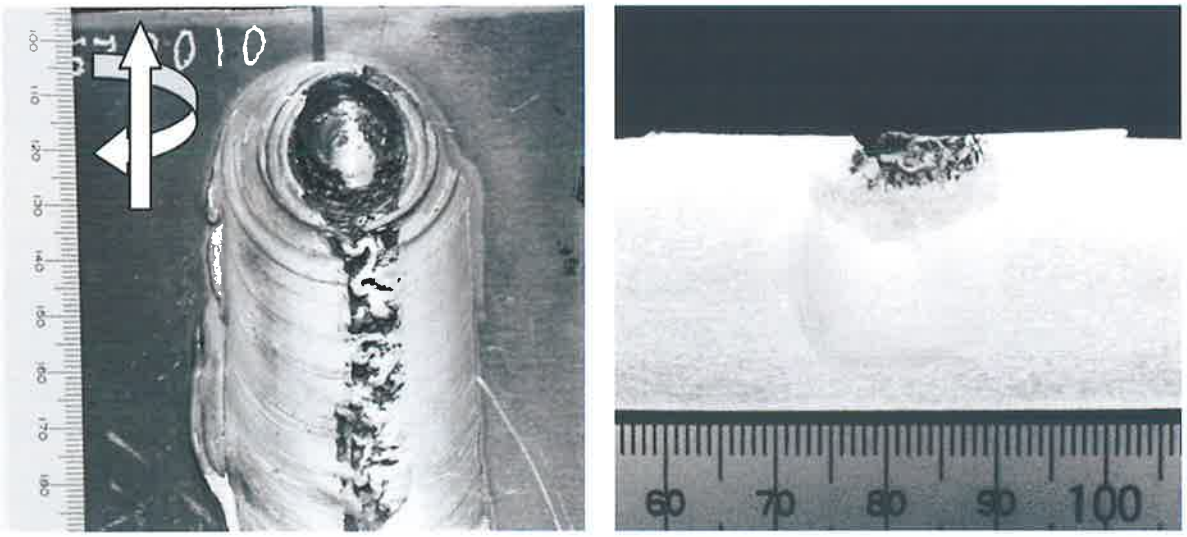

Figure 132 Weld 625B top view left and weld macrograph right demonstrating the surface breaking defect.

The increased size of the weld defect, (weld 625B) in comparison to weld 625A can be attributed to the increase in weld travel speed used to produce weld 625B. The increase in weld travel speed of 30mm/min in the weld travel speed however could not directly explain why the workpiece had grown by approximately 1mm in thickness. For this to have occurred it is estimated from the load vs. deflection plot, Figure 56 of Chapter 3 that an reactionary axial load in excess of 6000kg (60kN) must have been generated during welding. This upward axial force was sufficient to cause the spindle and support structure to deflect and resulted in the tool shoulder riding above the surface of the workpiece even though the tool shoulder had initially been seated in intimate contact with the surface of the workpiece during the initial tool plunge. Further evidence of the high processing forces encountered during the production of weld 625B can be inferred by the relatively high spindle motor output measured for weld 625B, Figure131 when compared to spindle motor output, weld 625A, Figure 130.

The fact that welds 625A and 625B suffered from volumetric defects as a result of their respective travel speeds it was decided to reduce the welding speed for weld 625C to 60mm/min. The overall tool plunge displacement was also reduced to 26mm. Plunge parameters for weld 625C can be found in Table 5-11.

Weld No.	Pin Stick out (mm)	Overall Plunge Displacement (mm)	Plunge Displacement To Reach Workpiece (mm)	Plunge Depth Compensation Into Workpiece (mm)
625C	*20*	*26.0*	*2.0*	*4.0*

Table 5-11 Plunge depth settings for weld 625C.

A two stage plunge was again programmed for weld 625C. Here an initial plunge travel speed of 5mm/min for the first 24.3mm of plunge was followed by a further reduced plunge travel speed of 2mm/min for a distance of 1.7mm, Figure 133.

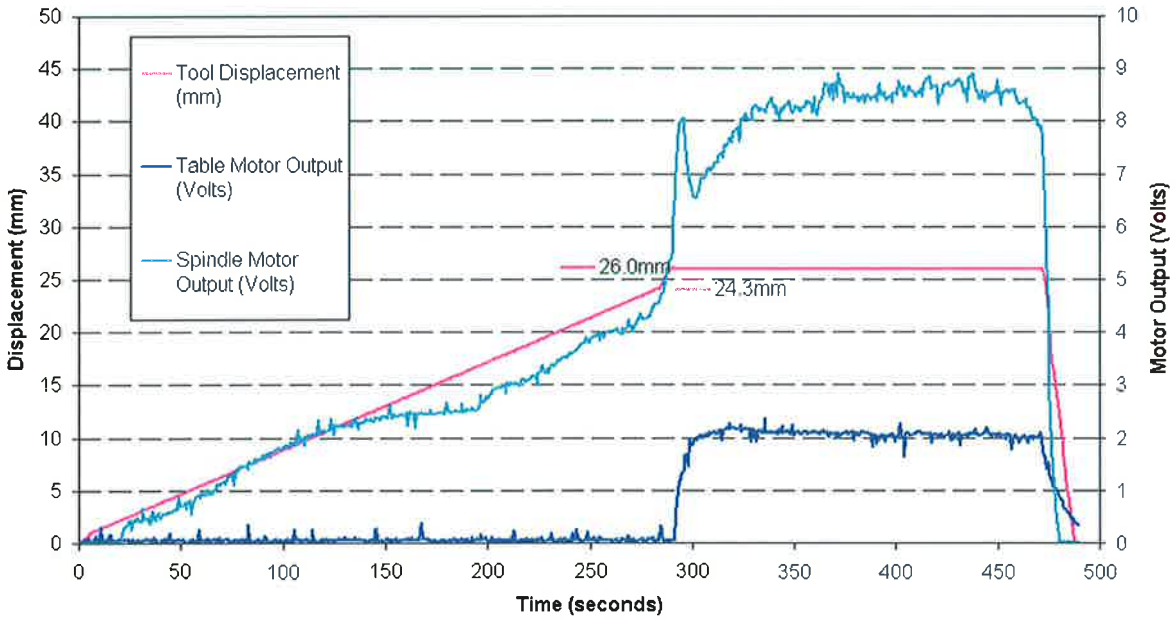

Figure 133 Tool displacement vs. motor output plot for B.O.P. weld 625C

The reduction in plunge depth and weld travel speed for weld 625C had an immediate effect in that the weld was free from defect, Figure 134 and there was an overall reduction in spindle motor output as can be seen from Figure 133 when compared to weld 625B, Figure 131. Since the spindle motor output was reduced this also infers that weld travel direction force had also been reduced, sufficient to avoid uplift of the tool and the formation of a weld defect.

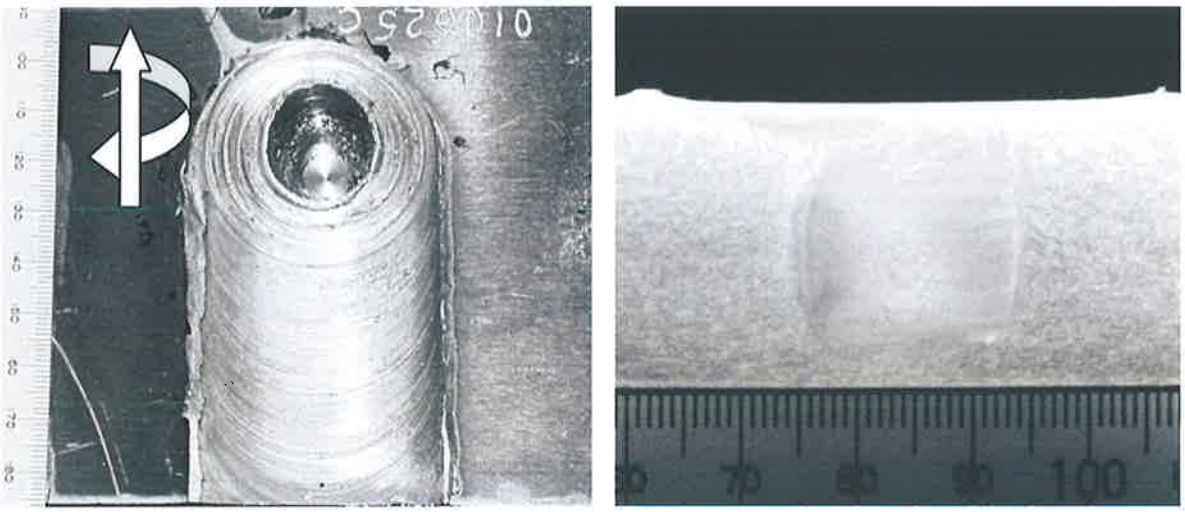

Figure 134 Weld 625C top view left and weld macrograph right demonstrating a sound and defect free weld.

The combined welds 625A-C had demonstrated that it was again possible to produce a defect free weld for a tool rotation speed of 250rpm and weld travel speed of 60mm/min, while using tool pin CT2-20 in conjunction with shoulder 50CR20. The increase of 50rpm in comparison to the friction stir welds produced in 25mm thick 5083 H111 alloy, section 5.4 had made possible a further increase of 10mm/min in the weld travel speed. The results however indicated that further increases in weld travel speed using the tool rotation speed of 250rpm were not possible due to an ability to prevent tool uplift from occurring during weld travel. This tool uplift could be clearly identified in the form of a swelling of the workpiece, which occurred directly under the tool shoulder in the stir zone of the weld. The reason for the uplift of the tool can be attributed to an increased axial force causing deflection, primarily to the spindle, Figure 56 of Chapter 3.

It should be recalled that welds 625A-C were produced as B.O.P. welds with a weld travel distance of approximately 160mm. This was because workpieces measured 200mm in length and 140mm in width. The results obtained from welds 625A-C are therefore only relative for the processing conditions encountered i.e. B.O.P. welding in relatively small workpieces. For these reasons it was decided to prove the capability of the welding tool and process parameters by producing a two metre long single pass butt weld, again in 25mm thick aluminium alloy 5083 H111 and compare this with the B.O.P. welds produced in section 5.5. The results from this weld are presented in section 5.6.

5.6 The Production of a 2m Long Friction Stir Weld Made in 25mm Thick Aluminium Alloy 5083 H111

Weld 716A was produced as a single pass butt weld in 25mm thick aluminium alloy 5083 H111. The weld length measured approximately two metres as can be seen in Figure 135. The weld was produced for a tool rotation speed of 250rpm and a weld travel speed of 60mm/min. as was used to produce B.O.P. welds in the same material, section 5.5.

Figure 135 The completed 2m long weld 716A produced in 25mm thick AA5083 H111

The welding tool pin employed to produce weld 716A, CT2-20. The pin was again coupled to the 50CR20 tool shoulder where a tool tilt of 3° away from the weld direction was employed.

Plunge parameters for weld 716A can be found in Table 5-12. The overall plunge depth compensation of 4mm maps that used to produce the defect free weld 625C, section 5.5.

Weld No.	Pin Stick out (mm)	Overall Plunge Displacement (mm)	Plunge Displacement To Reach Workpiece (mm)	Plunge Depth Compensation Into Workpiece (mm)
716A	*20*	*27.0*	*3.0*	*4.0*

Table 5-12 Plunge depth settings for weld 716A.

It was realized after the overall plunge displacement had taken place for weld 716A that the tool shoulder required further plunging into the workpiece. This was performed because it could be physically seen that the tool shoulder remained approximately 1mm above the surface of the workpiece. A plot of the tool displacement and spindle motor output for weld 716A can be found in Figure 136. As a consequence of the increased plunge it could be observed, Figure 136 that the spindle motor, for the majority of the weld length had had to operate at its maximum capacity i.e. 10 volts. This was approximately 10% higher than experienced by the spindle motor when producing the equivalent but much shorter weld length (160mm long) B.O.P. weld 625C, section 5.5. It is speculated that such a difference occurred because of joint configuration, in particular because of the size of each workpiece. Although no temperature measurements were taken during the production of either welds it is speculated that weld 625C because of the physical size of the workpiece produced a hotter weld and therefore produced the lower spindle load.

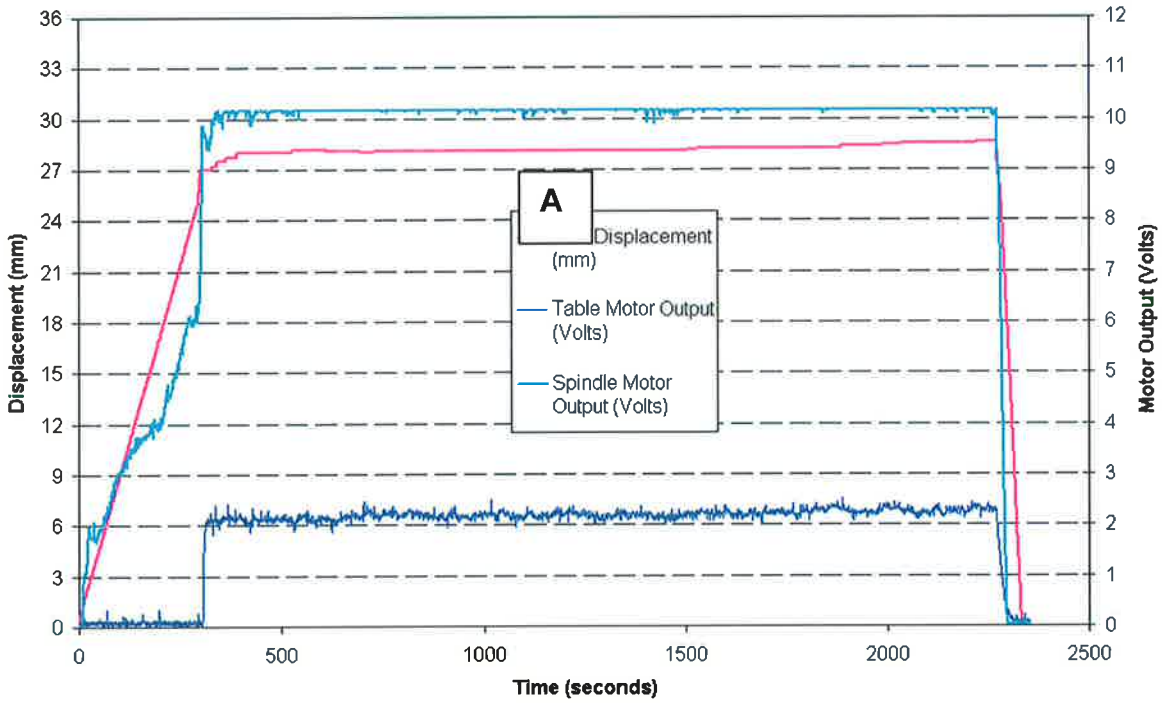

Figure 136 Tool displacement (mm) vs. motor output (Volt) plot for the 2m long butt weld 716A produced in 25mm thick aluminium alloy 5083 H111.

The surface of weld 716A appeared polished although at the outer edge of the weld could be seen a small quantity of flash, Figure 137. No volumetric defect could be detected when looking into the exit hole of the weld, Figure 138.

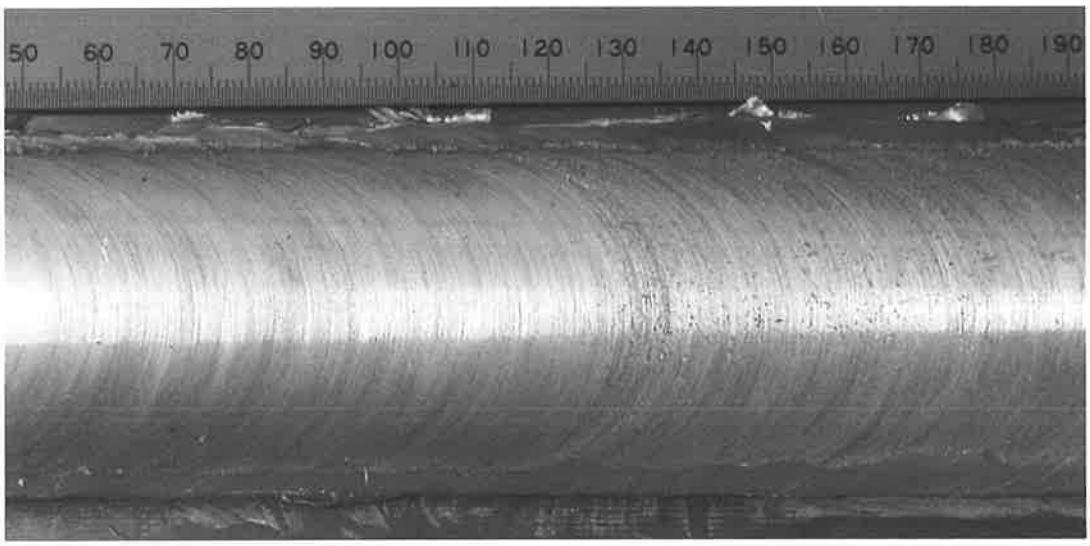

Figure 137 Weld surface appearance of weld 716A.

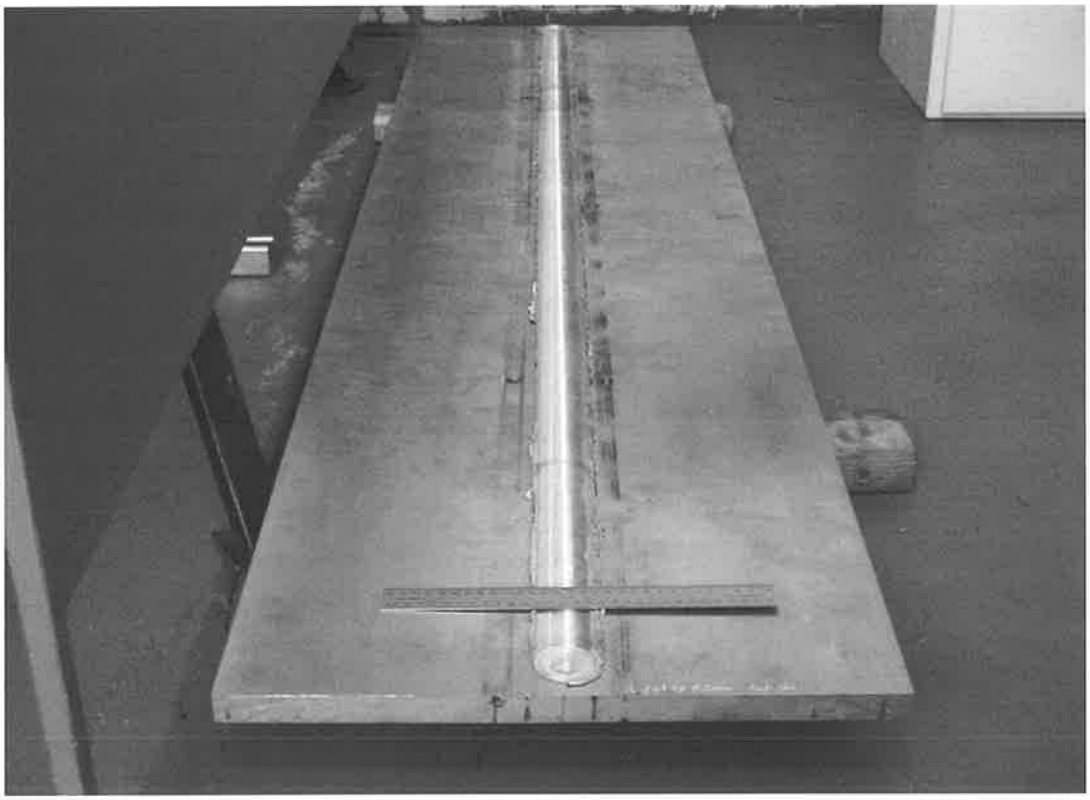

Figure 138 No volumetric defect was evident as viewed from the exit hole, weld 716A.

Although both the FSW tool and process parameters had proven capable of joining the 25mm thick 5083 H111alloy it became evident during the welding of weld 716A that the spindle motor of the friction stir welded was forced to operate at the limit of its capacity i.e. 10 volts. In order not to damage the spindle motor it was decided not to attempt any follow up friction stir welds in 25mm thick 5083 H111 alloy plate for this plate size and weld length.

5.7 A Dissimilar Aluminium Alloy Friction Stir Weld Between 12.5mm Thick 5083 H111 & 7075 T651 Alloys

The results from sections 5.3 had indicated that it was possible to weld both the 7075 and 5083 aluminium alloys using a common set of welding parameters and FSW tool pin (CT2-14). In order to fulfill the final objective (Objective 3), a dissimilar alloy weld between 12.5mm thick 5083 H111 and 7075 T651 alloys was produced. This was achieved in the form of weld 820A. The weld had the 7075 alloy placed in the advancing side of the weld and the 5083 alloy placed in the retreating side of the weld. The reason for the placement of each alloy was to enhance flow of the harder 7075 alloy into the body of the softer 5083 alloy and thereby achieve better mixing of the two alloys in the body of the stir zone. A macrograph of the stir zone (weld nugget) can be seen in Figure 139.

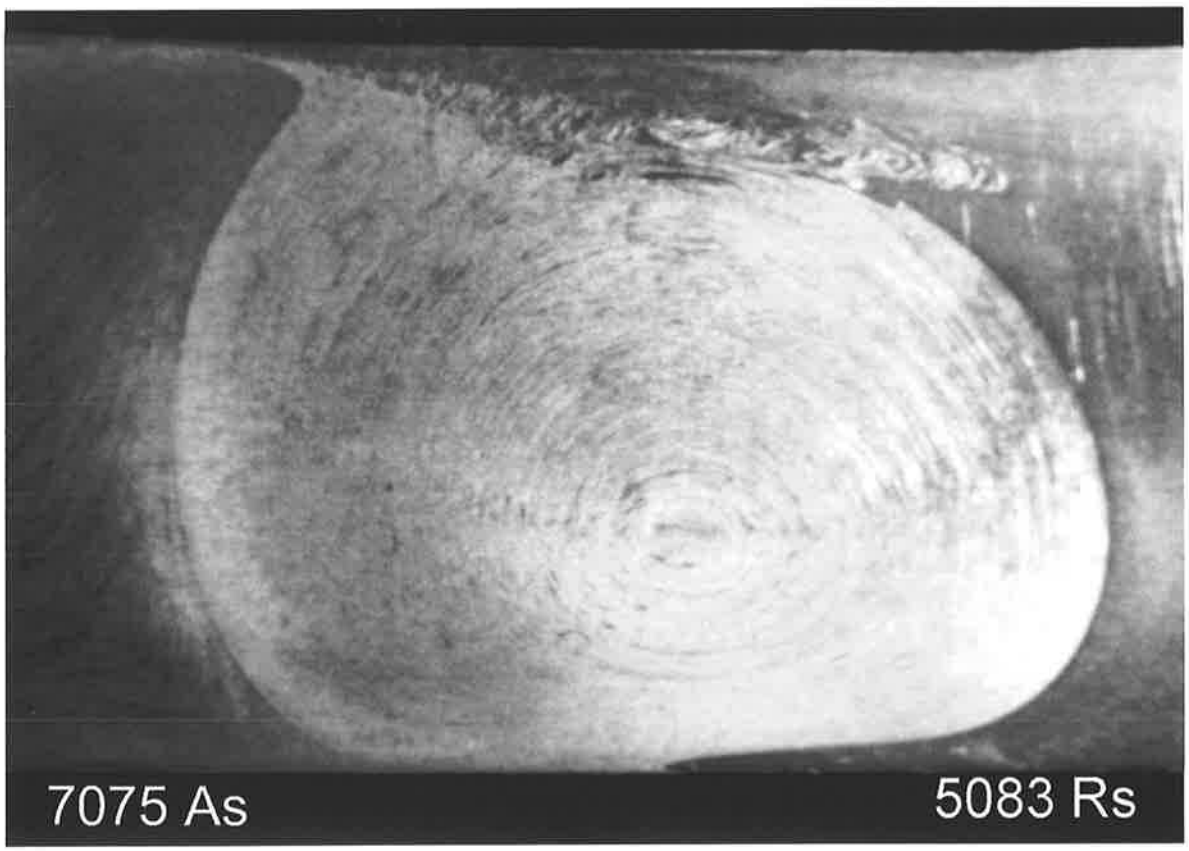

Figure 139 Weld macrograph of the dissimilar alloy weld 820A

Welding was performed using welding tool pin CT2-14 in conjunction with tool shoulder 30Cc14. This tool can be seen in the right hand caption of Figure 140. Weld 820A was produced for a tool rotation speed of 350rpm and for a weld travel speed of 60mm/min i.e. a tool rubbing velocity of 0.26m/sec for the pin and 0.55m/sec for the shoulder, as had

been used to produce friction stir welds in sections 5.3 and 5.6. Tool tilt was again set at 3° away from the direction of tool travel.

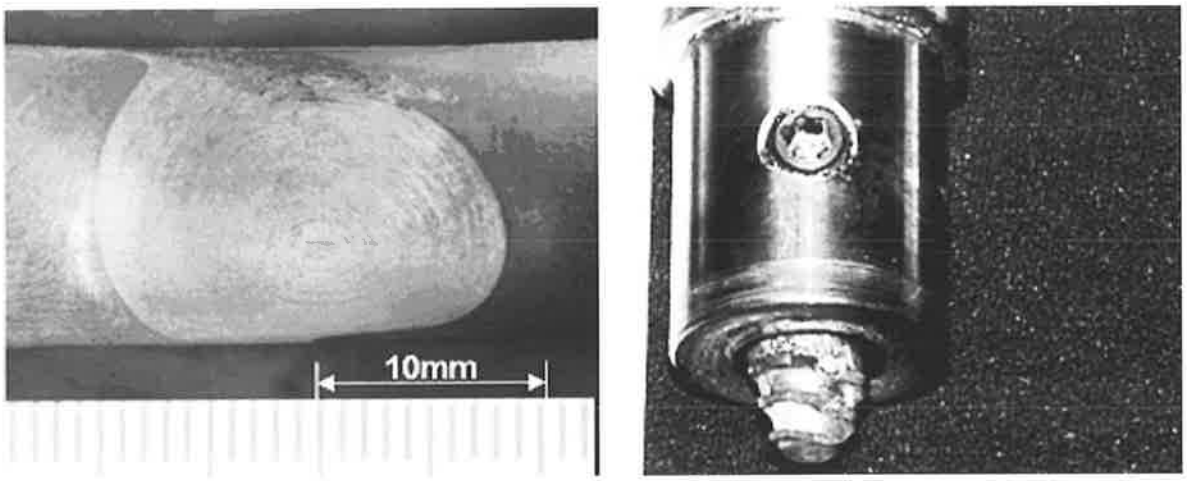

Figure 140 Weld macrograph (left caption) and welding tool (right caption) used in the production of weld 820A.

Plunge parameters used to produce weld 820A can be found in Table 5-13.

Weld No.	Pin Stick out (mm)	Overall Plunge Displacement (mm)	Plunge Displacement To Reach Workpiece (mm)	Plunge Depth Compensation Into Workpiece (mm)
820A	*11.7*	*14.5*	*1.0*	*1.5*

Table 5-13 Plunge depth settings for weld 820A.

Table 5-13 indicates that the overall plunge compensation for weld 820A was 1.5mm. A plot of tool plunge displacement vs. motor output (Volts) for weld 820A can be found in Figure 141.

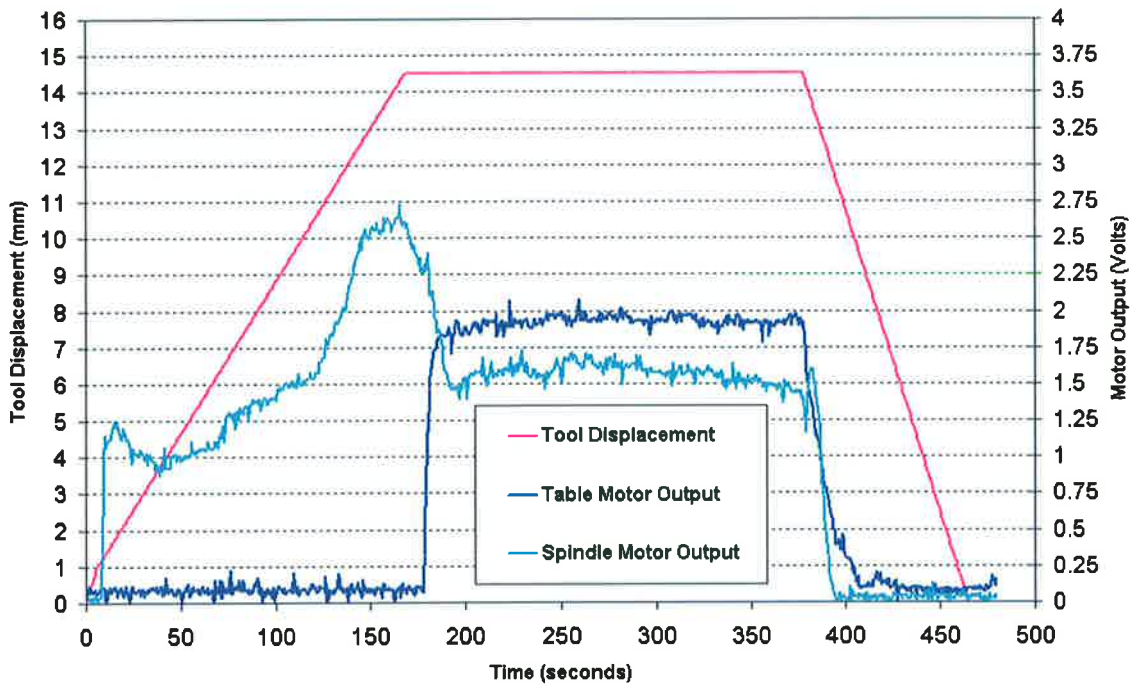

Figure 141 Tool displacement vs motor output for dissimilar friction stir weld produced between alloys 5083 H111 and 7075 T651 in 12.5mm of plate thickness

Micrographs produced for various locations of the stir zone for weld 820A, Figure 142 indicated that intimate mixing between the 5083 and 7075 alloys had occurred. This could be recognised by the very fine banding, which had formed in the weld nugget. The bands or streaks could be seen as individual light (5083) and darker (7075) patterns within the weld nugget. No visual evidence could be found suggesting that chemical mixing between the two alloys had occurred within the weld nugget. In addition to the very fine bands it was also found, Figure 142 that the average grain size at mid workpiece thickness for the weld nugget was extremely small, measuring on average around 10μm.

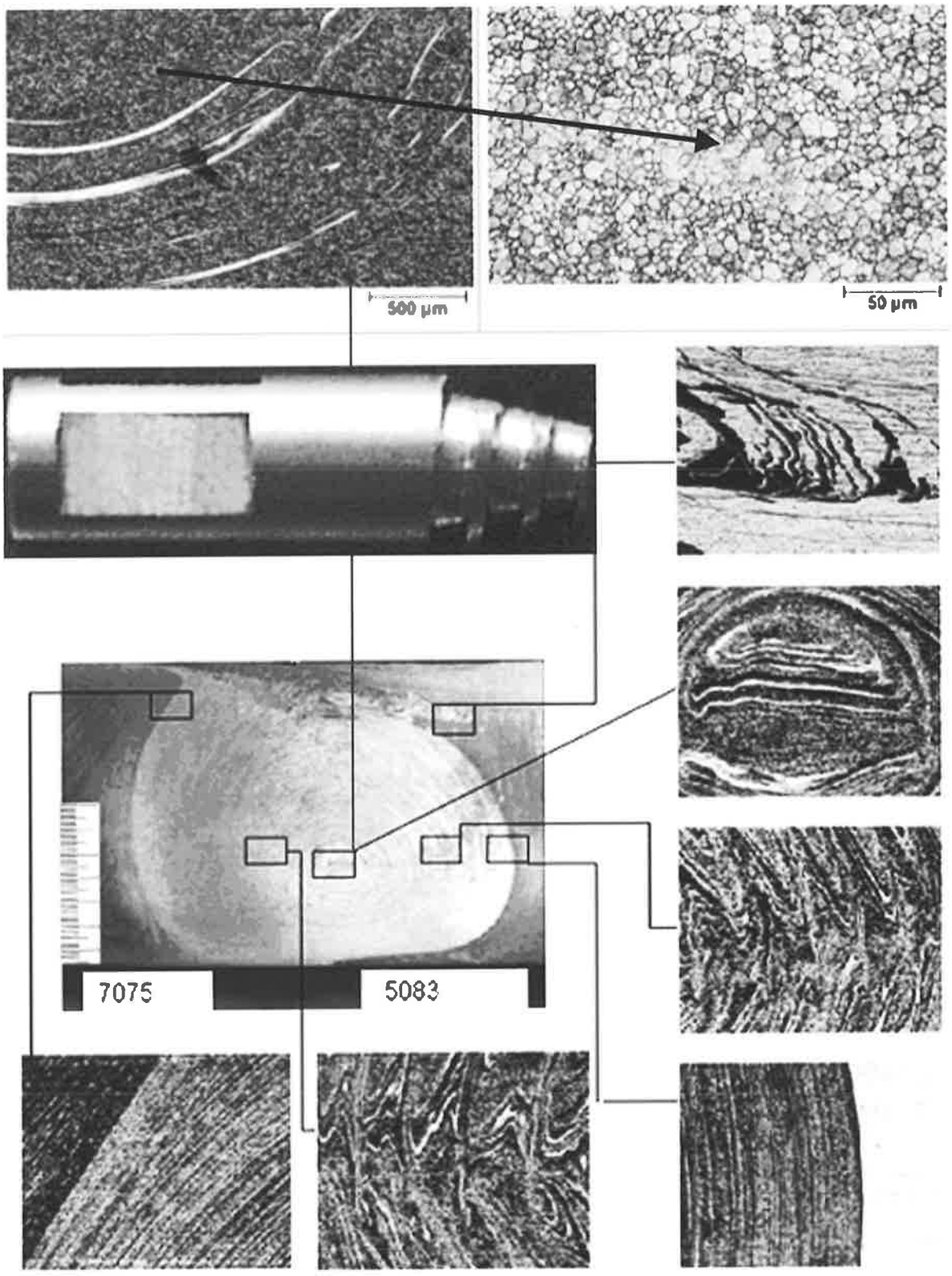

Figure 142 Weld pin (CT2-14), weld nugget and associated microstructure for weld 820A.

Microhardness (HV0.2) testing conducted from advancing to retreating side of the weld nugget and at mid workpiece thickness revealed that the weld nugget had hardness values approaching those of the 7075 alloy, Figure 143. These hardness values were found not to fluctuate significantly when measuring from the 7075 alloy side (advancing side) of the weld travelling across the weld nugget towards the 5083 (retreating) side. A clear demarcation in hardness was however found to exist between the weld nugget and the 5083 alloy, Figure 143.

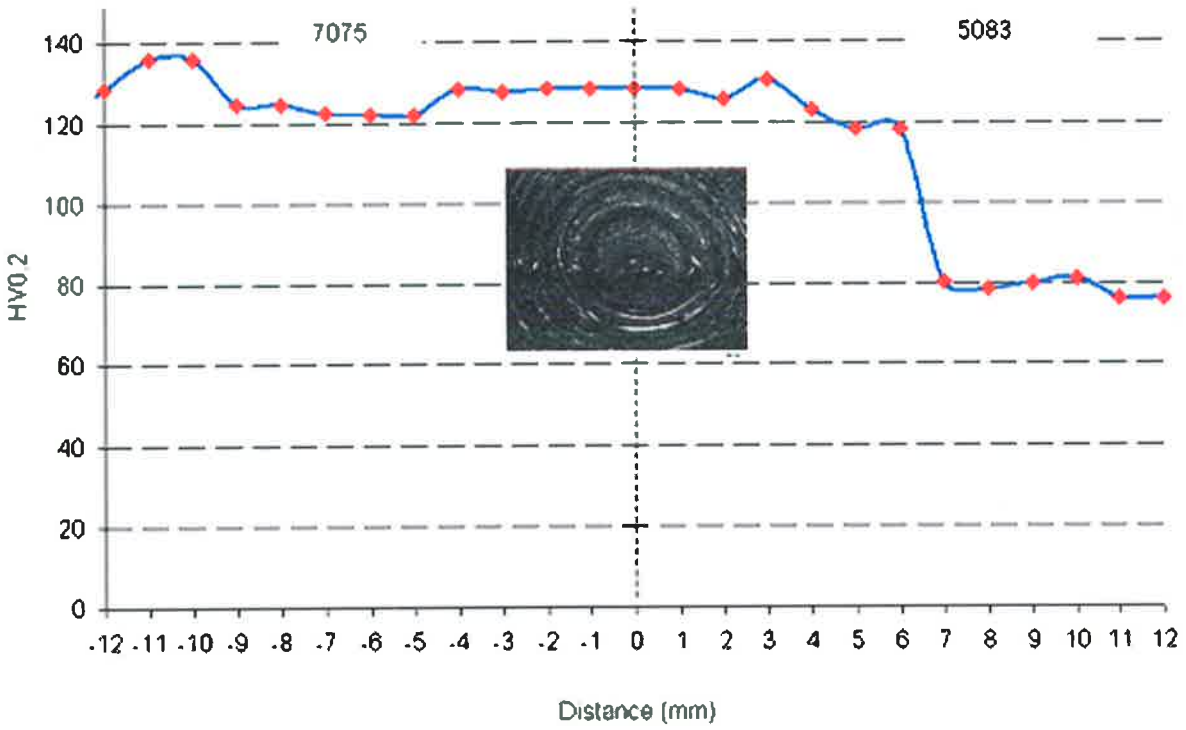

Figure 143 Microhardness (HV0.2) conducted at mid thickness for weld 820A. Note the HAZ varies between alloys but begins some 6mm either side of the join line.

The successful production of weld 820A completed the objectives set out in this thesis. Not only had the tool pin design CT2-14 in conjunction with the tool parameters (350rpm) demonstrated that when combined they were capable of both FSW 12.5mm thick 5083 and 7075 alloys, section 5.3 of this chapter but that this combination of tooling and weld parameters could also be used to produce a dissimilar friction stir weld which combined the same two alloys. This fact not only demonstrates the robustness of the tool pin design but also verifies the transferability of FSW parameters between both the 7075 T651 and 5083 H111 aluminium alloys.

6. DISCUSSION

The following sections discuss and analyze the results of the welding trials from sections 5.1 to 5.7 of Chapter 5.

6.1 FSW Process Parameter Investigation

Objective 1 of this thesis was to determine a set of weld parameters, which could be used to friction stir weld 12.5mm thick 5083 H111 and 7075 T651 aluminium alloys. Section 2.8 of the Literature Review highlighted and defined what most researchers in the field of FSW consider to be the key FSW parameters. These process parameters include:

1. Rotational speed of the welding tool.
2. Axial displacement or plunge depth of the tool shoulder into the surface of the workpieces as brought about by co-ordinate or axial load control.
3. Heating or dwell time.
4. Tool tilt angle.
5. Weld travel speed.

The following sections now discuss the results from Chapter 5 in relation to the investigated FSW parameters.

6.1.1 Rotational Speed of the FSW Tool

In terms of the weld parameter investigation, friction stir welds were produced in both the 5083 and 7075 alloys for tool rotation speeds, which ranged between 200 and 450 rpm. It should be recalled however that these welds were produced using two combinations of FSW tools, which had differing shoulder and pin diameters.

Section 2.10 of the Literature Review demonstrated that tool rotation speed could be converted into a linear tool rubbing velocity as measured at the periphery of each pin and shoulder. This allows for direct comparison for variation in tool size in relation to rotation speed of the tool. The equation for performing the conversion is reproduced below.

$$\text{Tool revs/sec} = \frac{Tool\ pin\ \ rubbing\ \ velocity\ \ for\ alloy\,(m/\sec)}{Pin\ \ circumference\,(m)}$$

Table 6-1 summarizes the relationship which exists between tool rotation speed and tool diameter i.e. pin and shoulder diameter as a function of tool rubbing velocity (m/sec), for all welds presented in sections 5.1 to 5.7 of Chapter 5.

Aluminium Alloys and Material Thickness (mm).	Tool Type (Pin-Shoulder)	Weld Rotation speed (revs/min)	Weld Rotation speed (revs/sec)	Equivalent Pin Rubbing Velocity (m/sec)	Equivalent Shoulder Rubbing Velocity (m/sec)
5083 H111 and 7075T651 x 12.5mm	*CT1-14 – 30Cc14*	*350*	*5.83*	*0.26*	*0.55*
5083 H111 and 7075T651 x 12.5mm	*CT1-14 – 30Cc14*	*300*	*5*	*0.22*	*0.47*
5083 H111 and 7075T651 x 12.5mm	*CT2-14 – 30Cc14*	*300*	*5*	*0.22*	*0.47*
Dissimilar 5083 H111-7075 T651 x 12.5mm	*CT2-14 – 30Cc14*	*350*	*5.83*	*0.26*	*0.55*
5083 H111 and 7075T651 x 12.5mm	*CT1-14 – 30Cc14*	*450*	*7.5*	*0.33*	*0.71*
5083 H111 and 7075T651 x 12.5mm	*CT2-14 – 30Cc14*	*450*	*7.5*	*0.33*	*0.71*
5083 H111 x 25mm	*CT1-20 – 50CR20*	*200*	*3.33*	*0.21*	*0.52*
5083 H111 x 25mm	*CT1-20 – 50CR20*	*200*	*3.33*	*0.21*	*0.52*
5083 H111 x 25mm	*CT2-20 – 50CR20*	*250*	*4.17*	*0.26*	*0.65*

Table 6-1 Tool diameter, rpm and rubbing velocity relationships for welds investigated in this thesis. Note tool pin CT2-xx proved capable of producing defect free welds over all weld parameters investigated.

Table 6-1 reveals that friction stir welds were attempted in both the 5083 H111 and 7075 T651 alloys for pin rubbing velocities which ranged between 0.21 to 0.33m/sec. The shoulder rubbing velocities for both alloys ranged between 0.47 to 0.71m/sec.

It should be noted that for each of the tool rubbing velocities investigated where a friction stir weld was produced using tool pin CT2, regardless of material thickness and alloy, it was possible to produce a successful i.e. defect free friction stir weld. Rubbing velocities were not only found to be transferable between alloys but also could be interchanged between tools of differing diameters i.e. pin diameter 14, pin diameter 20. Where equivalent rubbing velocities were investigated between the two tool pin forms CT1 and CT2, under identical welding conditions, it was found that successful welds could only be produced using the CT2 pin form.

Defect free friction stir welds in 12.5mm thick 5083 alloy could only be produced when sufficient axial down force was applied in the form of over plunging the tool. This will now be discussed in the following section.

6.1.2 Plunge Depth of the Tool Shoulder into the Surface of the Workpiece

All welds produced during the current investigation were performed using the Friction Stir Test Bed and produced under position, not load control because the FSW machine was not capable of load control. This meant that it was necessary to calculate not only tool pin stick out in relation to workpiece thickness but also tool shoulder penetration depth into the workpiece. For these reasons the pin stick out in relation to the workpiece material thickness was up to 0.8mm shorter for the 12.5mm thick workpieces and 5mm shorter for the 25mm thick workpieces. The danger existed that if the value of plunge depth was not correctly calculated two possible outcomes would result. The first and most serious was over plunging of the tool. This would compensate for any deflection experienced by the spindle and beam supporting the spindle but also meant that the tool pin had the potential of coming into contact with the backing bar. In the second instance if plunge was insufficient the tool shoulder contact with the workpiece was minimal and the weld would develop an open running void, which in most cases could be seen along the entire surface of the welded workpiece. These volumetric surface breaking defects in nearly all cases could not be healed by further plunging of the tool shoulder into the workpiece when using tool pin CT1.

Table 6-2 summarizes tool plunge compensatory depth (i.e. over plunging depth) in relation to maximum weld travel speed that was found capable of producing defect free welds in 12.5mm thick 5083 H111, 7075 O and 7075 T651 temper alloys as well as 25mm thick 5083 H111 alloy.

Aluminium Alloy and Material Thickness (mm).	Tool Type: Pin-Shoulder	Weld Travel Speed (mm/min)	Compensatory Tool Penetration Depth (mm)	Estimated Axial Force (kN)
5083 H111 x 12.5mm	*CT1-14 – 30Cc14*	*100*	*1.1*	*20-25*
7075 O x 12.5mm	*CT1-14 – 30Cc14*	*100*	*0.5*	*10-12*
7075 T651 x 12.5mm	*CT1-14 – 30Cc14*	*100*	*1.5*	*30-35*
5083 H111 x 12.5mm	*CT2-14 – 30Cc14*	*60*	*0.9*	*18-20*
5083 H111 x 25mm	*CT2-20 – 50CR20*	*60*	*4.0*	*60-65*
7075 T651 x 12.5mm	*CT2-14 – 30Cc14*	*60*	*0.9*	*18-20*
Dissimilar 5083 H111-7075 T651 x 12.5mm	*CT2-14 – 30Cc14*	*60*	*1.5*	*30-35*

Table 6-2. Tool compensatory plunge depth for successful friction stir welds as a function of welding tool type and weld travel speed. Note an estimate of axial (vertical down force) has been made for each weld based on Figure 56 of Chapter 3.

Although it was possible to estimate the required tool shoulder penetration depth into the surface of the workpiece for the FSW of 12.5mm thick 5083 and 7075 aluminium alloys this was much more difficult for welds produced in 25mm thick material. Not only was it necessary to increase the penetration depth by up to 4mm when FSW the 25mm thick material but results from section 5.5 of Chapter 5 also revealed that penetration depth could not be maintained along the entire weld length for weld travel speeds in excess of 60mm/min. For example weld 625B, refer section 5.5 produced for the weld travel speed of 100mm/min lifted the tool out of the workpiece such that a swelling of the workpiece material of approximately 1mm could be observed.

Axial load estimates required to produced successful friction stir welds in both the 5083 and 7075 alloys can be found in Table 6-2. The estimates have been calculated based on the measurements of load versus deflection for the spindle and associated support beam, Figure 56 of Chapter 3.

6.1.3 Heating or Dwell Time

The fact that all friction stir welds produced in this study were performed using position control does not mean that the rate of tool travel during tool plunge could not be programmed and thereby controlled. In all cases a plunge rate of 5mm/min was initiated to start plunge. This meant that a tool pin required approximately 150 seconds to penetrate 12.5mm thick plate. In the case of FSW the 25mm thick plate it was found necessary to use a two stage plunge to allow for adequate seating of the tool shoulder into the surface of the workpiece. Here an initial plunge rate of 5mm/min was used to bring the tool shoulder to where it just made contact with the workpiece followed by a plunge rate of 2mm/min for seating the tool shoulder into the workpiece. Hence plunging of the tool for friction stir welds produced in 25mm of workpiece thickness occurred over approximately 300 seconds. Due to this relatively slow plunge rate and from evidence of the temperatures as measured in the FSW tool, section 5.4 of Chapter 5 it was not found necessary to have a dwell time greater than 10 seconds prior to the commencement of weld travel.

6.1.4 Tool Tilt Angle

The Friction Stir Weld Test Bed could be adjusted to allow for FSW with the tool at either 0 degrees or 3 degrees of tilt away from the direction of welding. All welds conducted in this study were performed at 3 degrees of tilt, primarily because of the concave and concentric ring tool shoulder forms employed to friction stir weld the 5083 and 7075 alloys.

A tool tilt angle of 3 degrees when applied to a 30mm diameter tool shoulder provides 0.785mm of penetration at the heel (trailing end) of the tool shoulder as measured from the centre of the tool given that this point represents the exact surface of the workpiece. The penetration of a 50mm diameter shoulder is 1.31mm. Had the friction stir welder been capable of a further 2 degrees of tilt angle (5 degrees in total) this would have enabled a penetration of 1.31mm for the 30mm diameter shoulder and 2.17mm for the 50mm diameter shoulder. This may in part have aided in preventing welds produced using tool pin CT1 from suffering from surface breaking defects, section 5.1 of Chapter 5. This however is only speculative because the resultant increase in tool tilt angle (away from the direction of welding) is accompanied by a similar increase in the helix angle of the pin threads. A larger helix angle would increase forces transmitted along the axis of the threads and thereby not only generate increased torque but also axial (upward force) to try to lift the tool out of the workpiece.

Minimising the force transmitted along the thread axis of the pin can be achieved in several ways; remove the threads on the pin or friction stir weld at an angle of 0 degrees. This thesis study chose the first option in that a substantial portion of the thread form was removed from the FSW pin i.e. pin CT2. This pin form in conjunction with a tool shoulder design (such as the scroll shoulder, section 2.11 of the Literature Review) should be investigated. Secondly, this coupling of tool designs has the potential to deduce axial forces required during FSW and may offer enhanced weld travel speed capabilities.

6.1.5 Weld Travel Speed

Weld travel speeds of up to 100mm/min were investigated, both for the 12.5mm thick and 25mm thick workpieces. Friction stir welds produced in the 12.5mm thick 5083 and 7075 alloys using tool pin CT2-14 demonstrated that defect free welds could be produced in these alloys for this level of weld travel speed. Defect free welds were only possible in the 25mm thick 5083 alloy when FSW using tool pin CT2-20 for weld travel speeds up to 60mm/min. The reasons as to the relatively slow weld travel speeds for the 25mm thick workpiece lay in the fact that for weld travel speeds above 60mm/min the FSW tool had a tendency to climb out of the workpiece i.e. the vertical forces generated during FSW caused added deflection of the spindle and to a lesser extent its support beam taking away the necessary contact between the tool shoulder and the surface of the workpiece. As a consequence surface breaking volumetric defects formed.

6.2 Weld Tool, Process Loads, Weld Temperatures, And Weld Power Relationships When FSW 5083 And 7075 Aluminium Alloys

Objective 2 of this thesis aimed at developing a better understanding of the FSW process by examining relationships that exist between tool pin form i.e. pin profile and how this influences weld force (in the direction of welding), weld temperatures (both within the tool and workpiece), weld energy and weld formation when FSW 5083 and 7075 aluminium alloys.

6.2.1 FSW Tool Pin Design and Weld Force Relationships

Essentially two tool pin forms were designed and tested by the author for two levels of material thicknesses (12.5 and 25mm thick plate). These pin forms identified generically

as CT1 and CT2 have been well documented in Chapter 5 and technical drawings can be found in Appendix B.

The two pin forms examined in this study were identical to one another in that each pin employed to weld a given material thickness had the same shape and thread form (thread pitch) but differentiated in that the CT2 pin forms possessed three flats machined into the threaded portion of the pin at a spacing of 120°, such that the thread in these regions was completely removed from the pin.

Load measurements were conducted while using both the CT1-14 and CT2-14 pin forms in combination with the 30Cc14 shoulder. A schematic of the equipment used for measuring the horizontal force in 12.5mm thick workpiece material is presented in Figure 144. The apparatus is simple with the workpiece holder mounted in a carriage containing supporting rollers. These rollers were little more than 12mm diameter steel rods.

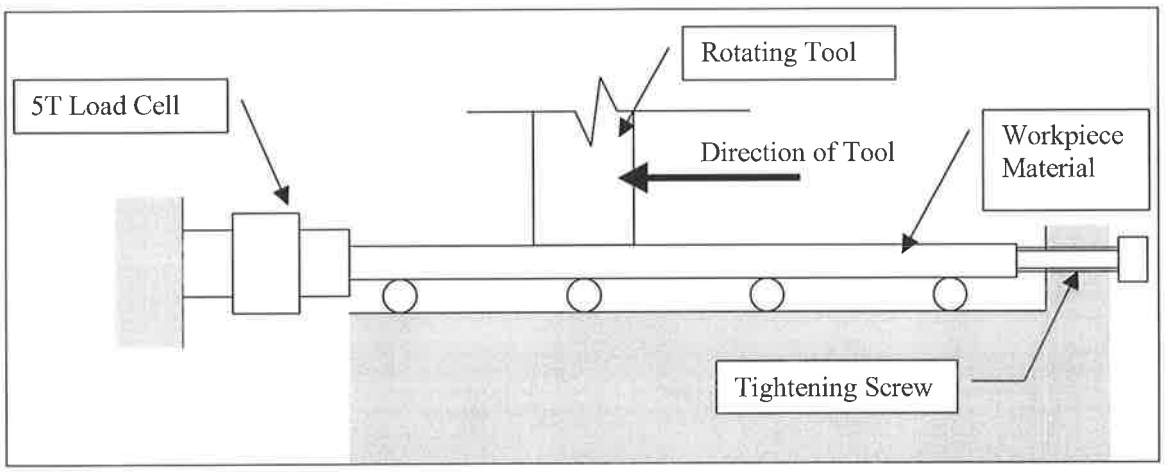

Figure 144 Load measurement as performed for 12.5mm thick 5083 and 7075 aluminium alloys

Load measurement was only performed for the 12.5mm thick plate because the carriage with its steel rollers was not robust enough to allow for the FSW of 25mm thick plate. What should be noted however is that the only modification to the standard workpiece clamping system (as presented in section 3.3.3 of Chapter 3) was that the backing plate was mounted on the rollers of the carriage and that a load cell was placed at the end of the assembly to measure forces in the direction of weld travel. During FSW the load cell operated in compression and gave an estimate of the load in kg produced during FSW.

Note a tightening screw is indicated at the end of the plate, Figure 144. This screw was used to secure the workpiece holder and prevent horizontal movement during tool plunge. It was found that if this screw was left tightened for the duration of the weld, the thermal input during FSW resulted in an expansion of the workpiece holder and caused an additional load on the load cell. Hence once the tool had been plunged into the material the screw had to be quickly released.

The results of load measurements performed in 12.5mm thick 5083 H111, 7075 O and 7075 T651 temper alloys, sections 5.1 to 5.3 of Chapter 5 demonstrated that the load generated in the direction of welding was influenced by several factors. These factors included:

- Alloy and temper condition e.g. 5083 H111, 7075 O and 7075 T651, This was observed in sections 5.1 and 5.2 of Chapter 5. It was found that the 7075 T651 alloy generated the highest loads of all investigated alloys. However, load as measured in the direction of weld travel between 7075 T651 and 5083 H111 alloys when friction stir welded under identical processing conditions showed that this difference in load between the two alloys was relatively small and that the resultant trend in relation to weld travel speed was almost identical, Figure 95 of Chapter 5.
- Weld travel speed. Again sections 5.1 and 5.2 of Chapter 5 revealed that load as measured in the direction of weld travel increased markedly as a result of increasing weld travel speed.
- Tool rotation speeds under a constant weld travel speed. Section 5.3 of Chapter 5 indicated that by changing tool rotation speed from 300 to 450rpm while maintaining all other welding conditions constant enabled a reduction of only 5% in the load as measured in the direction of weld travel regardless of tool pin form i.e. CT1 or CT2.
- Tool pin form. Section 5.3 of Chapter 5 highlighted that although an increase in rotational speed did not significantly reduced load as measured in the direction of weld travel the pin form CT2 always produced much lower processing loads in both the 12.5mm thick 7075 T651 and 5083 H111 alloys. In the case of the 7075 alloy this reduction in load could be observed to be as high as 40% between the two pin forms for a tool rotation speed of 450rpm.

Load as measured in the direction of weld travel is a critical variable as the load is a measure of the resistance to tool travel through the weld joint, particularly the FSW pin as

it contributes to the greatest portion of the tool entering the workpiece. The force on the welding tool pin when it becomes too large will cause it to break, not due only to the load in the travel direction but also due to bending as the tool is under rotation.

For a constant set of welding parameters and whilst using the same FSW tool it was demonstrated, section 5.2 of Chapter 5 that load in the direction of welding varied between all of the investigated aluminium alloys i.e. 5083 H111, 7075 O and 7075 T651. The most significant variation in load was observed for the 7075 O and 7075 T651 temper alloys. Annealing of the 7075 alloy meant that this alloy in the O temper, when friction stir welded was in a strain free condition and much softer in hardness compared to the same alloy in the artificially aged T651 temper condition. The variation in hardness HV0,2 was 68 for the O temper and 175 in the T651 temper. Hot working i.e. FSW both the 7075 O and 7075 T651 temper alloys under increasing weld travel speed and for a constant tool rotation speed, section 5.2 of Chapter 5 suggests that there may exist a constant ratio of load as measured between the 7075 O and 7075 T651 friction stir welded alloys. If the load generated in the T651 temper alloy is divided by the load in the O temper alloy this ratio appears to be approximately 1.6. This ratio could be seen to occur up to a weld travel speed of 90mm/min. The ratio may be a potential means for indicating when a deformation rate such as travel speed or too low a FSW temperature is reached weld defects begin to form. It is speculated although not tested that once this ratio increases this may in effect define the possible limit for weld travel speed for a given alloy and in a particular temper condition. This methodology could be applied not only to heat treatable aluminium alloys such as the 7075 alloy but also to alloys such as the 5083 alloy which is strengthened by cold working.

A comparison of FSW loads generated in the direction of weld travel between the 5083 H111 alloy and the 7075 T651 alloy, sections 5.2 and 5.3 of Chapter 5 revealed that FSW forces were always larger when welding the 7075 T651 alloy under identical parameter and weld tool conditions. A comparison of weld loads generated in both alloys over two rotational speeds (300 and 450rpm) whilst welding using tool pins CT1-14 and CT2-14, section 5.3 of Chapter 5 indicated that each alloy reacted differently to the FSW parameters and tool employed. Common features which existed when FSW both the 5083 H111 and the 7075 T651 alloys were that tool pin CT2-14 reduced load in the direction of weld travel in comparison to tool pin CT1-14 and that loads were higher in all cases when FSW the 7075 T651 alloy. Surprisingly however the difference in load between welds produced in the 5083 H111 alloy when welded using tool pins CT1-14 and CT2-14 were much smaller than that experienced by the same set of welds produced in

the 7075 T651 alloy. Certainly there is a difference in the thermal conductivity between the two alloys, with the 7075 alloy having the higher conductivity and therefore requiring a greater energy input in order to overcome any strain hardening during the time this alloy is experiencing peak processing temperatures.

6.2.2 FSW Tool Pin Design and Weld Tool/Workpiece Temperature Relationships

Sections 5.3 and 5.4 of Chapter 5 presented the results of temperature measurements both for the workpiece and in an instrumented FSW tool containing three thermocouples embedded in the pin and one embedded in the tool shoulder. Welds were conducted in 12.5mm thick 5083 H111 and 7075 T651 alloy as well as 25mm thick 5083 H111 alloy. Welds were performed using the CT1-14 and CT2-14 pins coupled to the 30Cc14 tool shoulder to compared temperature evolution in the 12.5mm thick alloys and the CT1-20-2 and CT2-20-2 pins coupled to the 50CR20 shoulder for the 25mm thick alloy.

Temperatures as measured in the workpiece when FSW the 12.5mm thick alloys, section 5.3 of Chapter 5 revealed that the temperatures generated in both sides of the workpieces varied by little more than 10°C regardless of the welding tool pin employed. This difference was seen to occur between temperatures measured for welds performed at 300rpm and at 450rpm and for a constant weld travel speed of 60mm/min.

Temperature measurements performed while using the instrumented FSW tool (designed by the author), section 5.4 of Chapter 5 revealed that the bulk temperature as recorded in the FSW tool and measured in 4 locations at a distance of 1mm removed from the tool / workpiece interface varied little (by less than 30°C) between the two tool pin forms employed while welding under identical processing conditions. In fact the temperature as measured in the FSW tool correlated well with the temperature measured in the region of the stir zone, Figure 124, section 5.4 of Chapter 5. This is not unexpected as temperature experienced by the FSW tool will eventually even out when the FSW process achieves a steady state due to the fact that the tool will eventually become saturated and temperatures developed between the surfaces of the tool and workpiece are continuously evened out across the interface during welding.

6.2.3 Weld Power and Weld Energy Relationships When FSW 5083 and 7075 Alloys

Section 5.2 of Chapter 5 revealed that the output as measured at the spindle motor (Volts) of the Friction Stir Weld Test Bed could be converted and used as a means of estimating spindle torque and thereby allowing for the calculation of the weld power (Watts) and specific weld energy (joules) per millimetre of weld length.

Certainly it can be argued that the degree of accuracy of any calculation very much depends on the accuracy of the measurement of the data and on the accuracy of interpreting the measured data. Since calibration of the spindle motor output to determine spindle torque was performed by Colegrove, refer Appendix C there is also the issue of interpreting another researcher´s data. If one looks at the range i.e band width of weld collected data, Figure 98 of section 5.2 there can be observed a relatively large scatter of data measurement points. For the area of interest however (spindle motor output of below 3 Volts) it can be considered that the calibration curve relating spindle motor torque to load (spindle torque), figure 98 is reasonably accurate. Even if an error were to have occurred this error only has the potential to shift the magnitude of the results vertically. Further calculations based on torque such as power and weld energy will therefore only be subject to an interpretation of their magnitude.

Friction stir welds were produced in both 12.5mm thick 5083 H111, 7075 O and 7075 T651 alloys using tool pin CT1-14 in conjunction with tool shoulder 30Cc14 for a constant tool rotation speed of 350rpm and a range of weld travel speeds starting at 30mm/min and terminating at 100mm/min. The results from these welds demonstrated that torque as measured at the spindle increased in response to an increase in weld direction load, which itself was seen to be a function of the weld travel speed i.e. load and spindle torque increased as a result of an increase in weld travel speed. In comparative terms however torque was seen to be only marginally affected by increasing travel speed where as load was notably affected.

When weld power was calculated from the spindle torque It could be observed that there were differences in weld power between the various alloys but that the level of weld power remained relatively constant over the range of investigated weld travel speeds. This was little more than what had already been seen for spindle torque. When the specific weld energy however was calculated for each weld and for each range of weld travel speed it was clear from the welds produced in the 5083 H111 alloy that the weld containing a

defect had a much reduced weld energy as compared to its counterpart weld, which was free from defect. Since the welding tool (both pin and shoulder) as well as processing parameters were the same for both welds the reason for defect formation can only be accounted for by the position of the shoulder in contact with the surface of the workpiece material. It should be recalled that a difference of over 1mm in plunge depth occurred between the two welds with the defective weld having the smaller plunge depth. Hence shoulder contact with the workpiece is the prime contributor to specific weld energy.

Determination of friction torque will depend on the nature of the pressure distribution between the contacting interfaces of the FSW tool with that of the workpiece. Since the tool shoulder has the largest surface in continuous contact with the workpiece, primarily because the tool pin can only present half of its circumference to the workpiece at any one time (due to rotation) it is the pressure that the tool shoulder brings onto the surface of the workpiece which will determine not only the torque as measured at the spindle but also whether a weld will defective or defect free. It is therefore essential that this force be known and actively controlled during FSW.

6.2 Producing Single Pass Friction Stir Butt Welds in 25mm thick 5083 H111 Aluminium Alloy And A Dissimilar 5083 H111 and 7075 T651 Alloy for 12.5mm Of Workpiece Thickness.

Objective 3 of this thesis set out to prove that from the investigated process parameters and for a given tool design, it was possible to friction stir weld both a 25mm thick 5083 H111 alloy and to join the dissimilar 5083 H111 and 7075 T651 alloy combination. This objective was achieved and demonstrated in sections 5.6 and 5.7 of Chapter 5.

Rubbing velocities based on the diameter of each tool i.e. pin and shoulder were 0.26m/sec for each pin however shoulder rubbing velocities 0.55m/sec for the 12.5mm thick workpieces and 0.65m/sec for the 25mm thick workpiece. Both welds were performed using the generic tool pin form CT2.

7. CONCLUSIONS

Friction Stir Welding (FSW) tools and conditions have been investigated for single pass butt welding of 12.5mm thick 5083 H111, 7075 O and 7075 T651 alloys. These tools comprise of tool pins CT1-14 and CT2-14 in conjunction with tool shoulder 30Cc14. The FSW parameters were established for tool pin CT2-14 in conjunction with shoulder 30CC14 for both similar and a dissimilar alloy weld between the 7075 T651 and 5083 H111 alloys for 12.5mm of material thickness. Technical drawings of both tool pins and shoulders can be found in Appendix A.

A FSW tool and friction stir welding parameter has been established for single pass butt welding of 25mm thick 5083 H111 alloy. This tool comprises of tool pin CT2-20 and tool shoulder 50CR20. Technical drawings of the tool can be found in Appendix A.

The following conclusions can be made from the results of this thesis:

- The tool pin CT2-14 in conjunction with tool shoulder 30Cc14 could successfully join 12.5mm thick 5083 H111 and 7075 T651 aluminium alloys for a weld travel speed of 60mm/min at peripheral tool rubbing velocities of 0.21 and 0.33m/sec for the tool pin and 0.47 and 0.71m/sec for the tool shoulder.

  A conversion allowing for calculation of tool rotation speed from rubbing velocity or vice versa is given by the following equation:

$$\text{Tool revs/sec} = \frac{Tool\ pin\ \ rubbing\ \ velocity\ \ for\ alloy\,(m/\sec)}{Pin\ \ circumference\,(m)}$$

  Note the equation above refers to a tool pin diameter but is also valid for calculating rubbing velocity for the tool shoulder by simply substituting the shoulder diameter in place of the pin diameter.

- The ability to produced successful (defect free) friction stir welds using tool pin CT1-14 in conjunction with tool shoulder 30Cc14 was dependant on the level of compensatory plunge depth. The compensatory plunge depth required to successfully friction stir weld 12.5mm thick workpieces using tool pin CT2-14 in was smaller than that required by tool pin CT1-14. This is attributed to the fact that

there is no continuous thread for tool pin CT2-14 and as such reduces the potential for tool uplift out of the workpiece during FSW.

- Weld forces as measured in the direction of weld travel when FSW 12.5mm thick workpieces were up to 40% reduced for tool pin CT2-14 in comparison to tool pin CT1-14 under identical weld conditions. This is attributed to the fact that the three flat tool form offers a reduction in tool contact area at the periphery of the tool with that of the workpiece material in comparison to tool CT1-14. The flats of tool pin CT2-14 also offer a much greater volume within the rotation zone to transfer thermally softened material around the tool thus reducing FSW force.
- FSW temperatures as measured either side of the join line in 12.5mm thick workpieces when friction stir welded using tool pin CT2-14 and CT1-14 revealed that under identical processing conditions temperatures varied by little more than 10°C as a result of tool pin form. Note in both cases welds were performed using tool shoulder 30Cc14. The influence of heat generation resulting from changes to the tool pin form under a constant set of welding conditions in 12.5mm workpiece thickness is marginal.
- FSW temperatures were able to be measured in 25mm thick 5083 H111 aluminium alloy using an instrumented tool containing thermocouples embedded in the pin and in the shoulder. Friction stir welds performed using tool pins CT1-20 and CT2-20 in the 25mm thick workpiece material indicated a tool temperature range of 510°C to 540°C for a tool rotation speed of 200rpm and a weld travel speed of 50mm/min. The higher temperature was measured for tool pin CT2. The lower temperature while welding using tool pin CT1-20 can be attributed to a volumetric defect having occurred in the stir zone of the weld. The influence of heat generation resulting from changes to the tool pin form under a constant set of welding conditions in 12.5mm workpiece thickness is marginal.
- Friction stir welding temperatures increase as a result of increasing tool rotation speed. This is attributed to an increase in the rate of adiabatic shear occurring due to the increase in tool rotation speed.
- Loads as measured in the direction of welding were not significantly reduced as a result of increasing tool rotation speed from 300 to 450rpm for a constant weld travel speed of 60mm/min when FSW 12.5mm thick workpiece material.
- A successful single pass friction stir butt weld was able to be produced in 25mm thick 5083 H111 alloy using tool pin CT2-20 in conjunction with shoulder 50CR20 for a tool pin rubbing velocity of 0.21m/sec and a shoulder rubbing velocity of 0.52m/sec. These rubbing velocities were initially trialed in 12.5mm thick 5083

H111 alloy using tool pin CT2-14 in conjunction with shoulder 30Cc14. The welds were free from defect. The findings indicate that it is possible once having established tool rubbing velocities for a given material in one level of material thickness to transfer these rubbing velocities across tools and workpiece thickness.

- A 2m long and successful single pass friction stir butt weld was produced in 25mm thick aluminium alloy 5083 H111 using tool pin CT2-20 in conjunction with shoulder 50CR20 for a tool pin rubbing velocity of 0.26m/sec and 0.65m/sec for the tool shoulder. The weld travel speed was 60mm/min. Friction stir weld produced in this material for identical processing conditions indicated that weld travel speeds greater than 60mm/min could not produce defect free welds due to uplift of the tool out of the workpiece. The level of tool compensatory plunge required to maintain adequate tool shoulder contact with the surface of the workpiece required that the spindle motor operate at its maximum capacity. The FSW of 25mm thick 5083 H111 alloy under the above welding conditions and using tool pin CT2-20 in conjunction with tool shoulder 50CR20 defines the process limit of the friction stir welder.
- Use of the tool pin CT2-14 in conjunction with tool shoulder 30Cc14 enabled the production of a successful dissimilar alloy friction stir weld between 12.5mm thick 5083 H111 and 7075 T651 aluminium alloys. The tool rubbing velocities used to produce this weld were 0.26m/sec for the pin and 0.55m/sec for the tool shoulder.

8. FUTURE WORK AND RECOMMENDATIONS

Objective 1 of this thesis set out to determine weld parameters for the FSW of 12.5 and up to 25mm thick 5083 H111 and 12.5mm thick 7075 T651 aluminium alloys. Welding conditions with a good tolerance to variation have been established.

Objective 2 of this thesis sought through an examination of tool pin forms to determine what extent the tool pin profile had on weld temperatures evolution, weld direction force and weld formation. The results of the experimental design have indicated that for the two tool pin forms investigated (pins CT1-xx and CT2-xx) when employed under identical processing parameters demonstrated that FSW temperatures varied by less than 5%. Hence, the conclusion from this investigation is that tool pin form does not significantly influence FSW temperature, both in the workpiece and FSW tool, rather this is determined by tool rotation speed. The key influence of pin form however, could be seen in weld direction force. Pin form CT2-xx possessing identical features as to pin form CT1-xx, with the exception that this pin form had three flats machined onto the threaded portion of the pin revealed significant benefits in its ablity to reduce weld direction force. This was observed to be a major benefit when FSW as it enabled the production of welds free from volumetric defects where pin CT1-xx could not.

Objective 3 of this thesis set out to develop a tool and welding conditions which would successfully join a dissimilar alloy 5083 H111 and 7075 T651 weld. The feasibility of this dissimilar alloy weld has been proven by the production of such a defect free weld.

Results from the experimental investigation have highlighted that it is a combination between how the FSW tool enters the workpiece, the tool geometry and material type (included here is the temper condition) that dictates possible weld process parameters such as travel speed. Loads and temperatures, as measured when FSW the aluminium alloys 7075 and 5083 for the various temper conditions demonstrated that there were significant differences in both the power required and welding force generated. These outcomes have implications in terms of machine robustness i.e. rigidity and power but also in terms of a tool design. For these reasons FSW machines must be capable of working in a wide range of processing conditions, the ultimate design being one where force and process monitoring are combined to create a self reacting system i.e. one in which weld parameter deviation allows for appropriate corrective measures to be instantaneously enacted.

Tool technology has been referred to as the most important feature of the FSW process, particularly because the tool shape determines the heating, shearing, crushing and forging action of the hot worked material. Tool size also determines the weld size, tool strength, working temperature and ultimately the range of materials to which a tool design can be applied. Tool design however, matters little if control over the tool cannot be maintained during welding. As such three areas have been identified by the author for future investigation.

8.1 Implementation Of A Load Control System

The inability to estimate correctly and then compensate for deflection characteristics of the Butler Friction Stir Test Bed spindle and support structure when FSW the thicker section (above 12mm in thickness) aluminium alloys during this study led to a considerable number of welds having defects. The recommendation here is to implement a force monitoring and control system on the welder, firstly to provide data as to the required downward forging force necessary to friction stir weld the aluminium alloys and secondly, to provide a system whereby this force can be continuously monitored and maintained during welding.

For the load control system to function the main software requirements are:

- high sampling rates with high feedback velocity
- the ability to allow online parameter adjustments during welding
- pre-setting of force and rotational speed ramps
- visualization of pre-set and actual parameter values
- communication with a motion controller, whether the Gallil or an external source.

During the study both plunging and welding was performed under positional control. Deviations in shoulder position from the surface of the workpiece could only be estimated making selection of plunge distance one of trial and error for each material and thickness. This system has flaws and requires modification.
Load control can be better realized for the Butler Friction Stir Test Bed in two ways. The first method would involve implementing a load sensor system (piezo-electric) within the FSW spindle housing and coupling this to the Galil motion controller for control of the z-axis motor. Integration of a measurement and control system however could prove difficult because of limited access within the spindle and because a

feedback mechanism needs to be implemented for the servo-electric motor controlling the z-axis. A much less complicated solution would be to realize a completely separate load control system via an additional linear axis mounted to the spindle head. This in short means redesigning the spindle head to accommodate a hydraulically activated force measurement flange containing piezo-electric load cells. The controller in this instance would be independent from the Galil control system and as such make the system far less complex.

8.2 Development Of A FSW Process Model

FSW is a thermo-mechanical joining process. Weld integrity requires that thermally softened material on both sides of the weld joint be intimately mixed. To better understand the deformation behaviour one must however be able to visualise material flow. The degree of material mixing, the thickness of the deformed aluminium lamellae and material flow patterns have been shown not only to depend on their relative positions in the weld nugget, but also on the tools and process parameters (temperatures) employed.

There exists a need to catalogue welding tool, parameter, weld geometry and mechanical property relationships for friction stir welded joints, particularly when joining thicker section aluminium alloys. This would not only provide for greater insight into the response of tooling and parameter selection in relation to weld joint properties i.e. a quality assurance catalogue, but also provide the basis for a FSW process model.

In order to make a meaningful evaluation of joint integrity it is important to understand;

- what weld structures (macros) are possible as a result of various tool designs
- what is the best weld structure obtainable from a given tool design in terms of joint integrity for a particular alloy and in a particular temper condition
- what minimum level of joint strength can be assured under static and cyclic loads to provide designers of friction stir welded components a reliable and accurate assessment of a welded components life expectancy.

The ability to assure weld quality or joint strength is critical if the process of FSW is to gain a wider acceptance, especially for the FSW of thicker section (greater than 12mm thick) aluminium alloys. Any future work should therefore be based on examining the influence that tool geometry has on such things as material flow patterns (mixing) and temperature cycles and forces generated during welding. The outcome of such a study would then allow for the correlation between tool geometry, weld structure formation

and weld integrity. The visible results could then be used as a map giving reference to industry as to the suitability or otherwise of a weld produced from observation of a single weld macro. The ground work required to achieve such a result would however rely on an in-depth understanding of joint formation (plastic deformation mechanics) both on the macroscopic and microstructural i.e. crystallographic level, but only for those aluminium alloys which show susceptibility for failure in the weld nugget.

8.3 Further Refinement Of The Instrumented Welding Tool

Distinct differences have been shown to occur for material flow and mixing between both sides of the same and dissimilar alloy welds. To successfully replicate material flow patterns and then to understand why these occur requires careful analysis of the temperature fields generated during welding. This is because material flow and temperature distribution throughout the weld zone are intimately linked. The development of the thermocouple welding tool has demonstrated that temperature fields can be measured as close as 1mm from the interface between the welding tool and the workpiece material and that these temperature fields are comparable with those measured by thermocouple placed in the workpiece itself. It is therefore recommended by this author that the instrumented tool be further refined and an induction heating system be coupled to the tool shoulder to allow for input of a constant temperature field for this region of the tool. The coupling of the heating system with that of a force control system i.e. downforce will provide for greater accuracy when developing heat source and heat sink relationships thus enabling steady state welding conditions to occur from start to end of weld.

9. REFERENCES:

1. Thomas WM, Nicholas ED, Needham JC, Church MG, Templesmith P, Dawes CJ: International Patent Application No. PCT/GB92/02203 and GB Patent Application No. 9125978.9, 1991.
2. Thomas WM. Friction Technology for The Aluminium Industries. Proceedings of the Seventh International Extrusion Technology Seminar May 16-19, 2000, Chicago, Illinois.
3. Nicholas ED. Exploiting Friction Welding In Production, Welding Institute 1978.
4. Vill VI. Friction Welding Of Materials, American Welding Society Inc., NY 1962.
5. Zhu XK and Chao YJ, Numerical simulation of transient temperature and residual stresses in friction stir welding of 304L stainless steel, Journal of materials processing Technology 146 (2004) 263-272.
6. Chen CM and Kovacevic R. Finite element modeling of friction stir welding-thermal and thermomechanical analysis, International Journal of Machine Tools and Manufacture, 43 (2003) 1319-1326.
7. Song M and Kovacevic R, Thermal Modeling of friction stir welding in a moving coordinate system and its validation, International Journal of Machine Tools and Manufacture, 43 (2003) 605-615.
8. Ulysse P. Three dimensional modeling of the friction stir welding process, International Journal of Machine Tools and Manufacture, 42 (2002) 1549-1557.
9. McClure JC, Tang W, Guo X, Feng Z, Gould JE. A Thermal Model Of Friction Stir Welding. 5th International Conference On Trends In Welding Research, pp. 590-594.
10. Chao YJ, Qi XH. Thermal And Thermo-mechanical Modeling Of Friction Stir Welding Of Aluminium Alloy 6061-T6. Journal of Materials Processing & Manufacturing Science, 7 (1999) 215-233.
11. Frigaard O, Grong O, Bjornklett B, Midling OT. Modeling of the Thermal and Microstructure Fields During Friction Stir Welding Of Aluminium Alloys, The 1st International Symposium on Friction Stir Welding, Thousand Oaks, Cal., USA, June 1999.
12. Chao YJ, Xinhai Q. Heat Transfer And Thermal-Mechanical Analysis Of Friction Stir Joining Of AA6061-T6 Plates. The 1st International Symposium on Friction Stir Welding, Thousand Oaks, CA, USA 14-16 June 1999.

13. Dong P, Lu F, Hong JK, Cao Z. Analysis Of Weld Formation Process In Friction Stir Welding. The 1st International Symposium on Friction Stir Welding, Thousand Oaks, CA, USA 14-16 June 1999.

14. Russel MJ, Shercliff HR, Analytic Modeling of Microstructure Development In Friction Stir Welding, The 1st International Symposium on Friction Stir Welding, Thousand Oaks, Cal., USA, June 1999.

15. Tang W, Guo X, McClure JC, Murr LE, Nunes A. Heat Input And Temperature Distribution. In Friction Stir Welding. Journal of Materials Processing & Manufacturing Science, 7, (1998) 163-172.

16. Frigaard O, Grong O, Midling OT. Modeling Of Heat Flow Phenomena In Friction Stir Welding Of Aluminium Alloys. INALCO 98, TWI, Cambridge, UK, 1998

17. Russel MJ, Shercliff HR. Analytic Modeling Of Friction Stir Welding. INALCO 98, TWI, Cambridge, UK, 1998.

18. McClure JC, Tang T, Guo X, Murr LE, Nunes A. Heat Input And Temperature Distribution In Friction Stir Welding. Journal of Material Processing & Manufacturing Science (USA), Vol. 7, Issue 2, (Oct. 1998), pp. 163-172.

19. Colegrove P. Three Dimensional Flow And Thermal Modeling Of The Friction Stir Welding Process, Proceedings of the second International Symposium on Friction Stir Welding, Gothenburg, Sweden, June 2000.

20. Bassett JC, Briley SS, Friction Stir Welding Of Aluminium Armor, Proceedings of the second International Symposium on Friction Stir Welding, Gothenburg, Sweden, June 2000.

21. Colligan K, Fisher JJ and Pickens JR. Friction Stir Welding (FSW) Of Aluminium Armor Alloy 2519, for the Advanced Amphibious Assault Vehicle (AAAV). AeroMat 2001, Long Beach, Cal., June 2001.

22. Jones C, Adams G. Assembly Of A Full Scale External Tank Barrel Section Using FSW. The 1st International Symposium on Friction Stir Welding, Thousand Oaks, Cal., June 1999.

23. Talwar R, Bolser D, Lederich R and Bauman J. Friction Stir Welding of Airframe Structures. Proceedings of the second International Symposium on Friction Stir Welding, Gothenburg, Sweden, June 2000.

24. Lohwasser D. Application of Friction Stir Welding For Aircraft Industry. Proceedings of the second International Symposium on Friction Stir Welding, Gothenburg, Sweden, June 2000.

25. Brooker MJ, van Deudekom AJM, Kallee SW, Sketchley PD. Applying Friction Stir Welding to the Ariane 5 Main Motor Thrust Frame. Proceedings of the second International Symposium on Friction Stir Welding, Gothenburg, Sweden, June 2001.

26. Pedwell R, Davies H, Jefferson A. The Application Of Friction Stir Welding To Aircraft Wing Structures. The 1st International Symposium on Friction Stir Welding, Thousand Oaks, Cal., June 1999.

27. Kallee SW, Mistry A. Friction Stir Welding in the Automotive Body in White Production. The 1st International Symposium on Friction Stir Welding, Thousand Oaks, Cal., June 1999.

28. Hori H, Makita S, Hino H. Friction Stir Welding of Rolling Stock For Subway. The 1st International Symposium on Friction Stir Welding, Thousand Oaks, Cal., June 1999.

29. Midling OT, Kvale JS. Industrialisation of Friction Stir Welding Technology In Panels Production For The Maritime Sector. The 1st International Symposium on Friction Stir Welding, Thousand Oaks, Cal., June 1999.

30. Pryzdatec J. A Ship Classification View on Friction Stir Welding. The 1st International Symposium on Friction Stir Welding, Thousand Oaks, Cal., June 1999.

31. Thomas WM, Gittos MF. Development of Friction Stir Welding Tools For the Welding Of Thick (25mm) Aluminium Alloys. TWI Research Report 692/1999, December 1999.

32. American Society of Metals, Aluminium and Aluminium Alloys, ASM Specialty Handbook 1996.

33. www.tennalum.com/AATT.html

34. Ringer SP and Hono K. Microstructural Evolution and Age Hardening in Aluminium Alloys: Atom probe field-Ion Microscopy and Transmission Electron Microscopy Studies. Materials Characterisation 44:101-131 (2000).

35. Verhoeven JD. Fundamentals of Physical Metallurgy, John Wiley and Sons, 1975.

36. Dieter GE. Mechanical Metallurgy, SI Metric Edition, McGraw-Hill Book Company, 1988.

37. Doherty RD, Hughes DA, Humphreys FJ, Jonas JJ, Juul Jensen D, Kassner ME, King WE, McNelly TR, McQueen HJ, Rollett AD. Current issues in recrystallisation: a review. Materials Science and Engineering A238 (1997) 219-274.

38. TWI Bulletin, Friction stir-where we are, and where we're going, May/June 1998.

39. AWS, Welding Handbook. 8th ed. Edited by. R.L. Obrien, Vol.2 1991, Miami American Welding Society. p. 955.

40. Threadgill P and Howes T. Rotary friction welding – a guide to best practice. www.twi.co.uk

41. Metals Handbook, Welding Brazing And Soldering, 9th Ed., V.6, 1983, pp.723-724.

42. Sahin M, Akata HE. Joining with friction welding of plastically deformed steel. Journal of Materials Processing Technology 142 (2003) pp. 239-246

43. Sketchley PD, Threadgill PL, and Wright IG. Rotary Friction Welding Of A Fe_3Al Based ODS Alloy. Materials Science and Engineering A329-331 (2002) pp. 756-762.

44. Midling OT and Grong O. A Process Model For Friction Welding Of Al-Mg-Si Alloys And Al-SiC Metal Matrix Composites-II. HAZ Microstructure and Strength Evolution. Acta Metallurgica et Materialia, Vol. 42, No. 5, pp. 1595-1609.

45. Spindler DE. What Industry Needs To Know About Friction Welding. Welding Journal, March, 1994: pp. 37-42.

46. Grewe KJ. Friction Welding Takes On New Applications. In Welding Journal 1997. Sept.: pp. 39-40.

47. Voinov VG. Mechanism of joint formation in Friction Welding. Welding Production, 1968. 15: pp. 8-13.

48. Ellis CRG. Continuous Drive Friction Welding of Mild Steel. Welding Journal, 1972 (April): pp. 183s-197s.

49. Lucas W. Process Parameters and Friction Welds, in Metal Construction and British Welding Journal 1973. 5(8): pp.293-297.

50. Suga Y. Miyakawa S and Ogawa K. Estimation of Temperature Distribution in the Friction Welding of Carbon Steel by Finite Element Method. In Welding International, 1999. 1384): pp. 262-269.

51. Petrucci LG. Temperature Distribution in Friction Welding. In General Engineer, 1978 (July-August): pp. 178-184.

52. Sergin SA. The distribution of temperature along the length of a bar in relation to the speed of rotation in friction welding of steels. In Welding Production, 1977(1): pp. 37-39.

53. Leinert TJ, Stellwag WL, Lehman Jr. and LR, Comparison of Heat Inputs: Friction Stir Welding vs. Arc Welding, American Welding Society Convention, 2002.

54. Cam G, Ventzke V, dos Santos JF, Kocak M, Dennequin G, Gonthier-Maurin P. Characterisation of electron beam welded aluminium alloys. In Science and Technology of Welding and Joining, Vol.4 (5), 1999: pp. 317-323.

55. Shinoda T, Tokisue H and Enomoto M, Recent trends of research and development of FSW technology in Japan, Proceedings of the 3rd International Symposium on FSW, Kobe, Japan 27-28 September 2001.

56. Cornet D, Guening D and Gregoire A, Engineering test report number ETR TSA/TP02/BE/s/N1, Sonaca S.A., Gosselies, Belgium.

57. Hori H, Makita S and Minaminda T, Joint strength of thick sheet welded by friction stir welding, Proceedings of the 3rd International Symposium on FSW, Kobe, Japan 27-28 September 2001.

58. Zettler R, Lomolino S, dos Santos JF, Donath T, Beckmann F, Lippman T, Lohwasser D, A study on Material Flow in FSW AA 2024-T351 and AA 6056 T4 Alloys, Proceedings of the 5th International Symposium on Friction Stir Welding, Metz France 14-16 September 2004.

59. London B, Mahoney M, Bingel W, Calabrese M, Waldron D; Experimental Methods For Determining Material Flow In Friction Stir Welds. The 3rd International Symposium on Friction Stir Welding, Kobe, Japan 27-28 September 2001.

60. Guerra M, McClure JC, Murr LE, Nunes AC. Metal Flow During Friction Stir Welding. Friction Stir Welding And Processing. Proceedings of Symposium, The Minerals, Metals & Materials Society, held Indianapolis, Indiana, USA, pp. 25-33, November 4-8, 2001.

61. Seidel TU, Reynolds AP; Visualization Of the Material Flow In AA2195 Friction Stir Welds Using A Marker Insert Technique. Metallurgical And Materials Transactions A, Vol. 32A, Issue 11, pp. 2879-2884, November 2001.

62. Askari A, Silling S, London B, Mahoney M; Modelling And Analysis Of Friction Stir Welding Processes. Friction Stir Welding and Processing. Proceedings of Symposium, The Minerals Metals & Materials Society, Indianapolis, Indiana USA, pp. 139-149, November 4-8, 2001.

63. Kazi SH, Murr LE; Complex Flow Phenomena Associated With Friction Stir Welding Of Aluminium Alloys. Friction Stir Welding and Processing.

Proceedings of Symposium, The Minerals Metals & Materials Society, Indianapolis, Indiana USA, pp. 139-149, November 4-8, 2001.

64. Ouyang JH, Kovacevic R. Material Flow And Microstructure In The Friction Stir Butt Welds Of The Same And Dissimilar Aluminium Alloys. Journal Of Materials Engineering And Performance. Vol. 11, (1), pp.51-63, Feb. 2000.
65. Reynolds AP. Visualisation of Material Flow In Autogeneous Friction Stir Welds. Science And Technology Of Welding And Joining. Vol. 5, No.2, pp. 120-124, 2000.
66. Bendzsak GJ, North TH, Smith CB. An Experimentally Validated 3D Model For Friction Stir Welding. The 2nd International Symposium on Friction Stir Welding, Gothenburg, Sweden, 26-28 June 2000.
67. Colligan K. Material Flow Behavior During Friction Stir Welding Of Aluminium. Supplement to the Welding Journal, pp.229-s to 237-s, July 1999.
68. Mahoney WM, Mishra R and Nelson T, High strain rate superplasticity in thick section 7050 aluminium created by friction stir processing, Proceedings of the 3rd International Symposium on FSW, Kobe, Japan 27-28 September 2001
69. Bhat BN, Carter RW, Ding RJ, Lawless KG, Nunes Jr. AC, Russel CK, Shah SR. Friction Stir Welding Development at NASA – Marshal Space Flight Center, In Friction Stir Welding and processing, TMS, Nov. 4-8, 2001, Indianapolis, Indiana, USA.
70. Manufacturing Engineering, March 2004, Vol.132, No.3.
71. Aluminium Now, Vol.5, No. 1, Jan/Feb. 2003.
72. www.aluminium.org/ANTemplate.cmf
73. www.twi.co.uk/j32k/unprotected band.1/fswjoint.html
74. Colligan KJ, Junde Xu, and Pickens JR. Welding Tool And Process Parameter Effects In Friction Stir Welding Of Aluminium Alloys. Friction Stir Welding And Processing II. Proceedings of Symposium, The Minerals Metals & Materials Society, San Diego, California USA, March 2-6, 2003. pp. 181-190.
75. Reynolds AP, Tang W; Alloy, Tool Geometry, and Process Parameter Effect On Friction Stir Weld Energies and Resultant FSW Joint Properties. Proceeding of Symposium (The Minerals Metals & Materials Society), pp.15-23, Indianapolis Indiana, USA, Nov. 4-8 2001.

76. Reynolds AP, Lockwood WD, Seidel TU, Processing-Property Correlation In Friction Stir Welds. Materials Science Forum, Vols. 331-337, 2000: pp. 1719-1724.

77. Su JQ, Nelson TW, Mishra R, Mahoney M, Microstructural investigation of friction stir welded 7050-T651 aluminium, Acta Materialia 51 (2003) 713-729.

78. Sato Y, Urata M, Kokowa H; Parameters Controlling Microstructure And Hardness During Friction Stir Welding Of Precipitation-Hardenable Aluminium Alloy 6063. Metallurgical and Materials Transactions A, Vol. 33A, pp. 625-653, March 2002.

79. Sutton MA, Yang B, Reynolds AP, Taylor R; Microstructural Studies Of Friction Stir Welds In 2024-T3 Aluminium. Materials Science and Engineering A323, pp. 160-166, 2002.

80. Salem HG, Reynolds AP, Lyons JS; Microstructure And Retention Of Superplasticity Of Friction Stir Welded Superplastic 2095 Sheet. Scripta Materialia 46, pp. 337-342, 2002.

81. Jin H, Saimoto S, Ball M, Threadgill PL; Characteristaion Of Microstructure And Texture In Friction Stir Welded Joints Of 5754 And 5182 Aluminium Alloy Sheet. Materials Science and Technology, Vol. 17, pp. 1605-1614, Dec. 2001.

82. Sato YS, Hwan S, Park C, Kokawa H. Microstructural Factors Governing Hardness In Friction Stir Welds Of Solid Solution Hardened Aluminium Alloys. Metallurgical And Materials Transactions A, Vol. 32A, Issue 12, pp. 3033-3042, Dec. 2001.

83. Field DP, Nelson TW, Horvanski Y, Jata KV; Heterogeneity Of Crystallographic Texture In Friction Stir Welds Of Aluminium. Metallurgical And Materials Transactions A, Vol. 32A, Issue 12, pp. 2869-2877, Nov. 2001.

84. Denquin A, Allehaux D, Campagnac M-H, Lapasset G. Microstructural Evolution And Strength Mismatch Within A Friction Stir Welded 6056 Aluminium Alloy. The 3rd International Symposium on Friction Stir Welding, Kobe, Japan 27-28 September 2001.

85. Friggard O, Grong O, Midling OT. A Process Model For Friction Stir Welding Of Age Hardening Aluminium Alloys. Metallurgical And Materials Transactions A, Vol. 32A, Issue 12, pp. 1189-1200, May 2001.

86. Sato Y, Kokowa H, Ikeda K, Enomoto M, Jogan S, Hashimoto T; Micro-texture In Friction Stir Weld Of An Aluminium Alloy. Metallurgical And Materials Transactions A, Vol. 32A, Issue 12, pp. 941-948, April 2001.

87. Juhas MC, Collins PC, Viswanathan GB, Fraser HL. Microstructural Characterisation Of Friction Stir Welds. Lightweight Alloys For Aerospace Applications. Aluminium Alloys TMS (The Minerals Metals & Materials Society), 2001.

88. Riddle YW, McIntosh M, Sanders Jr TH. Improving Recrystallisation Resistance In Wrought aluminium Alloys With Scandium Additions. Lightweight Alloys For Aerospace Applications. Aluminium Alloys TMS (The Minerals Metals & Materials Society), 2001.

89. Leonard AJ, Microstructure And Aging Behaviour Of Friction Stir Welds In Aluminium Alloys 2014A-T651 And 7075-T651, The 2nd International Symposium on Friction Stir Welding, Gothenburg, Sweden, June 2001.

90. Svensson LE, Karlson L, Larsson H, Karlsson B, Fazzini M, Karlsson J; Microstructure And Mechanical Properties Of Friction Stir Welded Aluminium Alloys With Special Reference To AA 5083 And AA 6082. Science And Technology Of Welding And Joining, Vol. 5, No. 5, pp. 285-295, 2000.

91. Jata KV, Sankaran KK, Ruschau JJ; Friction Stir Welding Effects on Microstructure And Fatigue Of Aluminium Alloy 7050-T7451. Metallurgical And Materials Transactions A, Vol. 30A, Issue 12, pp. 2181-2192, Sept. 2000.

92. Heinz B, Strotzki B, Eggeler G; Microstructure And Mechanical Characterisation Of A Friction Stir Welded Al-Alloy. Materials Science Forum Vols. 331-337, pp. 1757-1762, 2000.

93. Jata KV, Semiatin SL; Continuous Dynamic Recrystallisation During Friction Stir Welding Of High Strength Aluminium Alloys. Scripta Materialia 43, pp. 743-749, 2000.

94. Norman AF, Brough I, Pragnell PB; High Resolution EBSD Analysis Of The Grain Structure In An AA2024 Friction Stir Weld. Materials Science Forum Vols. 331-337, pp. 1713-1718, 2000.

95. Sato YS, Kokawa H, Enomoto M, Jogan S, Hashimoto T. Precipitation Sequence In Friction Stir Weld Of 6063 Aluminium During Aging. Metallurgical And Materials Transactions A, Vol. 30A, Issue 12, pp. 2181-2192, Sept. 2000.

96. Bjorneklett BI, Grong O, Myhr OR, Kluken AO; A Process Model For The Heat Affected Zone Microstructure Evolution In Al-ZN-Mg Weldments. Metallurgical And Materials Transactions A, Vol. 30A, pp. 2667-2677, October 1999.

97. Sato YS, Kokawa H, Enomoto M, Jogan S, Hashimoto T. Microstructural Evolution Of 6063 During Friction Stir Welding. Metallurgical And Materials Transactions A, Vol. 30A, Issue 9, pp. 2429-2437, Sept. 1999.

98. Russel MJ, Shercliff HR, Analytic Modeling of Microstructure Development In Friction Stir Welding, The 1st International Symposium on Friction Stir Welding, Thousand Oaks, Cal., USA, June 1999.

99. Frigaard O, Grong O, Hjelen J, Gulbrandsen-Dahl S, Midling OT; Characterisation Of The Subgrain Structure In Friction Stir Welded Aluminium Alloys Using The SEM-EBSD Technique. The 1st International Symposium on Friction Stir Welding, Thousand Oaks, Cal., USA, June 1999.

100. Bjorneklett BI, Frgaard O, Grong O, Myhr OR, Midling OT; Modeling Of Local Melting During Friction Stir Welding Of Al-Zn-Mg Alloys. 6th International Conference On Aluminium Alloys, ICAA-6, Vol. 3, pp. 1531-1536, Japan 1998.

101. Murr LE, Li Y, Trillo EA, Flores RD, McClure JC, Microstructures In Friction Stir Welded Metals. Journal of Materials Processing and Manufacturing Science, Vol.7, pp.145-161, October 1998.

102. Donne CD, Braubn R, Staniek G, Jung A, Kaysser WA; Mikrostrukturelle, Mechanische Und Korrosive Eigenschaften Reibrührgeschweißter Stümpfnähte In Aluminiumlegierungen. Material Wissenschaft und Werkstofftechnik, 29, pp. 609-617, 1998.

103. Flores OV, Kennedy C, Murr LE, Brown D, Pappu S, Nowak BM, McClure JC. Microstructural Issues In Friction Stir Welded Aluminium Alloy. Scripta Materialia, Vol. 38, pp. 703-708, 1998.

104. Lui G, Murr LE, Niou C-S, McClure JC, Vega FR. Microstructural Aspects Of The Friction Stir Welding Of 6061-T6 Aluminium. Scripta Materialia, Vol. 37, pp. 355-361, 1997.

105. Murr LE, Liu G, McClure JC; Dynamic Recrystallisation In Friction Stir Welding Of Aluminium Alloy 1100. Journal Of Materials Science Letters 16, pp.1801-1803, 1997.

106. Droenen P-E, Ryum N; Local Melting In Al-Mg-Zn Alloys. Metallurgical And Materials Transactions A, Vol. 25A, pp. 521-530, March 1994.

107. Threadgill PL, Friction Stir Welding-the state of the art, TWI Research Report 678/1999, May 1999.

108. Blum W, McQueen HJ; Dynamics Of Recovery And Recrystallisation. Materials Science Forum Vols. 217-222, pp.31-42, 1995.

109. Boz M and Kurt A. The influence of stirrer geometry on bonding and mechanical properties in friction stir welding process. Materials & Design, Vol.25 (4), June 2004: pp.343-347.

110. Dawes CJ, Thomas WM, Development Of Improved Tool Design For Friction Stir Welding Of Aluminium, The 1st International Symposium on Friction Stir Welding, Thousand Oaks, Cal., June 1999.

111. Dawes CJ, Spurgin EJR, Staines DG, Friction Stir Welding Of Aluminium Alloy 5083-increased welding speed, TWI Research Report 684/1999, August 1999.

112. Dawes CJ, Threadgill PL, Spurgin EJR, Staines DG, Development Of The New FSW Technique For Welding Aluminium-Phase II, TWI Report 5651/35/95, November 1995.

113. Dawes CJ, Almond DN, Watts ER, Development Of The New FSW Technique For Welding Aluminium-Phase I, TWI Report 5651/12/94, July 1994.

114. Midling OT, Rovik G. Effect Of Tool Shoulder Material On Heat Input During Friction Stir Welding. The 1st International Symposium on Friction Stir Welding, Thousand Oaks, Cal., USA, June 1999.

115. Thomas WM, Munn I, Smith PT, Friction Stir Welding Of An Aluminium Alloy-Effects Of Tool Geometry, TWI, World Center For Materials Joining Technology, 1995.

116. Zhao Y, Lin S, Wu L and Qu F. The Influence Of Pin Geometry On Bonding And Mechanical Properties In friction Stir Weld 2014 Al Alloy. Article in Press, Material Letters 2005.

117. Zettler R, Lomolino S, dos Santos JF, Donath T, Beckmann F, Lippman T, Lohwasser D, Effect Of Tool Geometry And Process Parameters On Material Flow In FSW Of An AA 2024 T351 Alloy. Welding in the World, Journal of the International Institute of Welding, Vol.49, No.3/4, 2005.

118. Thomas WM and Andrews RE. High performance tools for friction stir welding, International patent specification, PCT/GB99/01128, 13 April, 1999.

119. Marks' Standard Hand Book for Mechanical Engineers Tenth Ed., McGraw Hill 1996, 5-34 to 5-36.

120. Kallee SW, Knowledge Based Software Package For Friction Stir Welding, Proc. INALCO-7, pp.209-217, Cambridge, 26th April 1998.

121. Johnson R, Horrex NL, Preliminary Examination Of Forces Generated During The Friction Stir Welding Process, TWI Technology Briefing, 696/2000, January 2000.

122. Johnson R, Forces in Friction Stir Welding of Aluminium Alloys-further studies, TWI Research Report 716/2000, December 2000.

123. Lienert TJ, Stellwag WL, Shao H. Determination Of Load Torque And Tool Temperatures During Friction Stir Welding Of Aluminium Alloys. Summary Report SR0019, EWI, Dec. 2000.

124. GKSS-Forschungszentrum, Joining Technology Group, Geesthacht, Germany.

125. Larsson H, Karlsson L, Stoltz S, Bergqvist E-L. Joining Of Dissimilar Al-Alloys By Friction Stir Welding. 2nd World Symposium Friction Stir Welding, Gothenburg Sweden, June 2000.

126. Murr LE, Trillo EA, Li Y, Flores RD, Nowak JC. Solid State Flow Associated With Friction Stir Welding Of Dissimilar Metals. Fluid Flow Phenomena In Metals Processing. Proceedings of Symposium, The Minerals, Metals & Materials Society, pp. 31-40, 1999.

127. Li Y, Murr LE, McClure JC. Flow Visualisation And Residual Microstructures Associated With The Friction Stir Welding Of Aluminium To 6061 Aluminium. Materials Science and Engineering A271, pp. 213-223, 1999.

128. Srinivasan PB, Dietzel W, Zettler R, dos Santos JF, Sivan V. Stress corrossion cracking susceptibility of friction stir welded AA7075-AA6056 dissimilar joint. Materials Science and Engineering A 392 (2005), pp. 292-300.

129. Krishnan KN. On the Formation of Onion Rings in Friction Stir Welds. Materials Science and Engineering A327, pp. 246-251, 2000.

130. Schneider JA, Nunes Jr. AC. Thermo-mechanical Processing in Friction Stir Welds. Friction Stir Welding and Processing II, TMS (The Minerals, Metals & Materials Society), 2003: pp. 43-51.

131. Fonda RW, Bingert JF, Colligan KJ. Development of grain structure during friction stir welding. Scripta Materialia 51 (2004) 243-248.

132. Nunes Jr. AC. Wiping Metal Transfer in Friction Stir Welding, Aluminium 2001: Proceedings of the 2001 TMS Annual Meeting Automotive Joining Aluminium Symposia. (New Orleans LA, February 11-15). Edited by G.

Kaufmann, J. Green and S. Das. TMS (The Minerals, Metals & Materials Society), 2001: pp. 235-248.

133. Colegrove PA and Shercliff HR. 2-Dimensional CFD Modelling Of Flow Around Profiled FSW Tooling. Friction Stir Welding and Processing II, Ed. KV Jata, M Mahoney and R Mishra, Proceedings of Symposia, (The Minerals & Materials Society) San Diego, California March 2-6, 2003. pp. 13-22.

134. Hyoe T, Colegrove PA and Shercliff HR. Thermal And Microstructure Modelling In Thick Plate Aluminium Alloy 7075 Friction Stir Welds. I Friction Stir Welding And Processing II, Ed. KV Jata, M Mahoney and R Mishra, Proceedings of Symposia, (The Minerals & Materials Society) San Diego, California March 2-6, 2003. pp. 33-42.

135. Shercliff HR and Colegrove PA. Mathematical Modelling of Weld Phenomena 6, Ed. H Cerjak and H Bhadeshia, Maney Publishing, London, UK, 2002. pp. 927-974.

136. Colegrove P. Master of Science (MSc.) Thesis, University of Adelaide, 2000.

10. APPENDIX

Appendix A: Tool Designs

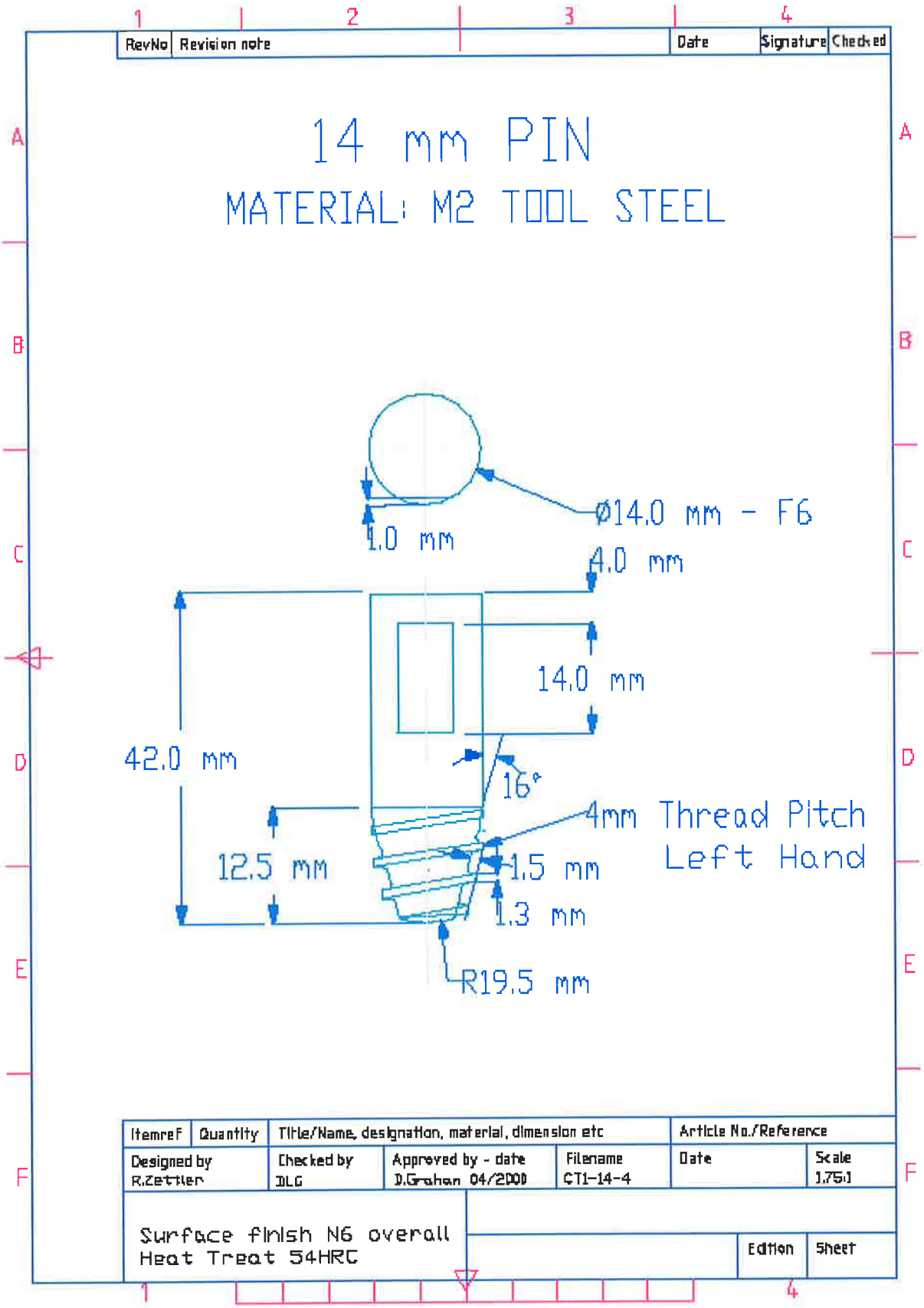

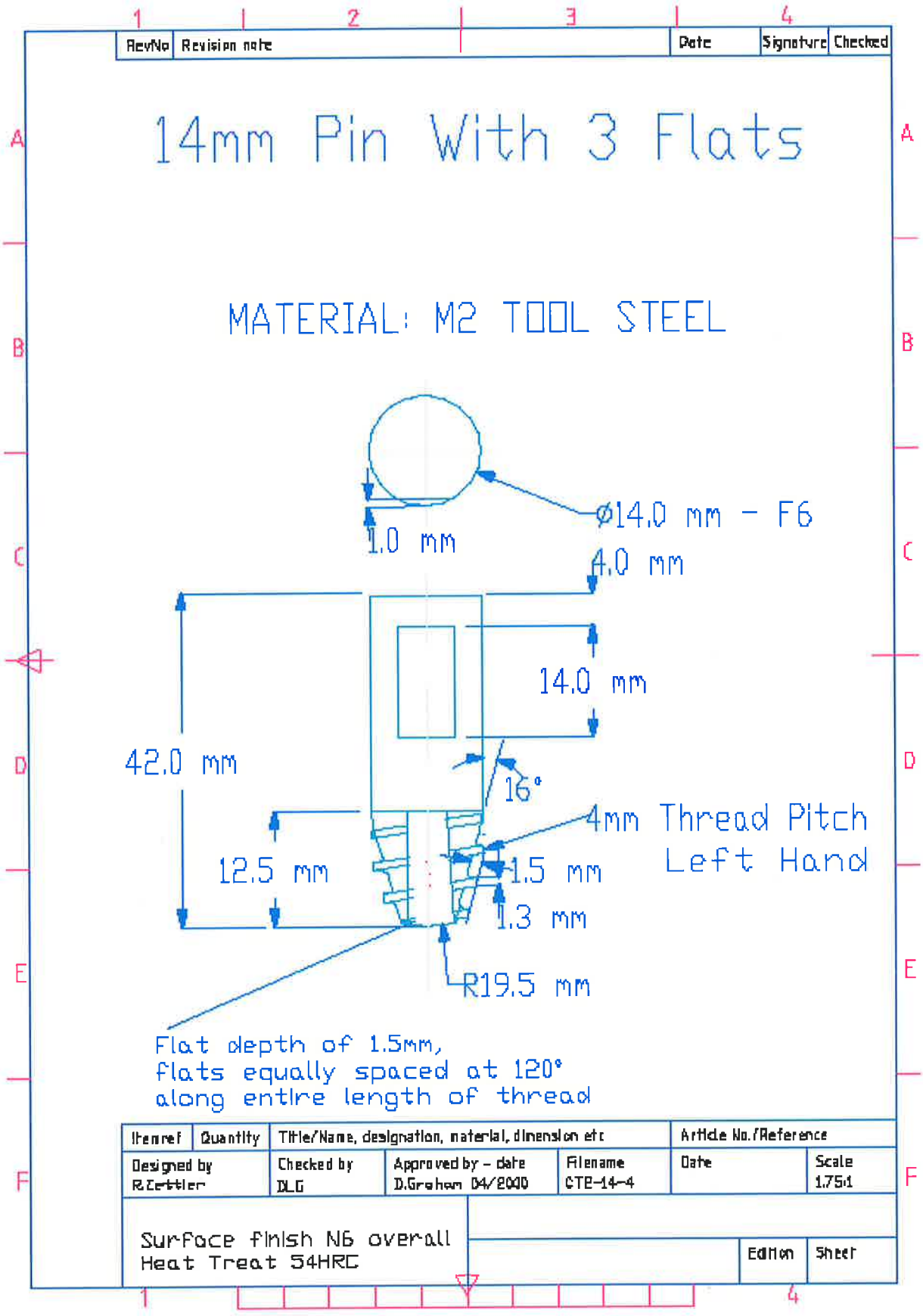
RevNo
Revision note
Date
Signature
Checked
14mm Pin With 3 Flats
MATERIAL: M2 TOOL STEEL
Ø14.0 mm - F6
1.0 mm
4.0 mm
14.0 mm
42.0 mm
16°
4mm Thread Pitch
Left Hand
12.5 mm
1.5 mm
1.3 mm
R19.5 mm
Flat depth of 1.5mm,
flats equally spaced at 120°
along entire length of thread
Itemref
Quantity
Title/Name, designation, material, dimension etc
Article No./Reference
Designed by
R.Zettler
Checked by
DLG
Approved by - date
D.Graham 04/2000
Filename
CTE-14-4
Date
Scale
1.75:1
Surface finish N6 overall
Heat Treat 54HRC
Edition
Sheet

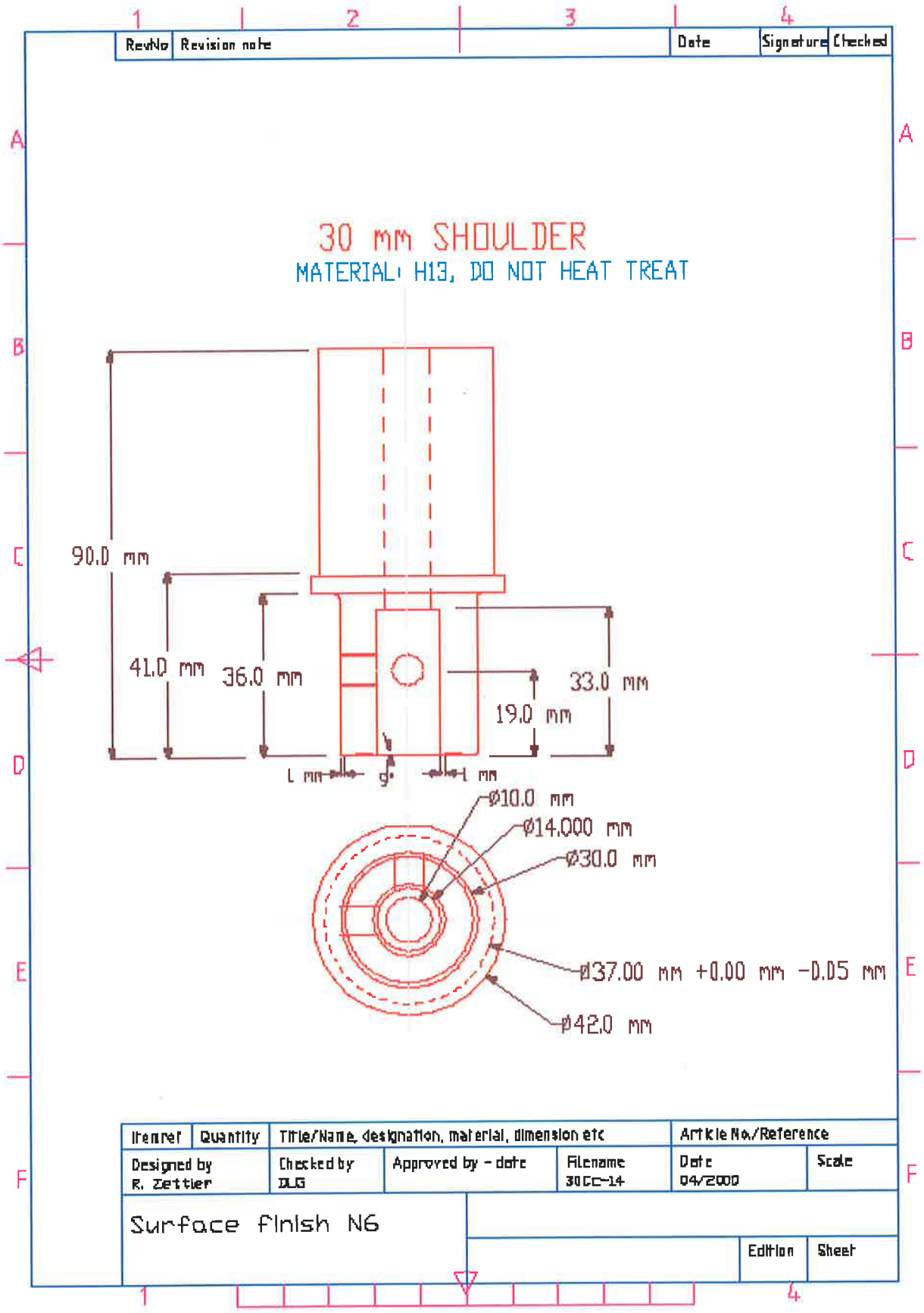
1
2
3
4
RevNo
Revision note
Date
Signature
Checked
A
B
C
D
E
F
30 mm SHOULDER
MATERIAL: H13, DO NOT HEAT TREAT
90.0 mm
41.0 mm
36.0 mm
33.0 mm
19.0 mm
Ø10.0 mm
Ø14.000 mm
Ø30.0 mm
Ø37.00 mm +0.00 mm -0.05 mm
Ø42.0 mm
Drawnr
Quantity
Title/Name, designation, material, dimension etc
Article No./Reference
Designed by
R. Zettler
Checked by
DLG
Approved by - date
Filename
30CC-14
Date
04/2000
Scale
Surface finish N6
Edition
Sheet

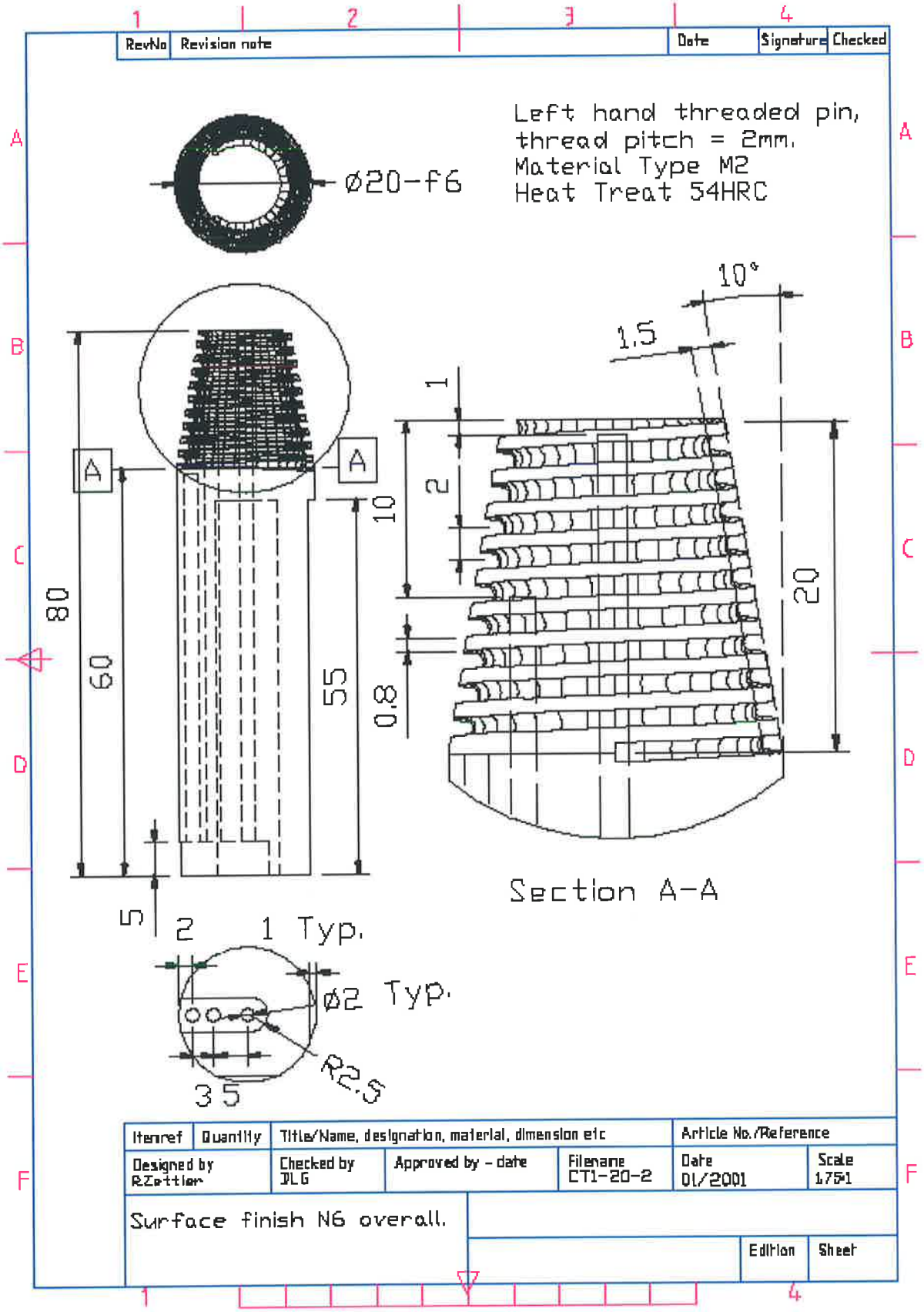
RevNo
Revision note
Date
Signature
Checked
Left hand threaded pin,
thread pitch = 2mm.
Material Type M2
Heat Treat 54HRC
Ø20-f6
10°
1.5
1
2
10
20
0.8
80
60
55
5
2
1 Typ.
Ø2 Typ.
R2.5
3.5
A
A
Section A-A
Itemref
Quantity
Title/Name, designation, material, dimension etc
Article No./Reference
Designed by
R.Zettler
Checked by
JLG
Approved by - date
Filename
CT1-20-2
Date
01/2001
Scale
1.75:1
Surface finish N6 overall.
Edition
Sheet

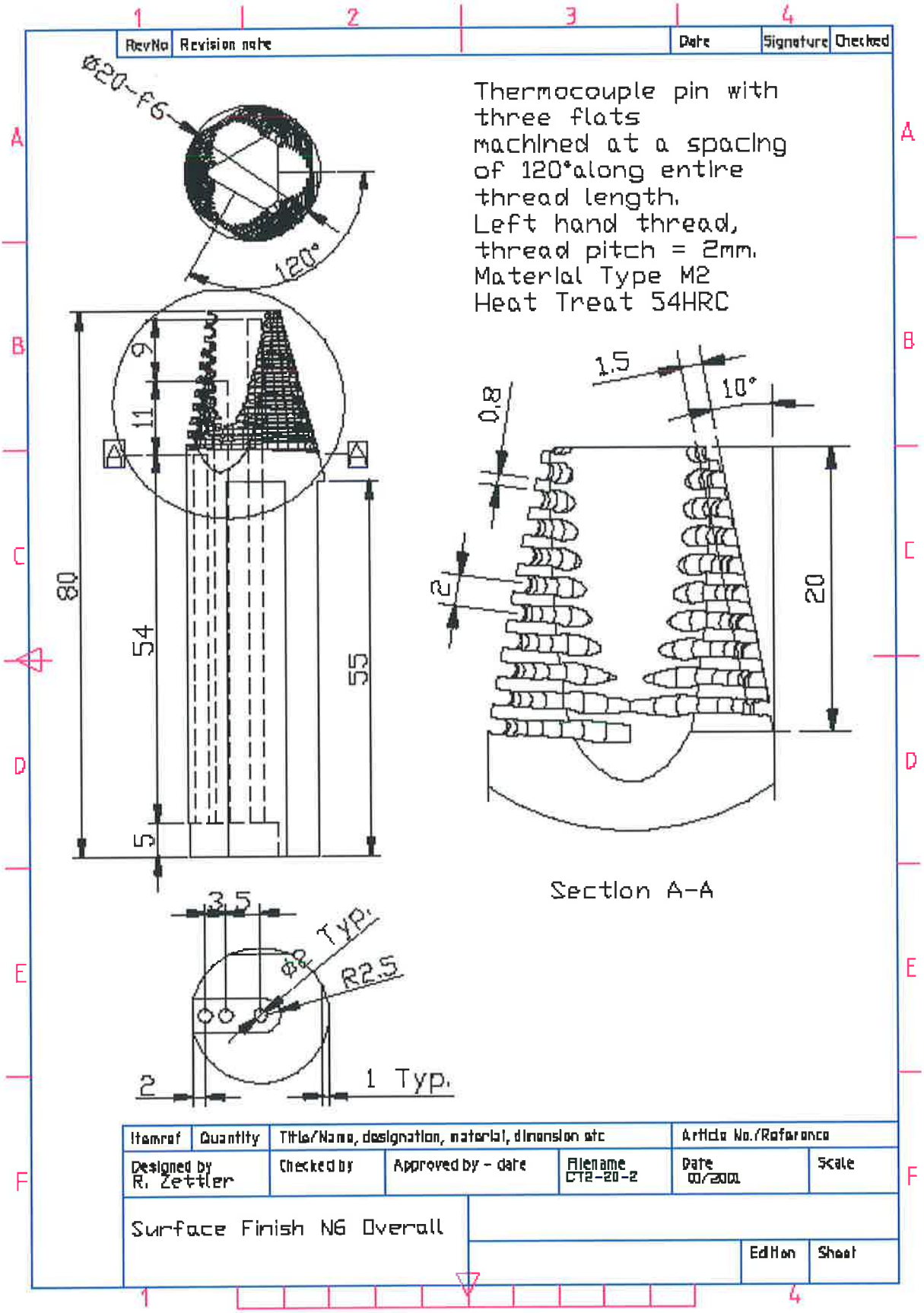
RevNo
Revision note
Date
Signature
Checked
Ø20-f6
120°
9
11
80
54
55
5
Thermocouple pin with three flats machined at a spacing of 120°along entire thread length.
Left hand thread, thread pitch = 2mm.
Material Type M2
Heat Treat 54HRC
1.5
10°
0.8
2
20
Section A-A
3.5
Ø2 Typ.
R2.5
2
1 Typ.
Itemref
Quantity
Title/Name, designation, material, dimension etc
Article No./Reference
Designed by R. Zettler
Checked by
Approved by - date
Filename CT2-20-2
Date 00/2001
Scale
Surface Finish N6 Overall
Edition
Sheet

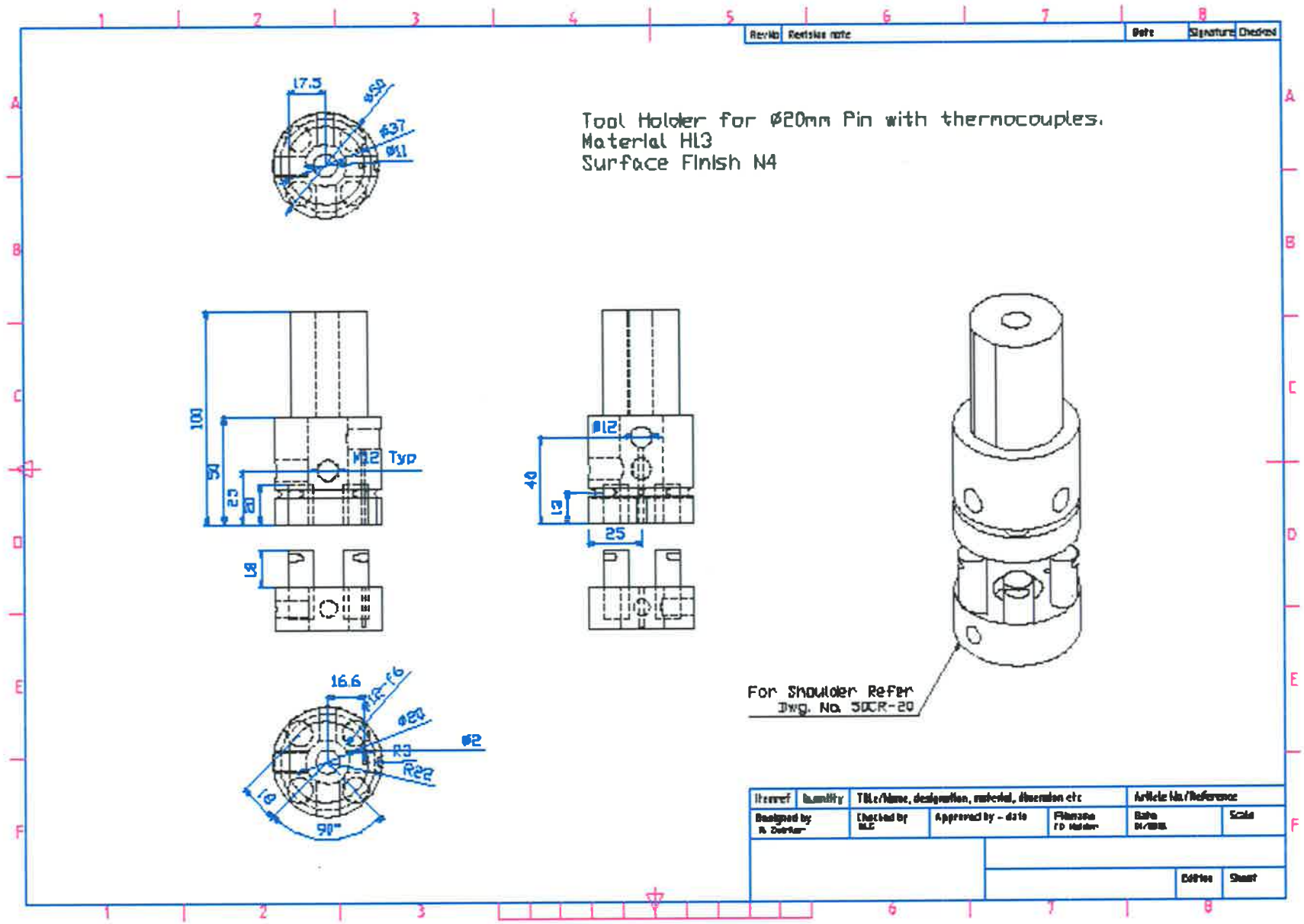
Tool Holder for Ø20mm Pin with thermocouples.
Material HL3
Surface Finish N4
17.5
Ø37
Ø11
100
50
25
20
M12 Typ
18
Ø12
40
13
25
16.6
R16
Ø22
Ø2
R3
R22
18
90°
For Shoulder Refer
Dwg. No. 50CR-20
Item ref
Quantity
Title/Name, designation, material, dimension etc
Article No./Reference
Designed by
Checked by
Approved by - date
Scale
Edition
Sheet

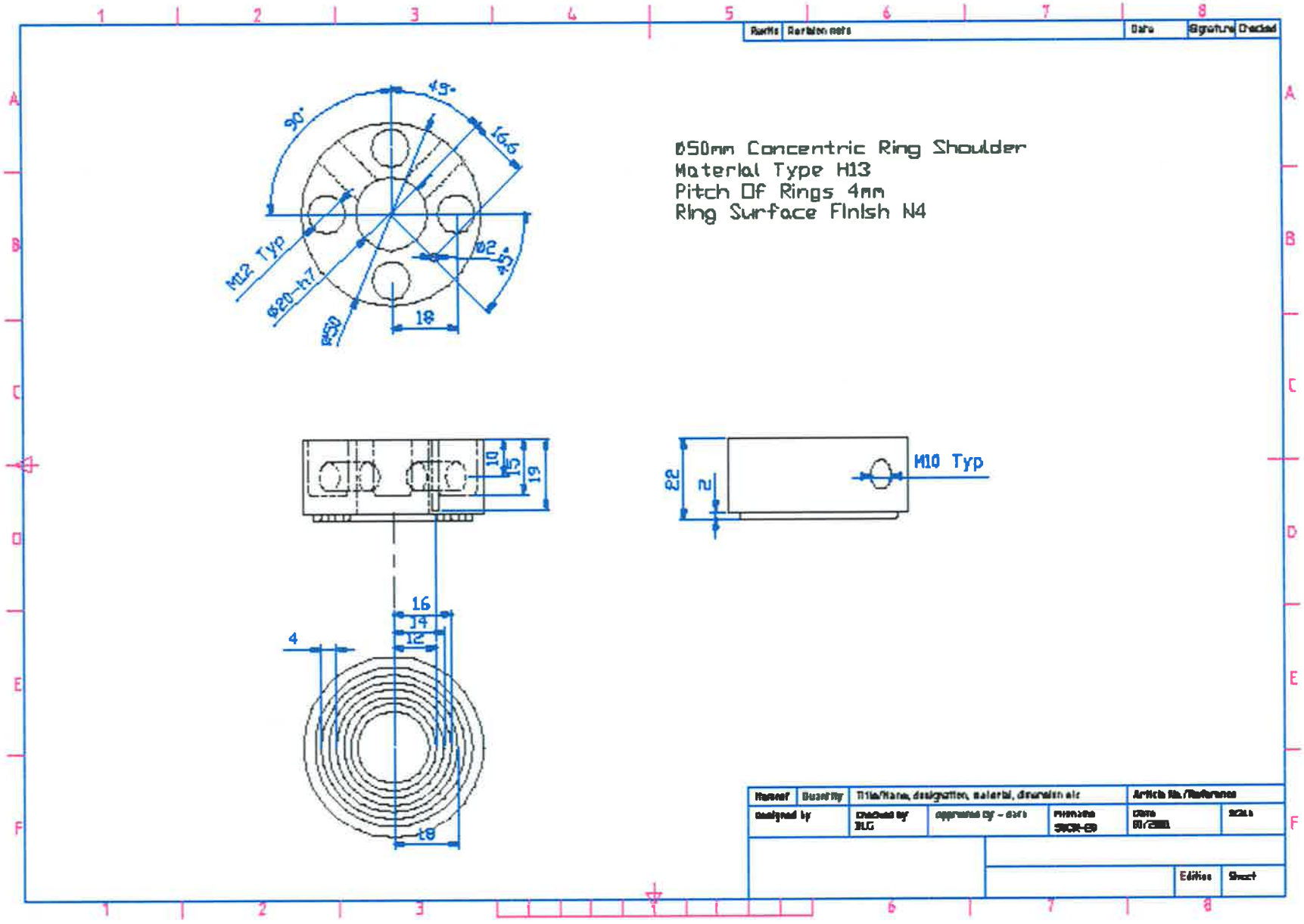
Marks
Revision note
Date
Signature
Checked
45°
90°
16.6
M12 Typ
Ø20-h7
Ø50
18
Ø2
45°
050mm Concentric Ring Shoulder
Material Type H13
Pitch Of Rings 4mm
Ring Surface Finish N4
10
15
19
M10 Typ
22
2
16
14
12
4
18
Number
Quantity
Title/Name, designation, material, drawing no.
Article No./Reference
assigned by
checked by
RLG
approved by - date
Format
Date
Scale
Edition
Sheet

Appendix B: A/D 597 Set Point Controller

ANALOG DEVICES

Thermocouple Conditioner and Setpoint Controller

AD596*/AD597*

FEATURES
Low Cost
Operates with Type J (AD596) or Type K (AD597) Thermocouples
Built-In Ice Point Compensation
Temperature Proportional Operation – 10 mV/°C
Temperature Setpoint Operation – ON/OFF
Programmable Switching Hysteresis
High Impedance Differential Input

GENERAL DESCRIPTION

The AD596/AD597 is a monolithic temperature setpoint controller that has been optimized for use at elevated temperatures such as those found in oven control applications. The device cold junction compensates and amplifies a type J or K thermocouple input to derive an internal signal proportional to temperature. The internal signal is then compared with an externally applied setpoint voltage to yield a low impedance switched output voltage. Dead-Band or switching hysteresis can be programmed using a single external resistor. Alternately, the AD596/AD597 can be configured to provide a voltage output (10 mV/°C) directly from a type J or K thermocouple signal. It can also be used as a stand-alone voltage output temperature sensor.

The AD596/AD597 can be powered with a single supply from +5 V to +30 V, or dual supplies up to a total span of 36 V. Typical quiescent supply current is 160 µA, which minimizes self-heating errors.

The AD596/AD597 H package option includes a thermocouple failure alarm that indicates an open thermocouple lead when operated in the temperature proportional measurement mode. The alarm output has a flexible format which can be used to drive relays, LEDs or TTL logic.

The device is packaged in a reliability qualified, cost effective 10-pin metal can or SOIC and is trimmed to operate over an ambient temperature range from +25°C to +100°C. Operation over an extended ambient temperature range is possible with slightly reduced accuracy. The AD596 will amplify thermocouple signals covering the entire –200°C to +760°C temperature range recommended for type J thermocouples while the AD597 can accommodate –200°C to +1250°C type K inputs.

The AD596/AD597 has a calibration accuracy of ±4°C at an ambient temperature of 60°C and an ambient temperature stability specification of 0.05°C/°C from +25°C to +100°C. If higher accuracy, or a lower ambient operating temperature is required, either the AD594 (J thermocouple) or AD595 (K thermocouple) should be considered.

*Protected by U.S. Patent No. 4,429,971.

REV. B

FUNCTIONAL BLOCK DIAGRAM

TO-100

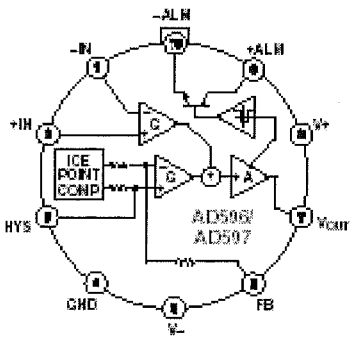

SOIC

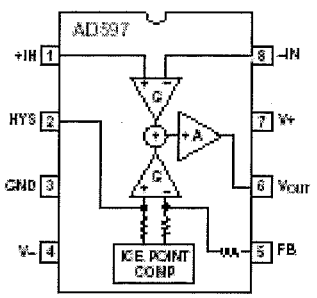

TOP VIEW
(Not to Scale)

PRODUCT HIGHLIGHTS

1. The AD596/AD597 provides cold junction compensation and a high gain amplifier which can be used as a setpoint comparator.
2. The input stage of the AD596/AD597 is a high quality instrumentation amplifier that allows the thermocouple to float over most of the supply voltage range.
3. Linearization not required for thermocouple temperatures close to 175°C (+100°C to +540°C for AD596J).
4. Cold junction compensation is optimized for ambient temperatures ranging from +25°C to +100°C.
5. In the stand-alone mode, the AD596/AD597 produces an output voltage that indicates its own temperature.

One Technology Way, P.O. Box 9106, Norwood, MA 02062-9106, U.S.A.
Tel: 781/329-4700 World Wide Web Site: http://www.analog.com
Fax: 781/326-8703

AD596/AD597–SPECIFICATIONS (@ +60°C and V_S = 10 V, Type J (AD596), Type K (AD597) Thermocouple, unless otherwise noted)

Model	AD596AH			AD597AH			AD597AR			Units
	Min	Typ	Max	Min	Typ	Max	Min	Typ	Max	
ABSOLUTE MAXIMUM RATINGS										
$+V_S$ to $-V_S$			36			36			36	Volts
Common-Mode Input Voltage	$(-V_S - 0.15)$		$+V_S$	$(-V_S - 0.15)$		$+V_S$	$(-V_S - 0.15)$		$+V_S$	Volts
Differential Input Voltage	$-V_S$		$+V_S$	$-V_S$		$+V_S$	$-V_S$		$+V_S$	Volts
Alarm Voltages										
+ALM	$-V_S$		$(-V_S + 36)$	$-V_S$		$(-V_S + 36)$	$-V_S$		$(-V_S + 36)$	Volts
–ALM	$-V_S$		$+V_S$	$-V_S$		$+V_S$	$-V_S$		$+V_S$	Volts
Operating Temperature Range	–55		+125	–55		+125	–40		+125	°C
Output Short Circuit to Common	Indefinite			Indefinite			Indefinite			
TEMPERATURE MEASUREMENT										
Specified Temperature Range +25°C to +100°C)										
Calibration Error[1]	–4		+4	–4		+4	–4		+4	°C
Stability vs. Temperature[2]		±0.02	±0.05		±0.02	±0.05		±0.02	±0.05	°C/°C
Gain Error	–1.5		+1.5	–1.5		+1.5	–1.5		+1.5	%
Nominal Transfer Function		10			10			10		mV/°C
AMPLIFIER CHARACTERISTICS										
Closed Loop Gain[3]		180.6			245.5			245.5		V/V
Input Offset Voltage		°C × 53.21 + 235			°C × 41.27 – 37			°C × 41.27 – 37		µV
Input Bias Current		0.1			0.1			0.1		µA
Differential Input Range	–10		+50	–10		+50	–10		+50	mV
Common-Mode Range	$(-V_S - 0.15)$		$(+V_S - 4)$	$(+V_S - 0.15)$		$(+V_S - 4)$	$(-V_S - 0.15)$		$(+V_S - 4)$	Volts
Common-Mode Sensitivity–RTO			10			10			10	mV/V
Power Supply Sensitivity–RTO		1	10		1	10		1	10	mV/V
Output Voltage Range										
Dual Supplies	$(-V_S + 2.5)$		$(+V_S - 2)$	$(-V_S + 2.5)$		$(+V_S - 2)$	$(-V_S + 2.5)$		$(+V_S - 2)$	Volts
Single Supply	0		$(+V_S - 2)$	0		$(+V_S - 2)$	0		$(+V_S - 2)$	Volts
Usable Output Current[4]	±5			±5			±5			mA
3 dB Bandwidth		15			15			15		kHz
ALARM CHARACTERISTICS[5]							Alarm Function Not Pinned Out			
$V_{CE(SAT)}$ at 2 mA		0.3			0.3					Volts
Leakage Current			±1			±1				µA
Operating Voltage at –ALM			$(+V_S - 4)$			$(+V_S - 4)$				Volts
Short Circuit Current		20			20					mA
POWER REQUIREMENTS										
Operating		$(+V_S$ to $-V_S) \leq 20$			$(+V_S$ to $-V_S) \leq 20$			$(+V_S$ to $-V_S) \leq 20$		Volts
Quiescent Current										
$+V_S$		160	300		160	300		160	300	µA
$-V_S$		100	200		100	200		100	200	µA

NOTES

[1]This is a measure of the deviation from ideal with a measuring thermocouple junction of 175°C and a chip temperature of 85°C. The ideal transfer function is given by:
AD596: $V_{OUT} = 180.57 \times (V_M - V_A + (\text{ambient in °C}) \times 53.21\ \mu V/°C + 235\ \mu V)$
AD597: $V_{OUT} = 245.69 \times (V_M - V_A + (\text{ambient in °C}) \times 41.27\ \mu V/°C - 37\ \mu V)$
where V_M and V_A represent the measuring and ambient temperatures and are taken from the appropriate J or K thermocouple table. The ideal transfer function minimizes the error over the ambient temperature range of 25°C to 100°C with a thermocouple temperature of approximately 175°C.
[2]Defined as the slope of the line connecting the AD596/AD597 CJC errors measured at 25°C and 100°C ambient temperatures.
[3]Pin 5 shorted to Pin 7.
[4]Current Sink Capability in single supply configuration is limited to current drawn to ground through a 5 kΩ resistor at output voltages below 2.5 V.
[5]Alarm function available on H package option only.

Specifications subject to change without notice.

Specifications shown in **boldface** are tested on all production units at final electrical test. Results from those tests are used to calculate outgoing quality levels. All min and max specifications are guaranteed, although only those shown in boldface are tested on all production units.

ORDERING GUIDE

Model	Package Description	Package Options
AD596AH	TO-100	H-10A
AD597AH	TO-100	H-10A
AD597AR*	Plastic SOIC	SO-8

*Consult factory for availability.

Table I. Output Voltage vs. Thermocouple Temperature (Ambient +60°C, V_S = −5 V, +15 V)

Thermocouple Temperature °C	Type J Voltage mV	AD595 Output mV	Type K Voltage mV	AD597 Output mV
−200	−7.890	−1370	−5.891	−1446
−190	−7.402	−1282	−5.730	−1362
−180	−6.821	−1177	−5.141	−1282
−170	−6.159	−1068	−4.669	−1146
−160	−5.426	−925	−4.138	−1016
−150	−4.632	−782	−3.553	−872
−80	−3.785	−629	−2.930	−717
−60	−2.892	−468	−2.243	−551
−40	−1.960	−299	−1.527	−375
−20	−.995	−125	−.777	−191
−10	−.501	−36	−.392	−96
0	0	54	0	0
10	.507	149	.397	97
20	1.019	238	.798	195
25	1.277	285	1.000	245
30	1.536	332	1.203	295
40	2.058	435	1.611	395
50	2.585	521	2.022	496
60	3.115	617	2.436	598
80	4.186	810	3.266	802
100	5.268	1006	4.095	1003
120	6.359	1203	4.919	1207
140	7.457	1401	5.733	1407
160	8.560	1600	6.539	1605
180	9.667	1800	7.338	1801
200	10.777	2000	8.137	1997
220	11.887	2201	8.938	2194
240	12.998	2401	9.745	2392
260	14.108	2602	10.560	2592
280	15.217	2802	11.381	2794
300	16.325	3002	12.207	2995
320	17.432	3202	13.039	3201
340	18.537	3402	13.874	3406
360	19.640	3601	14.712	3611
380	20.743	3800	15.552	3817
400	21.846	3999	16.395	4024
420	22.949	4198	17.241	4232
440	24.054	4398	18.088	4440
460	25.161	4598	18.935	4649
480	26.273	4798	19.788	4857

Thermocouple Temperature °C	Type J Voltage mV	AD595 Output mV	Type K Voltage mV	AD597 Output mV
500	27.388	5000	20.640	5066
520	28.511	5203	21.493	5276
540	29.642	5407	22.346	5485
560	30.782	5613	23.198	5694
580	31.933	5821	24.050	5903
600	33.096	6031	24.902	6112
620	34.273	6243	25.751	6321
640	35.464	6458	26.599	6529
660	36.671	6676	27.445	6737
680	37.893	6897	28.288	6944
700	39.130	7120	29.128	7150
720	40.382	7346	29.965	7355
740	41.647	7575	30.799	7560
760	42.923	7808	31.214	7662
780	–	–	31.629	7764
800	–	–	32.455	7966
820	–	–	33.277	8169
840	–	–	34.095	8369
860	–	–	35.718	8767
880	–	–	36.524	8965
900	–	–	37.325	9162
920	–	–	38.122	9357
940	–	–	38.915	9552
960	–	–	39.700	9746
980	–	–	40.488	9938
1000	–	–	41.269	10130
1020	–	–	42.045	10320
1040	–	–	42.817	10510
1060	–	–	43.585	10698
1080	–	–	44.439	10886
1100	–	–	45.108	11072
1120	–	–	45.863	11258
1140	–	–	46.613	11443
1160	–	–	47.356	11624
1180	–	–	48.095	11805
1200	–	–	48.828	11985
1220	–	–	49.555	12164
1240	–	–	50.276	12341
1260	–	–	50.533	13428

TEMPERATURE PROPORTIONAL OUTPUT MODE

The AD596/AD597 can be used to generate a temperature proportional output of 10 mV/°C when operated with J and K type thermocouples as shown in Figure 1. Thermocouples produce low level output voltages which are a function of both the temperature being measured and the reference or cold junction temperature. The AD596/AD597 compensates for the cold junction temperature and amplifies the thermocouple signal to produce a high level 10 mV/°C voltage output which is a function only of the temperature being measured. The temperature stability of the part indicates the sensitivity of the output voltage to changes in ambient or device temperatures. This is typically 0.02°C/°C over the +25°C to +100°C recommended ambient temperature range. The parts will operate over the extended ambient temperature ranges from –55°C to +125°C, but thermocouple nonlinearity at the reference junction will degrade the temperature stability over this extended range. Table I is a list of ideal AD596/AD597 output voltages as a function of Celsius temperature for type J and K ANSI standard thermocouples with package and reference junction at 0°C. As is normally the case, these outputs are subject to calibration and temperature sensitivity errors. These tables are derived using the ideal transfer functions:

AD596 output = (Type J voltage + 301.5 μV) × 180.57
AD597 output = (Type K voltage) × 245.46

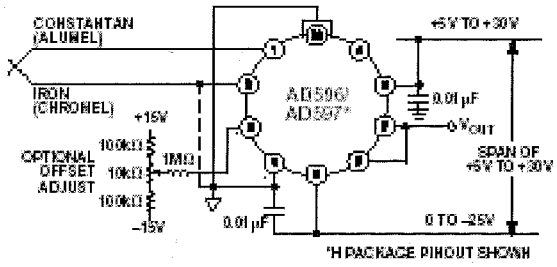

Figure 1. Temperature Proportional Output Connection

The offsets and gains of these devices have been laser trimmed to closely approximate thermocouple characteristics over measurement temperature ranges centered around 175°C with the AD596/AD597 at an ambient temperature between 25°C and 100°C. This eliminates the need for additional gain or offset adjustments to make the output voltage read:

V_{OUT} = 10 mV/°C × (thermocouple temperature in °C) (within specified tolerances).

Excluding calibration errors, the above transfer function is accurate to within 1°C from +80°C to +550°C for the AD596 and –20°C to +350°C for the AD597. The different temperature ranges are due to the differences in J and K type thermocouple curves.

European DIN FE-CuNi thermocouple vary slightly from ANSI type J thermocouples. Table I does not apply when these types of thermocouples are used. The transfer functions given previously and a thermocouple table should be used instead.

Figure 1 also shows an optional trimming network which can be used to change the device's offset voltage. Injecting or sinking 200 nA from Pin 3 will offset the output approximately 10 mV (1°C).

The AD596/AD597 can operate from a single supply from 5 V to 36 V or from split supplies totalling 36 V or less as shown. Since the output can only swing to within 2 V of the positive supply, the usable measurement temperature range will be restricted when positive supplies less than 15 V for the AD597 and 10 V for the AD596 are used. If the AD596/AD597 is to be used to indicate negative Celsius temperatures, then a negative supply is required.

Common-mode voltages on the thermocouple inputs must remain within the common-mode voltage range of the AD596/AD597, with a return path provided for the bias currents. If the thermocouple is not remotely grounded, then the dotted line connection shown in Figure 1 must be made to one of the thermocouple inputs. If there is no return path for the bias currents, the input stage will saturate, causing erroneous output voltages.

In this configuration, the AD596/AD597 H package option has circuitry which detects the presence of an open thermocouple. If the thermocouple loop becomes open, one or both of the inputs to the device will be deprived of bias current causing the output to saturate. It is this saturation which is detected internally and used to activate the alarm circuitry. The output of this feature has a flexible format which can be used to source or sink up to 20 mA of current. The collector (+ALM) should not be allowed to become more positive than ($-V_S$ + 36 V), however, it may be permitted to be more positive than $+V_S$. The emitter voltage (–ALM) should be constrained such that it does not become more positive than 4 V below $+V_S$. If the alarm feature is not used, this pin should be connected to Pins 4 or 5 as shown in Figure 1. The alarm function is unavailable on the AR package option.

SETPOINT CONTROL MODE

The AD596/AD597 can be connected as a setpoint controller as shown in Figure 2. The thermocouple voltage is cold junction compensated, amplified, and compared to an external setpoint voltage. The relationship between setpoint voltage and temperature is given in Table I. If the temperature to be controlled is within the operating range (–55°C to +125°C) of the device, it can monitor its own temperature by shorting the inputs to ground. The setpoint voltage with the thermocouple inputs grounded is given by the expressions:

AD596 Setpoint Voltage = °C × 9.6 mV/°C + 42 mV
AD597 Setpoint Voltage = °C × 10.1 mV/°C – 9.1 mV

The input impedance of the setpoint pin of the AD596/AD597 is approximately 50 kΩ. The temperature coefficient of this resistance is ±15 ppm/°C. Therefore, the 100 ppm/°C 5 kΩ pot shown in Figure 2 will only introduce an additional ±1°C degradation of temperature stability over the +25°C to +100°C ambient temperature range.

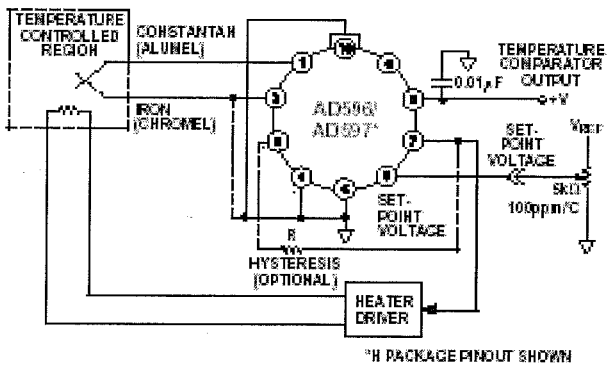

Figure 2. Setpoint Control Mode

Switching hysteresis is often used in setpoint systems of this type to provide noise immunity and increase system reliability. By reducing the frequency of on-off cycling, mechanical component wear is reduced leading to enhanced system reliability. This can easily be implemented with a single external resistor between Pins 7 and 3 of the AD596/AD597. Each 200 nA of current injected into Pin 3 when the output switches will cause about 1°C of hysteresis; that is:

$$R_{HYST}\ (\Omega) = \frac{V_{OUT}}{200\ nA} \times \frac{1}{°C_{HYST}}$$

In the setpoint configuration, the AD596/AD597 output is saturated at all times, so the alarm transistor will be ON regardless of whether there is an open circuit or not. However, –ALM must be tied to a voltage below $(+V_S - 4\ V)$ for proper operation of the rest of the circuit.

STAND-ALONE TEMPERATURE TRANSDUCER

The AD596/AD597 may be configured as a stand-alone Celsius thermometer as shown in Figure 3.

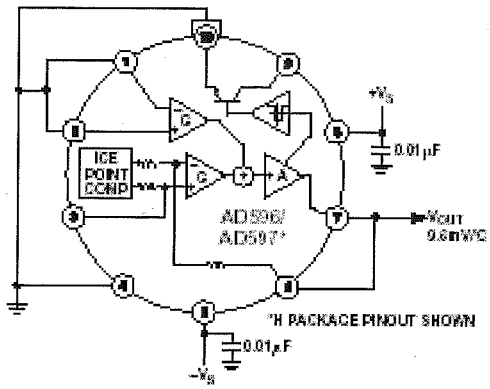

Figure 3. Stand-Alone Temperature Transducer Temperature Proportional Output Connection

Simply omit the thermocouple and connect the inputs (Pins 1 and 2) to common. The output will now reflect the compensation voltage and hence will indicate the AD596/AD597 temperature. In this three terminal, voltage output, temperature sensing mode, the AD596/AD597 will operate over the full extended –55°C to +125°C temperature range. The output scaling will be 9.6 mV per °C with the AD596 and 10.1 mV per °C with the AD597. Additionally there will be a 42 mV offset with the AD596 causing it to read slightly high when used in this mode.

THERMOCOUPLE CONNECTIONS

The connection of the thermocouple wire and the normal wire or printed circuit board traces going to the AD596/AD597 forms an effective reference junction as shown in Figure 4. This junction must be kept at the same temperature as the AD596/AD597 for the internal cold junction compensation to work properly. Unless the AD596/AD597 is in a thermally stable enclosure, the thermocouple leads should be brought in directly to Pins 1 and 2.

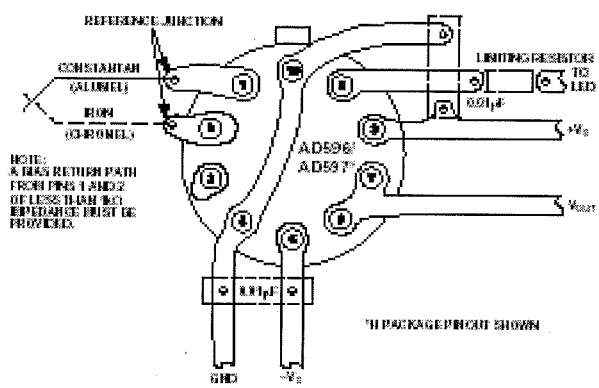

Figure 4. PCB Connections

To ensure secure bonding, the thermocouple wire should be cleaned to remove oxidization prior to soldering. Noncorrosive rosin flux is effective with iron, constantan, chromel, and alumel, and the following solders: 95% tin–5% silver, or 90% tin–10% lead.

SINGLE AND DUAL SUPPLY CONNECTIONS

In the single supply configuration as used in the setpoint controller of Figure 2, any convenient voltage from +5 V to +36 V may be used, with self-heating errors being minimized at lower supply levels. In this configuration, the $-V_S$ connection at Pin 5 is tied to ground. Temperatures below zero can be accommodated in the single supply setpoint mode, but not in the single supply temperature measuring mode (Figure 1 reconnected for single supply). Temperatures below zero can only be indicated by a negative output voltage, which is impossible in the single supply mode.

Common-mode voltages on the thermocouple inputs must remain below the positive supply, and not more than 0.15 V more negative than the minus supply. In addition, a return path for the input bias currents must be provided. If the thermocouple is not remotely grounded, then the dotted line connections in Figures 1 and 2 are mandatory.

STABILITY OVER TEMPERATURE

The AD596/AD597 is specified for a maximum error of ±4°C at an ambient temperature of 60°C and a measuring junction temperature at 175°C. The ambient temperature stability is specified to be a maximum of 0.05°C/°C. In other words, for every degree change in the ambient temperature, the output will change no more than 0.05 degrees. So, at 25°C the maximum deviation from the temperature-voltage characteristic of Table I is ±5.75°C, and at 100°C it is ±6°C maximum (see Figure 5). If the offset error of ±4°C is removed with a single offset adjustment, these errors will be reduced to ±1.75°C and ±2°C max. The optional trim circuit shown in Figure 1 demonstrates how the ambient offset error can be adjusted to zero.

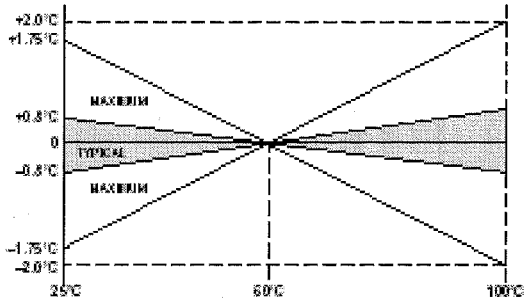

Figure 5. Drift Error vs. Temperature

THERMAL ENVIRONMENTAL EFFECTS

The inherent low power dissipation of the AD596/AD597 keeps self-heating errors to a minimum. However, device output is capable of delivering ±5 mA to an external load and the alarm circuitry can supply up to 20 mA. Since the typical junction to ambient thermal resistance in free air is 150°C/W, significant temperature difference between the package pins (where the reference junction is located) and the chip (where the cold junction temperature is measured and then compensated) can exist when the device is operated in a high dissipation mode. These temperature differences will result in a direct error at the output. In the temperature proportional mode, the alarm feature will only activate in the event of an open thermocouple or system transient which causes the device output to saturate. Self-Heating errors will not effect the operation of the alarm but two cases do need to be considered. First, after a fault is corrected and the alarm is reset, the AD596/AD597 must be allowed to cool before readings can again be accurate. This can take 5 minutes or more depending upon the thermal environment seen by the device. Second, the junction temperature of the part should not be allowed to exceed 150°C. If the alarm circuit of the AD596/AD597 is made to source or sink 20 mA with 30 V across it, the junction temperature will be 90°C above ambient causing the die temperature to exceed 150°C when ambient is above 60°C. In this case, either the load must be reduced, or a heat sink used to lower the thermal resistance.

TEMPERATURE READOUT AND CONTROL

Figure 6 shows a complete temperature indication and control system based on the AD596/AD597. Here the AD596/AD597 is being used as a closed-loop thermocouple signal conditioner and an external op amp is used to implement setpoint. This has two important advantages. It provides a high level (10 mV/°C) output for the A/D panel meter and also preserves the alarm function for open thermocouples.

The A/D panel meter can easily be offset and scaled as shown to read directly in degrees Fahrenheit. If a two temperature calibration scheme is used, the dominant residual errors will arise from two sources; the ambient temperature rejection (typically ±2°C over a 25°C to 100°C range) and thermocouple nonlinearity typical +1°C from 80°C to 550°C for type J and +1°C from –20°C to 350°C for type K.

An external voltage reference is used both to increase the stability of the A/D converter and supply a stable reference for the setpoint voltage.

A traditional requirement for the design of setpoint control thermocouple systems has been to configure the system such that the appropriate action is taken in the event of an open thermocouple. The open thermocouple alarm pin with its flexible current-limited output format supports this function when the part operates in the temperature proportional mode. In addition, if the thermocouple is not remotely grounded, it is possible to program the device for either a positive or negative full-scale output in the event of an open thermocouple. This is done by connecting the bias return resistor directly to Pin 1 if a high output voltage is desired to indicate a fault condition. Alternately, if the bias return is provided on the thermocouple lead connected to Pin 2, an open circuit will result in an output low reading. Figure 6 shows the ground return connected to Pin 1 so that if the thermocouple fails, the heater will remain off. At the same time, the alarm circuit lights the LED signalling the need to service the thermocouple. Grounding Pin 2 would lead to low output voltage saturation, and in this circuit would result in a potentially dangerous thermal runaway under fault conditions.

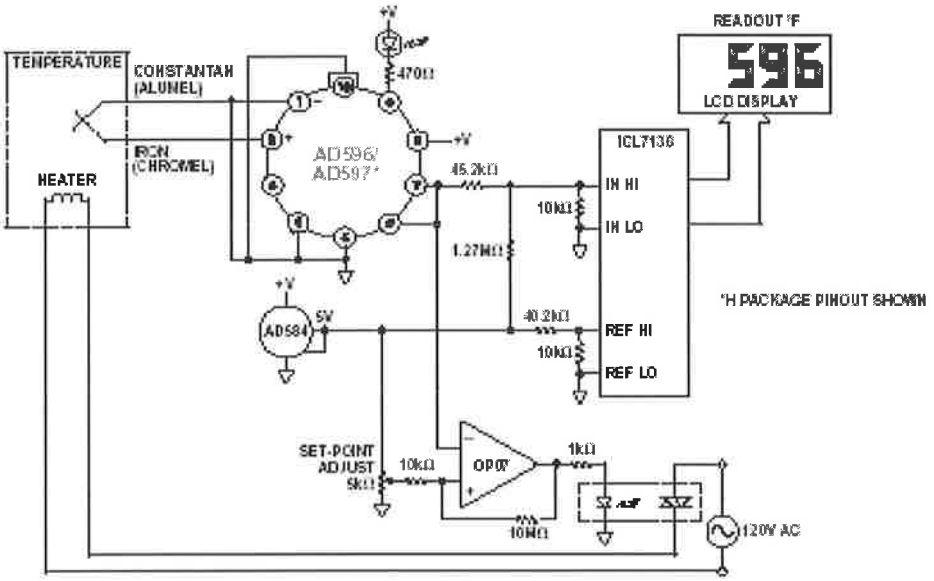

Figure 6. Temperature Measurement and Control

OUTLINE DIMENSIONS

Dimensions shown in inches and (mm).

10-Pin Metal Can (TO-100)

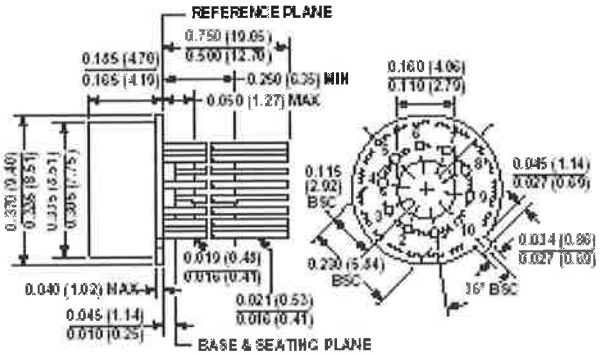

8-Lead Small Outline (SOIC) (SO-8)

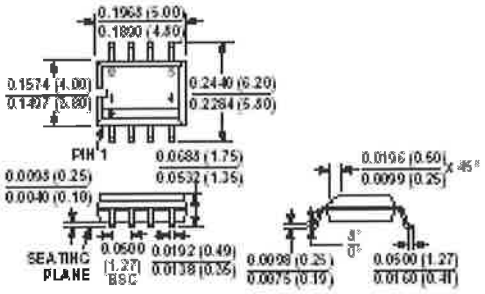

Appendix C: Colegrove: Calibration of Spindle Motor Torque For The Butler FSW Machine

Determining the Power Input

The verification of the thermal model requires that the heat input while welding should be known. This requires a knowledge of the torque produced by the FSW spindle and the horizontal load during welding. The heat input can be determined from these values plus the rotational speed of the spindle and the horizontal welding speed.

All the measurements have been done on the Butler Friction Stir Welding Machine. The vertical spindle motor of this machine is connected to an ABB ACS 600 Frequency Converter. This frequency converter produces a voltage, which depends on the output torque of the motor. The value varies between 0 and 10 Volts; 0 Volts indicating no load and 10 indicating that the motor is producing the full load torque. The value of this voltage is independent of the speed of the motor. The torque produced by the motor will not equal the torque at the spindle. There is a 2:1 gear reduction between the spindle and the FSW head plus there are bearings in the spindle head to support against horizontal loads and some losses will occur in the belt drive gear reduction. Referring to Figure 4-16 the actual power at the head will be equal to:

$$P_s = T_s\omega_s = 2T_m\omega_s - Q_{belt} - Q_{bearing} \qquad \text{Eq.4-1}$$

Hence, taking the power from the motor only without considering the losses through the belt drive and bearings will give an incorrect result. To solve this problem, direct torque measurement at the spindle is required. This section describes how this has been achieved so that a relationship between %max torque of the motor and torque at the spindle can be found.

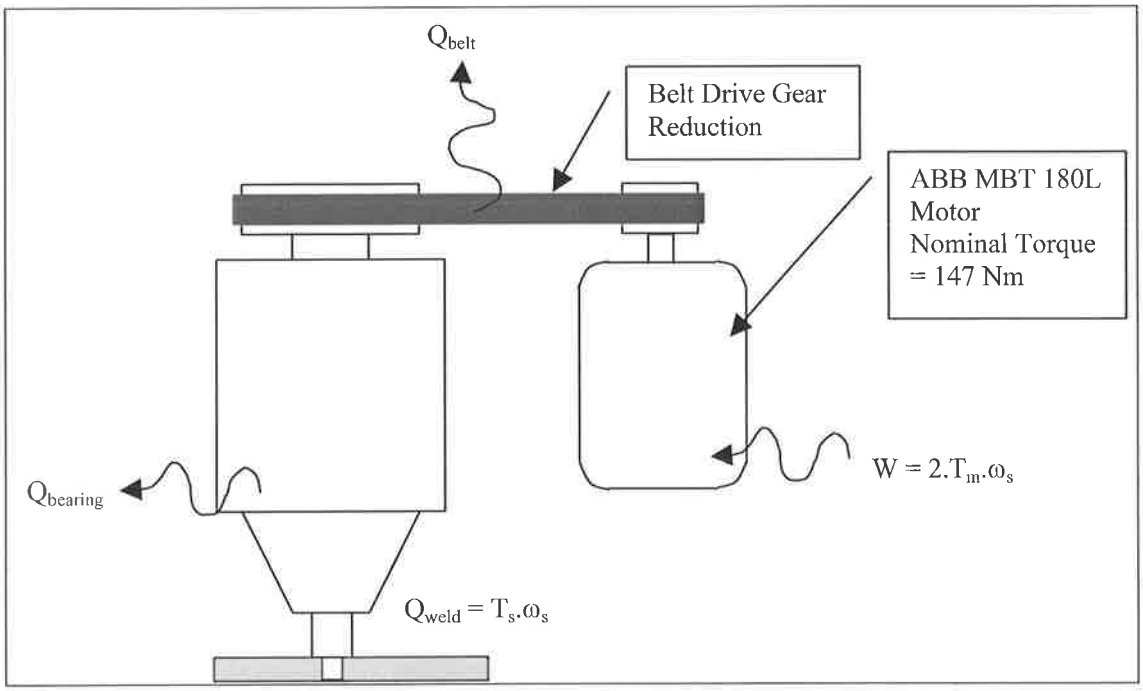

Figure 4-16 Spindle Drive on Butler FSW Machine

Measuring the horizontal load on the spindle is simpler. This is done by measuring the horizontal force with a load cell while welding, and is described in the second part of the document.

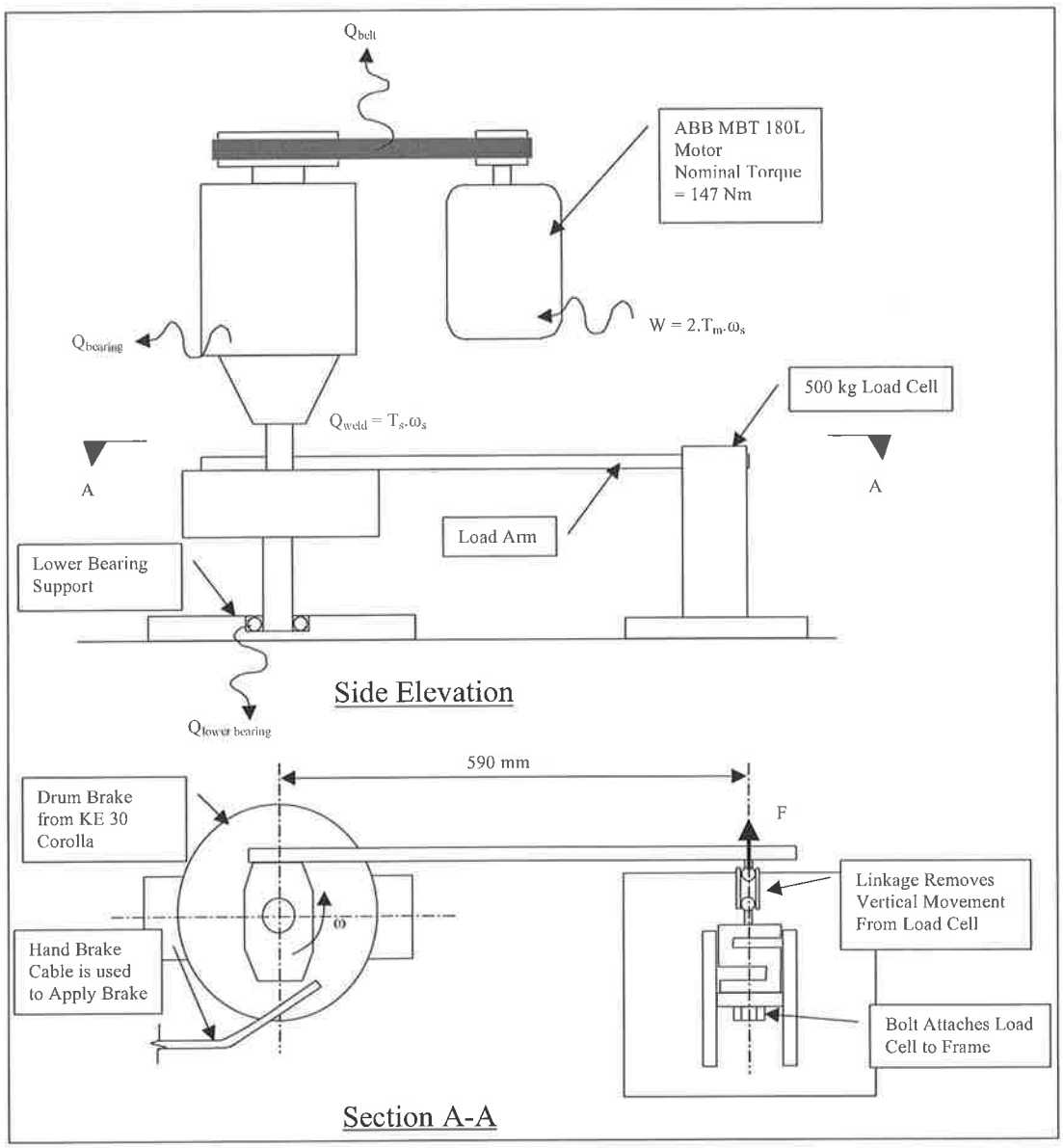

Figure 4-17 Layout of Torque Measuring Device

Torque Measuring Device

Description of Equipment

A layout of the equipment used for the Friction Stir Welding Torque Measuring Device is shown in Figure 4-17. The only problem with the design is the power loss from the lower bearing, which will tend to slightly lower the observed value of the force measured at the load cell. It is assumed that the resistance of this bearing is sufficiently low that it can be neglected. Note also

that there is a linkage between the load cell and the load arm. This stops any vertical movement of the load arm being transferred to the load cell.

An energy balance on the system shows that:

$$0.59F\omega_s + Q_{belt} + Q_{bearing} + Q_{lowerbearing} = 2T_m\omega_s \qquad \text{Eq. 4-2}$$

Hence the force on the end of the load cell will be given by:

$$T_s = 0.59F = \frac{2T_m\omega_s - Q_{belt} - Q_{bearing} - Q_{lowerbearing}}{\omega_s} \qquad \text{Eq. 4-3}$$

The force measured at the load cell is output as a voltage from the load cell amplifier. This voltage is monitored by the Galil Motion Controller, which controls the operation of the equipment.

Problems with the Device Operation

When performing the experiment the following problems were encountered:

- There was significant oscillation of the load arm when the spindle was rotating. This was caused by the spindle not being parallel to the drum brake housing, due to a misalignment of the bearing. Hence at a radius of 0.59m there was approximately 20mm oscillation of the load arm. Unfortunately, this oscillation may have also increased the energy loss in the system.
- There was significant noise in the readings from the load cell. Initially, it was thought that the noise was caused by the oscillation of the torque measuring device. However a test later showed that when the load cell was not connected there was still a significant amount of noise in the voltage output. Therefore, it was concluded that the noise was primarily caused by electrical RF noise from the spindle motor.

Because of these problems the following smoothing function was used when analysing the results:

$$T_i = \frac{T_{i-1} + 2T_i + T_{i+1}}{4} \qquad \text{Eq. 4-4}$$

This was repeated 10 times to get reasonably smooth data.

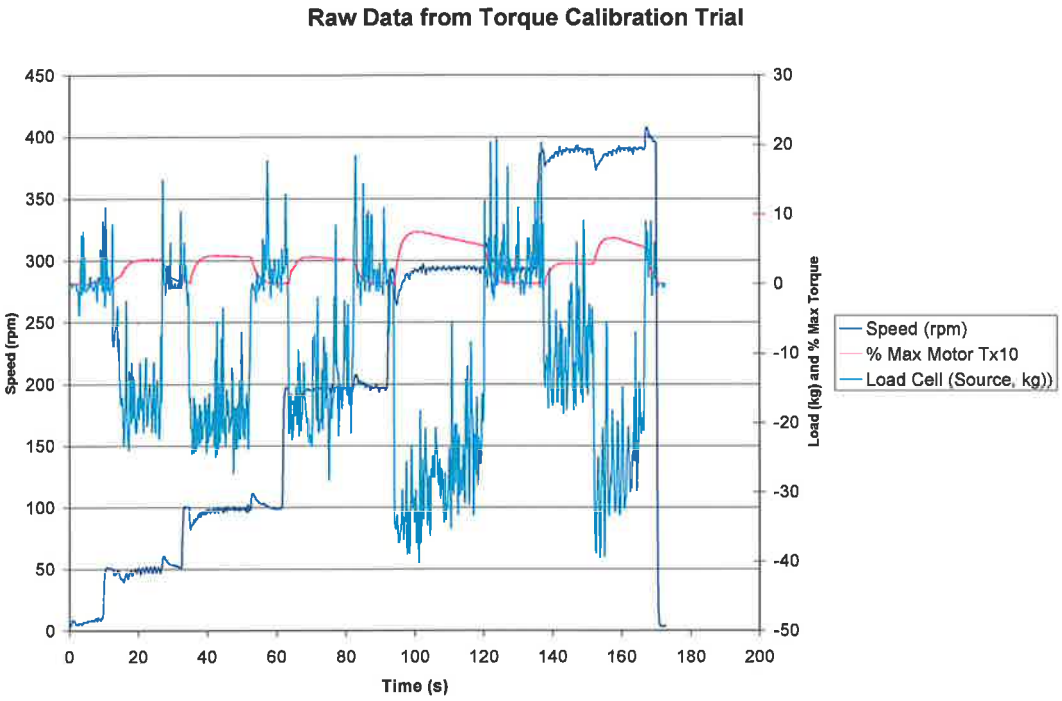

Figure 4-18 Raw Data

Results

The unsmoothed data is shown in Figure 4-18. The noise is clearly visible.

An example of the noise with no load on the load cell is shown in Figure 4-19. This clearly demonstrates that the bulk of the noise in the readings is not mechanical, but electrical. After smoothing this load data the curve shown in Figure 4-20was obtained. Selected areas were then used to produce calibration plots between the input torque of the motor and the torque output from the torque-measuring device. The first graph shown in Figure 4-21 demonstrates that the calibration curve is independent of speed. The second graph (Figure 4-22) shows all the data plotted together with a trendline to giving the calibration curve between the two results.

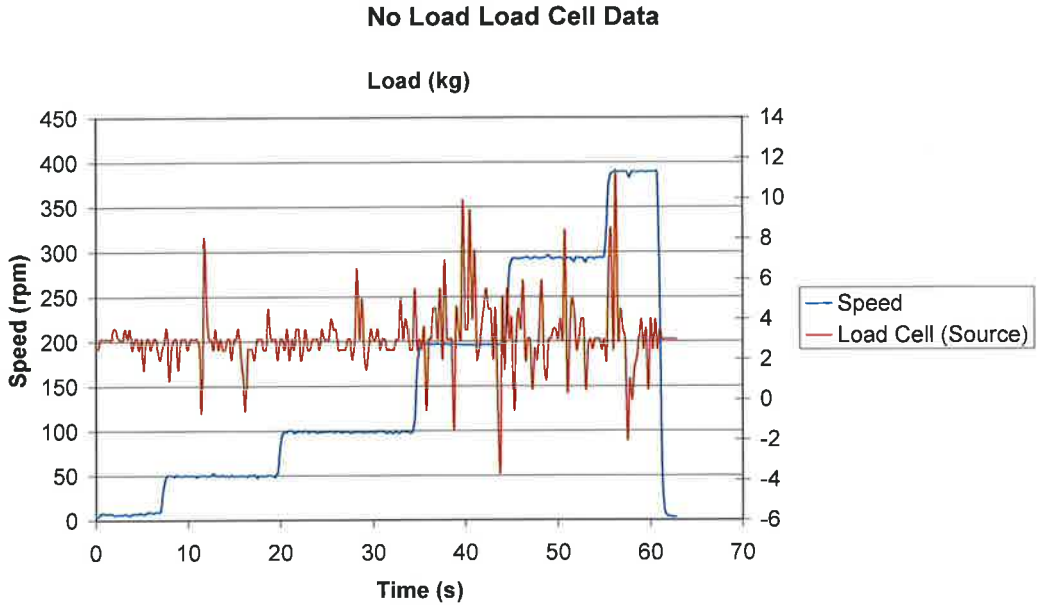

Figure 4-19 **No Load, Load Cell Data**

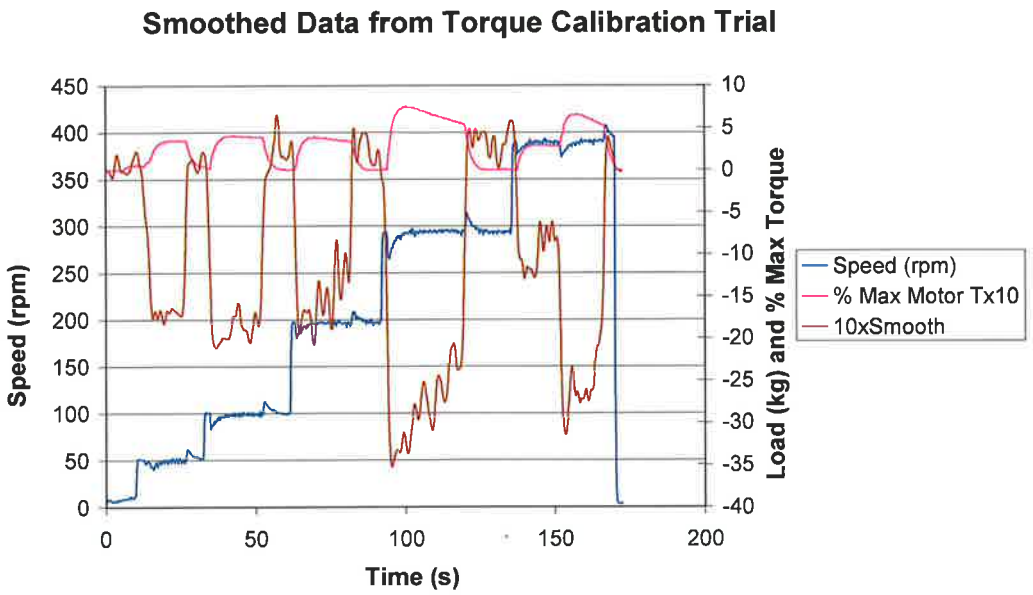

Figure 4-20 **Smoothed Data**

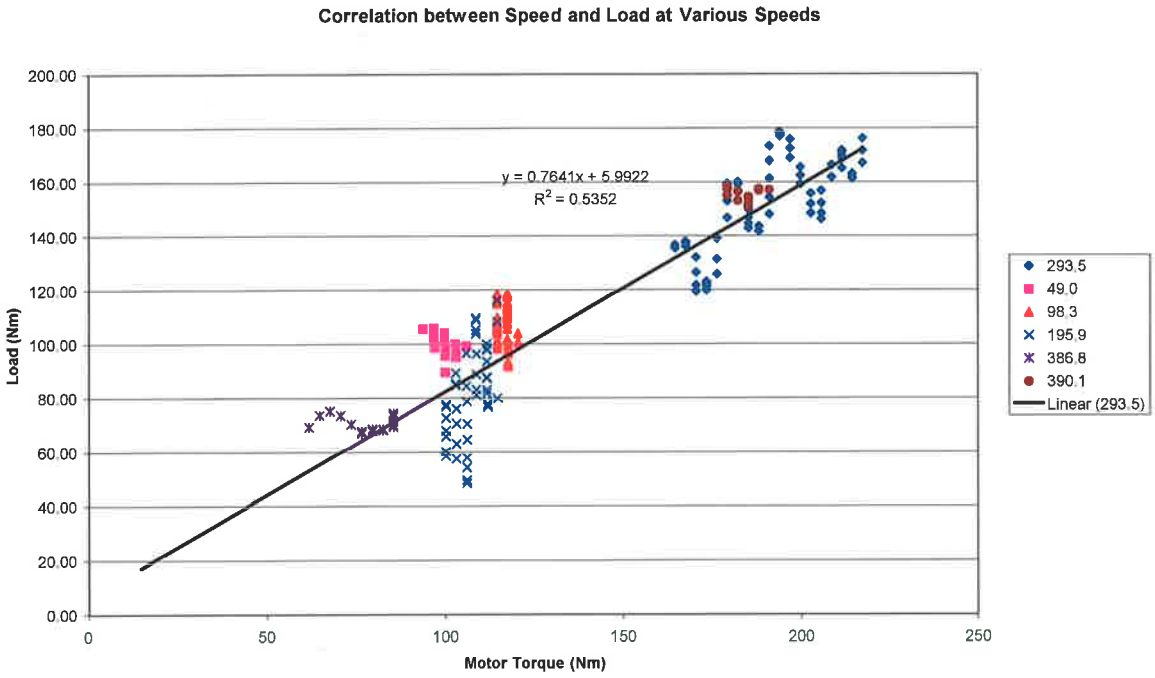

Figure 4-21 **Results at Different Speeds for Motor Torque vs. Load Cell Torque (Nm)**

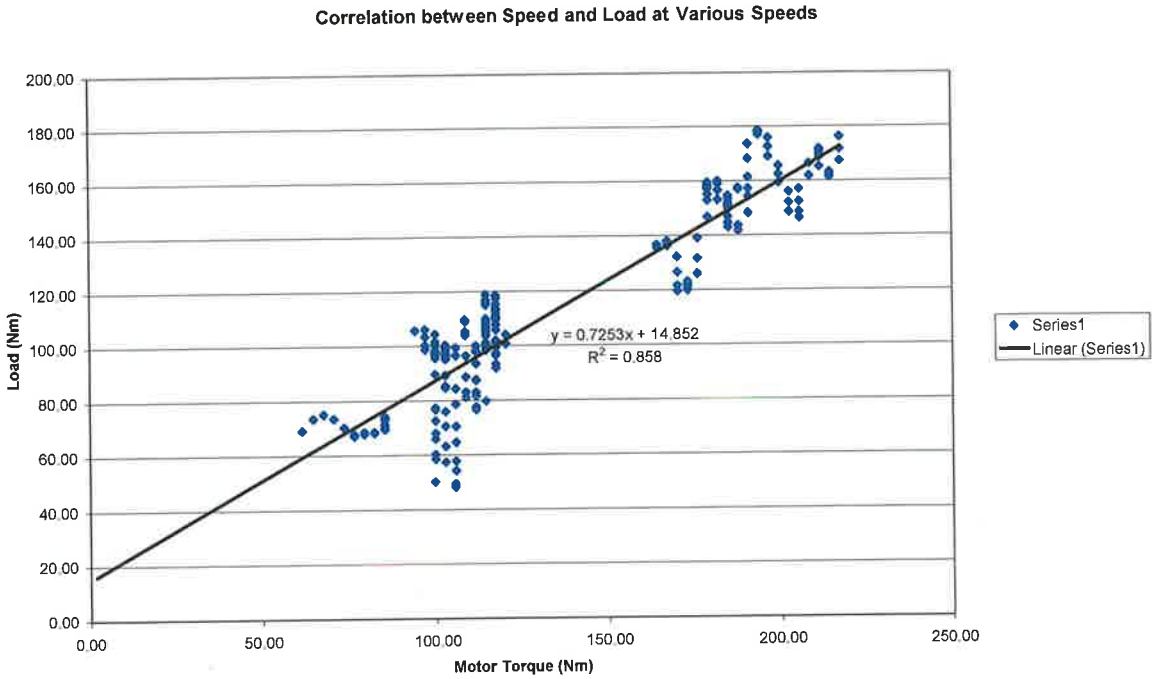

Figure 4-22 **Results for Motor Torque vs. Load Cell Torque (Nm)**

Discussion

One interesting feature that was observed in the results was how for a given setting on the hand brake, the load on both the load cell and the motor reduced over time. This was particularly noticeable at high speeds and braking loads and can be attributed to the brake pads heating up and losing their efficiency.

It was found that during weld 000313B, the %Max torque reading of the motor was 3.15. This resulted in a heat input of 2.96kW to the workpiece based on the calibration curve in Figure 4-22. The corresponding power output of the motor was 3.34 kW based on a nominal load of 147Nm. Hence there was a 12.9% energy loss through the drive system, based on the calibration curve.